To the Graduate Council:

I am submitting herewith a thesis written by Shawna R. Cyphers entitled "Detailed mapping of a terrane boundary, and structure and origin of block-in-matrix structures, central and eastern Blue Ridge, Jackson County, North Carolina" I have examined the final copy of this thesis for form and content and recommend that it be accepted in partial fulfillment of the requirements for the degree of Master of Science, with a major in Geology.

Robert D. Hatcher, Jr.
Major Professor

We have read this thesis
and recommend its acceptance:

Theodore C. Labotka

Harry Y. McSween

Acceptance for the Council:

Carolyn R. Hodges
Vice Provost and Dean of
The Graduate School

Detailed mapping of a terrane boundary, and structure and origin of block-in-matrix structures, central and eastern Blue Ridge, Jackson County, North Carolina

A thesis
Presented for the Master of Science Degree
University of Tennessee, Knoxville

Shawna R. Cyphers
May 2009

Acknowledgments

Many thanks to my primary advisor, Dr. Robert Hatcher, Jr., for his support, patience, time, and instruction over the course of this graduate program. I am so appreciative of the many opportunities you have provided me. I would also like to thank my other committee members, Dr. Harry McSween and Dr. Ted Labotka for their suggestions, comments, and helpful criticism throughout the duration of this project.

I am very appreciative to the department of geology and all of the professors who have been supportive during my time at the University of Tennessee. I also want to thank Allen Patchen for all of his help and advice on the use of the electron microprobe.

And to Nancy Meadows, thank you so much for your diligent editing, reassuring words, and kindness. We are so lucky to have you as 'da Mama' in the office.

To my fellow graduate students: Many thanks to Crystal Wilson, Chris and Jen Whisner, Mary Varnell, Heather Byars, Brittany Davis, and Ching Tu. You guys are great friends and it would not have been the same without you. And a special thanks to Arthur Merschat and Johnathan Evenick for being so helpful and supportive during my time at UTK, and most of all for being great friends

Special thanks to my parents Robert and Sue Ellen Cyphers, and to my brother, Aaron, for all of their support, encouragement, and love: you all are the best! Finally, a huge 'Thank You' to my husband, David Grant. Your patience, support, and love are more than anyone could ever hope for and I am forever grateful.

Abstract

Detailed geologic mapping of the Sylva South and Tuckaseegee quadrangles reveals the southern extent of the Great Balsam Mountains window (Great Balsam Mountains Window), which exposes the northeastern extension of the Dahlonega gold belt in western North Carolina. The Great Balsam Mountains Window is framed by the Soque River fault to the NW and SW, and by the Chattahoochee-Holland Mountain (Chattahoochee-Holland Mountain) fault to the SE. Emplacement and tight folding of the Chattahoochee-Holland Mountain fault is interpreted as an early Alleghanian (D_4) post-peak metamorphic, ductile event because it crosscuts the Rabun Granodiorite (335 Ma) south of the Great Balsam Mountains Window. The Soque River fault is a postmetamorphic late Taconic(?) fault separating two central Blue Ridge terranes: the Cartoogechaye terrane of upper amphibolite to granulite paragneisses, mafic and ultramafic rocks, pelitic schist and Grenvillian basement; and the Dahlonega gold belt of middle to upper amphibolite facies metasedimentary rocks and lesser mafic and altered ultramafic (soapstone to metaperidotite). The Chattahoochee-Holland Mountain fault separates Dahlonega gold belt rocks from Tallulah Falls-Ashe Formation middle to upper amphibolite facies rocks of the Tugaloo terrane in the eastern Blue Ridge and truncates the Soque River fault in the SW part of the window. The tripartite stratigraphy of the Tallulah Falls Formation was identified and mapped in the study area, along with the northern extent of the Walnut Creek granodiorite (355 Ma), Rabun Granodiorite (335 Ma), and Looking Glass granodiorite (333 ± 2 Ma). Geochemistry of felsic igneous rock samples indicates they are typical eastern Blue Ridge plutonic rocks that are likely derived from repeated intracrustal melting of accretionary wedge rocks. Geochemistry of mafic rocks collected from block-in-matrix structures have a geochemical signature typical of an igneous protolith and fall in the tholeiitic basalt field with a strong affinity for a MORB protolith. Penetrative (D_2) structures are dominant in the study area and probably formed during the Taconic orogeny. Rocks in the study area contain amphibolite facies assemblages (sillimanite–kyanite and sillimanite–kyanite–staurolite).

TABLE OF CONTENTS

CHAPTER I INTRODUCTION 1

Objectives 1
REGIONAL GEOLOGY 2
STUDY AREA 4
STRUCTURE 10
BLOCK-IN-MATRIX STRUCTURES 10

CHAPTER II ROCK UNITS 12

INTRODUCTION 12
ROCK UNITS 12
Dahlonega gold belt–Otto Formation 12
Metasandstone 14
Schist 16
Amphibolite 20
Catamount Gap 20
Savannah Church 23
Ultramafic Rocks 23
Cartoogechaye Terrane 23
Tugaloo Terrane 26
Lower Tallulah Falls Formation 28
Aluminous Schist 28
Upper Tallulah Falls Formation 29
Amphibolite 31
Dills Falls Shear Zone 31
Walnut Creek Granodiorite–Tonalite 32
Tuckaseegee Granodiorite–Monzodiorite 32
Rabun Granodiorite 36
Looking Glass Granodiorite 36

CHAPTER III GEOCHEMISTRY OF METAIGNEOUS ROCK 39

INTRODUCTION 39
SAMPLE COLLECTION AND ANALYTICAL METHODS 41
Samples 41
Analytical Techniques 41
PART 1: GRANITIC PLUTONS IN THE EASTERN BLUE RIDGE 42
Granitoid Geochemistry 46
Trace-element geochemistry 46
REE geochemistry 50
Tectonic discrimination diagrams 50
DISCUSSION OF GRANITOIDS 50
PART 2: GEOCHEMISTRY OF MAFIC ROCKS 54
AMPHIBOLITE GEOCHEMISTRY 56
Ortho- versus Para-amphibolite 56
Covariation diagrams 56
Trace-element geochemistry 68
REE geochemistry 74
Alkaline vs subalkaline basalts 74
Tectonic discrimination diagrams 74
SYNTHESIS AND DISCUSSION OF MAFIC ROCKS 80

CHAPTER IV METAMORPHISM 82

INTRODUCTION 82
GEOLOGIC SETTING AND TIMING OF METAMORPHISM 84
Western Blue Ridge *84*
Central Blue Ridge *86*
Eastern Blue Ridge *87*
SAMPLE DESCRIPTION 88
Methodology *88*
PETROGRAPHIC DESCRIPTION 90
Sample 311C (Dahlonega gold belt) *90*
Sample CGB (Dahlonega gold belt) *90*
Sample 478 (Upper Tallulah Falls) *92*
Sample 1498 (Upper Tallulah Falls) *92*
Sample 588 (Upper Tallulah Falls) *92*
Sample 862 (Upper Tallulah Falls) *94*
Phase Diagrams *94*
Mineral chemistry *97*
GEOTHERMOBAROMETRY 106
RESULTS OF P–T ESTIMATES 109
PRESSURE–TEMPERATURE–TIME PATHS 110
CONCLUSIONS 110

CHAPTER V DEFORMATION AND STRUCTURAL STYLE IN THE BLUE RIDGE 122

INTRODUCTION 122
DOMAINS 123
FAULTS 125
MAP PATTERNS AND CROSS SECTIONS 129
BLOCK-IN-MATRIX STRUCTURES 133
DEFORMATION AND OROGENIC EVENTS 137

CHAPTER VI CONCLUSIONS 145

REFERENCES CITED 147

APPENDIX I: ELECTRON MICROPROBE ANALYSES 160

APPENDIX II: STRUCTURAL DATA 210

VITA 227

LIST OF TABLES

CHAPTER II

TABLE 2-1. MODAL ANALYSES OF METASANDSTONE SAMPLES FROM THE SYLVA SOUTH AND TUCKASEEGEE QUADRANGLES 17
TABLE 2-2. MODAL ANALYSES OF AMPHIBOLITES SAMPLES FROM BLOCK-IN-MATRIX STRUCTURES ..... STRUCTURE 21
TABLE 2-3. MODAL ANALYSES OF SAMPLES COLLECTED FROM THE WCG AND TUCKASEEGEE GRANITOIDS 34

CHAPTER III

TABLE 3-1. WHOLE-ROCK MAJOR AND TRACE ELEMENT DATA FOR REPRESENTATIVE GRANITIC SAMPLES IN THE EASTERN BLUE RIDGE TERRANE 43
TABLE 3-2. CIPW NORMATIVE MINERALOGY OF GRANITIOD SAMPLES 45
TABLE 3-3. WHOLE-ROCK MAJOR AND TRACE ELEMENT DATA FOR REPRESENTATIVE SAVANNAH CHURCH AMPHIBOLITES SAMPLES IN THE DAHLONEGA GOLD BELT. 60
TABLE 3-4…WHOLE-ROCK MAJOR AND TRACE ELEMENT DATA FOR REPRESENTATIVE CATAMOUNT GAP AMPHIBOLITES SAMPLES IN THE DAHLONEGA GOLD BELT. 61

CHAPTER IV

TABLE 4-1. RESULTS OF PRESSURE-TEMPERATURE CALCULATIONS 118

CHAPTER V

TABLE 5-1. COMPILATION FROM PREVIOUS STUDIES OF DEFORMATION AND FOLDING IN THE CENTRAL AND EASTERN AND CENTRAL BLUE RIDGE 126

LIST OF FIGURES

CHAPTER I

FIGURE 1-1. REGIONAL MAP OF WESTERN, CENTRAL AND EASTERN BLUE RIDGE IN TENNESSEE, GEORGIA, NORTH CAROLINA AND SOUTH CAROLINA 3
FIGURE 1-2. COMPILED GEOLOGIC MAP OF A SECTION OF THE BLUE RIDGE..... 5-6
FIGURE 1-3. PREVIOUS WORK IN AND NEAR THE STUDY AREA..... 8

CHAPTER II

FIGURE 2-1. SIMPLIFIED GEOLOGIC MAP OF SYLVA SOUTH AND TUCKASEEGEE QUADRANGLES 13
FIGURE 2-2. REPRESENTATIVE SAMPLES OF DAHLONEGA GOLD BELT METASANDSTONE 15
FIGURE 2-3. QFM DIAGRAM (PETTIJOHN, 1954) COMPARING COMPOSITION OF METASEDIMENTARY ROCKS FROM THE DAHLONEGA GOLD BELT AND THE TALLULAH FALLS FORMATION..... 18
FIGURE 2-4. REPRESENTATIVE SAMPLES OF DAHLONEGA GOLD BELT SCHIST 19
FIGURE 2-5. AMPHIBOLITE SAMPLE FROM CATAMOUNT GAP 22
FIGURE 2-6. AMPHIBOLITE SAMPLE FROM SAVANNAH CHURCH 24
FIGURE 2-7. SAMPLES OF DAHLONEGA GOLD BELT SOAPSTONE AND MAFIC LITHOLOGY..... 25
FIGURE 2-8. REPRESENTATIVE LITHOLOGIES OF THE TALLULAH FALLS FORMATION 27
FIGURE 2-9. UPPER TALLULAH FALLS METASANDSTONE 30
FIGURE 2-10. WCG AND TUCKASEEGEE GRANITOIDS 33
FIGURE 2-11. CLASSIFICATION OF WCG AND TUCKASEEGEE SAMPLES 35
FIGURE 2-12. RABUN GRANODIORITE..... 37

CHAPTER III

FIGURE 3-1. COMPILED GEOLOGIC MAP OF A SECTION OF THE BLUE RIDGE. 40
FIGURE 3-2. NORMATIVE-FELDSPAR CLASSIFICATION AND SHAND'S INDEX OF GRANITOID SAMPLES 44
FIGURE 3-3. HARKER DIAGRAMS OF ALL MAJOR OXIDES FOR THE WALNUT CREEK AND TUCKASEEGEE GRANITE SAMPLE. 47
FIGURE 3-4. TiO_2 VARIATION DIAGRAMS OF WALNUT CREEK SAMPLES AND THE TUCKASEEGEE GRANITE SAMPLE. 48
FIGURE 3-5. TRACE ELEMENT DIAGRAMS FOR THE WALNUT CREEK AND TUCKASEEGEE GRANITE 49
FIGURE 3-6. REE DIAGRAMS (SUN AND MCDONOUGH, 1989) FOR WALNUT CREEK AND THE TUCKASEEGEE GRANITE SAMPLE.. 51
FIGURE 3-7. TECTONIC DISCRIMINATION DIAGRAMS FOR EASTERN BLUE RIDGE GRANITES WALNUT CREEK AND THE TUCKASEEGEE GRANITE (PEARCE ET AL., 1984).. 52
FIGURE 3-8..THE SAVANNAH CHURCH BLOCK-IN-MATRIX EXPOSURE.. 57-58
FIGURE 3-9. NIGGLI MG-(AL-ALK)-C DIAGRAMS FOR AMPHIBOLITE BLOCKS FROM THE SAVANNAH CHURCH EXPOSURE AND CATAMOUNT GAP EXPOSURSE. 59
FIGURE 3-10. BIVARIATE DIAGRAM OF MAJOR OXIDES (WT.%) COMPARED TO MG # FOR AMPHIBOLITE BLOCKS..... 62-67
FIGURE 3-11. BIVARIATE DIAGRAM OF MAJOR OXIDES (WT.%) COMPARED TO ZR (PPM) FOR AMPHIBOLITES BLOCKS.. 69-72
FIGURE 3-12. MORB NORMALIZED DIAGRAM OF PEARCE (1983) FOR SAVANNAH CHURCH AND CATAMOUNT GAP SAMPLES.. 73
FIGURE 3-13. RARE EARTH ELEMENT (REE) DIAGRAMS OF SUN AND MCDONOUGH (1989) OF SAVANNAH CHURCH AND CATAMOUNT GAP SAMPLES..... 75
FIGURE 3-14. VARIOUS DISCRIMINANT DIAGRAMS FOR AMPHIBOLITES BLOCKS FROM THE SAVANNAH CHURCH EXPOSURE AND CATAMOUNT GAP. 76
FIGURE 3-15. BIVARIATE DISCRIMINANT DIAGRAMS FOR ALKALI AND THOLEIITIC BASALTS 77
FIGURE 3-16. TECTONIC DISCRIMINANT DIAGRAMS FOR BASALTS..... 78
FIGURE 3-17. . TECTONIC DISCRIMINANT DIAGRAMS AND TH/YB VERSUS TA/YB DIAGRAMS 79

CHAPTER IV

FIGURE 4-1. SIMPLIFIED GEOLOGIC MAP OF SYLVA SOUTH AND TUCKASEEGEE QUADRANGLES WITH SAMPLES.LOCATIONS 83
FIGURE 4-2. METAMORPHIC ISOGRAD MAP OF THE SOUTHERN APPALACHIAN BLUE RIDGE AND INNER PIEDMONT COMPILED FROM VARIOUS STUDIES 85
FIGURE 4-3. METAMORPHIC ISOGRAD MAP OF THE STUDY AREA 89
FIGURE 4-4. PHOTOMICROGRAPHS OF REPRESENTATIVE SAMPLES. 91
FIGURE 4-5. PHOTOMICROGRAPHS OF REPRESENTATIVE SAMPLES. 93
FIGURE 4-6 AFM (THOMPSON, 1957) AND ACF DIAGRAM OF DAHLONEGA GOLD BELT SAMPLES 95
FIGURE 4-7 AFM (THOMPSON, 1957) OF TUGALOO TERRANE SAMPLES. 96
FIGURE 4-8 PARTIAL TERNARY PLOT SHOWING GARNET COMPOSITIONS.. 98
FIGURE 4-9 GARNET ZONING PROFILE OF SAMPLE 311C. 99
FIGURE 4-10 GARNET ZONING PROFILE OF SAMPLE 311C. 100
FIGURE 4-11 GARNET ZONING PROFILE OF SAMPLE CGB. 101
FIGURE 4-12 GARNET ZONING PROFILE OF SAMPLE 478. 102
FIGURE 4-13 GARNET ZONING PROFILE OF SAMPLE 1498.. 103
FIGURE 4-14 GARNET ZONING PROFILE OF SAMPLE 588 104
FIGURE 4-15 GARNET ZONING PROFILE OF SAMPLE 862 105
FIGURE 4-16 PLOTS OF BIOTITE AND ILMENITE COMPOSITION 107
FIGURE 4-17 THERMOBAROMETRY RESULTS FOR SAMPLE SS311C, GARNET #1. 111
FIGURE 4-18 THERMOBAROMETRY RESULTS FOR SAMPLE SS311C, GARNET #2.. 112
FIGURE 4-19 THERMOBAROMETRY RESULTS FOR SAMPLE CGB 113
FIGURE 4-20 THERMOBAROMETRY RESULTS FOR SAMPLE 478. 114
FIGURE 4-21 THERMOBAROMETRY RESULTS FOR SAMPLE 1498. 115
FIGURE 4-22 THERMOBAROMETRY RESULTS FOR SAMPLE 588. 116
FIGURE 4-23 THERMOBAROMETRY RESULTS FOR SAMPLE 862. 117
FIGURE 4-24 SIMPLIFIED GEOLOGIC MAP OF SHOWING LOCATIONS OF SAMPLES AND P-T ESTIMATES FOR THIS STUDY AND P-T ESTIMATES FROM PREVIOUS STUDIES 119
FIGURE 4-25 P-T-T PATHS 120

CHAPTER V

FIGURE 5-1. FORM-LINE MAP SHOWING GENERALIZED FOLIATION TRENDS, DOMAINS, AND EQUAL-AREA STEREONET PLOTS OF FOLIATION DATA. 124
FIGURE 5-2. EQUAL-AREA STEREONET PLOTS OF FOLD DATA. 127-128
FIGURE 5-3. MYLONITE IN UPPER TALLULAH FALLS FORMATION. 130
FIGURE 5-4. GEOLOGIC MAP OF THE STUDY AREA AND CROSS SECTIONS 131-132
FIGURE 5-5. AMPHIBOLITE BLOCK MORPHOLOGIES AT SAVANNAH CHURCH EXPOSURE 135
FIGURE 5-6. FOLDS AT SAVANNAH CHURCH EXPOSURE 136
FIGURE 5-7 MICROSCOPIC S_1 FOLIATION AND MESOSCOPIC S_2 FOLIATION 138
FIGURE 5-8. MIGMATITIC METASANDSTONE 140
FIGURE 5-9. EXPOSURE OF OTTO FORMATION METASANDSTONE AND PELITIC SCHIST 141
FIGURE 5-10 CRENULATED SCHIST AND OPEN FOLD IN THE OTTO FORMATION. 142

LIST OF ATTACHMENTS

PLATE I GEOLOGIC MAP OF THE SYLVA SOUTH AND TUCKASEEGEE QUADRANGLE .....*Attached*

PLATE II SAVANNAH CHURCH BLOCK-IN-MATRIX STRUCTURE .....*Attached*

CHAPTER I Introduction

The Appalachians are a deeply eroded mountain chain containing all of the components of a collisional orogenic belt: a foreland fold–thrust belt; a crystalline metamorphic core; and accreted native, suspect, and exotic terranes (Hatcher, 1989). In the southern Appalachians, the Blue Ridge composite megathrust sheet is one of the largest crystalline terranes in the world (Hatcher and Hooper, 1992). The Blue Ridge is a polydeformed, composite-crystalline terrane affected by three Paleozoic tectonothermal events: the Taconic, Neoacadian, and Alleghanian orogenies. Current errosional levels of the Appalachians expose mid–crustal sections of the mountain chain, which enables study of the internal parts of the orogen.

The Appalachians record a long history of deformation and detailed geologic mapping is needed to provide insight into the processes that have shaped and defined this orogen. Blue Ridge geology is complex, therefore detailed mapping integrated with structural, geochemical, and petrologic studies are required to better comprehend its history. In particular, the Blue Ridge in southwestern North Carolina has been identified for study because of recent detailed geologic mapping, geochronologic, structural, petrologic, and provenance studies conducted in this region (Shireman et al., 1985; Brumback, 1990; Quinn, 1991; Davidson, 1995; Cameron, 2001; Bream, 2003; Stahr, 2007).

This project focuses on a terrane boundary in SW North Carolina, the Chattahoochee–Holland Mountain fault, that separates rocks of the Dahlonega gold belt and eastern Blue Ridge. Detailed geologic mapping and structural, metamorphic, and geochemical analysis in this study should provide a better understanding of the tectonic evolution of the Blue Ridge.

Objectives

The objectives for this research are:

(1) create a detailed 1:24,000 scale geologic map of parts of the Sylva South and Tuckaseegee quadrangles;

(2) map the Chattahoochee–Holland Mountain fault, and the SW part of the Great Balsam Mountains window;

(3) provide a detailed description of rock units, metamorphism, and structure of the area; and

(4) compare the geochemistry of amphibolite samples from this and past studies with amphibolite blocks taken from two exposures of block-in-matrix structure;

(5) interpret the structure of this part of the Great Balsam Mountains Window and Tugaloo terrane;

(6) better understand the tectonic history of this part of the Blue Ridge.

Regional Geology

The Blue Ridge geologic province lies east of the Valley and Ridge, with the Great Smoky and Miller Cove faults separating the two provinces. To the east the Brevard fault zone defines the boundary between the eastern Blue Ridge and the Inner Piedmont. Tallulah Falls/Ashe Formation rocks are found on both sides of the Brevard fault zone, indicating that it is not a terrane boundary. Collectively, the Blue Ridge consists of western, central, and eastern geologic belts. The western Blue Ridge (Fig. 1–1) is composed of clastic rift-related metasedimentary rocks of the Neoproterozoic Ocoee Supergroup, Lower Cambrian Chilhowee Group, and Neoproterozoic and Cambrian volcanic-sedimentary assemblages, such as the Mount Rogers, Grandfather Mountain, and Catoctin Formations (King et al., 1958; Rast and Kohles, 1986; Aleinikoff et al., 1995; Brewer and Thomas, 2000). This sequence was deposited on the rifted margin of Laurentia, which is underlain by Middle Proterozoic continental

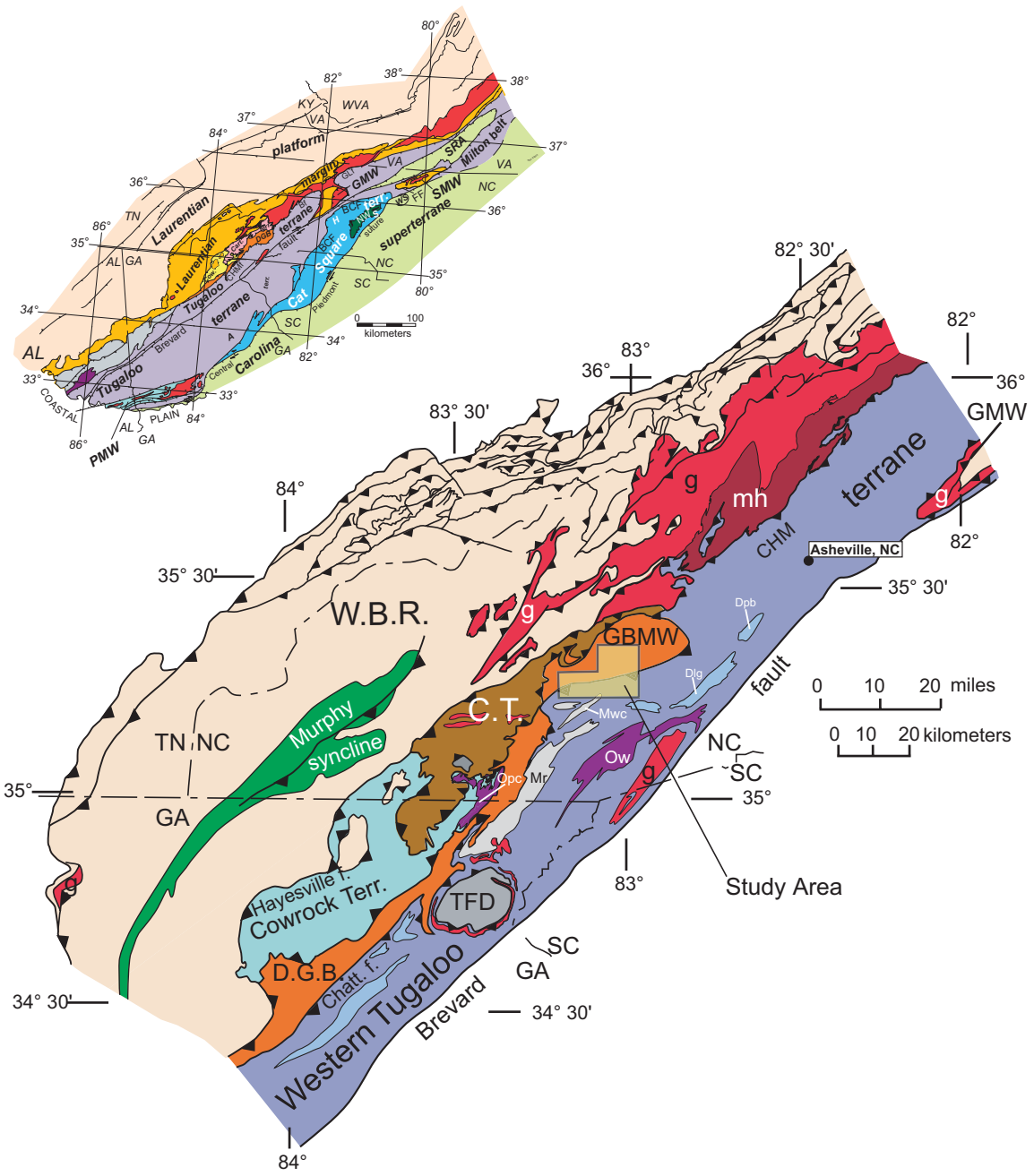


Figure 1–1. Regional map of the western, central and eastern Blue Ridge in Tennessee, Georgia, North Carolina and South Carolina. The study area is shaded yellow. C.T.–Cartoogechaye terrane; D.G.B.–Dahlonega gold belt; CHM–Chattahoochee-Holland Mountain fault; g–1.1 Ga (Grenvillian) mostly orthogneiss; GBMW–Great Balsam Mountains Window; GMW–Grandfather Mountain window; mh–Mars Hill terrane; TFD–Tallulah Falls Dome; W.B.R.–western Blue Ridge. Ordovician plutons (purple): Ow–Whiteside Granite; Opc–Persimmon Creek metatonalite. Devonian plutons (light blue): Dlg–Looking Glass Dpb–Pink beds. Mississippian plutons (light gray): Mr–Rabun Granodiorite; Mwc–Walnut Creek granodiorite. Modified from Hatcher (2005).

basement (Bream et al., 2004). The Hayesville fault (Fig. 1–2) separates the western and central Blue Ridge and was first identified as a major boundary by Hadley and Goldsmith (1963), and was later suggested to be a premetamorphic fault by Hatcher (1978).

The central Blue Ridge is made up of the Cowrock, Cartoogechaye, and Dahlonega gold belt terranes. Like the western Blue Ridge, these terranes contain metasandstone and pelitic schist, but the occurrence of granitic bodies and presence of mafic and ultramafic rocks distinguish these terranes and eastern Blue Ridge from the western Blue Ridge (Hurst, 1955; Hadley and Goldsmith, 1963; Hatcher, 1978).

Rocks of the eastern Blue Ridge belong to the Tugaloo terrane. The Brevard fault zone structurally separates the eastern Blue Ridge and the Inner Piedmont (eastern Tugaloo terrane), and together these belts make up the Neoacadian metamorphic core of the southern Appalachians (Hatcher and Merschat, 2006). The Tugaloo terrane extends from the Chattahoochee-Holland Mountain fault in the west, to the Brindle Creek fault (Inner Piedmont) to the east and is composed predominantly of Tallulah Falls-Ashe Formation metasandstone and pelitic schist, aluminous schist, mafic, and metaultramafic rocks.

Study Area

The study area is located in Jackson county in southwestern North Carolina, about 70 miles southwest of Asheville, N.C. (Figs. 1–1, 1–2). It includes the southern half of the Sylva South and all of the Tuckaseegee 7.5-minute quadrangles (Fig. 1–2).

Three tectonostratigraphic terranes located in the study area are the Cartoogechaye terrane, the Dahlonega gold belt, which lie in the central Blue Ridge and the Tugaloo terrane, which comprises the eastern Blue Ridge (Fig.1–2). The Dahlonega gold belt is situated east of the Cartoogechaye terrane and west of the Tugaloo terrane. The Cartoogechaye and Dahlonega gold belt terranes are separated by the Soque River fault (Fig. 1–2). Farther south, the

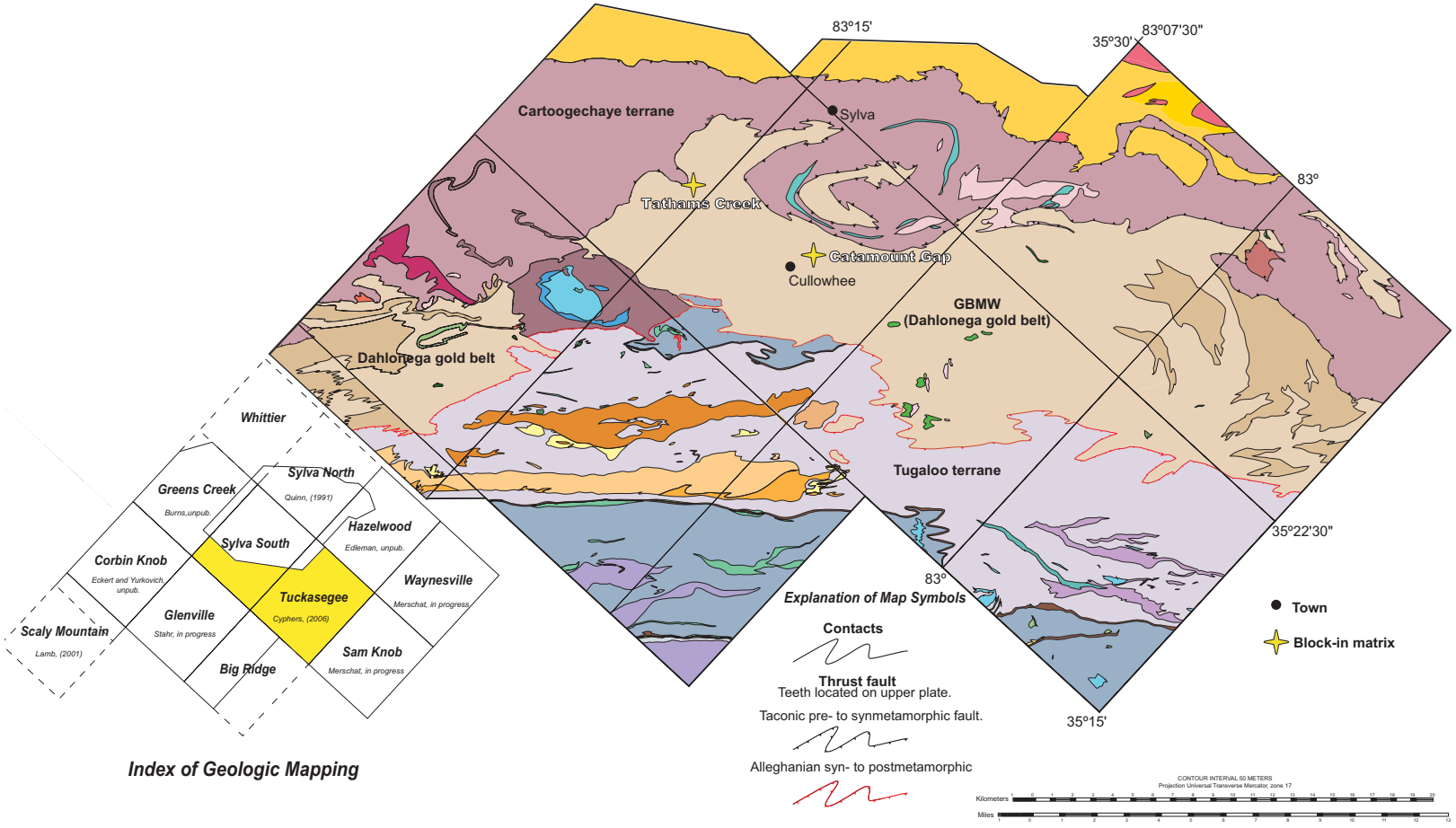


Figure 1–2. Compiled geologic map of a section of the Blue Ridge. Study area for this thesis is outlined in yellow in the index map below. GBMW–Great Balsam Mountains Window. Geology by: Greens Creek, Ann Burns; Sylva South (part), Tuckaseegee, Shawna Cyphers; Corbin Knob, James O. Eckert, Jr., and Steven P. Yurkovich; Hazelwood, Steven H. Edelman and Robert D. Hatcher, Jr.; Scaly Mountain, Dwight D. Lamb; Sam Knob, Waynesville, Arthur J. Merscha; Sylva South and Sylva North (parts), Michael J. Quinn; Glenville and Big Ridge (part), Donald W. Stahr, III. Modified from Merschat et al. (2006).

Rock Units

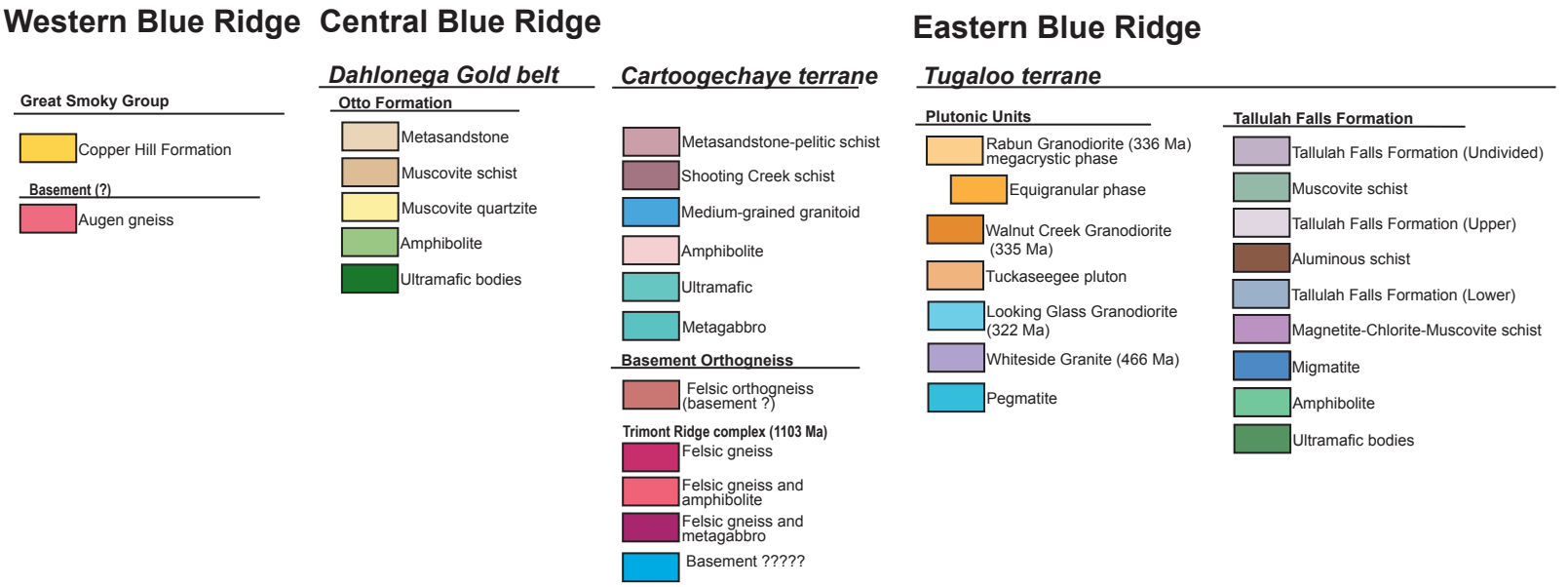


Figure 1–2 continued. Geologic units in and around study area, Blue Ridge geologic province.

pre-to-synmetamorphic Hayesville and Soque River faults join near Dahlonega, Georgia (Settles, 2002).

The earliest mapping in the eastern Blue Ridge of western North Carolina was conducted by Keith (1895, 1904, 1907). Later forerunners whose mapping provided much insight into Blue Ridge geology include King (1952); King et al. (1958); Hadley and Goldsmith (1963); Hamilton (1961); King (1964); Neuman and Nelson (1965) and Hadley and Nelson (1971). More recent detailed mapping in parts of this study area and surrounding areas were carried out by Hatcher, (1980); Eckert, (1983); Eckert et al., (1989); Cronin, (1983); Burns (unpublished); Quinn, (1991). Several projects emphasizing metamorphic petrology have also been completed in and around the study area, including those by Shireman (1985), Davidson (1994), and Cameron (2001) (Fig. 1–3). The projects carried out by Shireman (1985) and Davidson (1994) included some geologic mapping.

The Dahlonega gold belt was originally described by Yeates et al. (1896) in northeastern Georgia and has been traced from NW of Atlanta, Georgia, into western North Carolina (Hadley and Nelson, 1971; Hatcher, 1988; Hopson et al., 1989; Higgins et al, 2003) where it is exposed in the Great Balsam Mountains window (Great Balsam Mountains Window) (Figs. 1–1, 1–2) (Hatcher et al., 2005). Hadley (1970) suggested that the Dahlonega gold belt is a distal facies of the Ocoee Supergroup, as both are composed of two-mica, two-feldspar metasandstones, and almost all samples collected from the Dahlonega gold belt have a strong Laurentian component dominated by 1.1 Ga detrital zircons (Bream, 2003; Bream et al., 2004). One sample from the Dahlonega gold belt contains detrital zircons with ages ranging from 1.8-2.0 Ga, which indicates the detrital zircons originated from the Penokean province of the Canadian Shield (Hatcher et al., 2005, 2007) or is a suspect terrane of Gondwanan affinity (Bream, 2003; Bream et al., 2004).

The Dahlonega gold belt is separated from the Tugaloo terrane by the Chattahoochee-Holland Mountain fault. The Tugaloo terrane is composed of

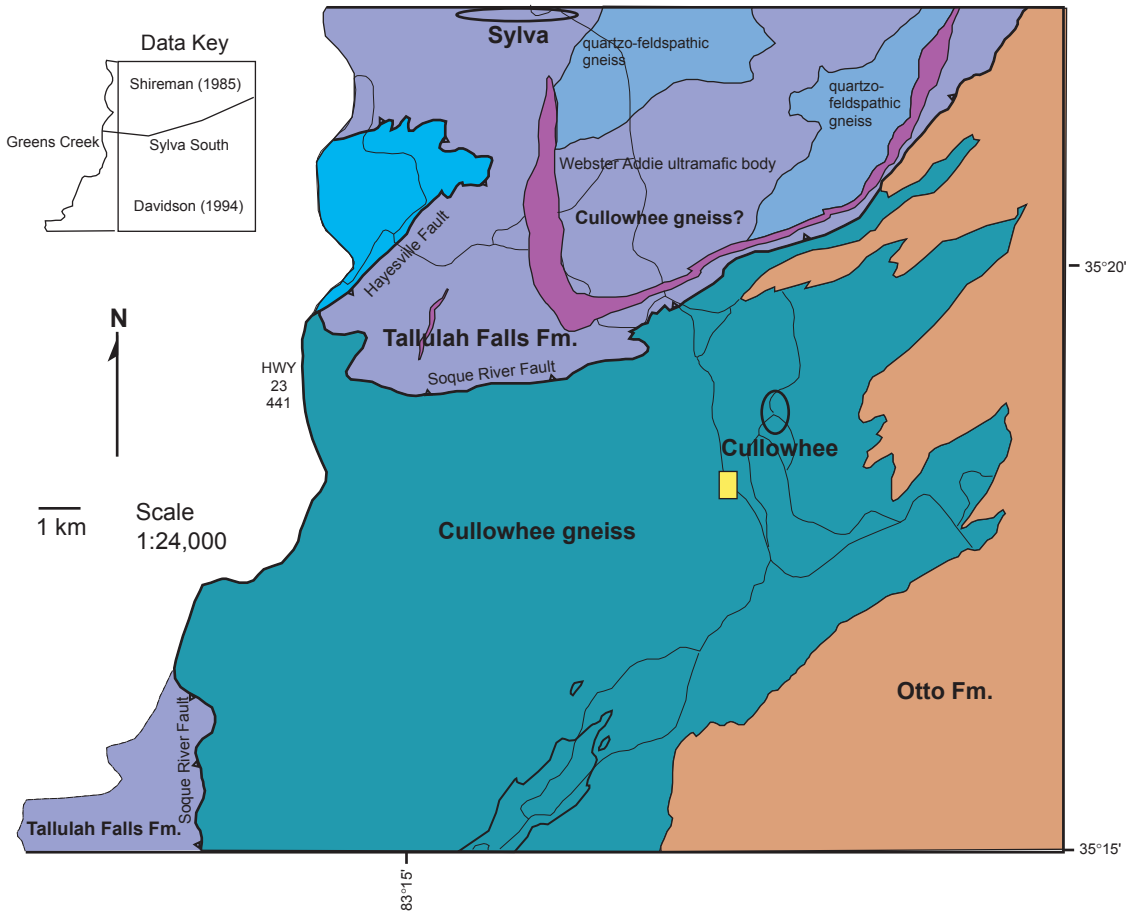


Figure 1–3. Previous metamorphic petrology projects in the study area. Geologic map of the Sylva South and eastern portion of the Greens Creek quadgrangles with geology by Cameron (2001), Davidson (1994), and Shireman (1985). The projects by Davidson (1994) and Shireman (1985) include some mapping. Note that the units labeled Cullowhee gneiss belong to the Otto Formation, most of the rocks labeled Otto Formation belong to the Tallulah Falls Formation, and the rocks labeled Tallulah Falls Formation belong to the Cartoogechaye terrane (see Fig. 1–2). Yellow rectangle indicates location of exposure studied by Cameron (2001). Modified after Cameron (2001).

metagraywacke and schist with interlayered amphibolite of the Tallulah Falls-Ashe Formation, the protolith of which consisted of a slope-and-rise sequence of deep–water sandstone and shale deposited on ocean crust and rifted blocks of Grenville continental basement (Hatcher, 1971, 1974; Hatcher and Goldberg, 1991; Hatcher et al., 2004). The Tallulah Falls Formation is divided into three members: the lower metagraywacke-pelitic schist-amphibolite unit, an aluminous schist member, and an upper metagraywacke-pelitic schist unit (Hatcher, 1971, 2002). Ultramafic bodies are also found throughout this terrane, and are commonly altered to soapstone (Hatcher and Goldberg, 1991).

A suite of Paleozoic plutons intruded parts of the Tugaloo terrane. Of this suite, three granitic bodies are located in the study area; the Rabun Granodiorite, Walnut Creek granodiorite–trondhjemite (WCG), and smaller granitic body identified in this study and herein named the Tuckaseegee granodiorite–trondhjemite (Fig.1–2). Zircon SHRIMP U-Pb ages indicate the Rabun (336 ± 2 Ma) and WCG (333 ± 2 Ma) plutons are Mississippian (Stahr et al., 2005). SW of the study area the Rabun Granodiorite is truncated by the Chattahoochee-Holland Mountain fault near Dillard, Georgia, indicating the fault was active after emplacement of the Rabun pluton.

A classic Barrovian-type metamorphic sequence is recognized in the southern Appalachians, with metamorphic grades increasing southeastward. From the Great Smoky fault metamorphic grade increases eastward, across the western Blue Ridge and into the central and eastern Blue Ridge, which preserve middle to upper amphibolite to granulite facies assemblages (Hatcher et al., 2005). Rb-Sr, K-Ar, $^{40}Ar/^{39}Ar$ dating, U-Pb ages of zircon metamorphic rims, and monazite chemical ages suggest Taconian peak metamorphism and deformation (~460 Ma) occurred throughout the western and central Blue Ridge (Hatcher and Goldberg, 1991; Moecher and Miller, 2000; Moecher et al., 2004).

More recent data, however, indicate a Neoacadian peak metamorphic event in the eastern Blue Ridge and Inner Piedmont (Dennis and Wright, 1997; Carrigan et al., 2001; Bream, 2003). Shireman et al. (1985) recognized three

primary metamorphic events and associated deformational events have affected the rocks in this area: 1) an early progressive metamorphic event that peaked at staurolite-kyanite grade (584° C and 5.6 kbars); 2) a peak metamorphic event that reached 705° C and 7.3 kbars (Labotka and Shireman, 1991); and 3) a later, lower temperature event (590° C and 5.5 kbars) that was interpreted to represent closure temperatures of the garnet-biotite geothermometer (Brumback, 1990). Peak P-T estimates for the Dahlonega gold belt near Cullowhee, North Carolina, are 720° C and 8.0 kbars (Cameron, 2001).

Structure

Structurally, the southern Appalachian Blue Ridge is composed of a series of transpressional, dominantly westward-vergent thrust faults, with deformational styles ranging from brittle to ductile (Hatcher and Goldberg, 1991). Three major deformational events and at least five fold generations are present in the central and eastern Blue Ridge. Early stage folds have tight to isoclinal geometries (F_1 and F_2), intermediate-stage folds have closed to tight geometries, and late-stage folds have open geometries (Quinn, 1991). Multiple transpositional events have obscured many of the earlier fabrics (Hatcher and Goldberg, 1991), with relicts preserved only in amphibolite boudins.

Block-in-Matrix Structures

Enigmatic block-in-matrix structures are found throughout the Blue Ridge province. Exactly how these structures formed is uncertain. Raymond et al. (1989) interpreted the block-in-matrix units as tectonic structures that mark terrane sutures in the central Blue Ridge. Raymond (1984) defined mélange as, “A body of rock mappable at a scale of 1:24,000 or smaller and characterized both by the lack of internal continuity of contacts or strata and by the inclusion of fragments and blocks of all sizes, both exotic and native, embedded in a fragmented matrix of finer grained material.” Possible origins of block-in-matrix structures include sedimentary, igneous, diapiric, and tectonic processes

(Raymond et al., 1989). Hatcher et al. (1984) suggested that these structures are the product of polyphase deformation involving folding, faulting, boudinage, and penetrative ductile shear.

The Tallulah Falls Formation and Dahlonega gold belt (Cullowhee terrane of Raymond et al., 1989) both contain bodies of block-in-matrix structures and two exposures are known in my study area: Catamount Gap and Savannah Church/Tathams Creek (Fig. 2–1). A geochemical, metamorphic, and structural analysis of amphibolite blocks in the block-in-matrix structures will also be included within this study. Geochemical and metamorphic analyses of the different amphibolite samples will be valuable in determining the tectonic origin of the amphibolite blocks, some or all of which may be a part of larger block-in-matrix structures.

Chapter II Rock Units

Introduction

Three tectonostratigraphic units are present in the Sylva South and Tuckaseegee quadrangles, each separated from the other by two major faults: the Soque River fault and the Chattahoochee-Holland Mountain fault (Fig. 2–1). The Dahlonega gold belt is the structurally lowest unit and is exposed in the Great Balsam Mountains Window. To the north and northwest, rocks of the Cartoogechaye terrane make up the intermediate thrust sheet, and, above this, rocks of the Tallulah Falls Formation (Tugaloo terrane) comprise the uppermost thrust sheet, overlying the other terranes. Mineralogical, textural, structural, and lithologic associations and observations were used to identify each of the three terranes.

Rock units

Dahlonega gold belt–Otto Formation

According to Yeates et al. (1896) the Dahlonega gold belt is composed of a “fairly“ clean metasandstone and interlayered schist. Interest in the Dahlonega gold belt originated from the occurrence of gold discovered in 1829 near Dahlonega, Georgia, which was traced from the Alabama–Georgia line to the Georgia–North Carolina line (Yeates et al., 1896; Jones, 1909; German 1985). Since its original description, rocks of this unit have been referred to by many different names: (1) Ashland–Wedowee belt (Hurst, 1973); (2) New Georgia Group (McConnell and Abrams, 1984); (3) Helen Group (Gillon, 1982 and Nelson and Gillon, 1985); and (4) Otto Formation metasandstone and schist (Hatcher, 1980).

The Dahlonega gold belt is made up of aluminous metasedimentary rocks and is lithologically similar to the Ocoee Super Group, leading Hadley (1970) and Hadley and Nelson (1971) to correlate the Dahlonega gold belt with the Great

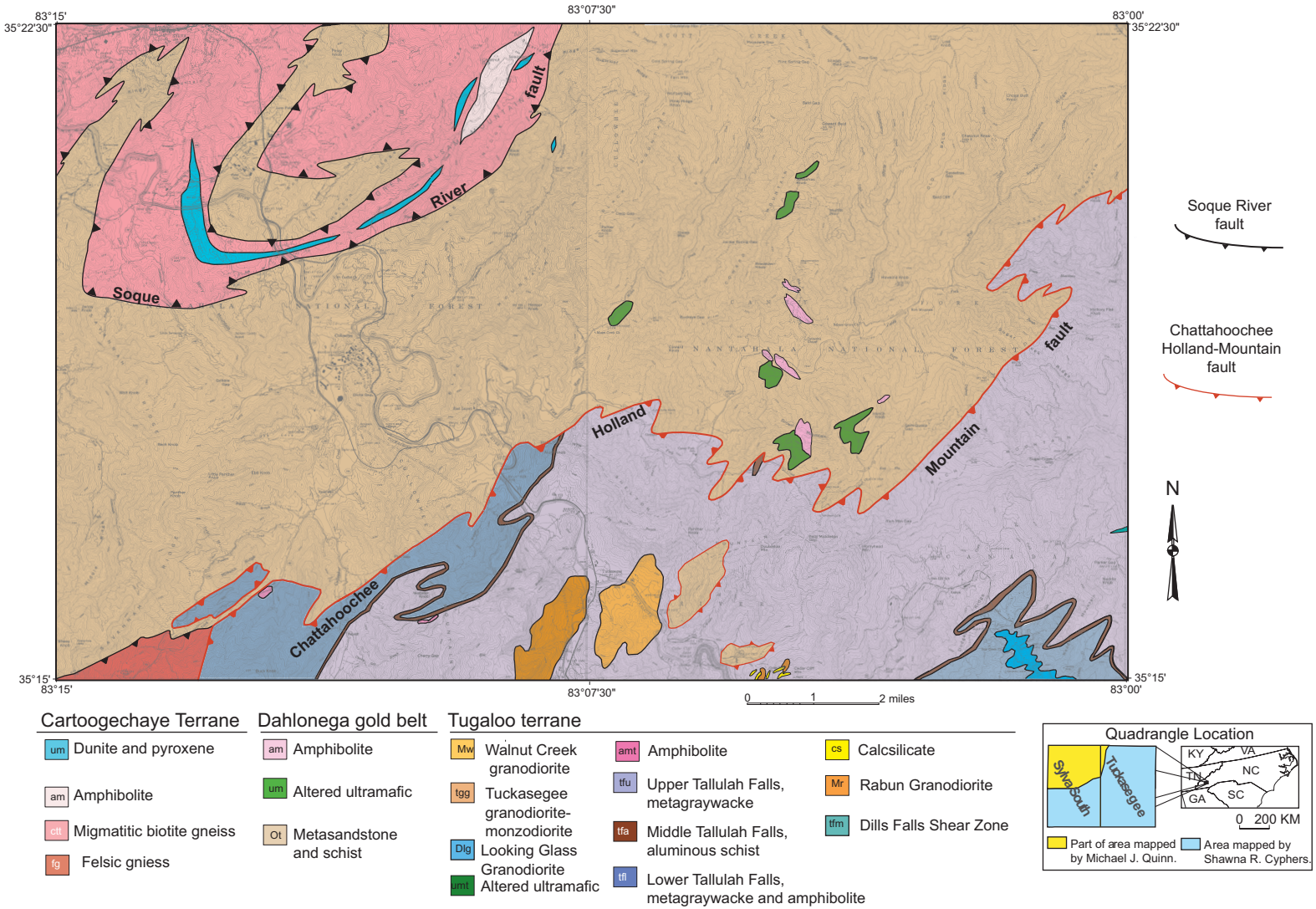


Figure 2–1. Simplified bedrock geologic map of Sylva South and Tuckaseegee quadrangles illustrating major rock units, faults, and topography. Mapping by Quinn (1989-1990) and Cyphers (2005-2006).

Smoky Group. Despite the lithologic similarities between the two units, the abundance of calc–silicate, and apparent lack of mafic rocks in the Great Smoky Group versus the lack of calc-silicate and abundance of mafic rocks in the gold belt make this correlation unlikely (Settles, 2002).

The Dahlonega gold belt is complex, and distinctive lithologic variations occur along its length. Felsic gneiss, such as the Cane Creek gneiss (482.1 ± 1.6 Ma, Bream, 2003), is present in the southwestern portion (central and northeast Georgia), but is uncommon to absent to the northeast. Similarly, mafic rocks are, in general, more abundant to the southwest than to the northeast (Hopson et al., 1989). Rocks of the Dahlonega gold belt are more aluminous than rocks of the Tallulah Falls Formation; however, the bulk composition of both terranes is made up of metagraywacke/biotite gneiss with interlayered two-mica schist and amphibolite.

Field Occurrence and Description

Metasandstone

Metasandstone of the Otto Formation is quartz-rich and feldspathic and can contain moderate amounts of garnet (Fig. 2–2a); muscovite is the dominant mica, but biotite is commonly present. Interlayers of two-mica schist are common; amphibolite and calc-silicate interlayers and boudins are also present, but less abundant. Sulfides are widespread and sulfide staining is present at many exposures. Texturally the metasandstone ranges from massive to well foliated, depending on the amount of mica present. Grain size ranges from fine- to medium-coarse, and is generally equigranular. Quartz, plagioclase, muscovite, garnet, biotite, opaque oxides, and ± sulfides are readily identified in hand sample.

In thin section the metasandstone is moderately foliated with compositional layers defined by biotite and lesser muscovite (Fig. 2–2b). The dominant mineral assemblage is quartz, plagioclase (An_{13-26}), and biotite with minor microcline. Grain size is generally homogenous, although some samples

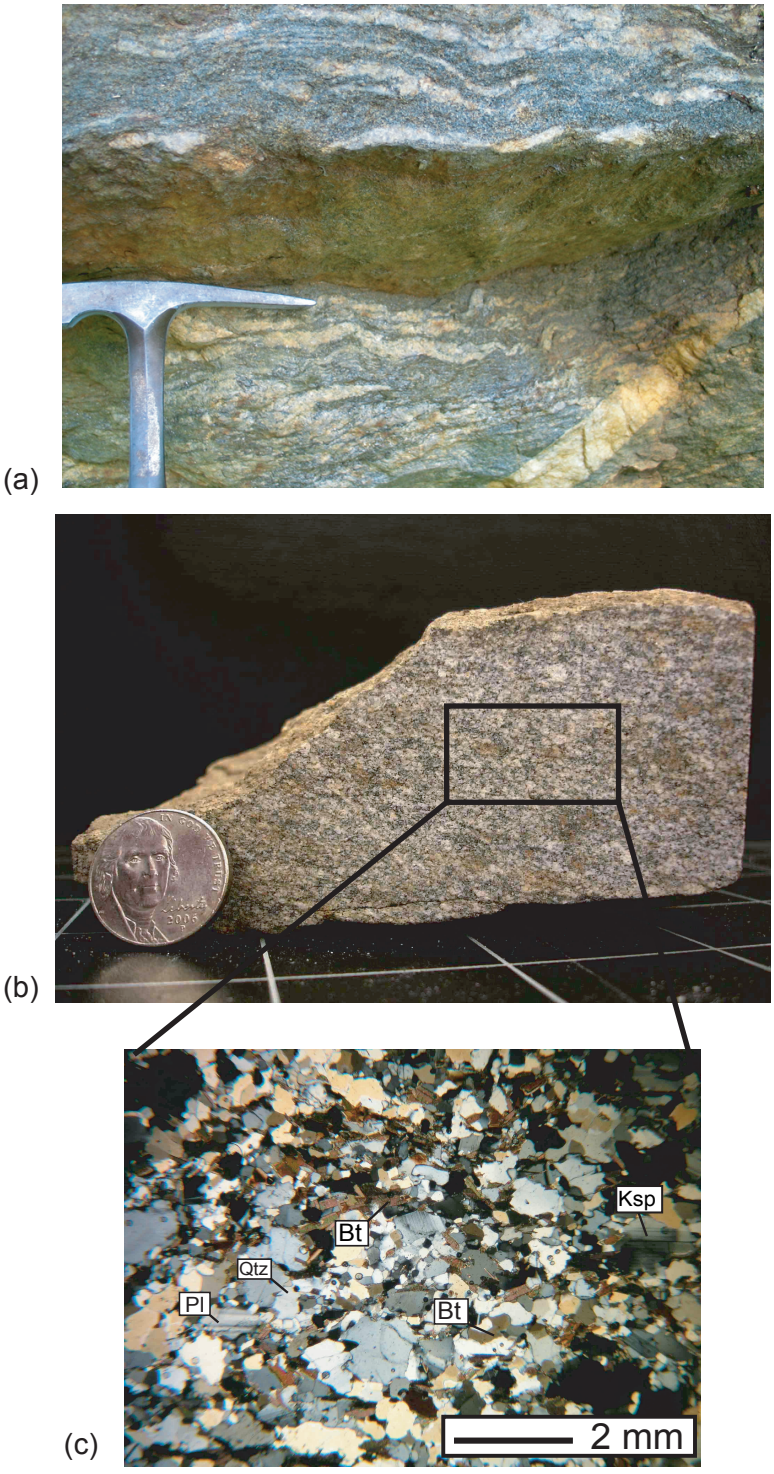


Figure 2–2. (a) Exposure of Dahlonega gold belt metasandstone, located in the western part of the Tuckaseegee quadrangle near Johns Creek Road. (b) Hand sample of Dahlonega gold belt metasand-stone, and (c) photomicrograph of Dahlonega gold belt metasandstone. Abbreviations: Bt–biotite; Ksp–potassium feldspar; Pl–plagioclase; Qtz–quartz.

contain larger plagioclase porphyroclasts and rare garnet porphyroblasts. Modal abundances of 2 metasandstone samples from the Dahlonega gold belt indicate that the protolith was likely metagraywacke (Pettijohn, 1954; Hadley and Goldsmith, 1963) (Table 2–1 and Fig. 2–3).

Plagioclase composition ranges from An_{13} to An_{26}, and albite and pericline twins are common throughout the samples; seritization of plagioclase occurs but is not pervasive. Round quartz inclusions are present in plagioclase grains. In plane light biotite laths are pleochroic green/brown to brown/yellow, and define compositional layering. Quartz has sutured grain boundaries, and subgrains of quartz are also present. Accessory minerals include zircon and chlorite. Garnets in the metasandstone are anhedral to subhedral and display a poikioblastic texture with inclusions of quartz, plagioclase, sillimanite (fibrolite), and biotite.

Schist

Schist in the Otto Formation is aluminous two–mica, garnet schist; layers range from 1 cm to 1 m, and are interlayered in the metasandstone. Schist is medium-grained, well-foliated, and often crenulated. Exposures consist of medium-grained muscovite-biotite-garnet schist. Some exposures are composed of granular schist with fine- to -medium grained quartz and plagioclase. Muscovite, biotite, and garnet are the most commonly observed minerals (Fig. 2–4a); kyanite, staurolite, chlorite, and sillimanite were also observed. Some exposures of schist were less aluminous and composed dominantly of biotite and garnet. Weathered exposures can occur with a reddish-brown or yellow-orange color, which is likely the result of weathering of sulfide minerals.

In thin section, Otto Formation schist is moderately to well foliated, and grain size ranges from medium to coarse (Fig. 2–4b). Biotite and muscovite are well–aligned, defining the dominant S_2 foliation. Biotite is found as pleochroic brown to light brown and pleochroic reddish brown. Garnet porphyroblasts are anhedral to subhedral and range from 0.5 mm to 1 mm. Some porphyroblasts of garnet contain inclusions of fibrolite, but biotite, muscovite, and quartz inclusions are more common. Kyanite and chlorite are abundant, and porphyroblasts are

Table 2–1. Modal analyses of metasandstone samples from the Sylva South and Tuckasegee quadrangles. DGB is Dahlonega gold belt and TFF is Tallulah Falls Formation.

Sample ID Unit	937 DGB	892 DGB	853 TFF	265 TFF
Description	Metagraywacke	Metagraywacke	Metagraywacke	Metagraywacke
points counted	612	521	504	503
Quartz	41.2	40.9	19.3	36.8
Plagioclase	32.7	36.3	40.1	31.2
K-feldspar	3.92	2.30	7.94	2.78
Biotite	21.9	16.5	31.2	26.8
Muscovite	0.00	2.30	0.00	0.60
Epidote	0.33	1.54	0.60	1.39
Sericite	0.00	0.00	0.20	0.00
Ilmenite	0.00	0.19	0.40	0.40
Zircon	0.00	0.00	0.20	0.00
Apatite	0.00	0.00	0.20	0.00
Total	100	100	100	100

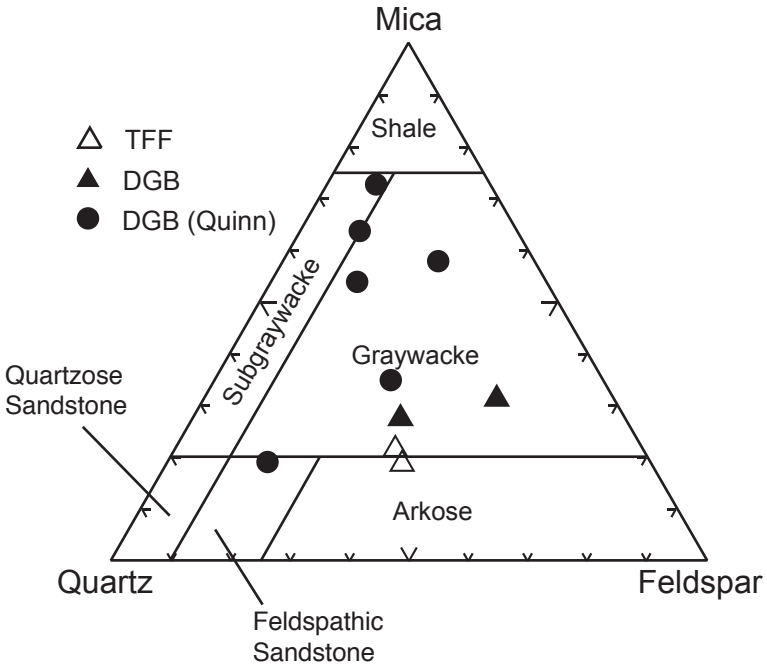


Figure 2–3. QFM diagram (Pettijohn, 1949) comparing the composition of metasedimentary rocks from the the Dahlonega gold belt (DGB) and the Tallulah Falls Formation (TFF). This diagram is used with the following assumptions (originally outlined by McClellan, 1988): mica represents metamorphosed clay (Hadley and Goldsmith, 1963); quartz and feldspar reactions are minimal; quartz and feldspar are present in their original abundances; and volume change is negligible.

(a)



(b)

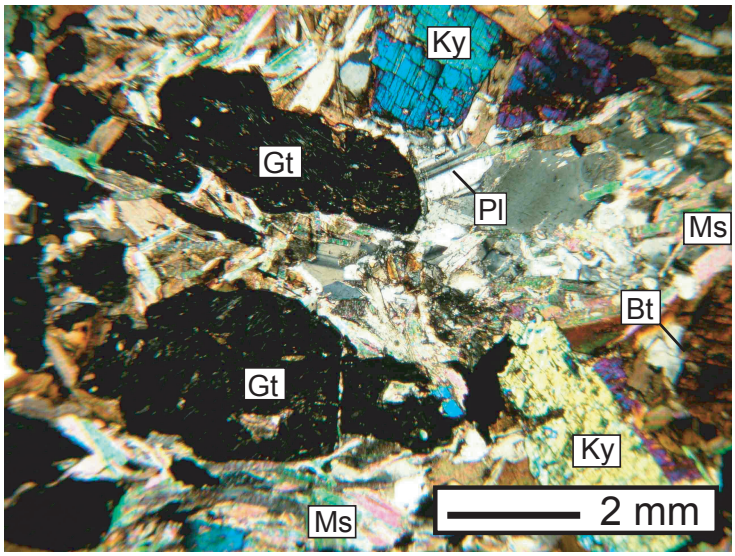


Figure 2–4. (a) Representative exposure of Dahlonega gold belt schist located off Johns Creek road in the Tuckaseegee quadrangle. At this location the schist is tightly crenulated. (b) Photomicrograph of representative Dahlonega gold belt schist. Abbreviations: Bt–biotite; Gt–garnet; Ky–kyanite; Ms–muscovite; Pl–plagioclase.

generally aligned in the dominant S_2 foliation. Kyanite porphyroblasts are likely a prograde phase, but chlorite is interpreted as a product of retrograde metamorphism, because it is commonly found in the embayments and cracks of garnet porphyroblasts, and is interpreted to be in disequlibrium with surrounding phases. Staurolite is present, but in lesser amounts (≤2%). Finer–grained quartz and feldspar are in the matrix; plagioclase has albite and pericline twins An_{12}–An_{26}, and seritization of feldspar is common. Accessory minerals include apatite and opaques.

Amphibolite

Amphibolite occurs as boudins and thin layers in metasandstone and is associated with ultramafic–mafic bodies. Amphibolite samples were collected from two block–in–matrix exposures, at Catamount Gap (CG) and Savannah Church (SC). Modal abundances of 2 CG samples and 2 SC samples are listed in Table 2–2.

Catamount Gap

The CG exposure consists of muscovite–rich schist and quartz–feldspar gneiss enclosing blocks and layers of amphibolite and calcsilicate (Fig. 2–5a). Block morphologies range from sub–rounded to angular. In thin section, the CG amphibolite samples are weakly foliated, and the foliation is defined by biotite and hornblende (Fig. 2–5b). Samples range from fine– to medium–grained garnet amphibolites; garnet porphyroblasts generally make up 5–20 percent of the sample. The general mineral assemblage of CG amphibolite is biotite, hornblende, and zoisite, along with quartz and plagioclase (An_{29}– An_{33}). Undulatory extinction was observed in quartz grains and some plagioclase grains display a myrmekitic texture. Garnet porphyroblasts are skeletal with inclusions of hornblende and quartz. Hornblende is pleochroic green to light green and brown to light brown. Biotite has reddish–brown pleochroism. CG samples are compositionally more variable than the SC amphibolites. Some are rich in biotite

Table 2–2. Modal analyses of amphibolite samples from block–in–matrix structures. Geochemical analyses of granitoid and amphibolite samples are discussed in Chapter 3. DGB is Dahlonega gold belt.

Sample ID Un it Description	SC2 DGB amphibolite	SC4 DGB amphibolite	CG2 DGB amphibolite	CG3 DGB amphibolite
points counted	863	869	843	868
Quartz	6.84	5.18	11.2	5.88
Plagioclase	23.4	25.0	20.3	12.2
K-feldspar	0.35	0.12	0.00	0.00
Biotite	4.52	0.00	15.9	2.30
Hornblende	60.4	60.9	28.1	48.9
Garnet	0.93	2.30	14.5	11.9
Epidote	2.09	1.27	2.25	2.76
Myrmekite	0.00	0.00	6.17	13.4
Opaques	1.16	0.58	0.59	0.92
Zoisite	0.00	4.26	0.00	1.38
Apatite	0.00	0.23	0.00	0.00
Rutile	0.35	0.23	0.59	0.35
Calcite	0.00	0.00	0.59	0.00
Total	100	100	100	100

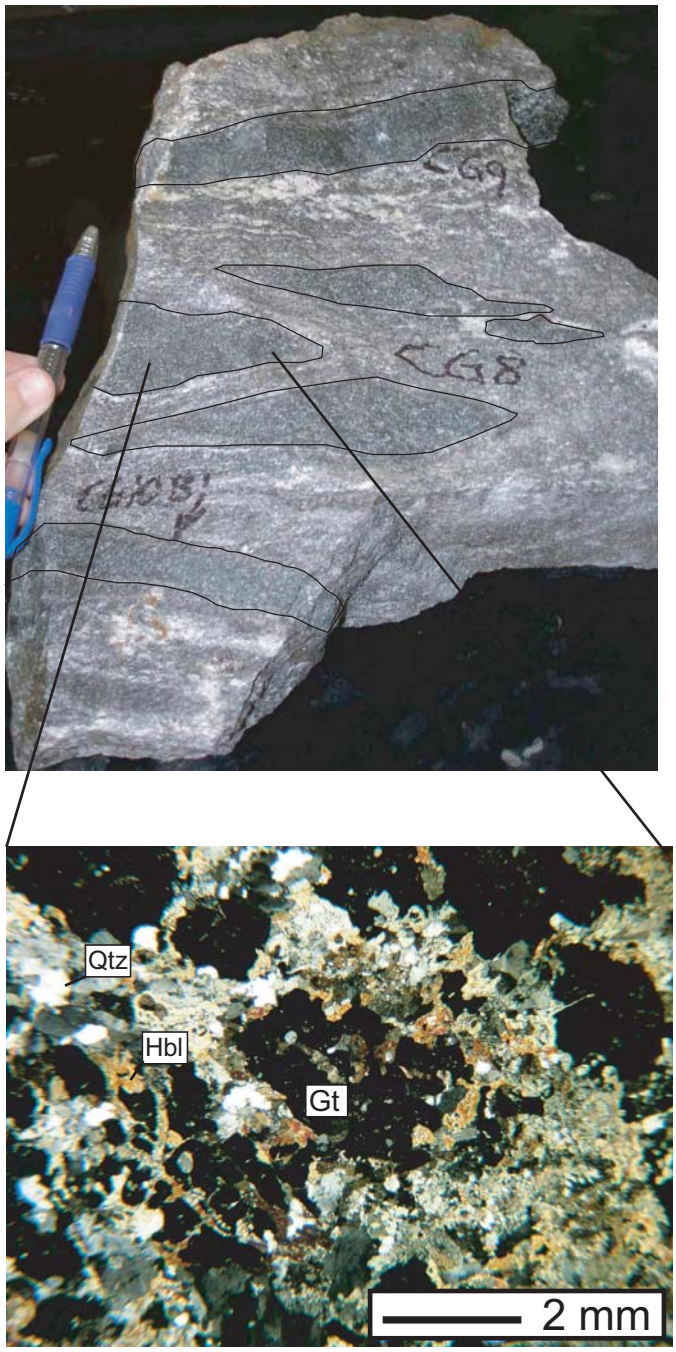


Figure 2–5. (a) Hand specimen of amphibolite blocks from Catamount Gap block–in –matrix exposure. (b) Photomicrograph of thin section of amphibolite block (CG–8). Abbreviations: Gt–garnet; Hbl–hornblende; Qtz–quartz.

and hornblende, while others are more felsic, with an abundance of myrmekite and sphene. Accessory minerals include calcite, rutile, and opaques. One highly altered calcsilicate block was collected from the Catamount Gap block-in-matrix exposure. Mineralogically it is composed of clinozoisite, zoisite, biotite, diopside, plagioclase (An_{34}), garnets, and cummingtonite. Garnets are skeletal and contain inclusions of diopside, epidote, plagioclase, and quartz.

Savannah Church

The SC exposure is composed of a migmatitic matrix of mostly biotite quartz–plagioclase–garnet semi-schist and biotite–quartz–feldspar migmatitic metasandstone; lesser leucosomes, amphibolite layers, and boudins, and calcsilicate schist are also present in the matrix. Blocks consist of amphibolite (Fig. 2–6a), with or without garnet, and commonly with a leucosome layer along the margin. Amphibolite blocks occur as rounded, tapered, and angular morphologies.

Petrographic analysis of SC amphibolites indicate samples are hornblende and plagioclase rich (An_{33}–An_{37}) (Fig. 2–6b). Hornblende can occur with or without quartz inclusions. Skeletal garnets are common and constitute 5–12 percent of the samples. Biotite is pleochroic tan to reddish-brown**.** Sutured grain boundaries occur in quartz grains. Accessory minerals include epidote, ilmenite, and opaques.

Ultramafic Rocks

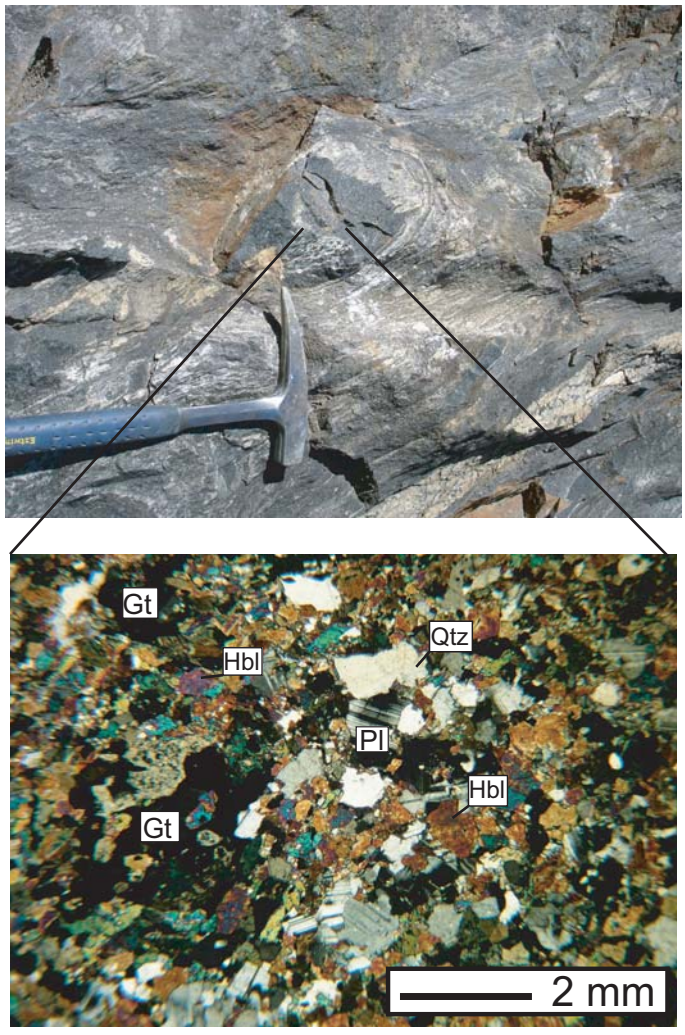
Highly altered ultramafic rocks (soapstone) are present in the Dahlonega gold belt and occur as map–scale bodies. The majority of ultramafic bodies are in the Tuckaseegee quadrangle. Ultramafic rocks are talc-chlorite schist with minor Fe-oxides (Fig. 2–7). No thin sections of the metaultramafic rocks were made for this study.

Cartoogechaye Terrane

The Cartoogechaye terrane (Hatcher et al., 2005) is exposed north and west of the Great Balsam Mountains Window and is made up of metasandstone,

(a)

(b)



(c)

Figure 2–6. (a) Amphibolite blocks from Savannah Church block–in–matrix exposure. (b) Amphibolite block, SC–4, (c) Photomicrograph of amphibolite block (SC–4). Abbreviations: Gt–garnet; Hbl–hornblende; Pl–plagioclase; Qtz–quartz.



(a)



(b)

Figure 2–7. (a) Hand sample of Dahlonega gold belt soapstone from Brown Mountain, Tuckaseegee quadrangle. (b) Hand sample of mafic lithology collected near Caney Fork Road, south of Brass Town Bald, Tuckaseegee quadrangle.

pelitic schist, and granulite facies ultramafic and mafic complexes (Hatcher et al., 2007). Amphibolite occurs in metasandstone as layers and boudins.

Exposures in the study area are composed of medium- to coarse-grained quartz and plagioclase-rich felsic orthogneiss with moderate amounts of muscovite, biotite, garnet, amphibole, and lesser calcsilicate. Felsic gneiss may be related to the Trimont Ridge basement complex (1103 Ma) (Bream, 2003; Hatcher et al., 2004). Muscovite–rich schist is also exposed in the study area and is composed of medium–grained muscovite–rich garnet schist with lesser biotite and sillimanite.

Tugaloo Terrane

The Tugaloo terrane consists of Ashe-Tallulah Falls Formation rocks, small amounts of Grenville basement, as well as middle and late Paleozoic plutons (Hatcher et al., 2005). The Tallulah Falls Formation and four plutonic bodies are exposed in the southern part of the study area. The Tallulah Falls Formation is one of the most extensive lithotectonoic units in the southern Appalachians, occurring in the Tugaloo terrane (eastern Blue Ridge and Inner Piedmont). This unit has been identified by Rankin (1970) as the Ashe Formation in the western Blue Ridge in NW North Carolina, and the Ashe Formation was subsequently correlated with the Tallulah Falls Formation by Hatcher (1971, 1978); Higgins and McConnell (1978) elevated this formation to Sandy Springs Group in NE Georgia and eastern Alabama. Rocks of the Tallulah Falls Formation have also been correlated with sequences in the Alto allochthon and Six Mile nappe in the western Inner Piedmont (Hopson and Hatcher, 1988). The Chattahoochee–Holland Mountain thrust sheet contains a predominantly deep-ocean assemblage of sedimentary and volcanic rocks, with fragments of ocean crust and mantle (Hatcher et al., 2004)

The Tallulah Falls Formation contains three units consisting of a lower graywacke– schist–amphibolite member (lower Tallulah Falls Formation) (Fig. 2–8a), a middle garnet–aluminous schist member, and an upper graywacke–schist

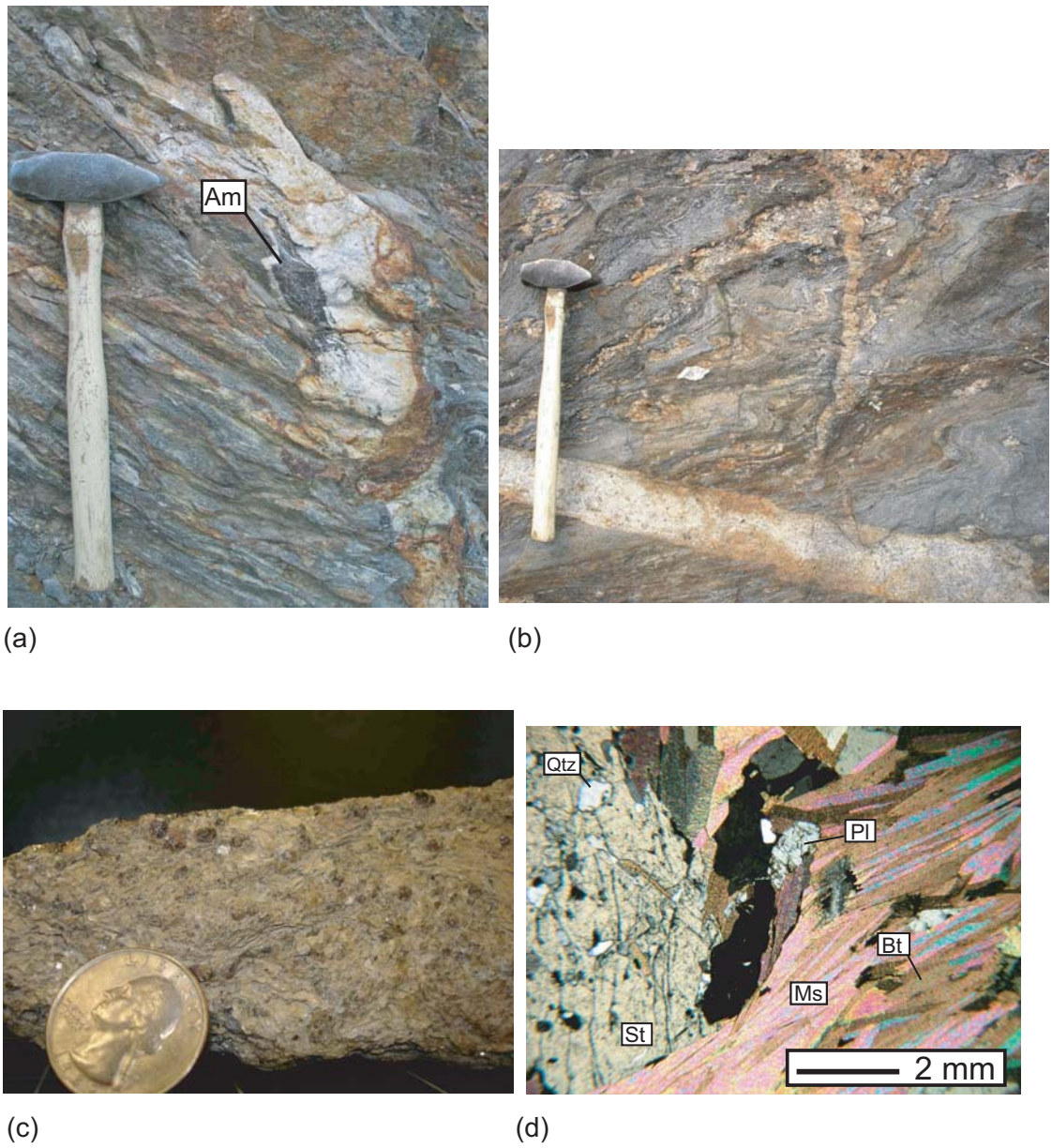


Figure 2–8. Representative photographs of lithologies of the TFF: (a) migmatitic LTFF with interlayered amphibolite. Exposure is located south of Milksick Ridge in the southern part of the Sylva South quadrangle; (b) exposure of UTFF on Woods Branch road in the southwest part of the Tuckaseegee quadrangle; (c) Sample of the aluminous schist, and (d) representative photomicrograph of the aluminous schist unit from the NE part of the Big Ridge quadrangle. Abbreviations: Am–amphibolite;Bt–biotite; Ms–muscovite; Pl–plagioclase; Qtz–quartz; St–staurolite.

member (upper Tallulah Falls Formation) (Fig. 2–8b). The lower, middle, and upper members were mapped in the study area.

Several plutonic suites have intruded the eastern Blue Ridge: a Middle Ordovician (Taconic) metaplutonic episode (Miller et al., 2000; McDowell et al., 2002; Bream, 2003), a Devonian (Acadian) episode of less–deformed plutons; and a late Mississippian (early Alleghanian) plutonic pulse (Miller et al., 2000; Stahr et al., 2005). Four plutons are exposed in the study area: the Walnut Creek granodiorite-trondhjemite; the Tuckaseegee granodiorite-trondhjemite; the Rabun granodiorite; and the Looking Glass granodiorite.

Field Occurrence and Description

Lower Tallulah Falls Formation

Medium–grained migmatitic, biotite-rich metagraywacke is the dominant lithology in the lower Tallulah Falls Formation with moderate amounts of interlayered amphibolite, and lesser calcsilicate, biotite–muscovite–garnet schist, and biotite–rich schist. Comparatively, the lower Tallulah Falls Formation contains less quartz and more biotite than the upper Tallulah Falls Formation. Exposures of lower Tallulah Falls Formation in the study area are composed of medium–grained biotite–rich paragneiss. Amphibolite is common and occurs as interlayers in the lower Tallulah Falls Formation, and likely originated as dikes and flows emplaced into the sequence during rifting and sedimentation (Hatcher and Goldberg, 1991). Hornblende gneiss consists of medium– to coarse–grained moderately to well–foliated hornblende+plagioclase+biotite +quartz±opaques.

Aluminous Schist

The middle schist of the Tallulah Falls Formation is a muscovite-rich aluminous schist, which separates the upper Tallulah Falls Formation from the lower Tallulah Falls Formation, and is composed of muscovite, feldspar, quartz,

biotite, garnet, aluminum silicate (kyanite and/or sillimanite), and staurolite (Fig. 2–8c, 2–8d). Garnets are ubiquitous in the aluminous schist member; porphyroblasts range in size from 0.5–2 mm and make up 10–20 percent of the lithology. Garnet-rich soil is indicative of weathered aluminous schist and is used to trace this member of the Tallulah Falls Formation where exposures are sparse. Sillimanite was the observed aluminum silicate in the aluminous schist in the study area. Some exposures are more quartz–rich, resulting in granular schist; however, a lepidoblastic texture is more common. Grain size ranges from medium to coarse, and coarse grains of muscovite were observed at several exposures. Crenulations were also observed at several exposures of aluminous schist. Amphibolite is commonly associated with the aluminous schist unit and is interlayered with the schist and metasandstone.

Upper Tallulah Falls Formation

The upper unit of the Tallulah Falls Formation is a biotite–rich metagraywacke, more quartz–rich than the lower Tallulah Falls Formation unit with layers enriched in garnet (Fig. 2–9a). Textures range from well-foliated metasandstone to migmatite. Hornblende gneiss occurs in the upper Tallulah Falls Formation, but is not common. The amphibolite gneiss is medium grained, with biotite and coarser–grained quartz and feldspar.

Petrographic analysis of upper Tallulah Falls Formation indicates a foliated medium– to fine–grained inequigranular quartz–plagioclase–biotite–muscovite metasandstone (Fig. 2–9b). The matrix is composed of quartz, plagioclase, biotite, and minor muscovite (< 1%), with porphyroclasts of plagioclase (An_{10}–An_{24}) composing ~ 15 percent of the sample. Albite and pericline twins occur in many plagioclase grains, and seritization is also present. The foliation is defined by aligned biotite crystals that are interlayered with quartz and feldspar grains. Quartz commonly displays sutured grain boundaries and subgrains. Accessory minerals include zircon, sphene, sericite, muscovite, chlorite, and sillimanite. Modal abundances of 2 metasandstone samples collected from the Tallulah Falls Formation indicate the protolith was

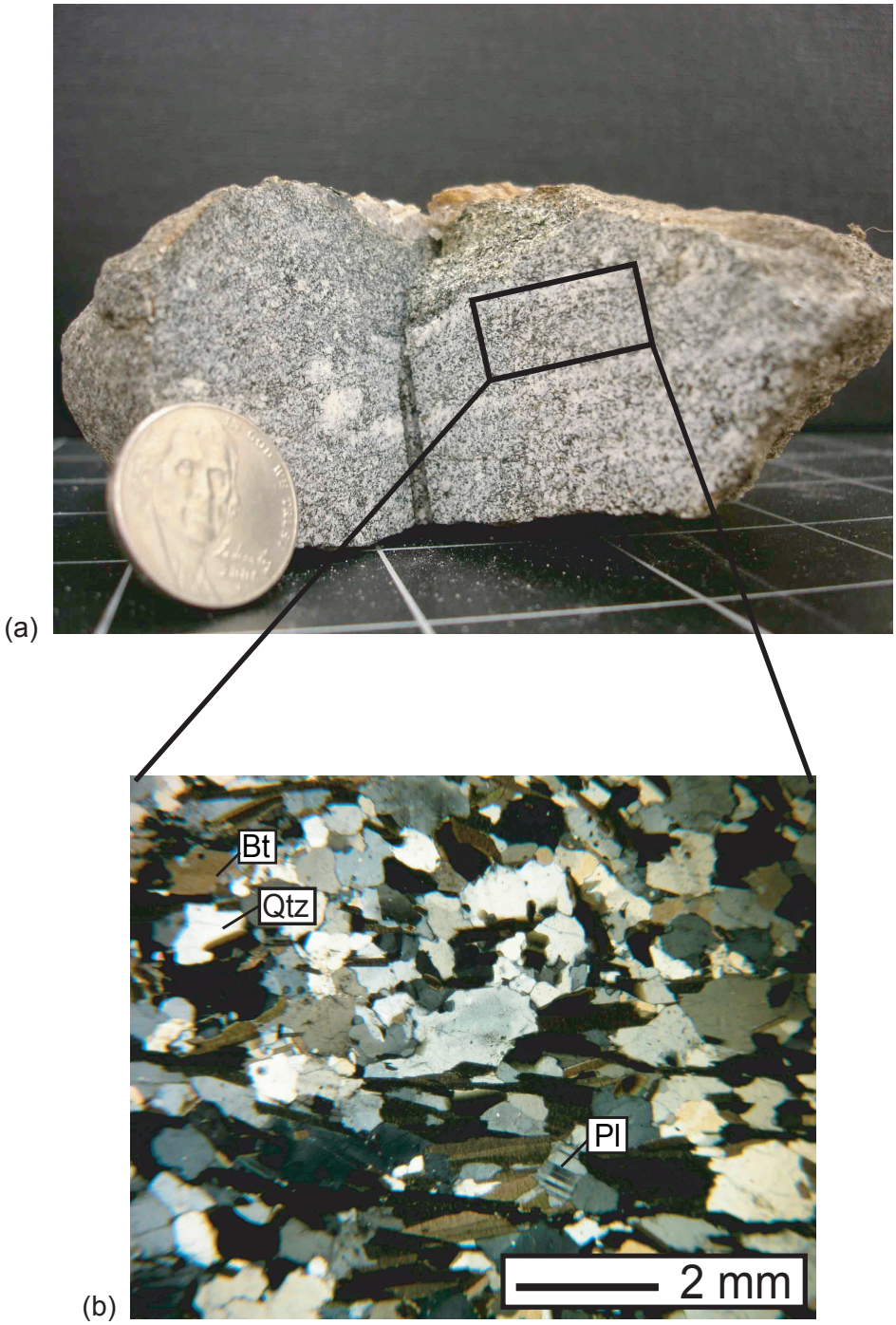


Figure 2–9. (a) Hand sample of upper Tallulah Falls metasandstone on Caney Fork Road in the Tuckaseegee quadrangle and , (b) photomicrograph of upper Tallulah Falls metasandstone. Abbreviations: Bt–biotite; Pl–plagioclase; Qtz–quartz.

metagraywacke, similar to the Otto Formation sandstones (Pettijohn, 1954; Hadley and Goldsmith, 1963; McClellan, 1988) (Table 2–1 and Fig. 2–3).

Schist can also be found as interlayers in the Tallulah Falls Formation and occurs as biotite, muscovite, garnet, kyanite, sillimanite schist. Grain size ranges from medium–fine with some samples containing granular layers of plagioclase and quartz. Petrographically the interlayered schist is a biotite+garnet+ muscovite± kyanite±staurolite±sillimanite. Garnets are 0.2–0.7 cm and occur as subhedral or anhedral porphyroblasts; they commonly contain inclusions of quartz, biotite, and opaques. Retrograde textures around garnets are composed of chlorite and biotite. Many garnets are fractured and are being replaced by biotite and chlorite. Euhedral, medium-grained muscovite is present throughout the matrix and possibly indicates later muscovite growth. Some later muscovite contains inclusions of biotite, plagioclase, fibrous sillimanite, and staurolite.

Plagioclase (An_{14}) is either untwinned or occurs as albite, pericline, and Carlsbad twins. Kyanite grains occur as subhedral to anhedral porphyroblasts, and some grains are twinned. Sillimanite commonly occurs as fibrolite; and occurs in the matrix and as inclusions in garnets, quartz, and muscovite. Where present, staurolite occurs as large porhpyroblasts and contains inclusions of feldspar, biotite, quartz, and muscovite.

Amphibolite

Amphibolite is medium– to coarse–grained, moderately to well–foliated, and is composed of hornblende+biotite+plagioclase±garnet±opaques. It occurs as layers and boudins commonly associated with the aluminous schist.

Dills Falls Shear Zone

The Dills Falls shear zone is a mylonitic metagraywacke schist described by Merschat (in progress); only a short segment of the shear zone is exposed in the study area and it terminates near the east side of the Tuckaseegee quadrangle (Fig. 2–1). It is composed of light– to medium–gray, medium–grained, migmatitic, porphyroclastic, muscovite, garnet, biotite, plagioclase,

quartz paragneiss with interlayers of porphyroclastic garnet–biotite–muscovite–schist, and muscovite– biotite granitoid gneiss (Merschat, pers comm.). Where it is exposed in the study area it is gray and white in color and composed of biotite-rich quartz-plagioclase- muscovite mylonite.

Walnut Creek Granodiorite–Tonalite

The Walnut Creek Granodiorite (WGC) is located ~7 km south of Cullowhee, NC (Fig. 2–1). It is an equigranular, medium–grained two–mica granodiorite–tonalite originally described by Stahr et al. (2005) in the Glenville quadrangle. U-Pb dating of zircons collected from the WCG yielded an age of 333 ± 2 Ma (Stahr et al., 2005; Stahr, 2007). Exposures of WCG are white to light gray, poorly foliated, medium–grained equigranular quartz, plagioclase, biotite, muscovite granodiorite–tonalite, with moderate amounts of muscovite and biotite (Fig. 2–10a). Modal abundances of granitiod are listed in Table 2–3.

Petrographic modal analysis shows that the WCG is a coarse–grained hypidiomorphic granular–granodiorite–trondhjemite (Fig. 2–10b) composed of quartz and plagioclase (An_{10}–An_{25}), with lesser biotite and muscovite accessory minerals (including clinozoisite and opaques). Modal abundances of the WCG sample indicate that it is compositionally a tonalite according to Streckeisen's (1976) IUGS classification scheme based on modal percent quartz, alkali feldspar, and plagioclase (Fig. 2–11).

Tuckaseegee Granodiorite–Monzodiorite

The Tuckaseegee granitic body is located just east of the WCG (Fig. 2–1). Exposed area of the Tuckaseegee granodiorite–monzodiorite (TG) is roughly 3.1 km^2. Lithologically it is an equigranular and poorly foliated medium–grained quartz, plagioclase, biotite, and primary muscovite granitoid (Fig. 2–10c).

In thin section, the Tuckaseegee granitoid is very similar to the WCG. It is medium– to coarse–grained with a hypidiomorphic granular texture and is composed of quartz, plagioclase (An_{13}–An_{22}), microcline, lesser biotite and

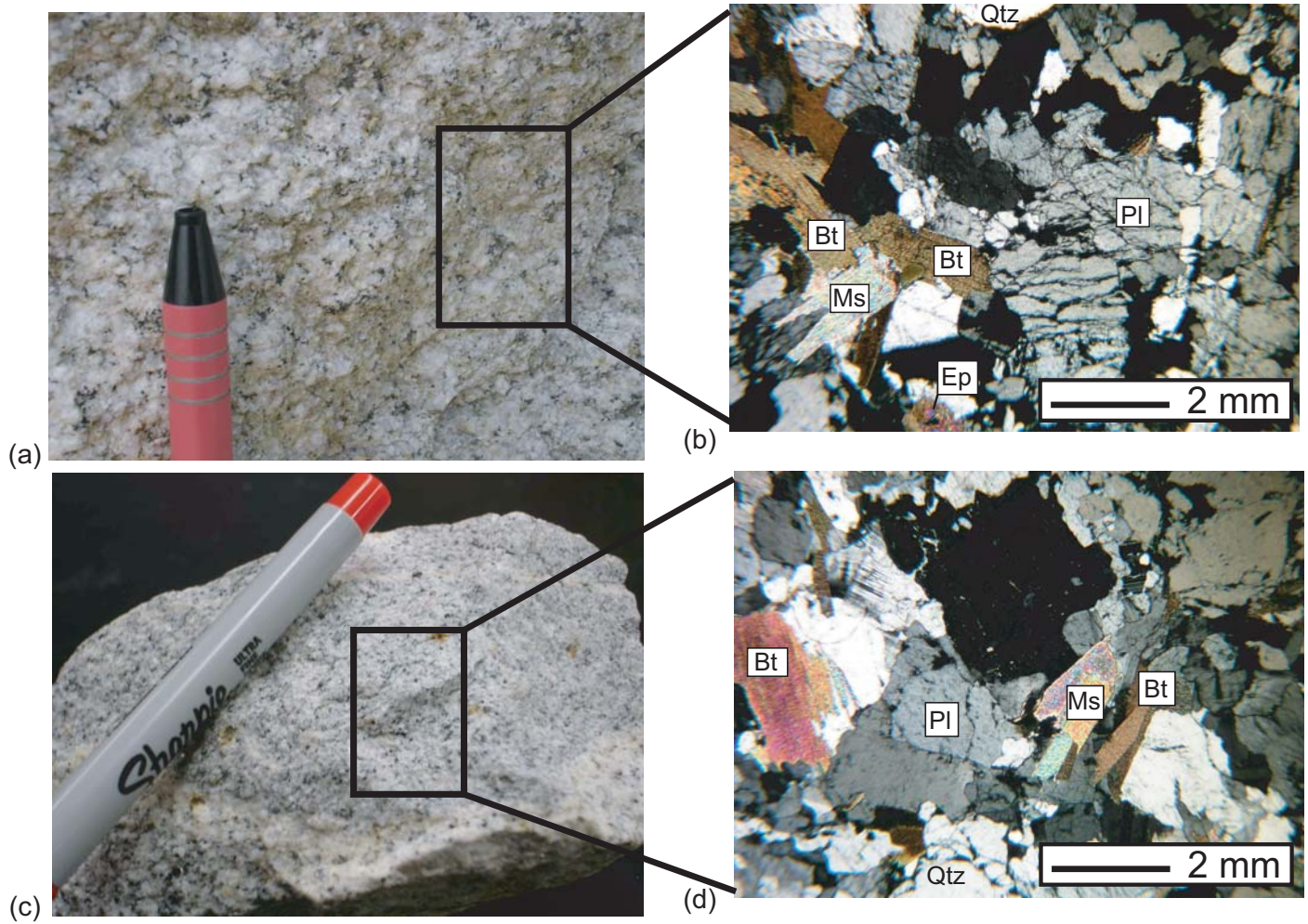


Figure 2–10. (a) Hand sample and photomicrograph (b) of the WCG. Sample collected at an exposure on Topez Lane southeast part of the Sylva South quadrangle. (c) Hand sample of Tuckaseegee granodiorite and photomicrograph. Sample collected on Shook Cove road, southwest part of the Tuckaseegee quadrangle. (d). Abbreviations: Abbreviations: Bt–biotite: Ep–epidote; Pl–plagioclase; Qtz–quartz.

Table 2–3. Modal analyses of samples collected from the WCG and Tuckaseegee granitoids. Geochemical analyses of the granitoid and amphibolite samples are discussed in Chapter 3.

Sample ID Unit Description	1066 WCG Tonalite/ Trondhjemite	T421 Tuckaseegee Granodiorite/ Quartz monzodiorite
points counted	819	825
Quartz	29.6	17.6
Plagioclase	58.6	58.2
K-feldspar	1.95	14.2
Biotite	4.40	4.36
Muscovite	4.03	3.64
Epidote	0.85	0.48
Myrmekite	0.00	1.09
Sericite	0.37	0.36
Opaques	0.12	0.00
Zircon	0.00	0.12
Titanite	0.12	0.00
Rutile	0.00	0.00
Total	100	100

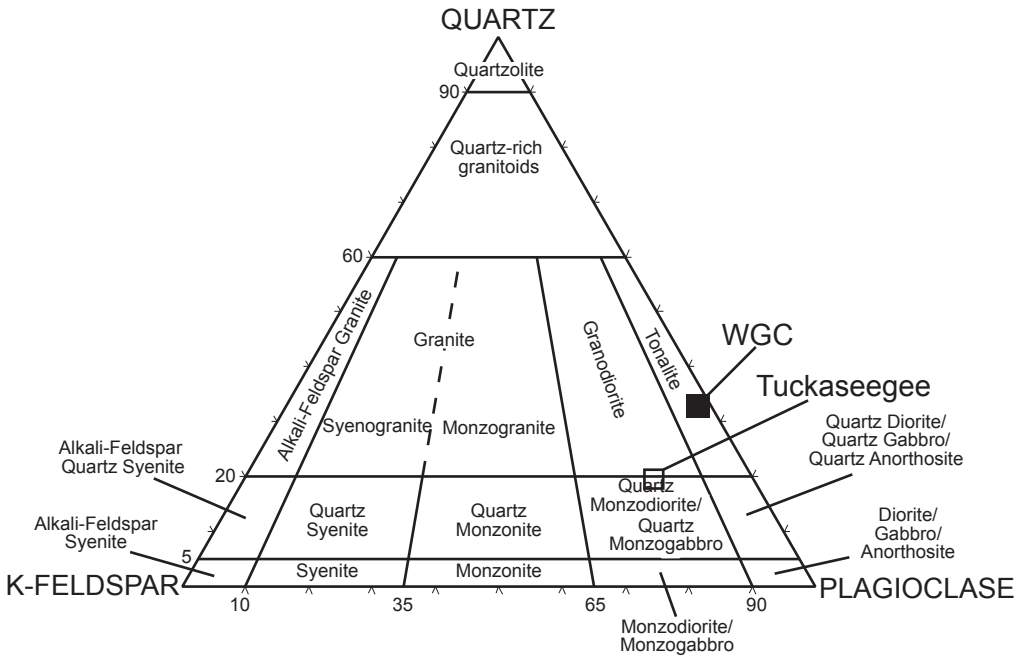


Figure 2–11. IUGS classification (Streckeisen, 1976) of WCG and Tuckaseegee samples.

muscovite (Fig. 2–10d). Plagioclase has both Carlsbad and albite twinning. Granophyric texture was also observed in a few of the plagioclase grains, along with minor seritization. Modal abundances of the Tuckaseegee sample indicate that it is compositionally a granodiorite–monzodiorite according to Streckeisen's (1976) IUGS classification scheme based on modal percent quartz, alkali feldspar, and plagioclase

Rabun Granodiorite

The Rabun granodiorite is a Mississippian (Miller and Stewart, 2002; Miller et al., 2006; Stahr, 2007) batholith–scale pluton (~125 km^2); it was originally named by Hatcher (1971). It is complexly folded and is truncated by the Chattahoochee-Holland Mountain fault SW of the study area (Acker and Hatcher, unpublished). Only a small portion of the NE end of the Rabun pluton is present in the study area (Fig. 2–1); xenoliths of upper Tallulah Falls Formation were observed at several exposures (Fig. 2–12).

Miller et al. (1997) described the Rabun as a weakly to well–foliated, medium– to coarse–grained, commonly porphyritic granite to quartz monzonite body. Two texturally distinct phases are present in the Rabun granodiorite: a dominant porphyritic to megacrystic phase and an equigranular phase (Miller et al., 1997; Stahr, 2008). Outcrops observed in the study area consist of the equigranular phase, are light gray to white, and poorly foliated. Mineralogically, the equigranular phase is composed of plagioclase–quartz–biotite±muscovite. Later aplite dikes cross–cut exposures of the Rabun.

Looking Glass Granodiorite

The Looking Glass granodiorite intruded the upper Tallulah Falls Formation in the SE corner of the study area. The Looking Glass (333 ± 2 Ma; Varnell, in progress) is a relatively small plutonic body, roughly 35 km^2, and only a small portion is exposed in the lower SE corner of the study area (Fig. 2–1). Miller et al. (1997) reported that the Looking Glass is metamorphosed and deformed, as indicated by hornfelsic schist and recrystallization textures in quartz

(a)



(b)



Figure 2–12. (a) Exposure of Rabun granodiorite with crosscutting trondhjemite dike. (b) Exposure of Rabun granodiorite with xenoliths of upper Tallulah Falls Formation. Both exposures are located in the southeast section of the Tuckaseegee quadrangle near Cedar Creek Farm road.

grains (M. G. Varnell, pers. comm., 2008); the pluton is also moderately deformed as indicated by its interfolded contact with the Tallulah Falls Formation (Fig. 2-1). It is an equigranular medium–grained quartz–plagioclase–K-feldspar–biotite–muscovite granodiorite with a moderately to well–foliated granoblastic texture (Miller et al., 1997). Exposures are often composed of light tan saprolite.

CHAPTER III Geochemistry of Metaigneous Rock

Introduction

Polyphase deformational and thermal events are responsible for the complexity of the geology in the southern Appalachians and obscure the structures, relationships, petrology, and chemistry indicative of the protoliths of metaigneous rocks present therein. As a result, field observations, along with an understanding of the petrology and geochemistry of metaigneous rocks, are intergral to piecing together the history of the Appalachian orogen.

Metaigneous rocks occur throughout the southern Appalachian Blue Ridge. There are, however, important distinctions in occurrence of granitoid, mafic, and ultramafic rocks in different terranes in the Blue Ridge. For example, mafic and ultramafic rocks are common in central and eastern Blue Ridge terranes, whereas, the western Blue Ridge contains few or no igneous rocks (Hurst, 1955; Hadley, 1970).

In this chapter the geochemistry of both felsic and mafic metaigneous rocks exposed in the study area (Fig. 3–1) will be discussed to better understand the geologic evolution of this area. Similarities and differences between two plutons in the Tugaloo terrane of the eastern Blue Ridge in the southern part of the study area are explored in the first part of the chapter. The geochemistry of amphibolite samples taken from enigmatic block-in-matrix structures located in the Dahlonega gold belt are then examined and compared to other occurrences of mafic and ultramafic rocks in this terrane in the second part of the chapter. Observations of geochemical signatures and trends of both granitic and mafic samples are an important step in understanding the evolution of the Blue Ridge geologic province.

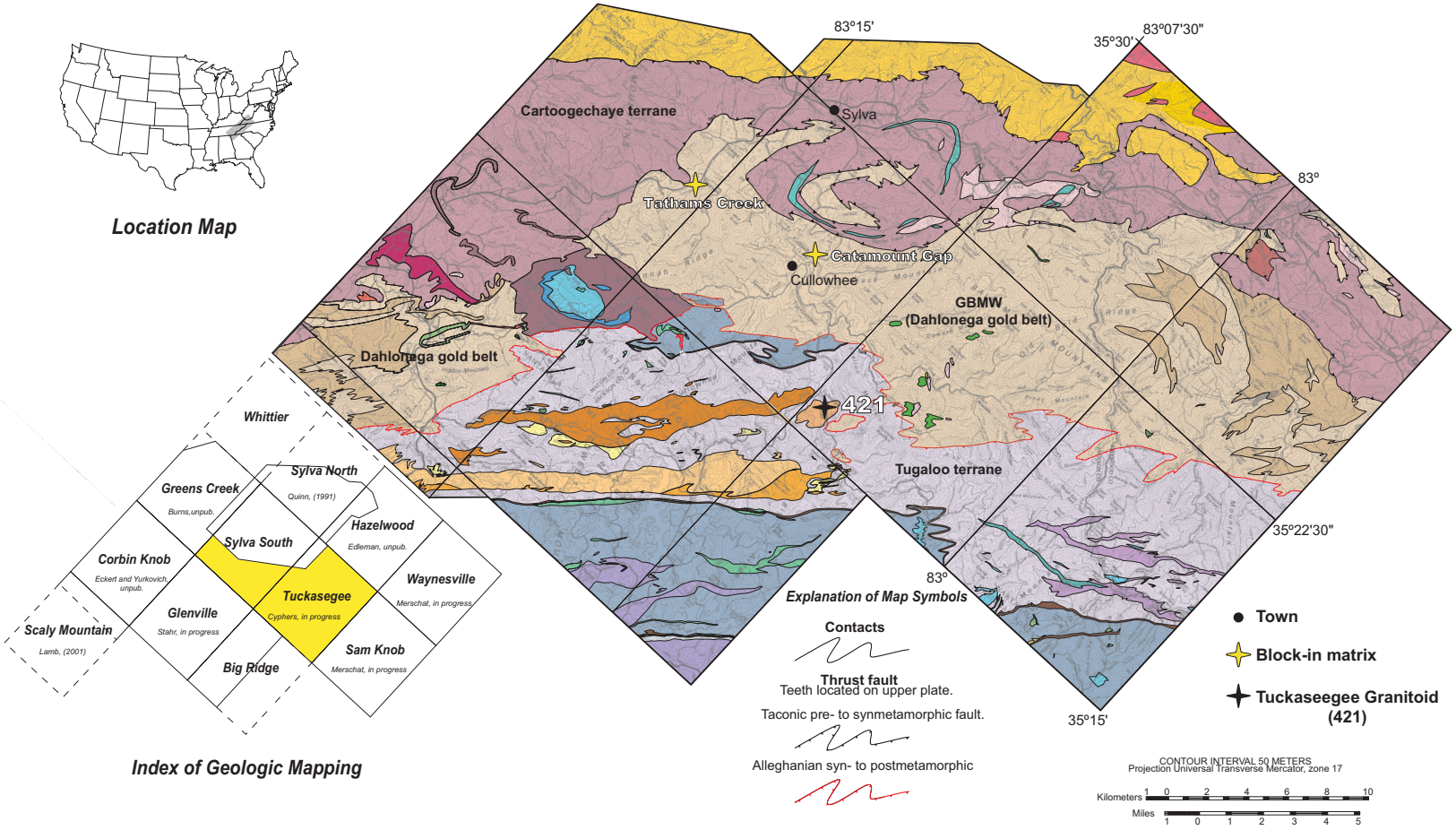


Figure 3-1. Compiled geologic map of a section of the Blue Ridge. Study area for this thesis is outlined in yellow. Geology: Greens Creek–Ann Burns; Sylva South (part), Tuckaseegee–Shawna Cyphers; Corbin Knob–James O. Eckert, Jr., and Steven P. Yurkovich; Hazelwood–Steven H. Edelman and Robert D. Hatcher, Jr.; Scaly Mountain–Dwight D. Lamb; Sam Knob, Waynesville–Arthur J. Merschat; Sylva South and Sylva North (parts)–Michael J. Quinn; Glenville and Big Ridge (part)–Donald W. Stahr, III. Modified from Merschat et al. (2006).

Sample Collection and Analytical Methods

Samples

Samples of representative metaigneous lithologies were collected in the study area for geochemical analysis. These samples were chosen in order to address questions of provenance and/or their association with surrounding units and rock types. One sample (T421) of the recently named Tuckaseegee granitoid (Fig. 3-1) mapped in the study area was selected for comparison with previous geochemical results of the Walnut Creek granodiorite/trondhjemite (Stahr et al., 2005). The majority of the samples selected (20) are amphibolite blocks taken from the Savannah Church (SC) and Catamount Gap (CG) block-in-matrix structures (Fig. 3-1). The lithology of these samples was discussed in Chapter II and will not be revisited here. A more detailed investigation of the geochemistry of each sample is a significant part of this chapter, in particular to determine the protoliths of amphibolite blocks from the block-in-matrix structures.

Analytical Techniques

Samples collected for analysis were extracted from the exposure using a sledge hammer and chisel, and then were cut into smaller slabs on a prep saw. In addition to the above preparation, samples collected for geochemical analysis were also washed, broken into smaller sections with a hammer, and powdered using an alumina shatter box. Multi-element whole-rock analyses were performed at ACTLABS (Ancaster, ON) using lithium metaborate/tetraborate fusion and inductively coupled plasma emission spectroscopy (FUS-ICP) and total digestion inductively coupled plasma analysis (TD-ICP). Inductively coupled plasma (ICP) mass spectrometry (ICP-MS) and Instrumental Neutron Activation Analysis (INAA) were also used. A standard thin section was made of each sample.

Part 1: Granitic plutons in the Eastern Blue Ridge

Paleozoic granitic plutons in the eastern Blue Ridge are generally peraluminous, two-mica, low-K, generally garnet-bearing, heavy rare earth element (HREE) depleted trondhjemites to granodiorites (Miller et al., 2006). The Whiteside and Persimmon Creek granitic bodies were emplaced in the Middle Ordovician (Miller et al., 2000, 2006; McDowell et al., 2002; Bream, 2003); a younger suite of

Devonian and Mississippian plutons (Miller et al., 2000, 2006; Stahr et al., 2005) provide evidence of a later pulse of plutonism in the eastern Blue Ridge. Several origins have been suggested for the magmas that produced these granitic bodies, including continental convergent-margin magmas, which would account for the peraluminous chemistry of the trondhjemitic plutons or subduction-related magmas related to the granodiorites (McSween et al., 1991). Contamination of mantle-derived melt by crustal sources is another hypothesis suggested for the petrogenesis of felsic plutonic rocks in the eastern Blue Ridge (Sando et al., 1983).

Sample T421 is compared here with Walnut Creek Granodiorite studied by Stahr et al. (2005). This sample is representative of the lithology of the Tuckaseegee granodiorite/ trondhjemite observed in the mapped area. Because only one sample was collected from the Tuckaseegee granitoid, any comparisons between it and the WCG are tentative; and analyses are needed to better understand the geochemistry of the Tuckaseegee granitoid and its relationship with the WCG.

As noted in Chapter II, this unit is a medium– to fine–grained plagioclase-quartz–rich granitic body found within the southern part of the mapped area. The extent of this body is about 2 km^2, relatively small when compared to the nearby Walnut Creek and Rabun plutons. All samples are peraluminous, as shown in table 3-1 and figure 3-2, and indicated by mineralogy in the previous chapter. Normative feldspar compositions (Table 3-2) (Barker, 1979) indicate all Walnut Creek samples but one are trondhjemite; the remaining two samples, one Walnut

Table 3-1 - Whole-rock major and trace element data for representative granitic samples in the Eastern Blue Ridge terrane.

Granite			Walnut Creek							Tuckaseegee
Sample ID			GQ-203	GQ-221	GQ-542	GQ-547	GQ-878B	GQ-1081	GQ-1213	T421
Analysis Type	Detection Limit									
FUS-ICP	Major Oxides (wt%)									
	SiO_2	0.01	72.21	75.81	71.63	70.98	68.61	70.97	70.94	73.63
	Al_2O_3	0.01	15.65	13.8	16.35	15.98	16.15	16.09	16.48	14.2
	Fe_2O_3 (T)	0.01	0.9	1.24	0.89	1.3	2.55	1.52	1.13	1.18
	MnO	0.001	0.014	0.014	0.025	0.026	0.029	0.019	0.026	0.039
	MgO	0.01	0.22	0.36	0.23	0.43	0.71	0.62	0.42	0.42
	CaO	0.01	1.58	2.3	2.36	2.23	2.51	2.91	2.22	0.73
	Na_2O	0.01	4.96	4.75	5.97	5.29	4.6	5.31	5.56	3.91
	K_2O	0.01	3.57	0.99	1.21	1.37	2.78	1.03	2.25	4.12
	TiO_2	0.001	0.113	0.141	0.105	0.175	0.428	0.209	0.167	0.111
	P_2O_5	0.01	0.05	0.03	0.05	0.07	0.15	0.09	0.05	0.05
	LOI	0.01	0.76	0.35	0.58	1.38	0.74	0.7	0.65	0.776
	TOTAL		99.76	99.78	99.4	99.24	99.24	99.48	99.89	99.17
	Trace Elements (ppm)									
	Ba	1	660	269	183	285	1096	293	1222	976
	Be	1								1
	Sr	2	284	498	594	586	628	594	1018	107
	V	5	6	11	8	14	36	18	12	11
	Y	1	14	1	7	3	7	4	5	13
INAA	Trace Elements (ppm, *-ppb)									
	As	1	n.d.	n.d.	n.d.	n.d.	n.d.	n.d.	n.d.	< 1
	Au	1*	n.d.	n.d.	n.d.	n.d.	n.d.	n.d.	n.d.	1
	Br	0.5	n.d.	n.d.	n.d.	n.d.	n.d.	n.d.	n.d.	< 0.5
	Co	0.1	1	1.4	1.2	2	3.2	3.2	2	3
	Cr	0.5	3.1	<0.5	<0.5	<0.5	1.2	4.9	3.4	1.2
	Hg	1	n.d.	n.d.	n.d.	n.d.	n.d.	n.d.	n.d.	< 1
	Ir	1	n.d.	n.d.	n.d.	n.d.	n.d.	n.d.	n.d.	< 1
	Mo	2	n.d.	n.d.	n.d.	n.d.	n.d.	n.d.	n.d.	
	Sb	0.1	n.d.	n.d.	n.d.	n.d.	n.d.	n.d.	n.d.	< 0.1
	Sc	0.01	2.86	0.71	1.68	1.49	3.4	2.44	2.28	3.22
	Se	0.5	n.d.	n.d.	n.d.	n.d.	n.d.	n.d.	n.d.	< 0.5
	W	1	n.d.	n.d.	n.d.	n.d.	n.d.	n.d.	n.d.	< 1
FUS-MS	Trace Elements (ppm)									
	Bi	0.1								< 0.1
	Ce	0.1	34.6	11.2	9.27	11.5	35.4	5.19	5.45	16
	Cs	0.1	2	0.6	0.7	1.1	1.5	0.8	0.9	1.2
	Dy	0.02	2.2	0.35	0.93	0.54	1.35	0.88	0.82	2.13
	Er	0.01	1.1	0.23	0.66	0.33	0.57	0.44	0.46	1.27
	Eu	0.005	0.671	0.348	0.366	0.439	1.03	0.488	0.341	0.356
	Ga	1	n.d.	n.d.	n.d.	n.d.	0.9	n.d.	n.d.	21
	Gd	0.02	2.58	0.54	0.76	0.72	2.34	1.15	0.75	2.1
	Ge	0.5	n.d.	n.d.	n.d.	n.d.	n.d.	n.d.	n.d.	0.9
	Hf	0.1	1.8	2.7	2	2.3	3.8	2.4	2.3	1.3
	Ho	0.01	0.39	0.07	0.2	0.11	0.22	0.16	0.16	0.42
	In	0.1								< 0.1
	La	0.05	18	5.75	4.27	5.94	18.8	7.22	2.98	6.83
	Lu	0.002	0.146	0.045	0.116	0.066	0.067	0.051	0.073	0.193
	Nb	0.2	10.2	1.4	4.1	2.2	5.4	1.5	2.3	4.9
	Nd	0.05	14.6	4.73	4.16	5.64	17.3	6.99	2.97	8.14
	Pr	0.02	3.97	1.26	1.12	1.42	4.67	1.81	0.74	1.89
	Rb	2	120	33	37	40	82	32	40	90
	Sm	0.01	3.01	0.64	0.73	0.85	3.05	1.16	0.59	2.09
	Sn	1								< 1
	Ta	0.1	0.89	0.1	0.57	0.24	0.29	0.1	0.24	0.7
	Tb	0.01	0.42	0.07	0.14	0.1	0.29	0.17	0.14	0.36
	Th	0.05	6.8	0.8	1.5	1.2	8.6	1	1.6	2.45
	Tl	0.05								0.5
	Tm	0.005	0.165	0.04	0.111	0.056	0.077	0.062	0.075	0.2
	U	0.05	2.6	0.4	1.7	0.7	0.6	0.6	0.9	1.66
	Yb	0.01	1.06	0.31	0.78	0.41	0.47	0.37	0.5	1.31
	Zr	1	50	85	61	75	136	74	69	26
TD-ICP	Trace Elements (ppm, *-%)									
	Ag	0.5								< 0.5
	Cd	0.5								< 0.5
	Cu	1	5	5	17	10	19	6	11	4
	Ni	1	2	2	2	1	1	5	1	1
	Pb	5	35	7	17	10	18	8	15	26
	S	0.001*								0.002
	Zn	1	42	36	33	46	66	46	43	60

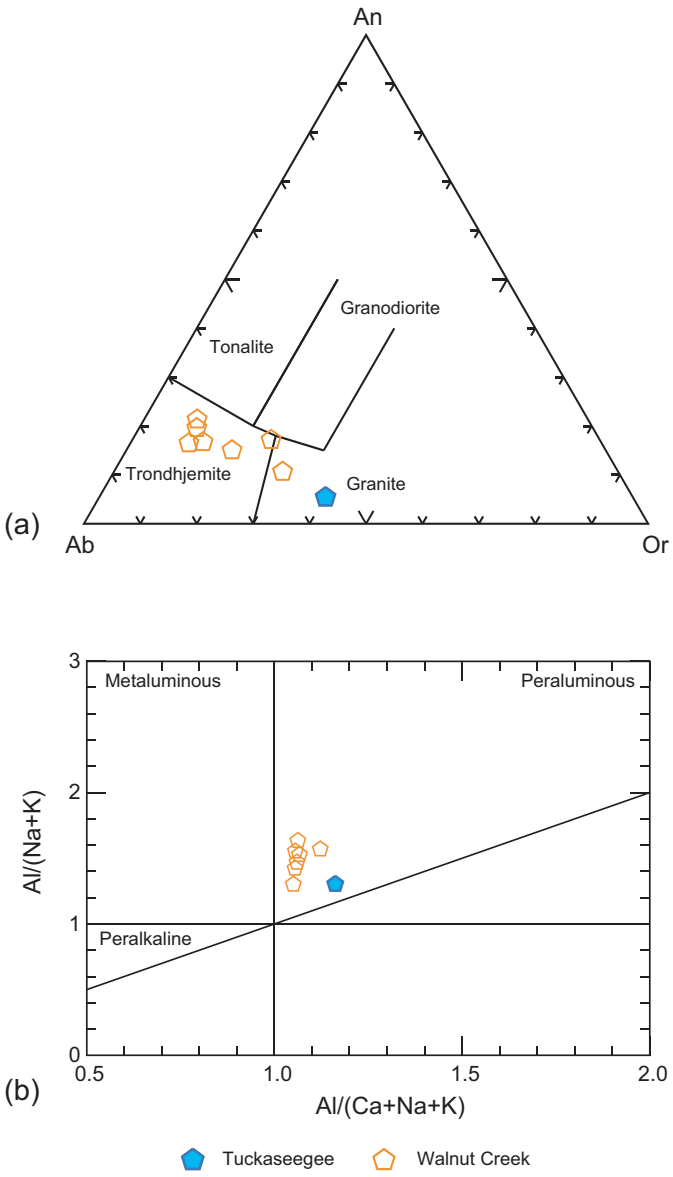


Figure 3-2. (a) Normative-feldspar classification (Barker, 1979) of Walnut Creek and the Tuckaseegee granitoids. (b) Shand's Index (Maniar and Piccoli, 1989) showing all Walnut Creek samples with the Tuckaseegee sample. All plot in the peraluminous field.

Table 3-2. CIPW normative results. WC is Walnut Creek.

Sample ID	GQ-203	GQ-221	GQ-542	GQ-547	GQ-878B	GQ-1081	GQ-1213	T421
unit	WC	WC	WC	WC	WC	WC	WC	Tuckaseegee
Normative Mineralogy								
Quartz	26.12	39.01	27.01	29.74	25.20	29.23	24.74	33.07
Corundum	0.88	0.81	1.05	1.91	1.37	1.17	0.99	2.10
Orthoclase	21.10	5.85	7.15	8.10	16.43	6.09	13.30	24.35
Albite	41.97	40.19	50.52	44.76	38.92	44.93	47.05	33.09
Anorthite	7.51	11.21	11.38	10.61	11.47	13.85	10.69	3.29
Hypersthene	1.65	2.42	1.70	2.65	4.70	3.36	2.40	1.05
en	0.55	0.90	0.57	1.07	1.77	1.54	1.05	1.05
fs	0.00	0.00	0.00	0.00	0.00	0.00	0.00	0.00
Magnetite	1.02	1.42	1.07	1.49	2.55	1.66	1.24	1.52
Chromite	0.00	0.00	0.00	0.00	0.00	0.00	0.00	0.00
Ilmenite	0.02	0.02	0.04	0.06	0.06	0.04	0.06	0.21
Apatite	0.12	0.07	0.12	0.16	0.35	0.21	0.12	0.12

Creek and the Tuckaseegee granite, plot within the granite field (Fig. 3-2).

Granitoid Geochemistry

Harker diagrams indicate that the Tuckaseegee granite is more silica rich compared to all but one sample collected from the Walnut Creek pluton (Fig. 3-3). Covariation diagrams of trace elements plotted against TiO_2 (Fig. 3-4) show that almost all samples have similar TiO_2 values and Nb/Y and U/Th ratios. One Walnut Creek sample is enriched in TiO_2 compared to all other samples.

Trace-element geochemistry

Major elements are highly mobile in rocks that have been metamorphosed, but trace element chemistry can be useful because of the decreased mobility of trace elements compared to major elements (Rollinson, 1993). Decreased mobility means that these elements will retain the signature of the protolith; therefore, select trace elements can be indicative of particular petrogenetic processes (Pearce and Cann, 1973; Pearce, 1982; Rollinson, 1993).

Normalized multi-element diagrams sometimes called incompatible element diagrams or spider diagrams are useful in identifying different compositions and can be helpful in determining provenance and differentiating trends. With respect to mantle mineralogy, compatible elements have a high ionic potential, prefer the solid phase, and are immobile or less mobile. Incompatible elements have a low ionic potential, prefer the melt phase, are highly mobile, and are easily leached by hydrous fluids (Rollinson, 1993).

Incompatible element diagrams (Fig. 3-5) plot the light ion lithophile elements (LILE) on the left side of the diagram and the high field strength elements (HFSE) to the right. LILE are more mobile; their abundance is controlled by the fluid phase and therefore shows variable enrichment. Incompatible HFSE are the most immobile and are a function of the chemistry of the source and crystal/melt processes normally depleted relative to the LILE (Rollinson, 1993).

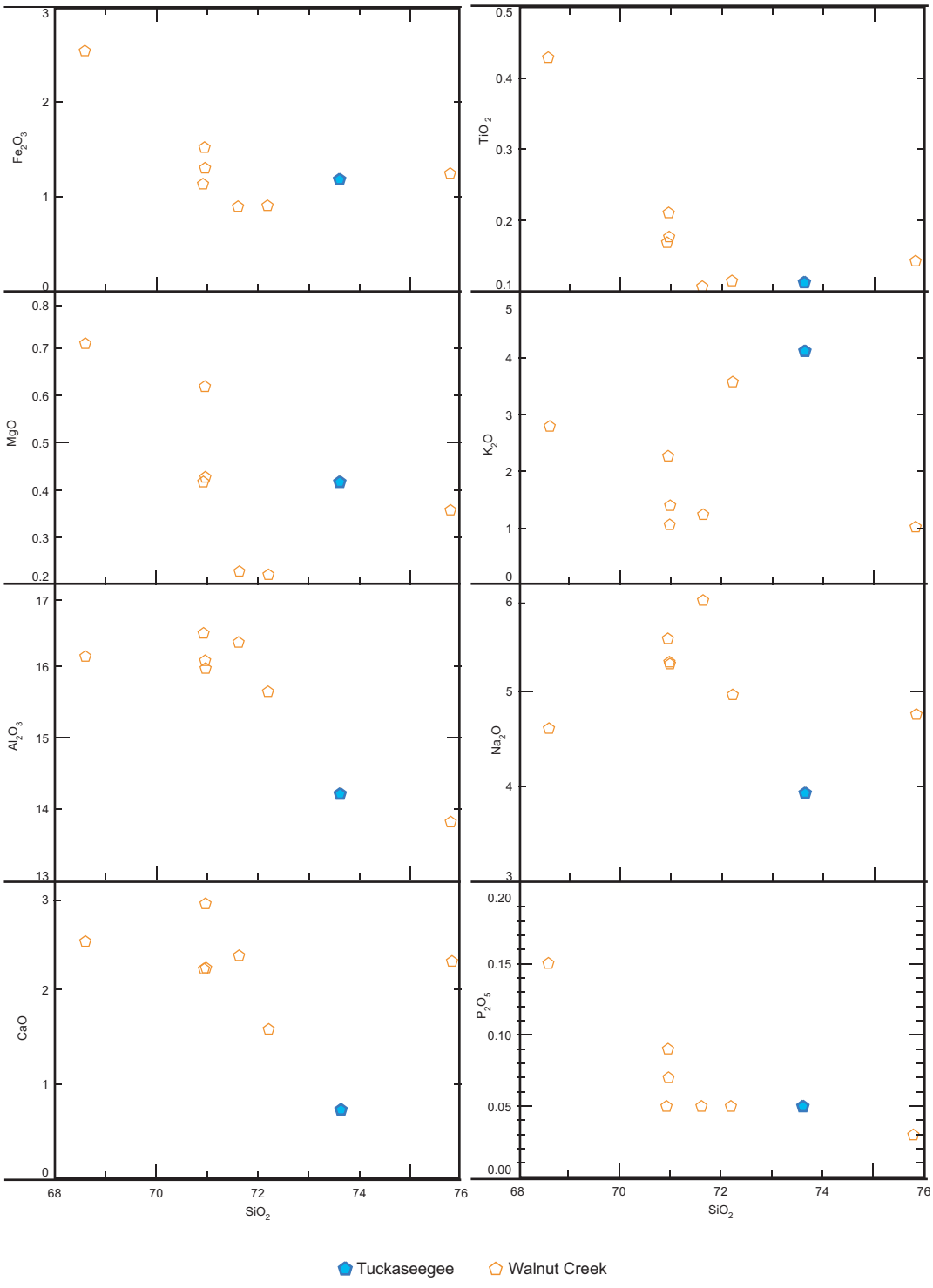


Figure 3-3. Harker diagrams of all major oxides for the Walnut Creek and Tuckaseegee granite samples.

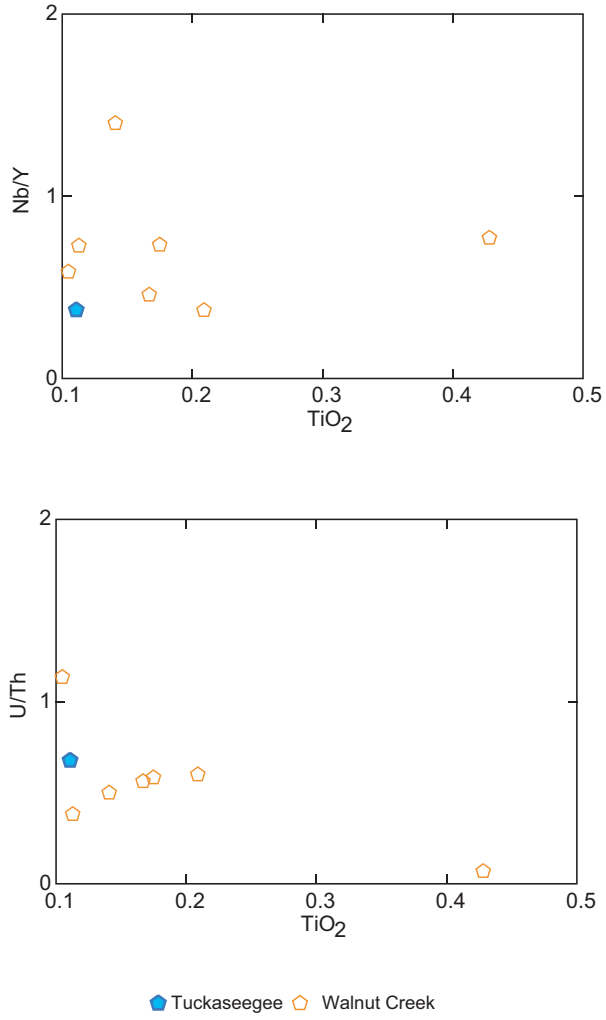


Figure 3-4. TiO_2 variation diagrams of Walnut Creek samples and the Tuckaseegee granite samples.

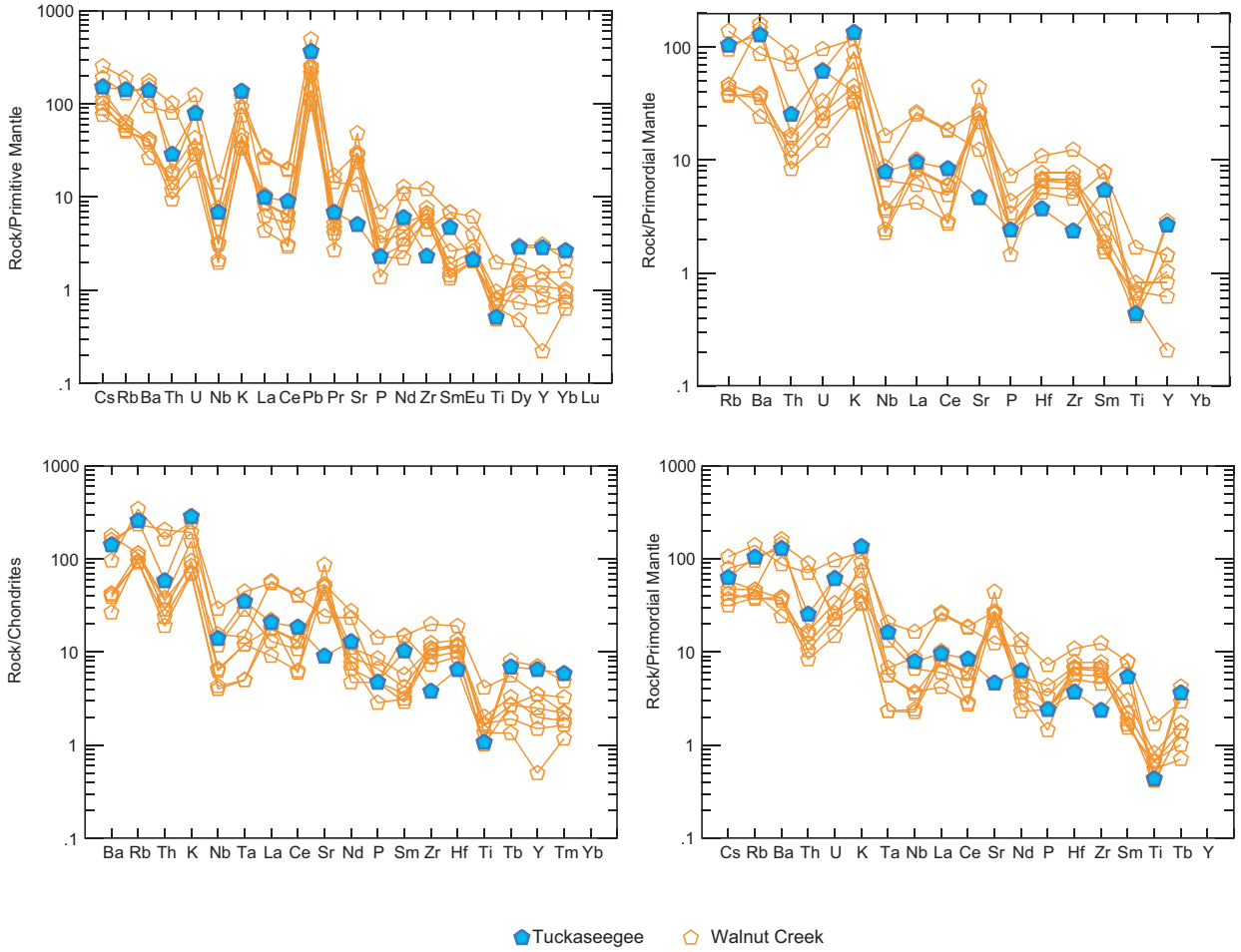


Figure 3-5. Trace element diagrams for the Walnut Creek and Tuckaseegee granite sample (Sun and McDonough, 1989; Thompson, 1982; Holm, 1985; Wood, et al., 1979).

REE geochemistry

The rare earth element (REE) diagram (Fig. 3-6) normalized to chondrite values displays light rare earth elements (LREE) to the left of the diagram and heavy rare earth elements (HREE) to the right. Almost all REE form stable 3+ ions of similar size; however, as the atomic number increases and the ionic size decreases, so these elements behave differently and will fractionate relative to each other.

All granitic samples have a similar trend on trace element discriminant diagrams (Fig. 3-6). Both the Walnut Creek and Tuckaseegee granitoids are enriched in the LREE and depleted in the HREE (Fig. 3-6). They are all enriched in K and depleted in Ti and Nb. Differences are apparent, however, in the two trace elements Sr and Zr, which are depleted in the Tuckaseegee granite sample when compared to Walnut Creek samples. Walnut Creek samples have a positive Eu anomaly while the Tuckaseegee granitoid has a negative anomaly.

Tectonic discrimination diagrams

The Walnut Creek samples and the Tuckaseegee granite sample plot in the volcanic arc granites field on the tectonic discrimination diagrams Rb vs Yb+Ta, Rb vs Y+Nb, Ta vs Yb, and Nb vs Y (Fig. 3-7). The Hf-Rb/10-Ta diagram discriminates between ocean-ridge granites, volcanic-arc granites and within-plate granites (Fig. 3-7e). Two samples, one Walnut Creek sample and the Tuckaseegee granite, fall within the syn-collisional zone on the Hf, Rb/30, Ta x 3 diagram (Fig. 3-7f), which provides distinction between syn-and post-collisional granites (Rollinson, 1993).

Discussion of Granitoids

Miller et al. (1997) compared the geochemistry of the Rabun granodiorite, Pink Beds, Looking Glass, and Whiteside granitoids; in particular, trace element chemistry was utilized in order to distinguish between trondhjemitic and granodioritic compositions. Trondhjemites are generally very poor in

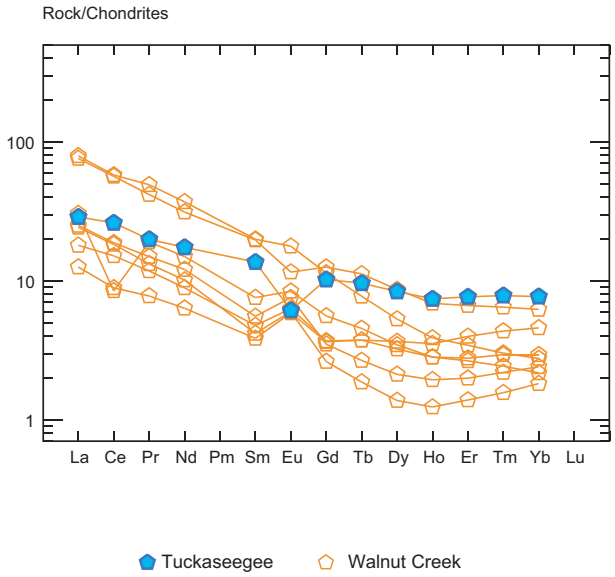


Figure 3-6. REE diagrams (Sun and McDonough, 1989) for Walnut Creek and the Tuckaseegee granite sample.

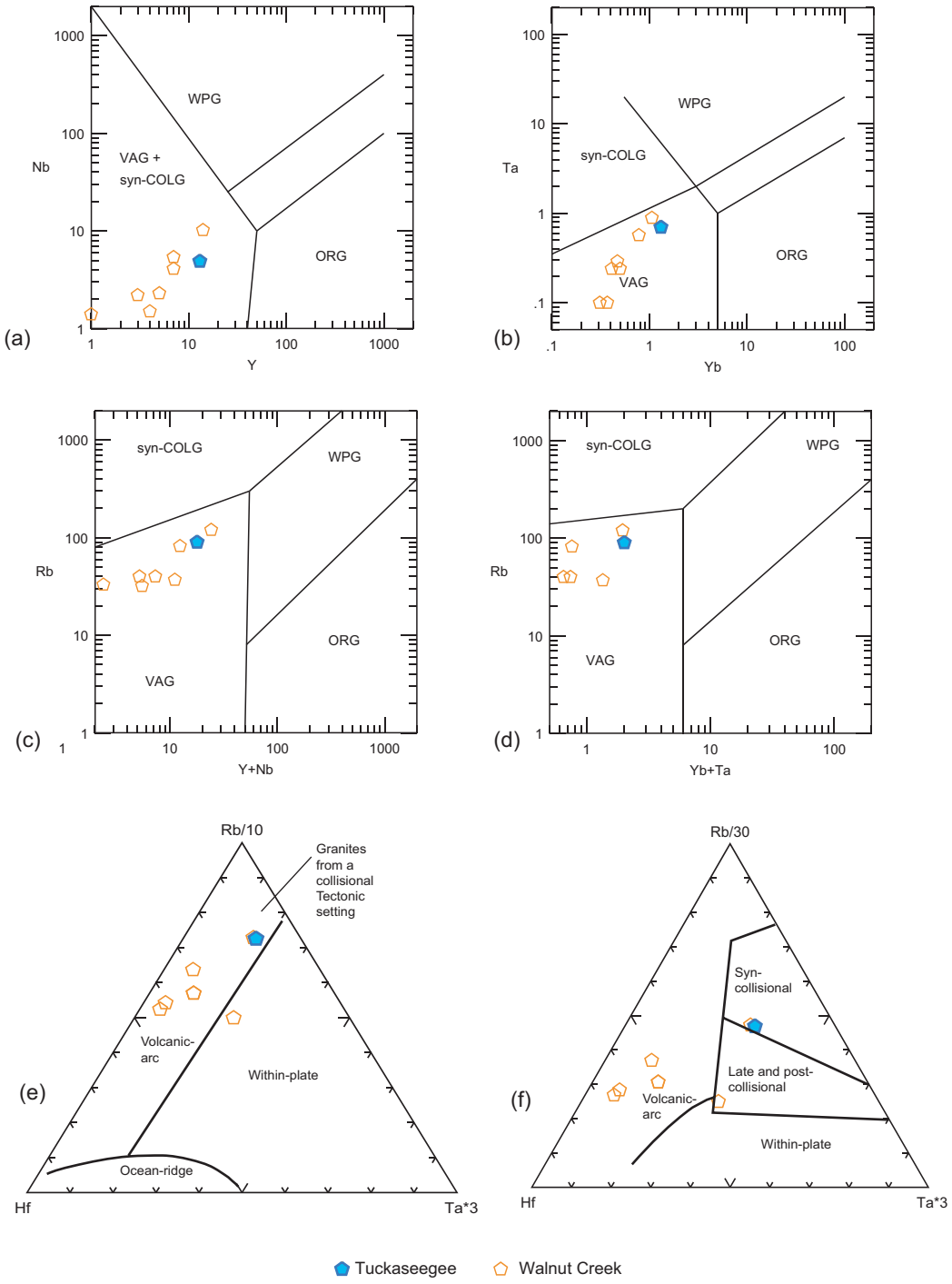


Figure 3-7. Tectonic discrimination diagrams for eastern Blue Ridge granites Walnut Creek and the Tuckaseegee granite (Pearce et al., 1984). Abbreviations ORG – orogenic granite; syn-COLG – syn-collisional granite; VAG – volcanic-arc granite; and WPG – within-plate granite.

incompatible elements such as Rb, LREE, Ba, Th, and U; tend to have minor Eu anomalies; and are very rich in Sr**.**

In comparison, granodiorites have more typical incompatible element concentrations, and have small negative Eu anomalies and moderate Sr concentrations. Both are poor in HFSE and HREEs, although, trondhjemites are especially poor in HREEs and in the HFSE element Ta (Miller et al., 1997). In addition, high Sr and low HREE suggest an entirely crustal derivation from a deep (garnet bearing, feldspar-poor) mafic source (Miller et al., 1997). Both the Walnut Creek and Tuckaseegee granitoids are similar mineralogically and are located within less than a kilometer of each other (Fig. 3-1). Due to the close proximity of the two granitic bodies, the Tuckaseegee could be a satellite pluton of the WCG. Both are also located very near the Rabun and

Pink Beds plutons (Fig. 3-1)**.** REE and spider diagrams show that the Tuckaseegee granitoid sample has a very similar trend when compared to the Walnut Creek granodiorite /trondhjemite samples (Figs. 3-5, 3-6). Despite similarities between the Tuckaseegee sample and Walnut Creek samples, the Tuckaseegee granite sample shows distinctions that are worth mentioning, including a small negative Eu anomaly, moderate to low Sr values, and enrichment in Ta in comparison to all but two Walnut Creek samples. This geochemistry is also typical of eastern Blue Ridge plutonic rocks like the granodiorites discussed by Miller et al. (1997).

Discriminant diagrams indicate all granitic samples discussed herein are immature volcanic–arc granites (Fig. 3-7). Rollinson (1993) cautioned that careful consideration should be applied to tectonic discriminant diagrams, because of the effects of element mobility and crystal fractionation. In addition, differences in trace-element chemistry can be a function of variable source chemistry as well as differences in tectonic environment (Twist and Harmer, 1987). An alternative model suggests that repeated intracrustal melting of accretionary wedge rocks would provide the necessary source material for low-K tonalite-trondhjemite plutonism in the eastern Blue Ridge (Miller et al., 2006).

This interpretation is a more likely explanation for the provenance and emplacement of the WCG and Tuckaseegee granitoids.

Part 2: Geochemistry of Mafic Rocks

Pratt and Lewis (1905) collected data on ultramafic rocks in the NC Appalachians. Later, Hess (1955) identified a mafic-ultramafic belt that extends from Newfoundland to Alabama, the length of the Appalachian orogen; this work was continued by Larrabee (1966), who further defined the locations and extent of the ultramafic bodies. Misra and McSween (1984) noted that mafic-ultramafic rocks in the Appalachians are a heterogeneous group in terms of distribution, stratigraphic position, form and size, tectonic setting, and ages (which range from Neoproterozoic to Paleozoic).

In the central Blue Ridge, amphibolite samples collected from the Cartoogechaye terrane were interpreted by Quinn (1991) as ocean–floor basalt (MORB). Geochemical studies of the Buck Creek (Cartoogechaye terrane) and the Lake Chatuge (Cowrock terrane) mafic-ultramafic bodies indicated these bodies have a depleted mantle source (Shaw and Wasserburg, 1984). Eggers (1983) suggested an island-arc origin for the Kimsey Bald amphibolite, which occur in the Cartoogechaye terrane. Amphibolites from the Chunky Gal Mountain, Kimsey Bald, and many of the Lake Chatuge amphibolites were originally tholeiitic and likely formed in an ocean floor or within-plate setting (Walter, 1990). The geochemistry of the mafic rocks from the Carroll Knob complex have different trace and minor element composition from other mafic rocks in the Cartoogechaye terrane (Hatcher et al., 1984; Walter, 1990). Hatcher et al. (1984) suggested that the Carroll Knob complex may have originated as an ophiolite or as a complex differentiated pluton. Walter (1990) concluded that the chemistry of the Carroll Knob complex indicates the original composition was a tholeiitic arc basalt (Walter, 1990).

Several mafic-ultramafic complexes that have been studied in the Dahlonega gold belt include rocks of the Lake Burton metavolcanic suite, Ellijay

area, and Corundum Hill. Each is interpreted as a harzburgite-type (HOT) ophiolite (Nicolas and Boudier, 2003), because of the abundance of dunite, and presence of harzburgite and chromitite (Swanson et al., 2005). McConnell and Abrams (1984) and German (1985) favored a back-arc origin for the mafic rocks in the Dahlonega gold belt in Georgia. In another geochemical study, mafic rocks of the Lake Burton metavolcanic suite near Helen, Georgia, were interpreted as low-potassium tholeiite indicative of immature island arcs (Hopson, 1988; Gillon, 1989; Hopson et al., 1989; Hopson, 1994).

In the Dahlonega gold belt of northeast Georgia (Settles, 2001), trace element trends of amphibolite in the Sally Free mafic complex and Otto Formation indicate an oceanic origin for Dahlonega gold belt metaigneous rocks. Chemical tectonomagmatic discrimination diagrams plot amphibolites associated with the Otto Formation and Sally Free mafic complex as tholeiites, and mid-ocean ridge to island-arc basalts (Settles, 2001). The interlayered relationship of amphibolite and Otto Formation pelitic units northwest of the Sally Free mafic complex delimits sediment deposition to the Early Ordovician (or earlier) in this portion of the Dahlonega gold belt (Settles, 2001). Similarly, Quinn (1991) used trace element chemistry and field observations to interpret amphibolites of the Dahlonega gold belt in Sylva, NC and the surrounding area as oceanic basalt that was emplaced into the sediments as flow, dikes or sills.

Block-in-matrix structures are blocks of one lithology enclosed in a matrix of a different lithology. The term block-in-matrix has been used to describe structures formed through a variety of processes ranging from sedimentary, diapiric, igneous, and tectonic (Raymond et al., 1989). For this study, amphibolite blocks were collected from two exposures of block-in-matrix structures in the Dahlonega gold belt. Though block-in-matrix structures are found throughout the Blue Ridge of North Carolina (Raymond et al., 1989) occurrences of these structures are very numerous in the Dahlonega gold belt (Toe and Cullowhee terranes of Raymond et al., 1989). Amphibolite blocks from two exposures of block-in-matrix structures–Savannah Church (SC) and

Catamount Gap (CG)–were sampled for this study (Fig. 3-1), both occur in the Dahlonega gold belt. A diagram of compiled photographs of the SC block-in-matrix structure is shown in figure 3-8a and figure 3-8b details amphibolite blocks, major folds, and crosscutting felsic dikes that are present at this exposure.

Amphibolite Geochemistry

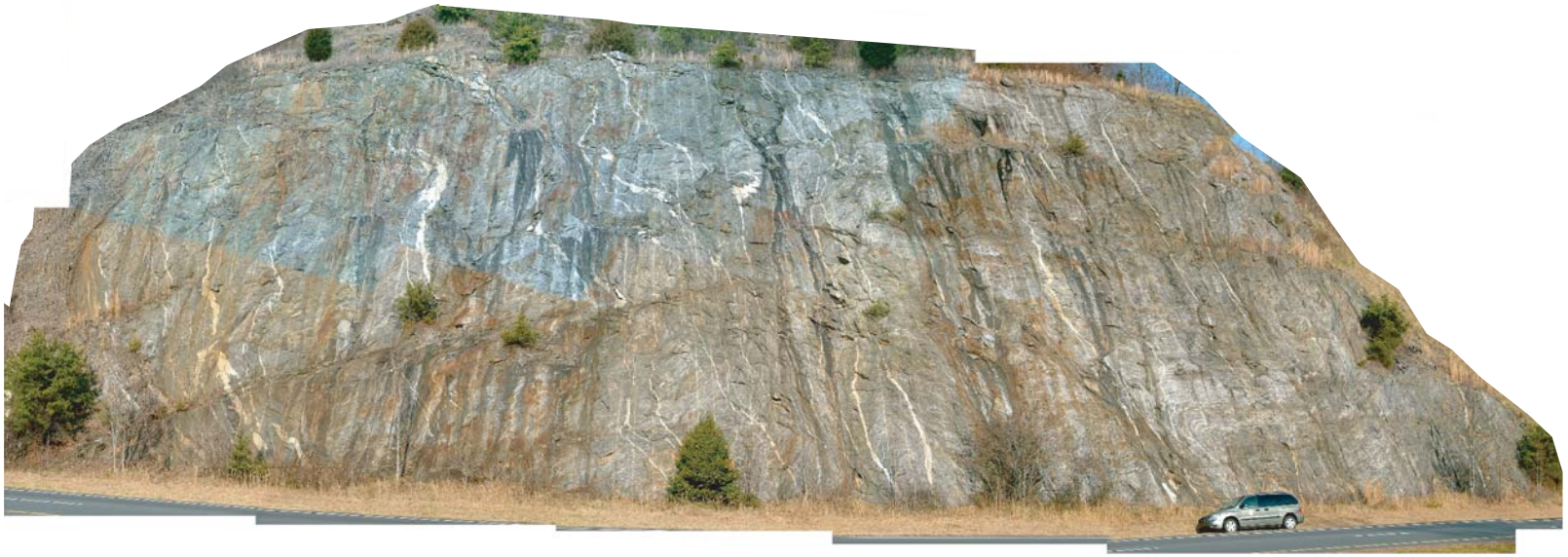
Ortho- versus Para-amphibolite

The Niggli values mg-(al-alk)-c ternary diagram (Fig. 3-9) is used to distinguish between para- and ortho-amphibolites (Leake, 1964). All but one CG sample plots in a linear cluster roughly parallel to the line showing an igneous trend indicating they are orthoamphibolites. The samples are not immediate to the igneous trend because of their higher alumina values.

Covariation diagrams

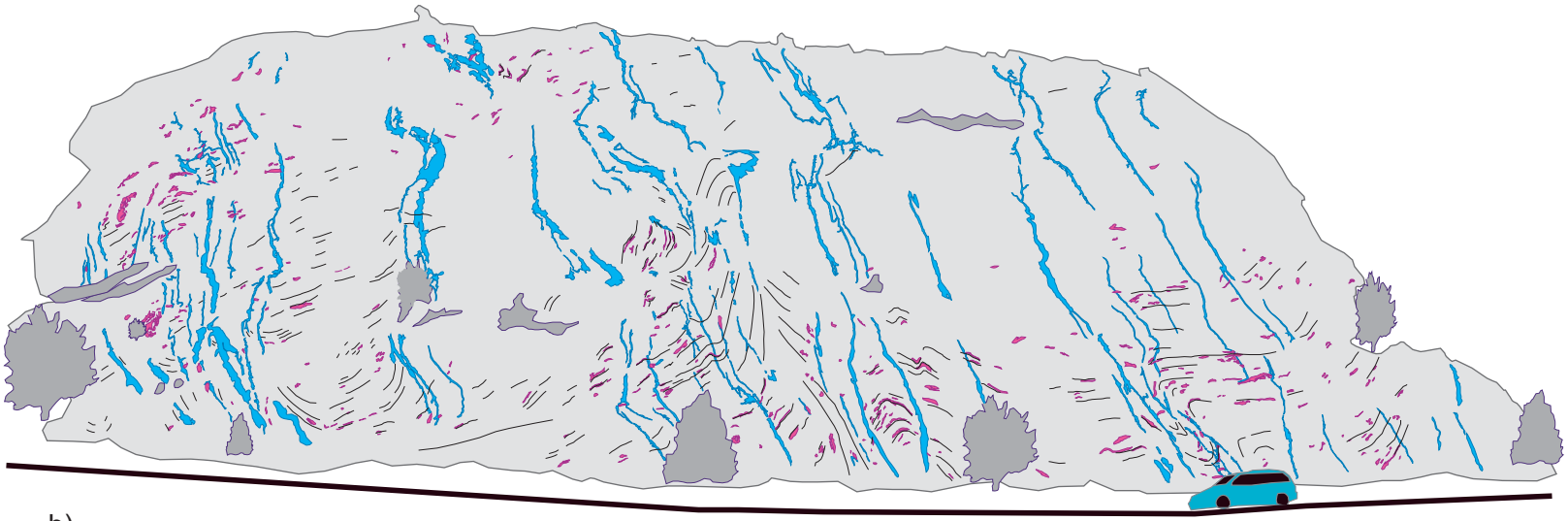
Trends of covariation diagrams using SiO_2 as a fractionation index (Harker diagrams) are not reliable for mafic rocks, because SiO_2 is highly mobile during metamorphic processes following initial crystallization. It is important to note, however, the amount of SiO_2 in each dataset. Most samples from SC and CG are silica–poor (<52% SiO_2); silica content are between 43.65 and 55.9 (wt. % SiO_2) and 47.04 and 53.87 SiO_2 (wt. %), respectively (Tables 3-3 and 3-4).

An alternative fractionation index is the magnesium number (100[MgO/(MgO+FeO)]), which is plotted against major oxides and trace elements (Fig. 3-10) for each sample (Oskarsson et al., 1982; Wilkinson, 1982). As fractionation proceeds, the Mg number decreases; this occurs because the Mg-Fe ratio changes drastically in the early stages of crystallization as a result of the higher distribution coefficient of Mg in comparison to Fe (Rollinson, 1993). The major oxides P_2O_5 and SiO_2 display a moderate decrease when compared to the Mg number in the SC samples; in contrast, there is an increase in CaO



a)

Figure 3-8. Savannah Church block-in-matrick structure at Tathams Creek. a) Compiled photographs of Savannah Church. b) Detail of amphibolite blocks (pink), major foliation and folds (black form lines), and felsic dikes (blue). Dark gray represents vegetation.



b)

Figure 3-8 (continued).

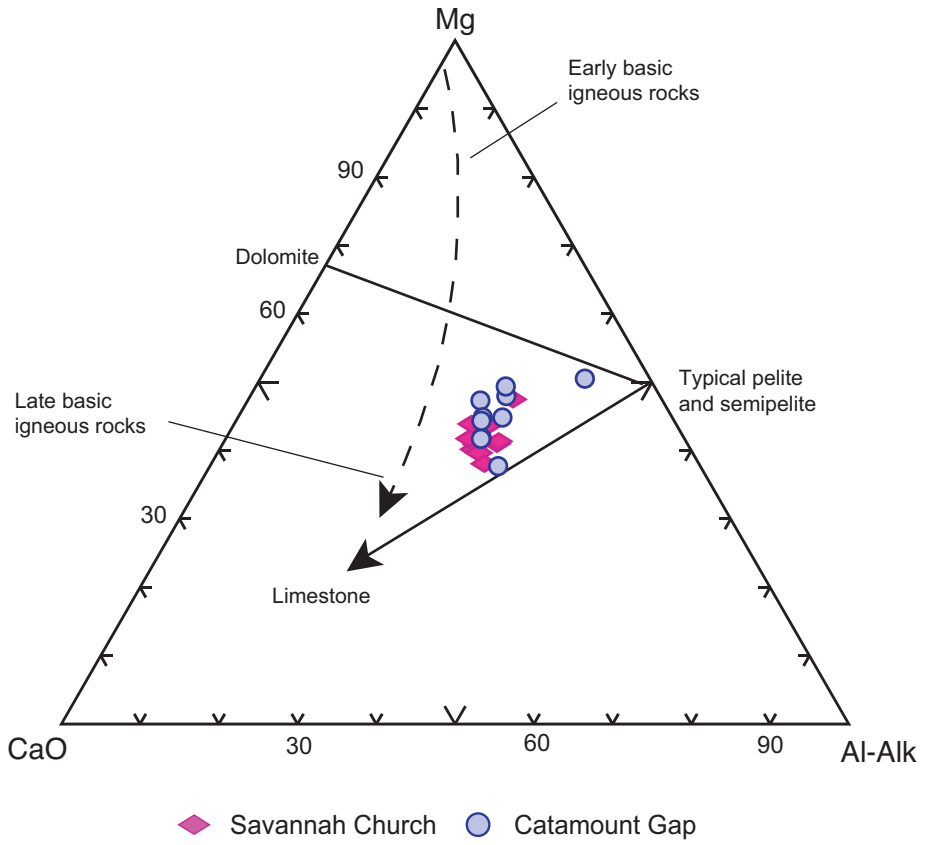


Figure 3-9. Niggli mg-(al-alk)-c diagrams for amphibolite blocks from the Savannah Church (pink diamonds) exposure and Catamount Gap (gray-filled circles) exposure. Dashed line indicates igneous trend. Mg=100x(MgO/FeO+MnO+2+MgO), al-alk=Al_2O_3-(Na_2O+K_2O), and C=CaO (Leake, 1964).

Table 3-3 - Whole-rock major and trace element data for representative Savannah Church amphibolite samples in the Dahlonega gold belt.

			Savannah Church amphibolite									
Sample ID			SC-1	SC-2	SC-3	SC-4	SC-5	SC-6	SC-7	SC-8A	SC-9A	SC-9C
Analysis Type	Detection Limit											
FUS-ICP												
	SiO_2	0.0001	55.9	49.35	52.66	48.58	47.58	43.65	49.57	44.98	45.8	48.07
	Al_2O_3	0.0001	14.69	14.48	14.29	16.15	15.87	14.75	15.04	18.18	16.82	14.66
	Fe_2O_3 (T)	0.0001	11.9	15.14	13.84	13.18	13.18	18.31	14.62	12.95	16.02	14.84
	MnO	0.00001	0.168	0.217	0.194	0.193	0.199	0.249	0.21	0.191	0.24	0.228
	MgO	0.0001	4.87	6.44	5.47	6.7	7.89	8.37	6.53	6.6	7.12	6.77
	CaO	0.0001	5.67	10.08	8.15	11.22	11.56	8.53	10.5	12.25	8.79	10.21
	Na_2O	0.0001	2.49	2.04	2.09	2.03	1.79	1.23	1.79	1.88	2.23	2.22
	K_2O	0.0001	2.13	0.62	0.46	0.6	0.67	1.92	0.42	0.69	1.71	0.88
	TiO_2	0.00001	1.504	1.89	1.918	1.507	1.409	2.301	1.962	1.548	1.81	2.025
	P_2O_5	0.0001	0.17	0.18	0.22	0.15	0.13	0.11	0.2	0.17	0.14	0.23
	LOI	0.0001	1.5	1.15	1.59	1.25	1.25	1.59	1.04	1.21	0.81	1.29
	TOTAL		99.96	100.1	99.58	100.3	100.3	99.16	100.5	99.45	99.89	99.98
	Trace Elements (ppm)											
	Ba	1	506	76	137	214	198	1345	79	252	511	136
	Be	1	3	3	4	2	2	3	3	3	4	3
	Sr	2	146	169	188	416	419	67	187	363	172	218
	V	5	271	361	334	298	281	377	354	323	378	358
	Y	1	45	41	44	32	35	34	54	33	49	48
INAA	Trace Elements (ppm, *-ppb)											
	As	1	< 1	< 1	< 1	< 1	< 1	< 1	< 1	< 1	< 1	< 1
	Au	1*	4	< 1	< 1	< 1	< 1	< 1	< 1	< 1	3	< 1
	Br	0.5	< 0.5	< 0.5	< 0.5	< 0.5	< 0.5	< 0.5	< 0.5	< 0.5	< 0.5	< 0.5
	Co	0.1	60.2	49.9	46.1	57.9	56.1	52.4	55.3	54.8	52.2	58.4
	Cr	0.5	131	161	100	169	178	235	158	163	226	176
	Hg	1	< 1	< 1	< 1	< 1	< 1	< 1	< 1	< 1	< 1	< 1
	Ir	1	< 1	< 1	< 1	< 1	< 1	< 1	< 1	< 1	< 1	< 1
	Mo	2	< 2	< 2	< 2	< 2	< 2	< 2	< 2	< 2	< 2	< 2
	Sb	0.1	< 0.1	< 0.1	< 0.1	< 0.1	< 0.1	< 0.1	< 0.1	< 0.1	< 0.1	< 0.1
	Sc	0.01	32.7	41.6	41.5	34.9	34.8	45.7	40.9	36	47.6	39.9
	Se	0.5	< 0.5	< 0.5	< 0.5	< 0.5	< 0.5	< 0.5	< 0.5	< 0.5	< 0.5	< 0.5
	W	1	399	326	759	346	247	192	240	226	239	244
FUS-MS	Trace Elements (ppm)											
	Bi	0.1	< 0.1	< 0.1	< 0.1	0.2	1.2	0.4	0.1	0.2	< 0.1	0.1
	Ce	0.1	45.1	23.2	41.7	21.5	13.5	20.9	27.7	18.9	24.2	33.3
	Cs	0.1	< 0.1	< 0.1	< 0.1	< 0.1	< 0.1	0.2	< 0.1	< 0.1	< 0.1	< 0.1
	Dy	0.02	9.23	7.48	8.5	6.09	5.95	6.74	9.56	6.01	8.66	8.84
	Er	0.01	4.56	4.41	4.92	3.54	3.64	3.58	5.59	3.5	5.2	5.08
	Eu	0.005	2.21	2.12	1.83	1.59	1.42	1.65	1.99	1.6	1.98	2.35
	Ga	1	19	19	23	18	17	26	20	30	29	21
	Gd	0.02	8.74	6.92	7.62	5.66	5.18	7.06	8.62	5.65	7.88	8.56
	Ge	0.5	1.9	2.2	2	2.4	2.3	1.9	2.8	3.1	3	3.3
	Hf	0.1	3.2	3.7	4.3	2.9	2.5	4.2	3.7	3	2.6	3.9
	Ho	0.01	1.63	1.47	1.63	1.19	1.19	1.21	1.83	1.19	1.73	1.7
	In	0.1	< 0.1	< 0.1	< 0.1	< 0.1	< 0.1	< 0.1	< 0.1	< 0.1	0.1	< 0.1
	La	0.05	17.2	7.97	18.4	8.67	4.66	6.92	10.4	6.91	7.93	12.8
	Lu	0.002	0.568	0.605	0.668	0.49	0.511	0.494	0.775	0.506	0.726	0.702
	Nb	0.2	9	4.7	11.3	3.5	2.8	8.7	6.1	8.9	7	5.5
	Nd	0.05	27.4	17.6	23.2	14.5	11.3	18.4	20.7	14.2	20.1	22.6
	Pr	0.02	6.02	3.49	5.1	3.03	2.13	3.44	4.01	2.79	3.77	4.74
	Rb	2	55	5	7	4	3	58	3	7	36	12
	Sm	0.01	7.68	5.42	6.37	4.44	3.71	5.68	6.35	4.43	6.27	6.59
	Sn	1	< 1	< 1	< 1	1	1	2	1	4	1	1
	Ta	0.1	2.4	1.6	3	1.7	1.3	1.1	1.6	1.3	1.4	1.4
	Tb	0.01	1.59	1.22	1.44	1.03	0.97	1.23	1.6	1.01	1.44	1.46
	Th	0.05	0.6	0.78	1.48	0.73	0.53	0.29	1.12	0.95	0.58	0.65
	Tl	0.05	0.38	< 0.05	0.06	0.05	< 0.05	0.34	< 0.05	< 0.05	0.15	0.07
	Tm	0.005	0.664	0.679	0.744	0.564	0.557	0.548	0.883	0.551	0.805	0.772
	U	0.05	1.21	0.75	0.76	0.54	0.64	0.67	2.43	0.87	0.32	0.36
	Yb	0.01	4.16	4.37	4.78	3.54	3.54	3.52	5.65	3.53	5.13	4.91
	Zr	1	114	143	157	107	96	163	141	115	78	155
TD-ICP	Trace Elements (ppm, *-%)											
	Ag	0.5	< 0.5	< 0.5	< 0.5	< 0.5	< 0.5	< 0.5	< 0.5	< 0.5	< 0.5	< 0.5
	Cd	0.5	0.7	0.7	1.4	0.6	0.7	0.9	0.7	1	0.7	1
	Cu	1	28	29	446	27	6	191	133	12	39	19
	Ni	1	31	27	14	65	85	86	47	62	44	36
	Pb	5	< 5	< 5	< 5	< 5	7	< 5	< 5	9	< 5	< 5
	S	0.00001*	0.093	0.118	0.284	0.038	0.007	0.432	0.205	0.008	0.124	0.064
	Zn	1	149	123	189	88	97	261	110	251	149	135

Table 3-4 - Whole-rock major and trace element data for representative Catamount Gap amphibolite samples in the Dahlonega gold belt.

			Catamount Gap amphibolite									
Sample ID			CG1	CG2	CG3	CG4	CG6	CG7B	CG8	CG9	CG10	CG11
Analysis Type	Detection Limit											
FUS-ICP												
	SiO_2	0.01	53.87	52.07	48.43	48.09	47.77	47.04	47.66	48.95	49.7	48.06
	Al_2O_3	0.01	15.98	15.64	14.62	16.7	18.91	16.52	14.6	14.47	16.78	16.24
	Fe_2O_3 (T)	0.01	10.32	10.87	13.06	10.59	14.82	12.02	15.61	12.69	11.54	12.17
	MnO	0.001	0.163	0.154	0.219	0.159	0.2	0.201	0.283	0.222	0.172	0.204
	MgO	0.01	6.27	6.6	6.89	8.27	7.7	6.63	6	6.81	6.49	6.89
	CaO	0.01	8.03	7.56	10.81	11.75	2.85	11.32	9.17	9.57	8.93	10.31
	Na_2O	0.01	1.47	1.18	0.73	0.96	1.89	1.53	0.95	1.25	2.01	2.29
	K_2O	0.01	1.12	1.75	0.22	0.73	2.81	0.79	0.57	0.85	0.85	0.83
	TiO_2	0.001	1.453	1.686	1.758	1.299	1.75	1.806	2.813	1.889	1.64	1.714
	P_2O_5	0.01	0.2	0.22	0.17	0.2	0.12	0.19	0.42	0.21	0.19	0.17
	LOI	0.01	1.25	2.396	3.092	1.679	0.968	2.116	2.298	3	1.764	1.017
	TOTAL		100.1	100.1	99.99	100.4	99.8	100.2	100.4	99.92	100.1	99.89
	Trace Elements (ppm)											
	Ba	1	149	686	146	30	902	116	122	192	224	118
	Be	1	4	5	3	5	1	2	2	3	2	3
	Sr	2	217	170	176	196	136	370	143	220	236	298
	V	5	265	285	339	260	341	305	425	364	288	322
	Y	1	29	45	41	25	44	37	73	38	37	32
INAA	Trace Elements (ppm, *-ppb)											
	As	1	< 1	< 1	< 1	< 1	< 1	< 1	< 1	< 1	< 1	< 1
	Au	1	1	< 1	2	< 1	1	< 1	1	< 1	< 1	3
	Br	0.5	< 0.5	< 0.5	< 0.5	< 0.5	< 0.5	< 0.5	< 0.5	< 0.5	< 0.5	< 0.5
	Co	0.1	38.4	34.8	46.5	47.2	36.3	42.4	42.3	39	39.3	41.9
	Cr	0.5	179	215	240	194	284	179	126	198	182	201
	Hg	1	< 1	< 1	< 1	< 1	< 1	< 1	< 1	< 1	< 1	< 1
	Ir	1	< 1	< 1	< 1	< 1	< 1	< 1	< 1	< 1	< 1	< 1
	Mo	2										
	Sb	0.1	< 0.1	< 0.1	< 0.1	< 0.1	0.6	< 0.1	< 0.1	< 0.1	< 0.1	< 0.1
	Sc	0.01	33.4	40	47.7	35.9	47.9	35.4	41.3	48.5	35	37.9
	Se	0.5	0.7	< 0.5	< 0.5	< 0.5	< 0.5	< 0.5	< 0.5	< 0.5	< 0.5	< 0.5
	W	1	2	< 1	< 1	< 1	< 1	< 1	1	< 1	< 1	< 1
FUS-MS	Trace Elements (ppm)											
	Bi	0.1	< 0.1	< 0.1	< 0.1	0.1	< 0.1	< 0.1	< 0.1	< 0.1	< 0.1	< 0.1
	Ce	0.1	25.5	50.1	19.9	12	20.1	17.4	40.6	28.1	31.2	18.5
	Cs	0.1	0.4	0.1	< 0.1	< 0.1	0.4	< 0.1	< 0.1	< 0.1	< 0.1	0.1
	Dy	0.02	5.65	9	7.87	4.62	8.17	6.95	13.4	7.34	7.07	6.26
	Er	0.01	3.17	5.11	4.71	2.75	4.92	4.17	8.18	4.38	4.14	3.74
	Eu	0.005	1.52	1.95	1.91	1.33	1.49	1.72	2.94	2.15	1.89	1.63
	Ga	1	20	21	22	24	26	19	21	20	20	19
	Gd	0.02	5.19	8.33	6.48	4.07	6.73	5.94	11.6	6.57	6.34	5.41
	Ge	0.5	1.3	1.5	1.5	1.7	1.5	1.4	1.6	2	1.5	1.7
	Hf	0.1	3.1	5.2	3.2	2.2	2.8	3.3	6.9	3.5	4.1	3
	Ho	0.01	1.1	1.76	1.6	0.94	1.68	1.41	2.8	1.48	1.43	1.27
	In	0.1	< 0.1	< 0.1	< 0.1	< 0.1	< 0.1	< 0.1	< 0.1	< 0.1	< 0.1	< 0.1
	La	0.05	9.95	20.6	7.16	3.77	9.1	5.48	13	10.4	11.7	6.22
	Lu	0.002	0.464	0.699	0.671	0.4	0.692	0.585	1.17	0.611	0.61	0.532
	Nb	0.2	5.8	8.4	3	4.2	5.2	2.7	5.6	3.9	4.3	3.5
	Nd	0.05	16.1	29.4	15.5	9.84	11.6	14.1	31.3	18.9	19.4	14
	Pr	0.02	3.33	6.32	2.95	1.83	2.37	2.64	5.9	3.81	4.02	2.7
	Rb	2	48	51	< 2	9	180	6	14	20	22	14
	Sm	0.01	4.18	7.06	4.69	3	3.8	4.29	8.98	5.16	5.13	4.05
	Sn	1	2	2	6	4	< 1	1	2	1	< 1	1
	Ta	0.1	0.6	0.5	0.2	0.1	0.2	0.2	0.4	0.2	0.2	0.2
	Tb	0.01	0.93	1.52	1.23	0.73	1.33	1.12	2.15	1.19	1.16	0.99
	Th	0.05	1.26	4.02	0.75	0.25	1.05	0.6	1.3	0.67	1.62	0.44
	Tl	0.05	0.24	0.28	< 0.05	0.07	0.97	0.06	0.07	0.08	0.12	0.11
	Tm	0.005	0.471	0.737	0.696	0.41	0.742	0.619	1.21	0.648	0.621	0.555
	U	0.05	0.93	1.25	0.54	0.32	0.33	0.45	0.91	0.29	0.71	0.46
	Yb	0.01	3.06	4.65	4.46	2.66	4.75	3.96	7.93	4.18	4.05	3.59
	Zr	1	116	179	118	79	103	126	254	125	150	109
TD-ICP	Trace Elements (ppm, *-%)											
	Ag	0.5	< 0.5	< 0.5	< 0.5	< 0.5	< 0.5	< 0.5	< 0.5	< 0.5	< 0.5	< 0.5
	Cd	0.5	< 0.5	< 0.5	< 0.5	< 0.5	< 0.5	< 0.5	< 0.5	< 0.5	< 0.5	< 0.5
	Cu	1	10	2	15	3	14	18	33	6	12	6
	Ni	1	69	53	45	122	59	74	58	32	42	54
	Pb	5	17	15	18	16	12	15	12	9	10	11
	S	0.001*	0.063	0.013	0.03	0.018	0.075	0.098	0.209	0.051	0.049	0.041
	Zn	1	94	181	89	116	305	77	109	120	115	95

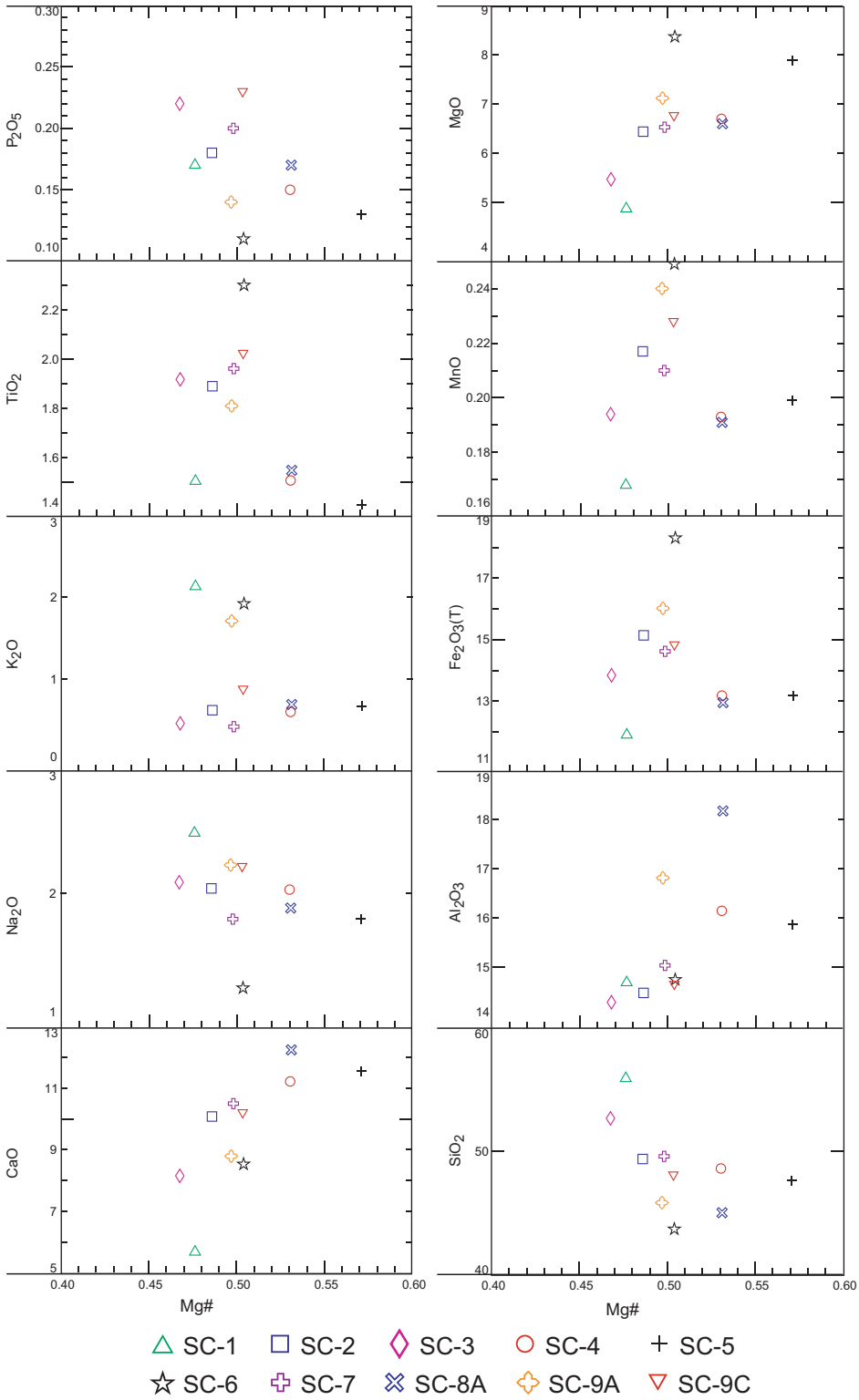


Figure 3-10. Bivariate diagram of major oxides (wt/ %) compared to Mg # for amphibolite blocks collected from the Savannah Church block-in-matrix exposure. Mg # is 100[MgO/(MgO+FeO)].

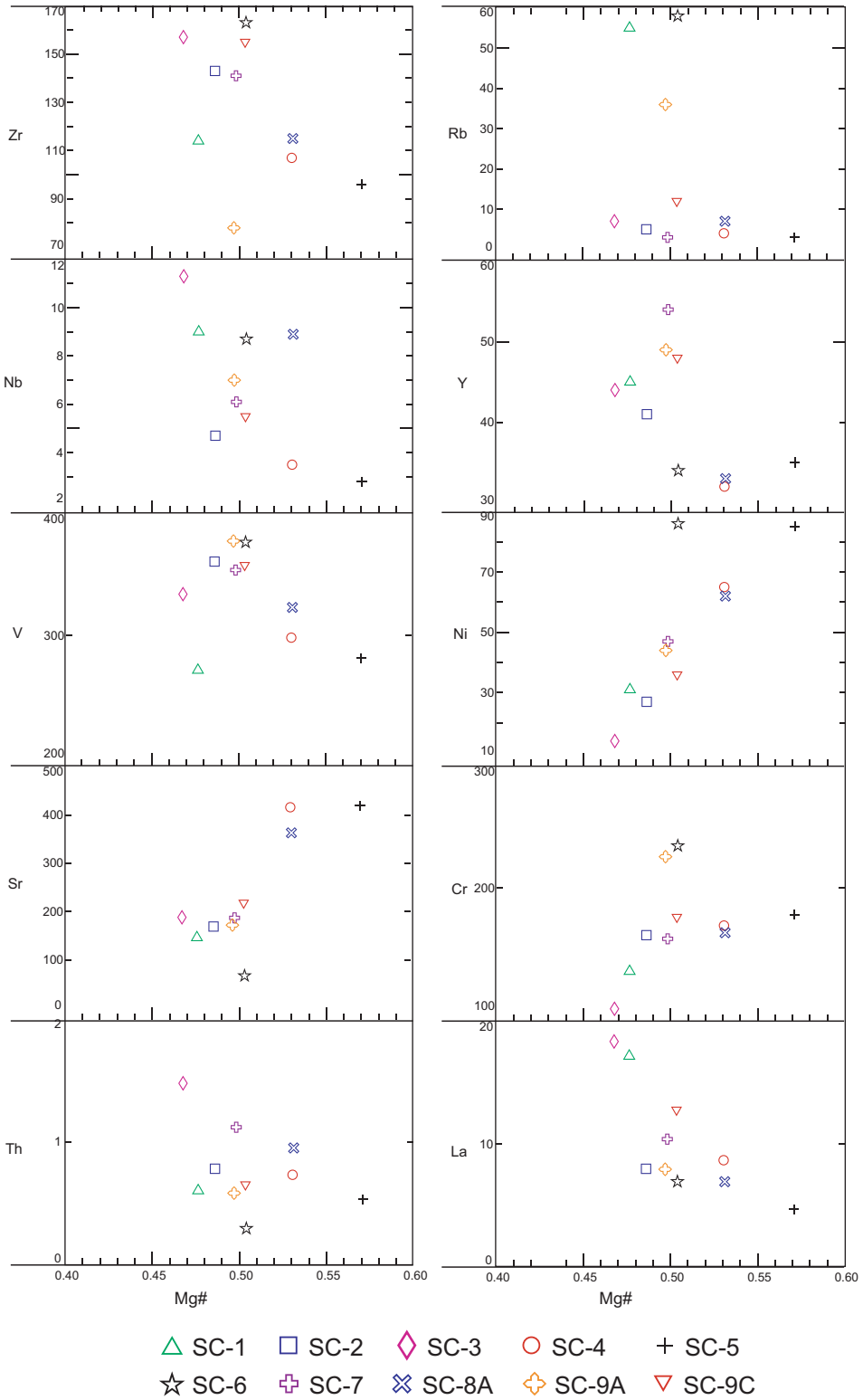


Figure 3-10 (continued). Bivariate diagram of major oxides (wt/ %) compared to Mg # for amphibolite blocks collected from the Savannah Church block-in-matrix exposure. Mg # is 100[MgO/(MgO+FeO)].

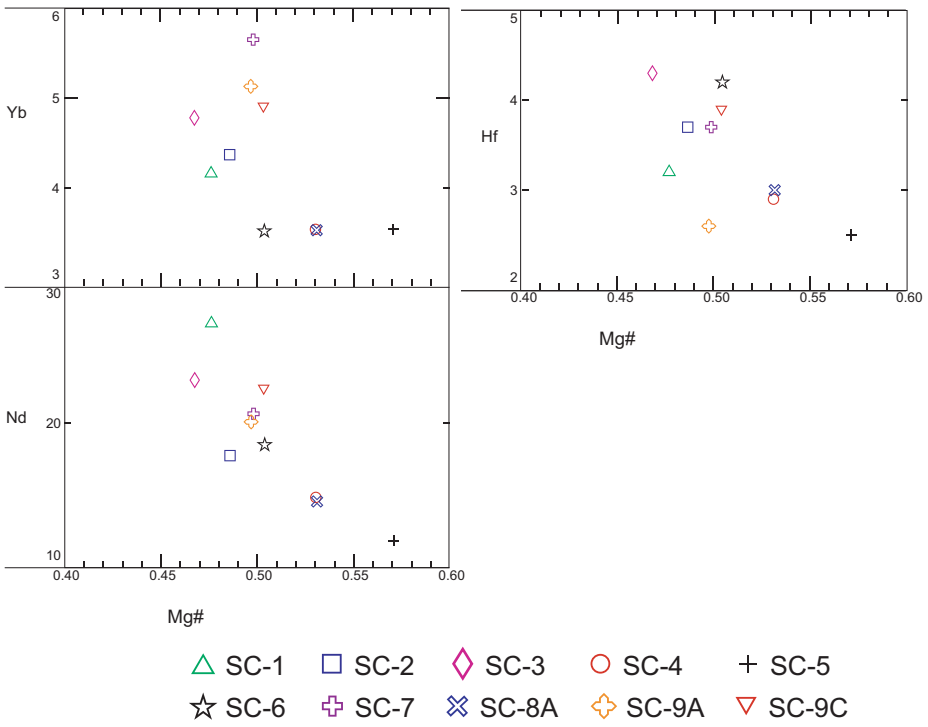


Figure 3-10 (continued). Bivariate diagram of major oxides (wt/ %) compared to Mg # for amphibolite blocks collected from the Savannah Church block-in-matrix exposure. Mg # is 100[MgO/(MgO+FeOz)].

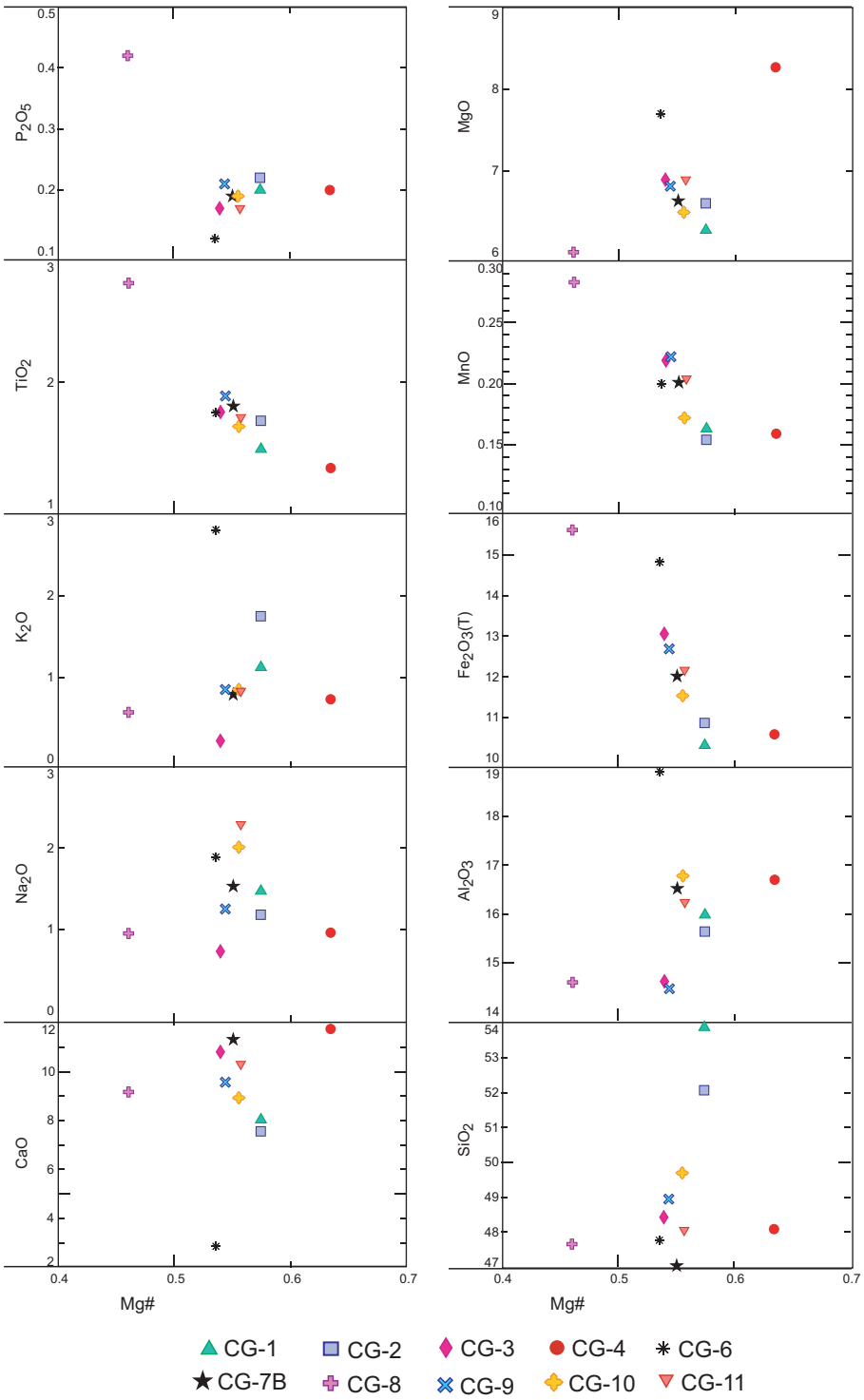


Figure 3-10 (continued). Bivariate diagram of select trace elements (ppm) compared to Mg # for amphibolite blocks collected from the Catamount Gap block-in-matrix exposure. Mg # is 100[MgO/(MgO+FeO)].

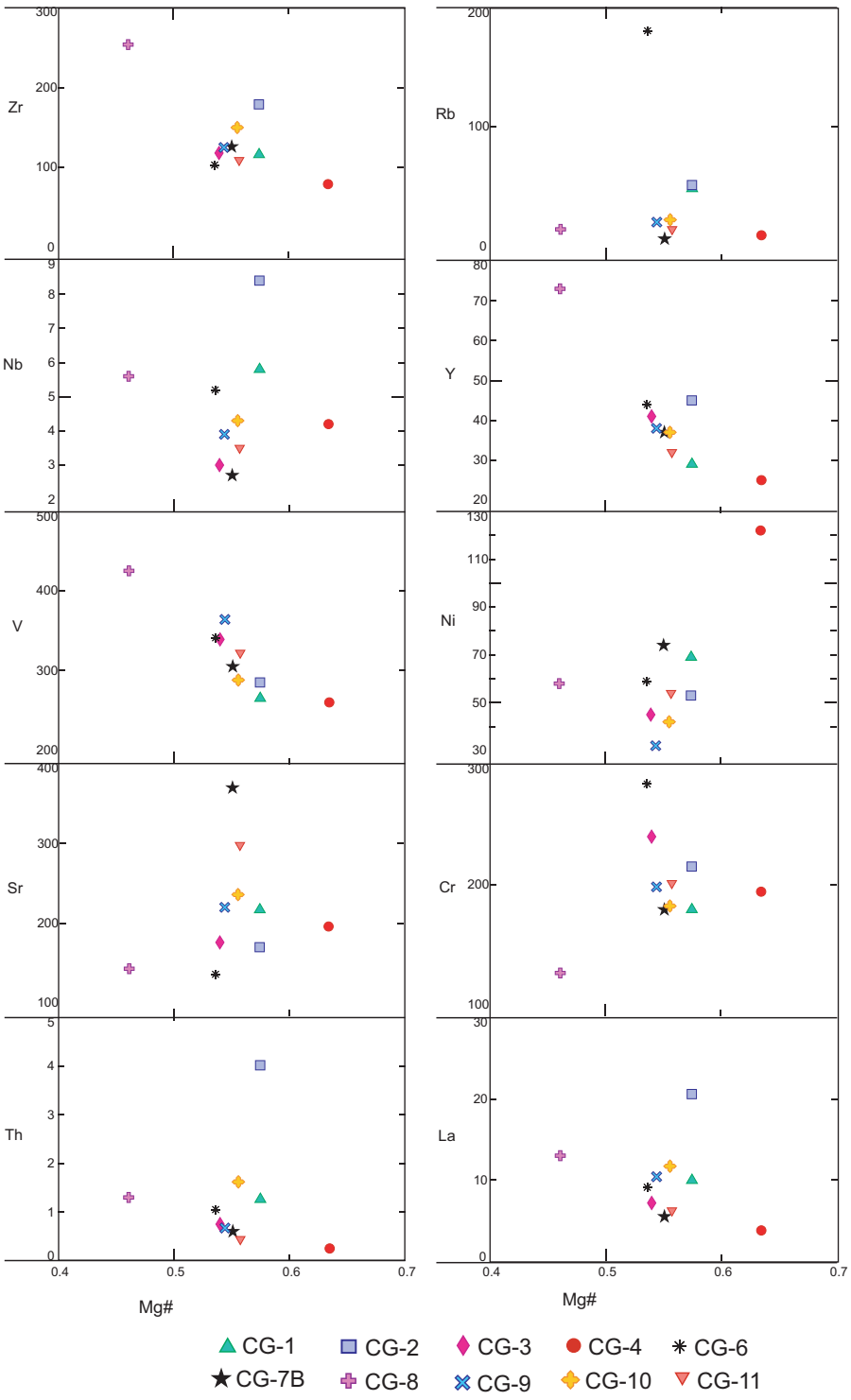


Figure 3-10 (continued). Bivariate diagram of major oxides (wt/ %) compared to Mg # for amphibolite blocks collected from the Catamount Gap block-in-matrix exposure. Mg # is 100[MgO/(MgO+FeO)].

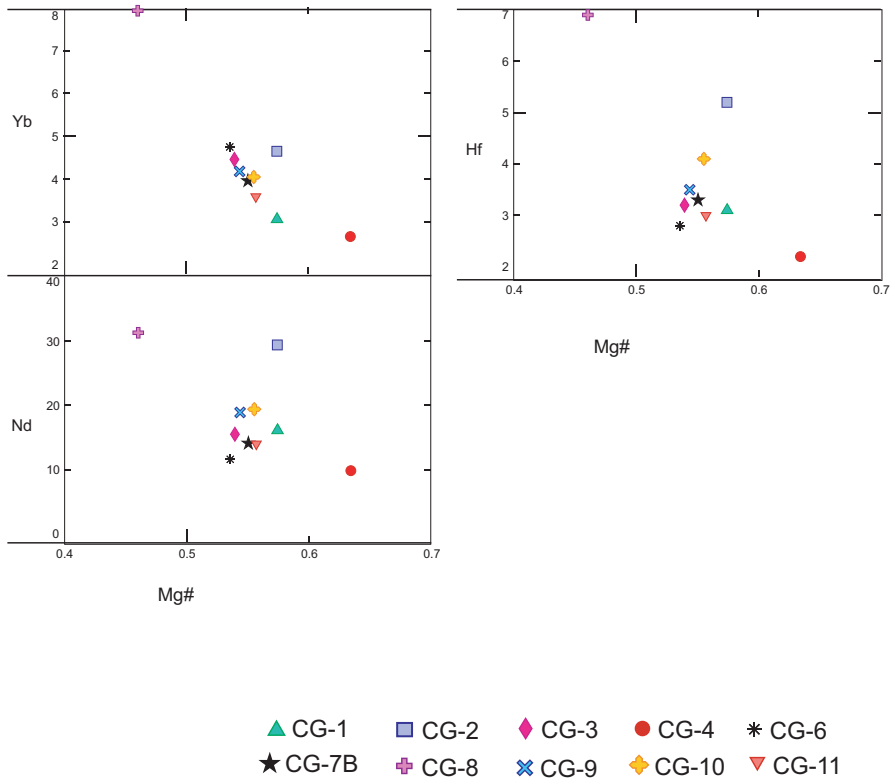


Figure 3-10 (continued). Bivariate diagram of major oxides (wt/ %) compared to Mg # for amphibolite blocks collected from the Catamount Gap block-in-matrix exposure. Mg # is 100[MgO/(MgO+FeO)].

and Al_2O_3. The elements Nb, Y, and La all decrease with increasing Mg number, and Sr, Cr, and Ni increase. In the CG samples TiO_2, MnO, Zr, V, and Y decrease with increasing Mg number. Alumina (Al_2O_3) and Cr, however, display a positive trend with increasing Mg number.

The trace element Zr is also useful as a fractionation index. Unlike the Mg number, Zr concentration increases as fractionation proceeds. For all SC samples (Fig. 3-11) both Al_2O_3 and Na_2O decrease. There is an increase in V, Th, Yb, Nd, La, and Hf with increasing Zr. In the CG samples (Fig. 3-11) there is an increase in K_2O and SiO_2 and a slight increase in TiO_2 and P_2O_5 with increasing Zr, and a decrease in MgO and Al_2O_3. The trace elements that increase with increasing Zr are Y, Th, Yb, Nd, La, and Hf; Cr is the only trace element that decreases. The major oxides TiO_2, P_2O_5, and MnO increase with increasing Zr.

Trace-element geochemistry

Amphibolite samples collected from the SC and CG exposures are normalized for the MORB diagram of Pearce (1983) (Fig. 3-12). Excluding Sr, which is depleted in comparison to other LILE, both data sets are enriched in the majority of the LILE giving the elements an overall “spikey” appearance on the left side of the diagram. The HFSE to the right side of the diagram have a relatively flat pattern and are lesser in abundance than the LILE. This trend does not include La, Cs, and Nd, which are slightly enriched.

All SC samples are greatly depleted in P compared to CG samples. SC-1 SC-6, and SC-9A have a spike in Rb between 10 and 100. All samples contain relatively high amounts of Ba, some more so than others. Samples SC6, SC1, SC9A contain Ba amounts between 80–20; all other samples contain Ba values between 3 and 12. For the SC samples, SC6 exhibits the greatest variance in LILE and has the lowest values of Sr and Th and highest values of Rb and Ba.

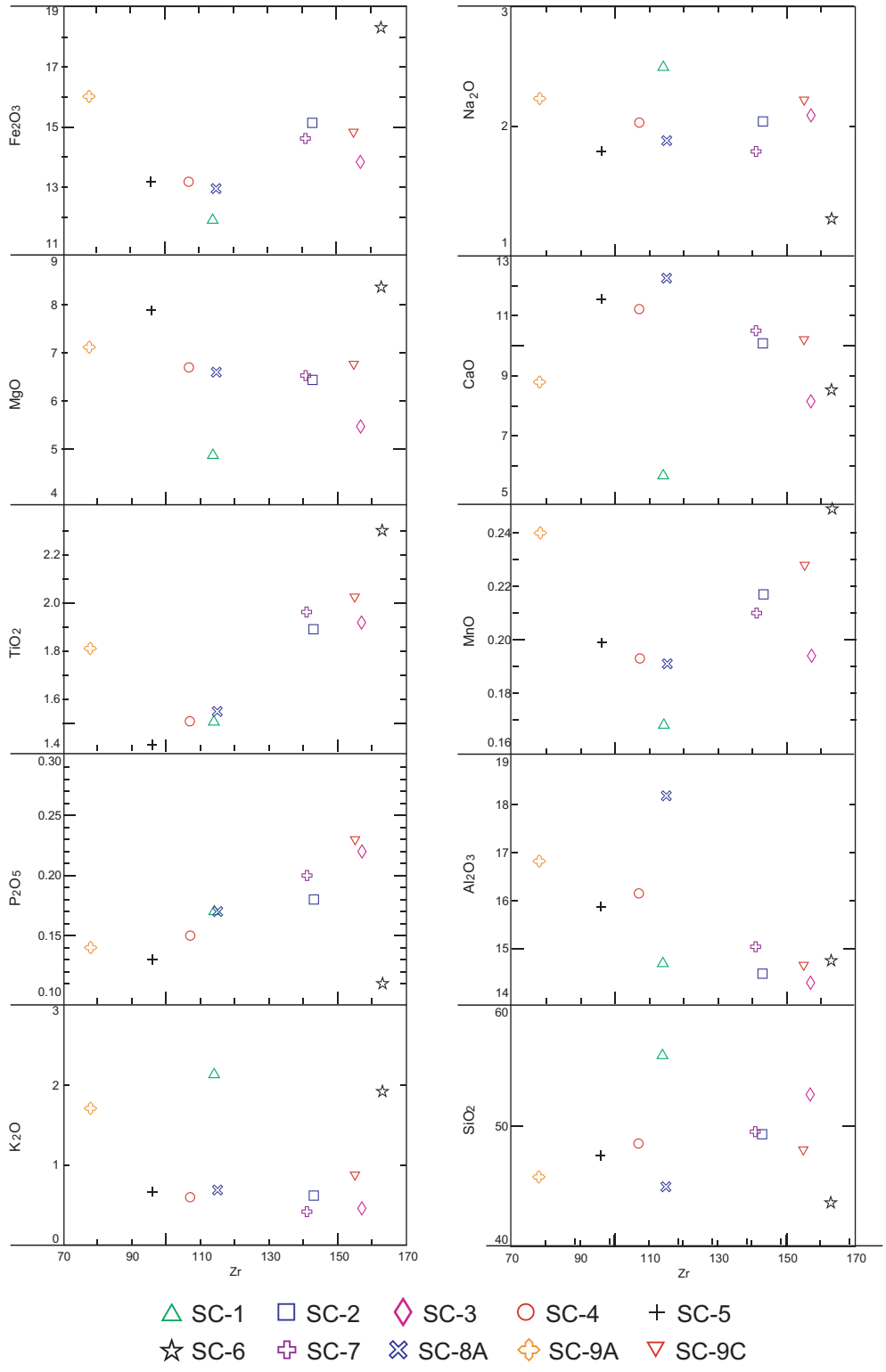


Figure 3-11. Bivariate diagram of major oxides (wt. %) compared to Zr (ppm) for amphibolite blocks collected from the Savannah Church block-in-matrix exposure.

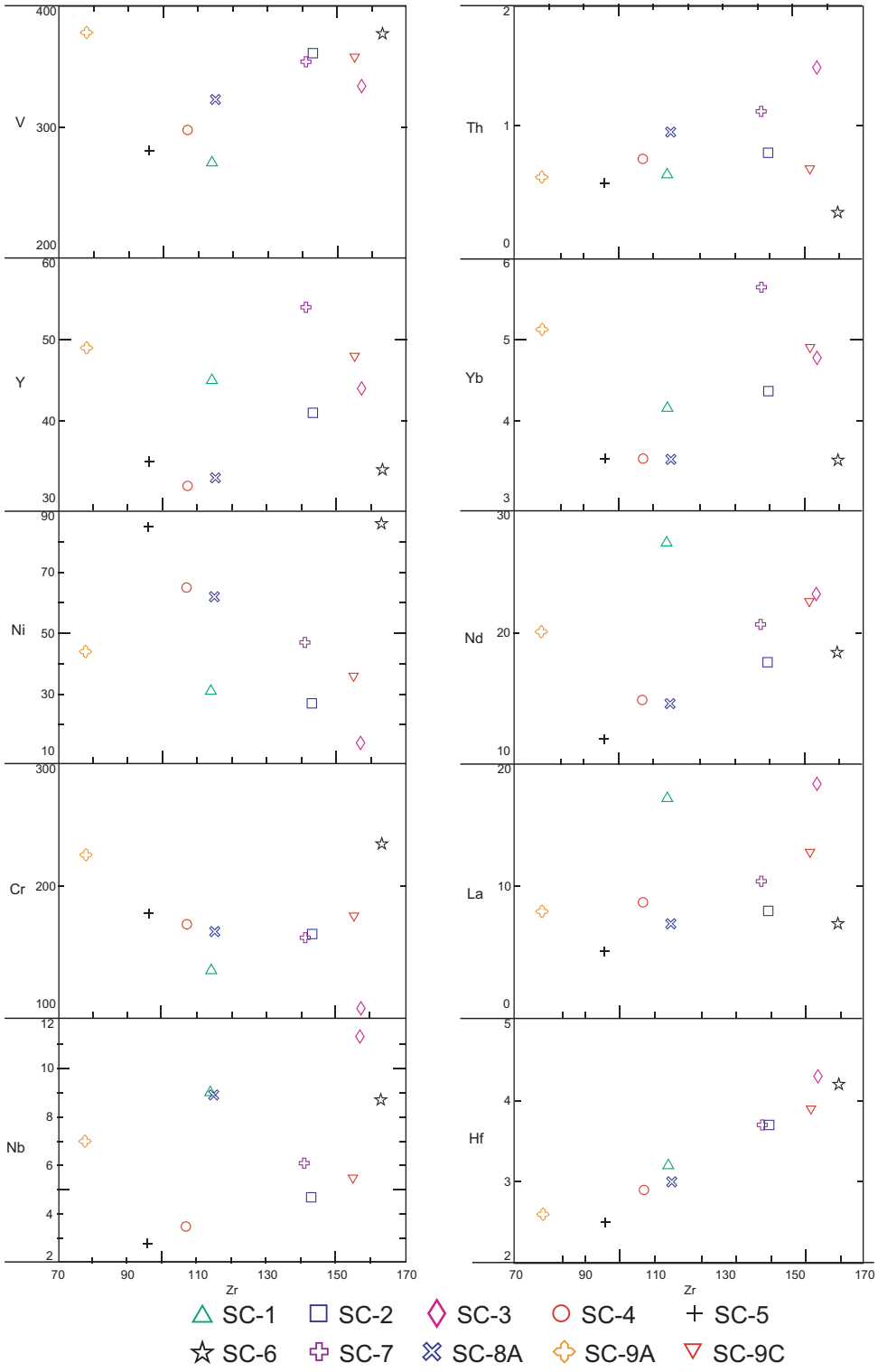


Figure 3-11 (continued). Bivariate diagram of major oxides (wt. %) compared to Zr (ppm) for amphibolite blocks collected from the Savannah Church block-in-matrix exposure.

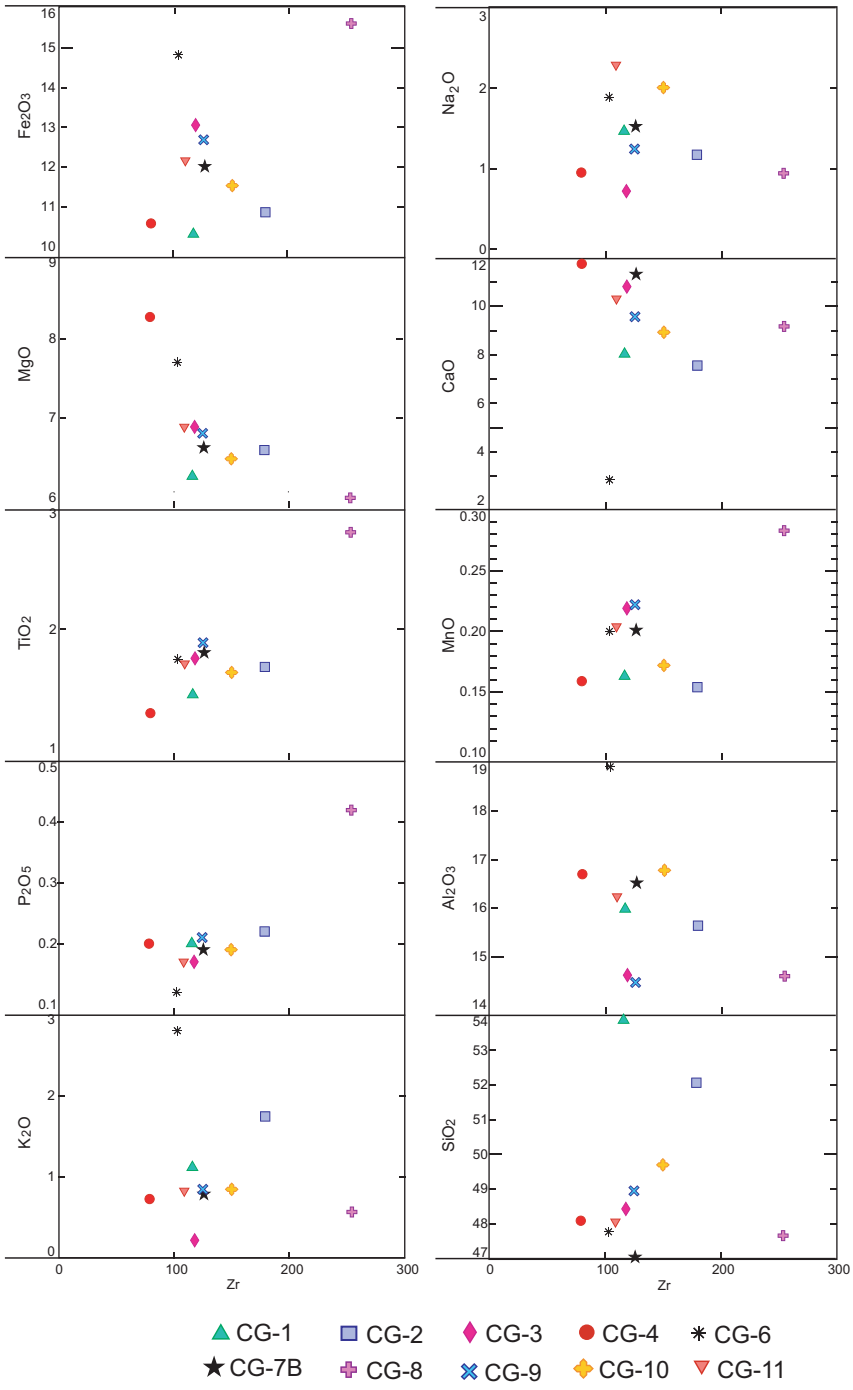


Figure 3-11 (continued). Bivariate diagram of major oxides (wt. %) compared to Zr (ppm) for amphibolite blocks collected from the Catamount Gap block-in-matrix exposure.

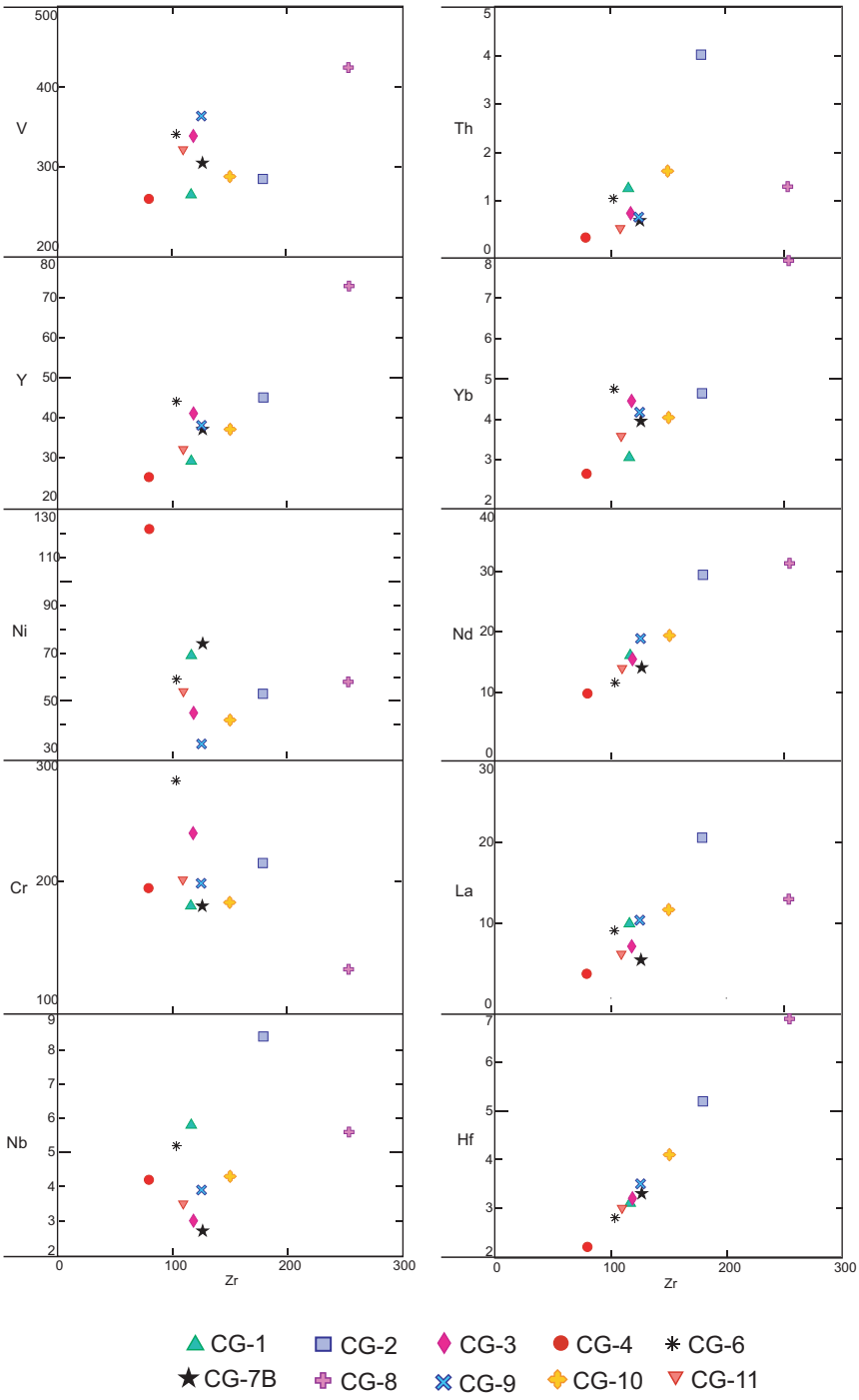


Figure 3-11 (continued). Bivariate diagram of major oxides (wt. %) compared to Zr (ppm) for amphibolite blocks collected from the Catamount Gap block-in-matrix exposure.

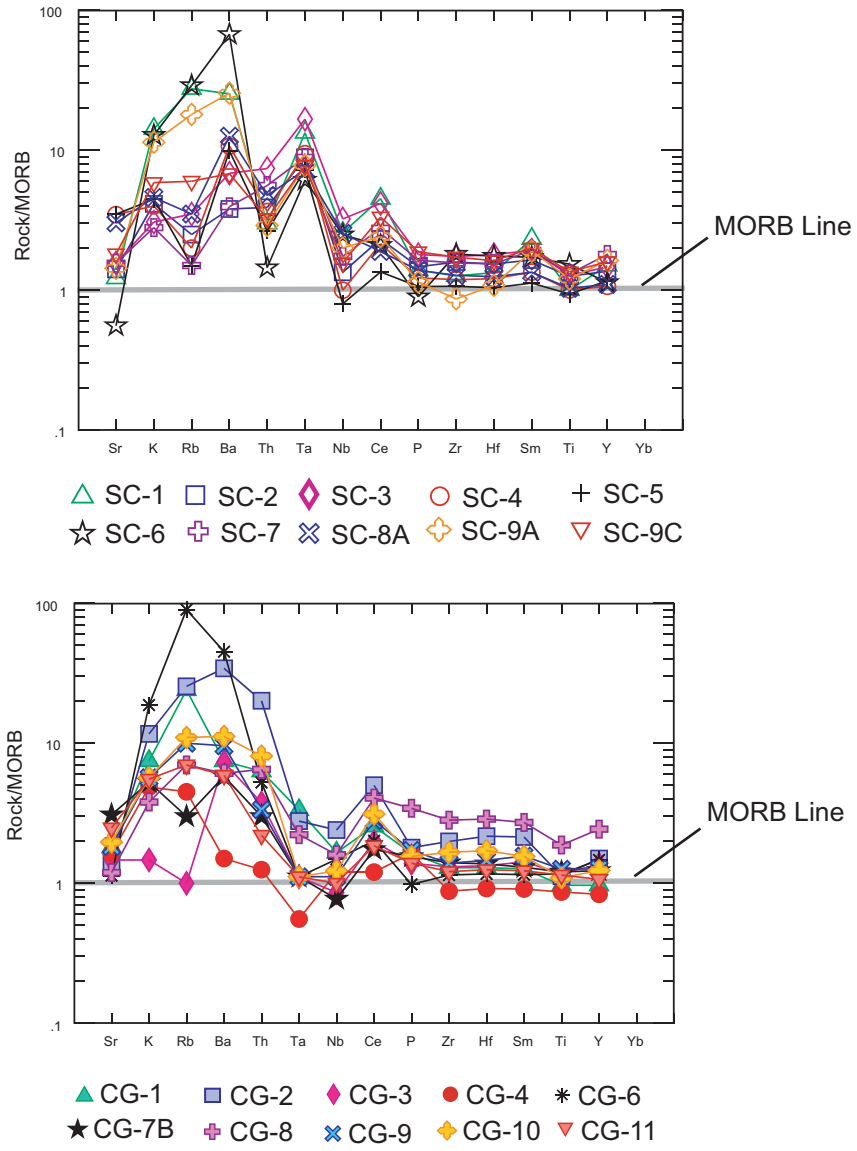


Figure 3-12. Normalized MORB diagram of Pearce (1983) for Savannah Church (SC) and Catamount Gap (CG) samples.

Amphibolite samples collected at the CG exposure have a similar trend to the SC samples in that they are enriched in LILE and display a flat HFSE pattern. Some differences are apparent: for example CG samples have a greater range in K, Rb, Ba, and Th compared with to the SC samples. In addition, CG samples have a negative Ta anomaly, whereas SC samples show a positive Ta anomaly. Sample CG2 and CG6 contain the largest range in LILE values, and have a relatively flat HFSE trend; CG4 has low values for Ba, Th, and Ta. The remaining CG samples have a similar trend in the LILE, between values of 1 and 10. All CG samples have a minor Nb depletion and a minor spike in Ce. Both SC and CG samples have a positive spike for Ba in the MORB normalized spider diagram (Fig. 3-12).

REE geochemistry

The overall trend for the REE diagrams for the SC and CG datasets is very similar. The chondrite-normalized diagram (Sun and McDonough, 1989) are slightly enriched in LREE and contain less HREE in comparison (Fig. 3-13).

Alkaline vs subalkaline basalts

Alkali and subalkaline (tholeiitic) basalt diagrams (Fig. 3-14 a) show that both SC and CG samples plot in the tholeiite basalt field indicating that these samples are silica enriched. The AFM diagram of Irvine and Baragar (1971) plot the samples as immature calc-alkaline basalts (Fig. 3-14b). Figure 3-15 also plots the samples as sub-alkaline tholeiitic basalts (Floyd and Winchester, 1975; Winchester and Floyd, 1976).

Tectonic discrimination diagrams

The majority of the tectonic discrimination diagrams indicate that both the SC and CG samples plot within the MORB field; this includes the discriminant diagrams of Pearce and Cann (1973); Floyd and Winchester (1975); and the Ti-Zr diagram from Pearce and Cann (1973) (Fig. 3-16). Two diagrams plot distinctive trends between the two datasets (Fig. 3-17). The HF/3-Ta-Th diagram of Wood (1980) (Fig. 3-17b) plots a distinct difference between the SC and CG

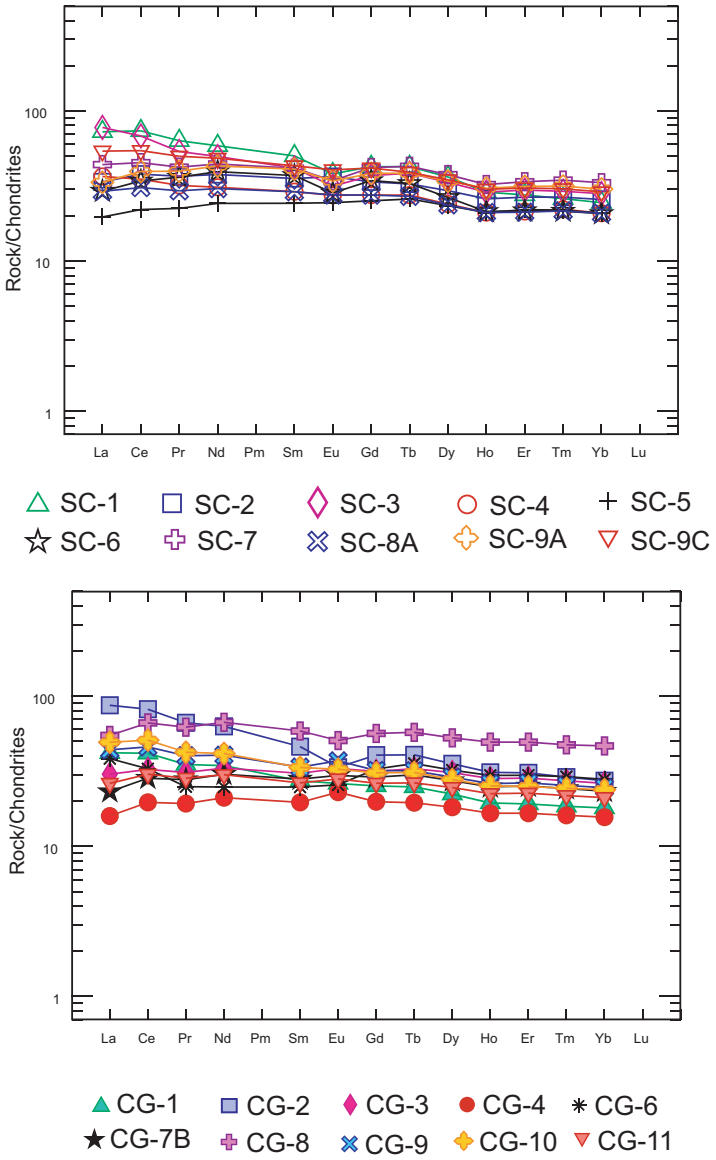


Figure 3-13. Rare earth element (REE) diagrams of Sun and McDonough (1989) of Savannah Chruch (SC) and Catamount Gap (CG) samples.

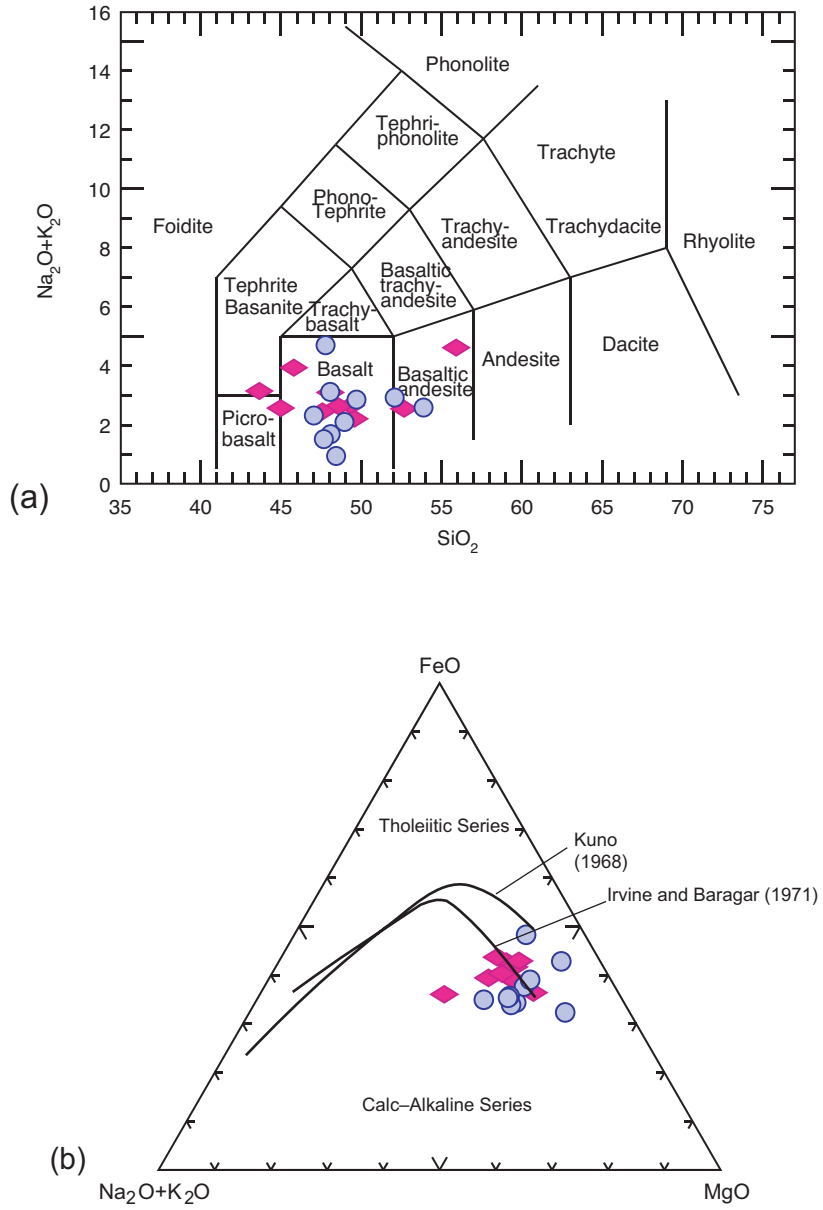


Figure 3-14. Various discriminant diagrams for amphibolite blocks from the Savannah Church (pink diamond) exposure and Catamount Gap (blue circle) exposure. (a) Alkali versus silica plot after Cox et al. (1979). (b) AFM diagram from Irvine and Baragar (1971).

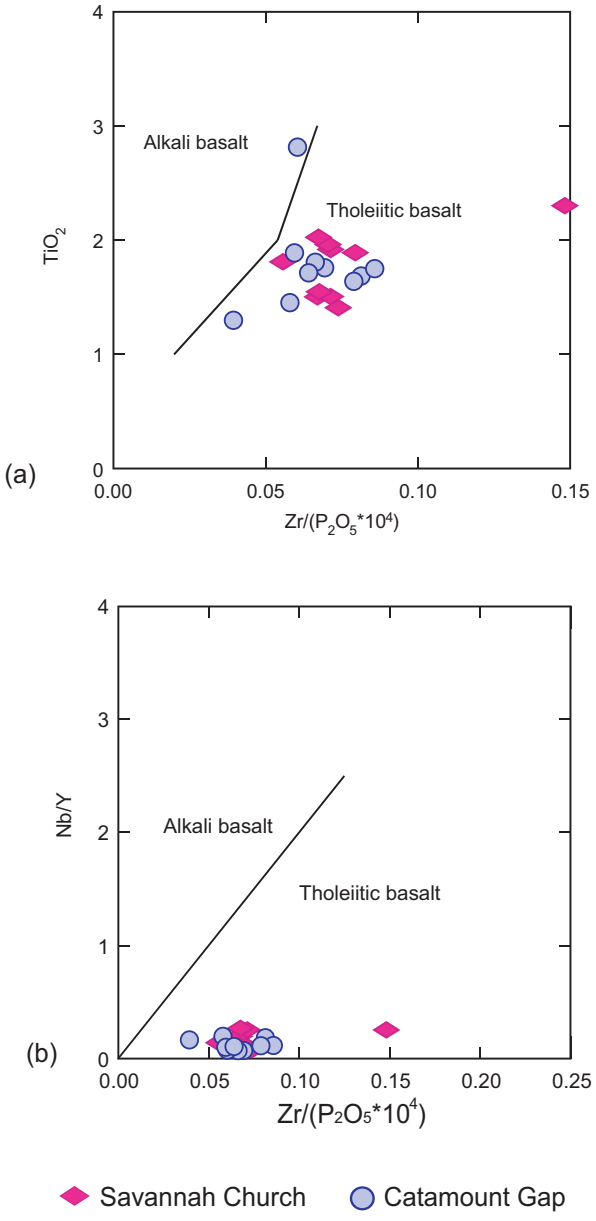


Figure 3-15. (a) TiO_2 versus $Zr/(P_2O_5*10^4)$ after Winchester and Floyd (1976). (b) Nb/Y versus $Zr/(P_2O_5*10^4)$ of Savannah Church and Catamount Gap amphibolites after Floyd and Winchester (1975).

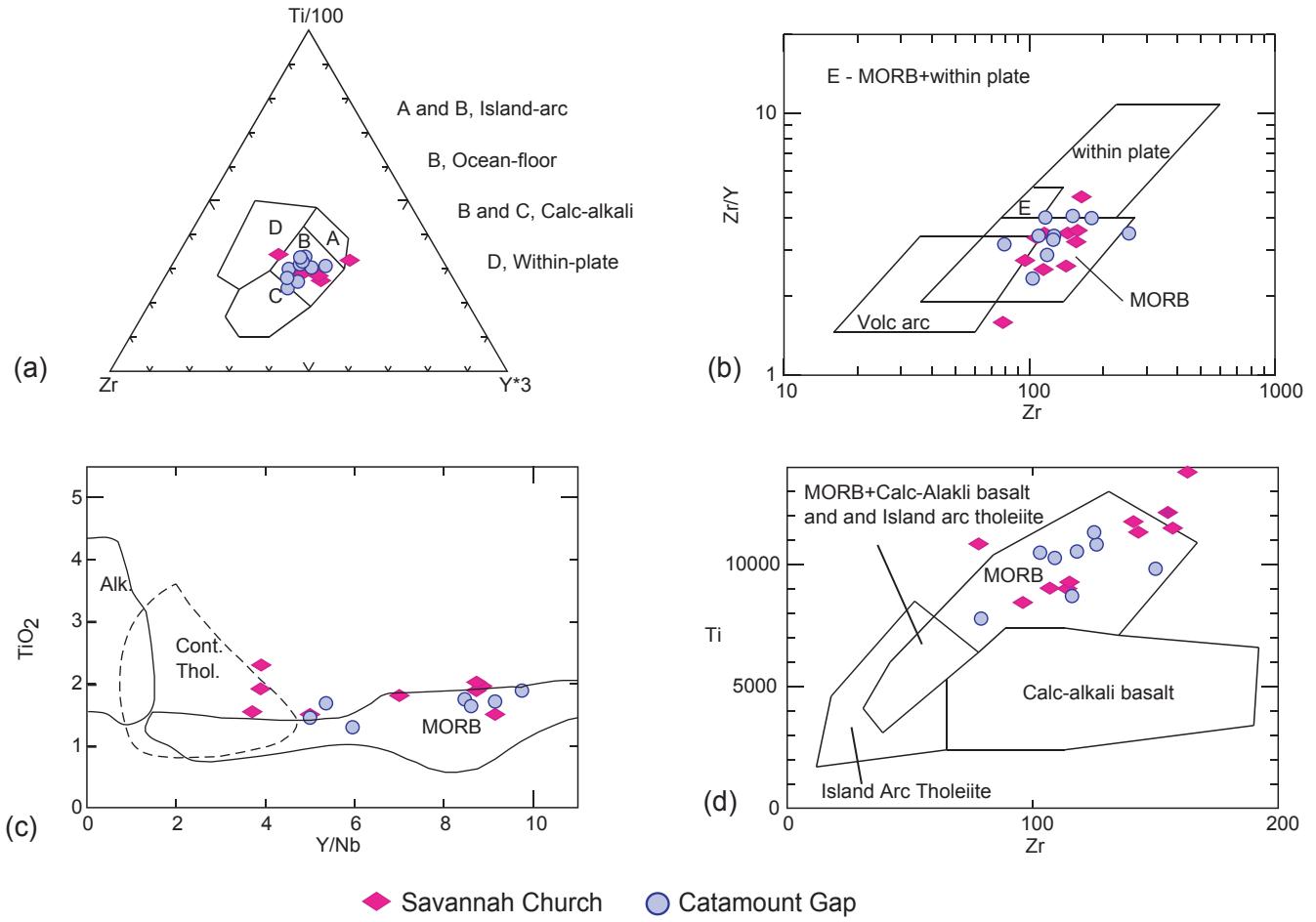


Figure 3-16. (a) Ti/100–Yx3–Zr diagram from Pearce and Cann (1973). (b) Zr/Y– Zr diagram (Pearce and Norry, 1979). (c) TiO2–Y/Nb diagram after Floyd and Winchester (1975). (d) Ti–Zr diagram from Pearce and Cann (1973).

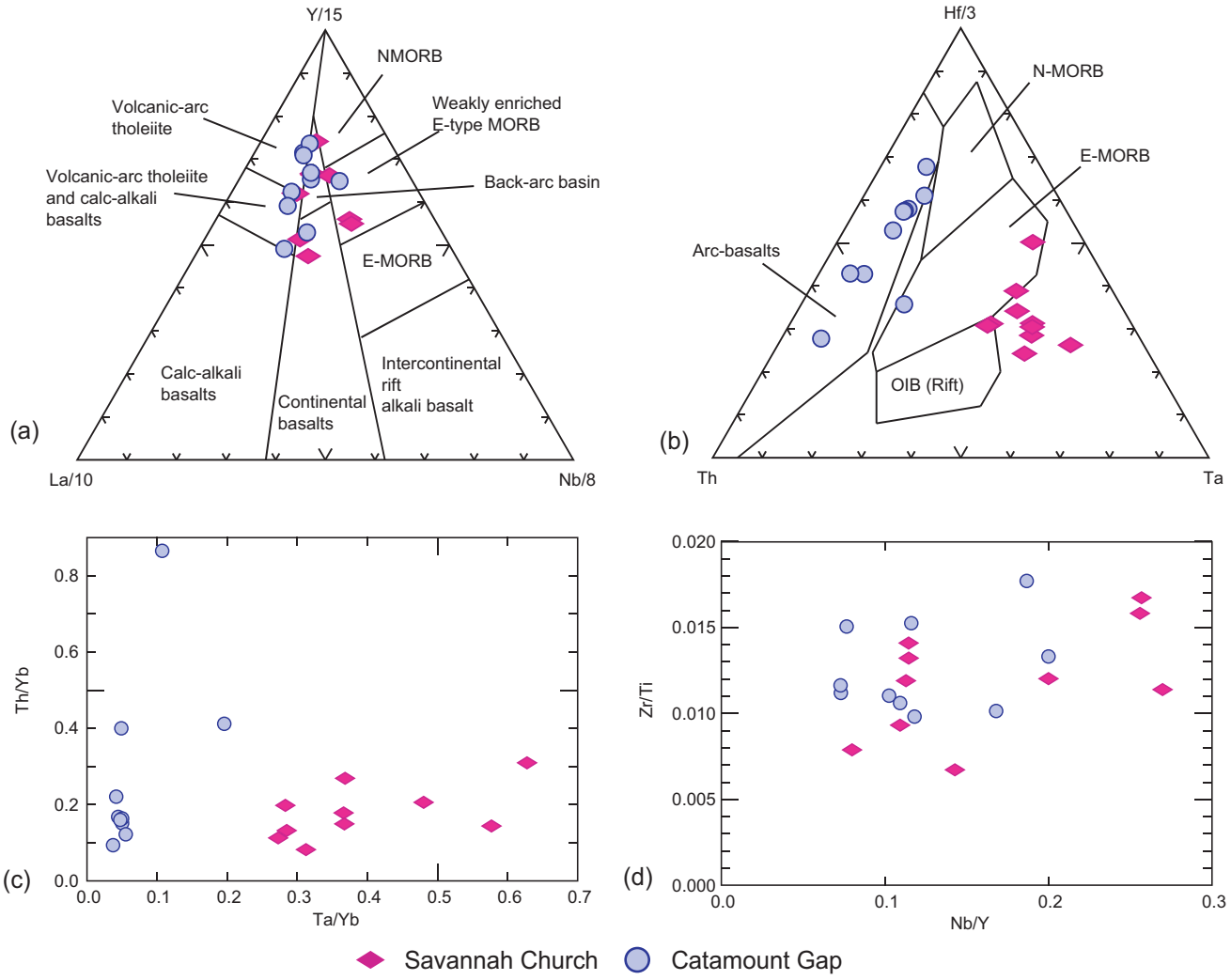


Figure 3-17. (a) La/10–Y/15–Nb/8 diagram after Cabanis and Lecolle (1989). (b) Hf/3–Ta–Th diagram Wood (1980). (c) Th/Yb versus Ta/Yb diagram (Pearce, 1983). (d) Zr/Ti–Nb/Y classification from Winchester and Floyd (1976).

samples wherein the CG samples are depleted in Ta when compared to the SC samples. Similarly, the Th/Yb versus Ta/Yb diagrams of Pearce (1983) (Fig. 3-17c) show that the CG samples have lower values of Ta/Yb when compared to the SC samples. This relationship is also notable in the multi–element diagrams mentioned earlier.

Synthesis and Discussion of Mafic Rocks

Upper-amphibolite metamorphism and multiple deformational events that affected the rocks in this area have altered the original mineral assemblage and destroyed original textures. Despite this, some conclusions are clear: amphibolite blocks collected from the SC and CG exposures have a geochemical signature indicative of an igneous protolith (Fig. 3-9). In particular, all samples consistently fall in the tholeiitic basalt field and show a clear affinity for a MORB protolith (Figs. 3-15 and 3-16). Multi-element diagrams of the SC and CG samples are somewhat inconsistent with a typical MORB trend, however; enriched LILE and the large variation in Ba, Rb, K and Ta on the

MORB normalized multi-element diagram indicate increased mobility of these elements during metasomatism that was caused by interaction with hydrothermal fluids (Plank et al., 2001). Contamination of continental signatures during metamorphism may also be a contributing factor (Fig. 3-12), and the negative Nb anomaly present in both SC and CG samples provides further evidence for crustal contamination. It is important to note that less mobile elements to the right side of the diagram fall roughly on the MORB–normalized line (Fig. 3-12). In addition, there is an overall REE trend consisting of higher concentration of LREE and relatively lower amounts of HREE in both SC and CG samples (Fig. 3-13). Fractionation of the LREE in comparison to the HREE is further evidence for continental contamination.

There is a greater range in K, Rb, Ba, and Th in the CG samples. All SC samples are greatly depleted in P; this could be due to the uptake of P as apatite is crystallized and removed from the melt. Other notable differences between the

SC and CG amphibolites are apparent in discriminant diagrams using Ta (Fig. 3-17 b-c); SC samples contain a higher amount of Ta than the CG samples. This distinction may be caused by the preferential uptake of Ta through the crystallization of illmentie, rutile, or sphene.

Most tectonic discriminant diagrams plot amphibolites from both the SC and CG block-in-matrix exposures as oceanic basalts with some scatter into the calc-alkaline and within-plate basalt fields (Fig. 3-16 a-d). The La/10–Y/15–Nb/8 diagram of Cabanis and Lecolle (1989) is the least distinctive, and all samples scatter between volcanic arc tholeiite, volcanic arc tholeiite, and calc-alkaline basalts, weakly enriched E-type MORB, back arc–basin, and continental basalts (Fig. 3-17a).

Minor inconsistencies are present in the geochemical analysis of the amphibolite samples due to crustal contamination and element mobility as a result of multiple metamorphic events. Despite these inconsistencies, there is an overall similarity in the major and trace element geochemistry of both datasets, which points toward a shared magmatic protolith. Extensive geochemical analysis indicates that amphibolites from the SC and CG exposures originated as tholeiitic basalt, which originated as MORB.

CHAPTER IV Metamorphism

Introduction

The southern Appalachians exhibit a classic Barrovian prograde metamorphic sequence from anchizone to lower greenschist facies in the western Blue Ridge foothills to granulite facies in the central Blue Ridge (Drake et al., 1989; Eckert et al., 1989; Hatcher and Goldberg, 1991). Three tectonothermal pulses have affected the Appalachians: the Taconian (510-460 Ma), Acadian (410-360 Ma), and Alleghanian (325-265 Ma), and the multiple events produce complicated overprinting of metamorphic and structural relationships.

The Soque River fault is a postmetamorphic (early to mid–Paleozoic) fault separating two central Blue Ridge terranes: the upper amphibolite to granulite paragneisses, mafic and ultramafic rocks, pelitic schist and Grenvillian basement of the Cartoogechaye terrane; and the middle to upper amphibolite facies meta-sedimentary and lesser mafic and ultramafic rocks of the Dahlonega gold belt. Southwest of the Great Balsam Mountains Window the Soque River fault separates the Cartoogechaye terrane and the Dahlonega gold belt. The postmetamorphic Chattahoochee-Holland Mountain fault frames the southerly portion of the Great Balsam Mountains Window, juxtaposing rocks of the Dahlonega gold belt and migmatitic Tugaloo terrane (Fig. 4–1).

Acker and Hatcher (unpublished) recognized that the Chattahoochee-Holland Mountain fault truncates the Rabun granodiorite. More recent work by Miller et al. (2006) and Stahr et al. (2006) demonstrated that the Rabun is a Mississippian granitoid (~335 Ma). This relationship limits emplacement of this fault to early Mississippian. Moreover, the Chattahoochee-Holland Mountain fault is tightly folded. Crosscutting relationships and geochronologic data indicate the Chattahoochee-Holland Mountain fault is Alleghanian and was emplaced at relatively high temperatures. Timing of a later, relatively high-grade metamorphic event and emplacement of the Chattahoochee-Holland Mountain

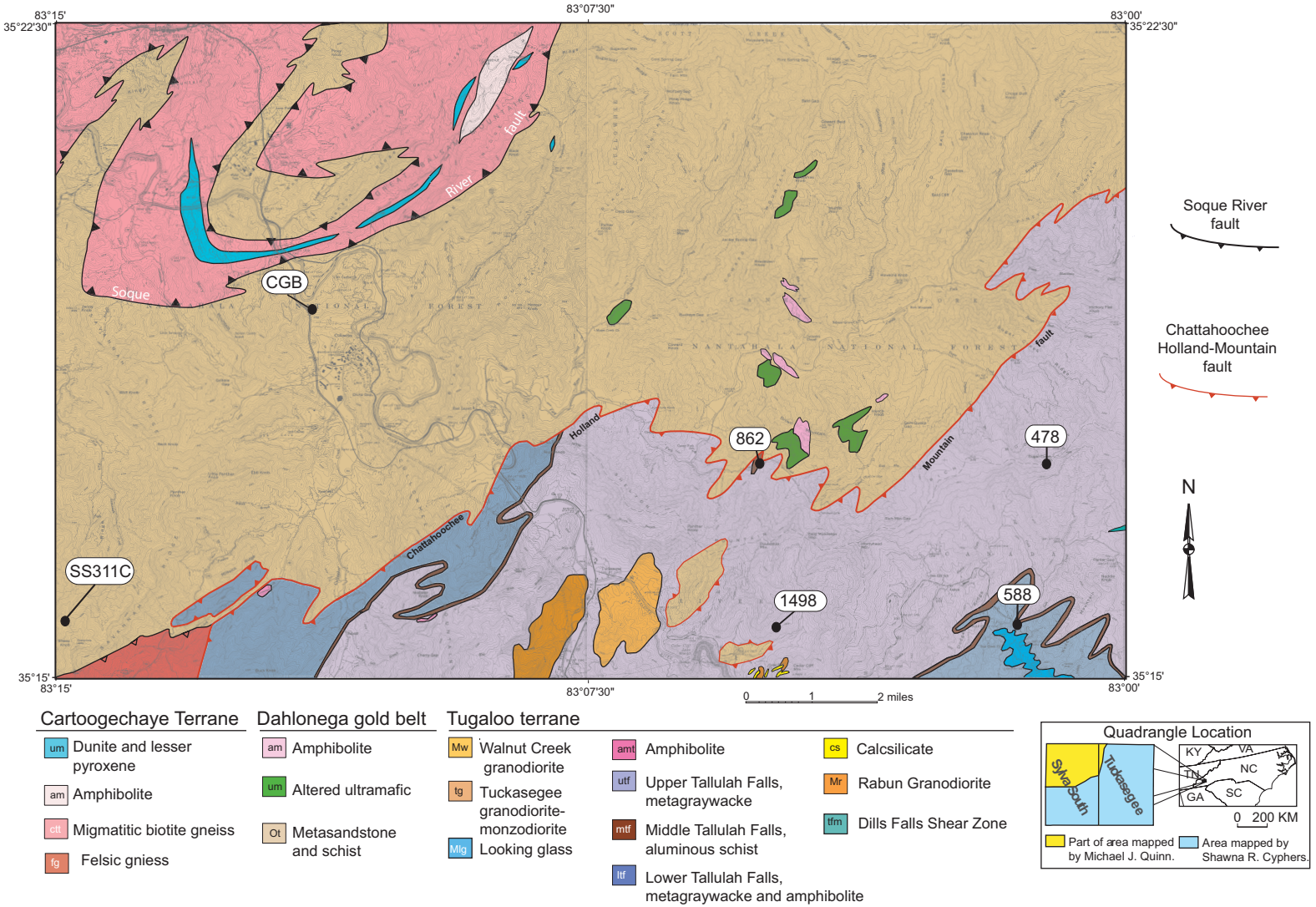


Figure 4–1. Simplified bedrock geologic map of Sylva South and Tuckaseegee quadrangles illustrating major lithologies, faults, and locations of samples collected for electron probe microanalysis.

fault during the Alleghanian complicate the previous understanding of the area and require reconsideration of the metamorphic history of this portion of the Blue Ridge and its broader implications.

Geologic Setting and Timing of Metamorphism

Hadley and Goldsmith (1963) stated that regional metamorphism in the southern Appalachians was contemporaneous with deformation likely beginning in the Ordovician and continuing throughout the Paleozoic as later orogenic pulses (Acadian and Alleghanian) shaped the mountain chain. The Blue Ridge thrust sheet comprises a large portion of the southern Appalachians and is made up of three distinct geologic regions: the western, central, and eastern Blue Ridge.

The peak metamorphic event of the western, central, and eastern Blue Ridge (western Tugaloo terrane) occurred during the Taconic (480-460 Ma) and at this time the Blue Ridge formed the metamorphic core of the Taconic orogen (Butler, 1991; Moecher et al, 2004; Hatcher et al., 2005; Merschat et al., 2006). The study area is in a section of the Blue Ridge that contains predominantly amphibolite facies assemblages with a large area to the southwest in the Cartoogechaye terrane containing granulite facies assemblages (Force, 1976; Absher and McSween, 1985; Eckert et al., 1989).

Western Blue Ridge

The western Blue Ridge is made up of Grenville basement and Neoproterozoic rifted margin to stable platform transition rocks emplaced on unmetamorphosed rocks of the Valley and Ridge. This relationship is evident in windows such as Wear Cove, Tuckaleechee Cove, and Cades Cove (Butler, 1973; Hatcher and Goldberg, 1991). Metamorphic grade in the western Blue Ridge ranges from anchizone to sillimanite grade (Fig. 4–2). Moecher et al. (2005) reported Th-U-Pb chemical ages of monazite from Great Smoky Group rocks near the Hayesville fault as 476-459 Ma. Corrie and Kohn (2007) reported U-Pb ages of monazite from the Great Smoky Mountains National Park at ~455

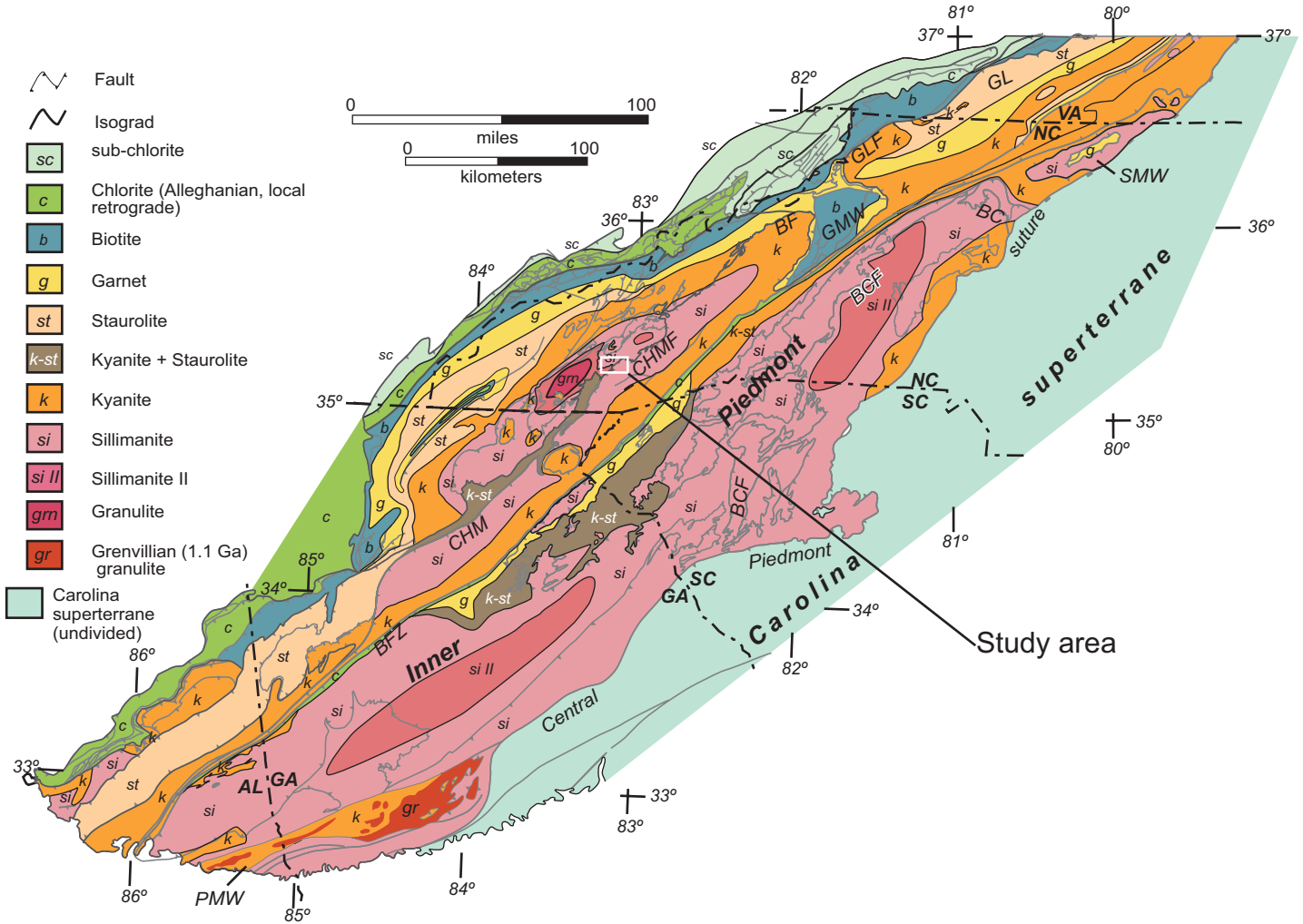


Figure 4–2. Metamorphic isograd map of the southern Appalachian Blue Ridge and Inner Piedmont compiled from various studies including (Hadley and Goldsmith, 1963; Carpenter, 1970; Hadley and Nelson, 1971; Rankin et al., 1972; Espenshade et al., 1975; Goldsmith et al., 1988; Merschat and Wiener, 1988; Eckert et al., 1989; Hopson et al., 1989; Butler, 1991; Hatcher and Goldberg, 1991; Nelson et al., 1992; Quinn, 1993; Settles, 2002; Higgins et al., 2003; Merschat, 2003; Tull and Holm, 2005; Hatcher and Merschat, 2006; Hatcher et al., 2007;Tull, 2007; Merschat et al., 2008). Modified from Merschat, Bream and Hatcher in progress.

Ma. Together these recent ages suggest a Taconic timing of peak metamorphism in the western Blue Ridge.

Samples from the chlorite zone (460-440 Ma) in the western Blue Ridge in Tennessee and North Carolina (Connelly and Dallmeyer, 1991), and metamorphic zircon rims and chemical ages of monazite indicate that the western Blue Ridge reached upper amphibolite to granulite facies conditions during the Ordovician (Moecher and Miller, 2000; Moecher et al, 2004). Whole-rock cooling ages ($^{40}Ar/^{39}Ar$) for samples from the biotite and garnet zones (350–340 Ma) in the western Blue Ridge in Tennessee and North Carolina (Connelly and Dallmeyer, 1991), along with SHRIMP ages on zircon rims (Carrigan et al., 2001; Bream, 2003; Merschat et al, 2006) indicate that a 360–350 Ma Neoacadian event and an early Alleghanian 325 Ma event affected the eastern Blue Ridge and Inner Piedmont (Dennis and Wright, 1997).

The Hayesville fault separates the western Blue Ridge from the central and eastern Blue Ridge. Metamorphism increases west to east across the Hayesville fault from upper greenschist facies to lower granulite facies in the central Blue Ridge (Miller et al., 1997). Eckert et al. (1989) determined that metamorphic isograds cross the Hayesville fault indicating the fault is premetamorphic, and that the central Blue Ridge was affected by the same 460-450 Ma event as the western Blue Ridge.

Central Blue Ridge

The central Blue Ridge is made up of the Cowrock and Cartoogechaye terranes, and the Dahlonega gold belt (Hatcher et al., 2007). A small portion of the Cartoogechaye terrane is exposed in the study area, with the Dahlonega gold belt comprising a large part of the mapped area. Metamorphic grade in the central Blue Ridge increases southwestward to upper amphibolite or lower granulite facies in the central part of the belt (Butler, 1973). The granulite facies rocks were first identified by Force (1976) who defined a hypersthene isograd (Fig. 4–2); including Winding Stair Gap (Absher and McSween, 1985; 1986). Moecher et al. (2005) reported an age of 460 Ma for metamorphic monazite

within the Hayesville thrust sheet near Sylva, North Carolina, supporting a Middle Ordovician age of Taconian metamorphism in the central Blue Ridge.

Cartoogechaye terrane rocks are exposed in the SW part of the field area (Fig. 4–1). Metamorphism in the Cartoogechaye terrane is amphibolite to granulite facies (Absher and McSween, 1985; Eckert et al., 1989; Moecher et al., 2004) and may have reached eclogite facies in the southern part of the Dellwood quadrangle (Anderson and Moecher, 2006). Zircon ages collected by Moecher et al. (2004) from the core of the granulite facies metamorphism at Winding Stair Gap agree with the youngest proposed limit of the Taconian orogeny (485 Ma); more recent geochronologic data agree with this interpretation (Berquist, 2005; Merschat et al., 2006). Moecher et al. (2004) suggested a counterclockwise P–T path that reached thermal maximum at 458 Ma. Evidence for this includes kyanite forming after sillimanite and leucosomes dated at 460 Ma in samples collected at Winding Stair Gap (Moecher et al., 2004).

Lower metamorphic grade was observed in the Dahlonega gold belt relative to the surrounding thrust sheets (Gillon, 1982; McConnell and Abrams, 1984; German, 1985). Merschat et al. (2006) obtained a U-Pb zircon rim age of ~420 Ma for a trondhjemite dike that truncates metamorphic layering at an exposure in the Dahlonega gold belt, which provides further control on the suggested Taconic timing of metamorphism in the Great Balsam Mountains Window window (Merschat et al., 2006). Felsic gneiss samples collected by Thomas (2001) and Settles (2002) in the Dahlonega gold belt SW of the Great Balsam Mountains Window yield SHRIMP U-Pb ages ranging from 482-458 Ma.

Eastern Blue Ridge

The Soque River fault places rocks of the eastern Blue Ridge structurally above rocks of the central and western Blue Ridge. This fault truncates foliation and juxtaposes terranes of different grade demonstrating that it is post-metamorphic (Hopson et al., 1989). Metamorphic grade remains middle to

upper amphibolite facies in the eastern Blue Ridge, with sillimanite grade in the western Blue Ridge, and kyanite and garnet grade farther east near the Brevard fault zone (Butler, 1973).

U-Pb analyses of zircons collected from the Lick Ridge eclogite near Bakersville, NC, yielded a ~459 Ma age from zircon cores, a 420 ± 15 Ma age from rims, and a 333.7 ± 0.4 Ma age for rutile inclusions in the zircon grains (Miller, et al., 2000); ages are correlated with the Taconic, Acadian, and Alleghanian events, respectively. Traditionally, peak metamorphism in the eastern Blue Ridge was thought to be Taconic, although, recent $^{40}Ar/^{39}Ar$ cooling ages and U-Pb chemical ages on monazite indicate overprinting of earlier fabrics by a Late Devonian event (Goldberg and Dallmeyer, 1997; Moecher et al., 2005).

Sample Description

Rocks in the study area consist of metagraywacke and schist, and are composed of quartz, plagioclase (An_{10}– An_{26}), biotite and/or muscovite, garnet, aluminum silicates (either sillimanite or kyanite), staurolite, and opaques. Garnet and biotite are common, and sillimanite, kyanite, and staurolite were also found throughout the study area. Rocks in the study area are well foliated with some being migmatitic. Representative samples were collected from the study area and mineral assemblages were identified in order to understand metamorphic conditions and reactions, and pressure–temperature (P–T) conditions. Metamorphic grade was mapped using index mineral data collected in the field and observed in thin sections (Fig. 4–3).

Methodology

Six samples (311C, CGB, 478, 1498, 588, 862) were analyzed using a four-spectrometer CAMECA SX-50 electron microprobe (EMP) (University of Tennessee, Knoxville). Standard calibrations for each session include ~20 KeV accelerating voltage; beam current was set at 10nA and 20nA depending on the phase being analyzed, and beam size also varied depending on the mineralogy. Counting times were 20-40 seconds. Elemental analysis on the EMP was also

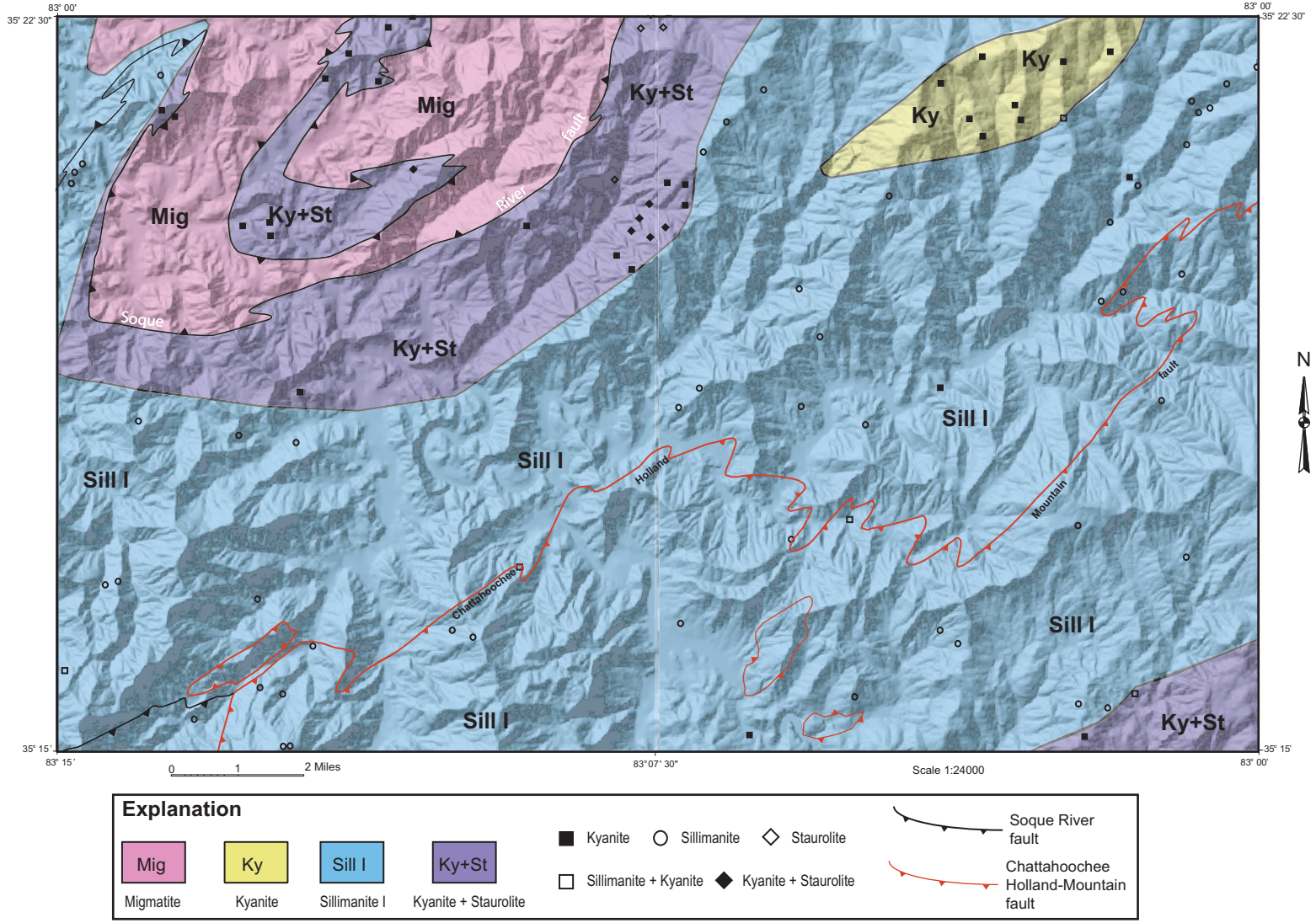


Figure 4–3. Metamorphic isograd map of Sylva South and Tuckasegee quadrangles displaying locations of observed index minerals (field observation and thin section). Mapping by Quinn (1991) and Shawna Cyphers (2006).

calibrated with a set of in-house standards before each session.

Single-point and line-scan analyses were determined from garnet, feldspar, and biotite phases within the sample. Single–point analyses of the rim and core of each mineral was performed to determine elemental variations in garnet, biotite, plagioclase, ilmenite, and muscovite phases, as well as spot analyses of surrounding minerals and mineral inclusions within each garnet. Line traverses were collected of each garnet selected for P–T determination; X-ray maps of two garnets were also made.

Petrographic Description

Sample 311C (Dahlonega gold belt)

Sample 311C is a medium to coarse-grained biotite gneiss. It is composed of large porphyroblasts of subhedral garnets (~1.5mm) surrounded by only slightly finer biotite, feldspar, and lesser amounts of quartz. Kyanite and sillimanite are visible only at a finer scale. Biotite grains define a moderate to poorly developed foliation, and the sample has a granular texture due to the relative abundance of quartz and feldspar. All garnets within the sample have inclusion-free outer rims and poikioblastic cores. Inclusions in garnet cores consist of biotite, quartz, plagioclase, and ilmenite. Two biotite crystals contain zircon inclusions, which have distinctive pleochroic halos. Both fibrous and prismatic sillimanite are present, and the finer prismatic (fibrolite) sillimanite is commonly associated with plagioclase (An_{12}– An_{26}) (Fig. 4–4a). Kyanite is euhedral with irregular and embayed margins, and interpreted to be in disequilibrium (Fig. 4–4b).

Sample CGB (Dahlonega gold belt)

Sample CGB was collected from the Catamount Gap block–in–matrix exposure just north of Cullowhee, NC. It is a poorly foliated, highly altered calcsilicate. Garnet porphyroblasts are skeletal with inclusions of diopside, epidote, plagioclase, and quartz (Fig. 4–4c). Clinozoisite, zoisite, biotite, diopside, plagioclase, and cummingtonite are present throughout the matrix.

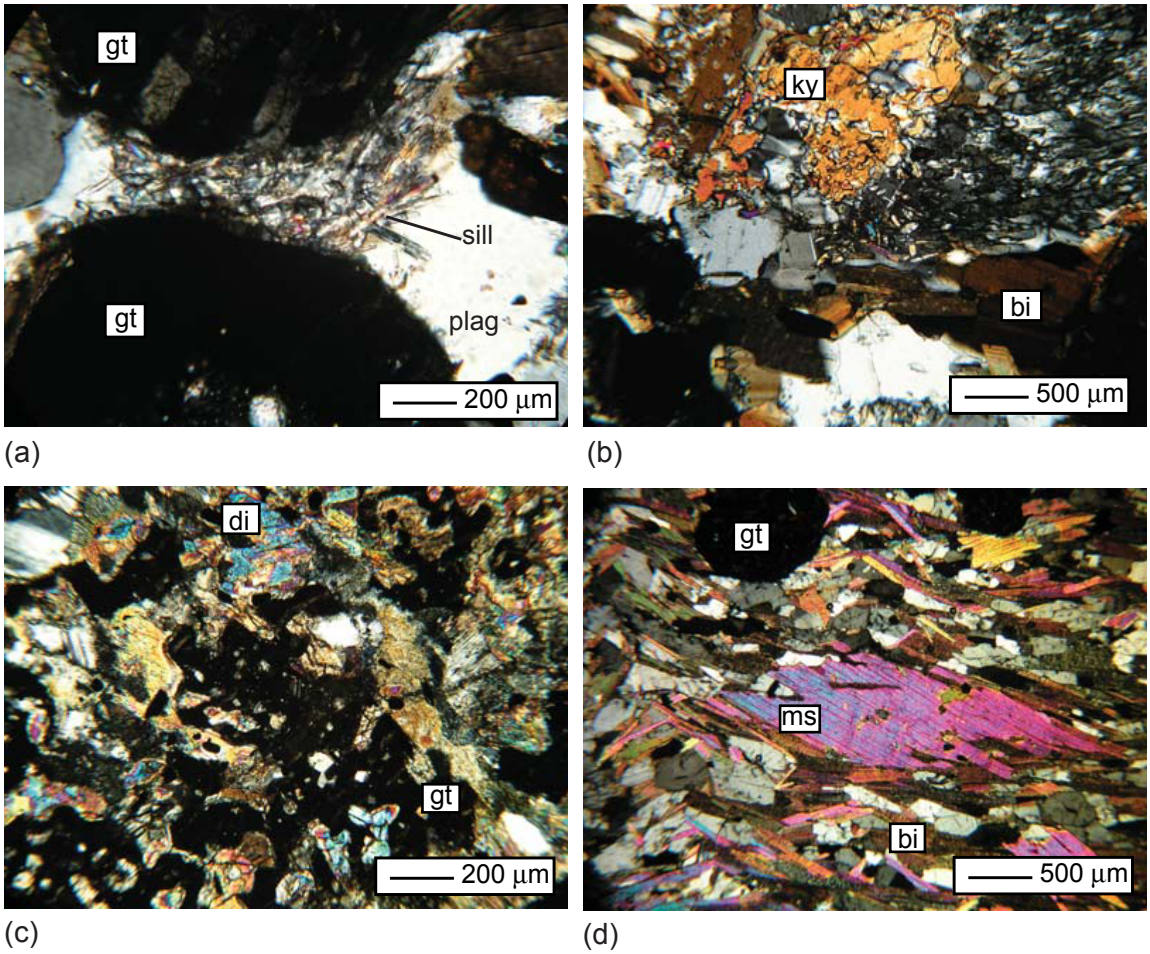


Figure 4–4. Photomicrographs of representative samples. (a) Matrix sillimanite (fibrolite) formed between two garnet porphyroblasts in sample 311C. (b) Kyanite in disequilibrium with surrounding phases, sample 311C. (c) Disequilibrium textures associated with fragmented garnet, sample CGB. (d) Sample 1498, late muscovite crosscutting the dominant F_2 foliation. Abbreviations: bt–biotite; di–diopside; gt–garnet; ky–kyanite; ms–muscovite; plag–plagioclase; sill–sillimanite.

Plagioclase (An_{34}) displays pericline and albite twinning. A felsic vein cross cuts the original mafic assemblage and is composed of quartz, plagioclase, and biotite.

Sample 478 (Upper Tallulah Falls)

Sample 478 is a muscovite–biotite–garnet schist. A medium fine-grained matrix of mica surrounds coarse-grained garnets, and micas are crenulated. All garnets contain inclusions of quartz, biotite, and opaques, and garnets are subhedral to anhedral. The foliation wraps around garnets, with larger euhedral crystals of muscovite and lesser biotite are present in pressure shadows. Reaction textures around garnets are composed of chlorite and biotite; many garnets are fractured, with chlorite and biotite present in fractures; some garnets are broken and are being replaced by biotite and chlorite. Later euhedral, medium-grained muscovite is present throughout the matrix.

Sample 1498 (Upper Tallulah Falls)

Sample 1498 is a well–foliated muscovite-biotite-garnet schist with granular layers of quartz and feldspar. Later larger muscovite cross cuts the dominant foliation (Fig. 4–4d). Some of the muscovite grains contain inclusions of biotite, plagioclase, and fibrous sillimanite. Smaller garnets are subhedral, larger garnets are anhedral, and others are fragmented. Plagioclase (An_{14}–An_{24}) and quartz occur as inclusions in garnets. Plagioclase in the sample is either untwinned or occurs as albite, pericline, and Carlsbad twins.

Sample 588 (Upper Tallulah Falls)

Sample 588 is an inequigranular kyanite-muscovite-garnet schist with coarse– to medium–coarse garnets and medium– to fine–grained micas. The sample is strongly foliated and is dominated by muscovite and biotite with fewer quartz and plagioclase (An_{13}– An_{26}) layers. Two aluminum silicate minerals are present in the sample; kyanite grains occur throughout the sample as does minor fibrous sillimanite. Some of the kyanite grains in this sample cross cut the dominant foliation (Fig. 4–5a,b). Sillimanite occurs in the matrix and as

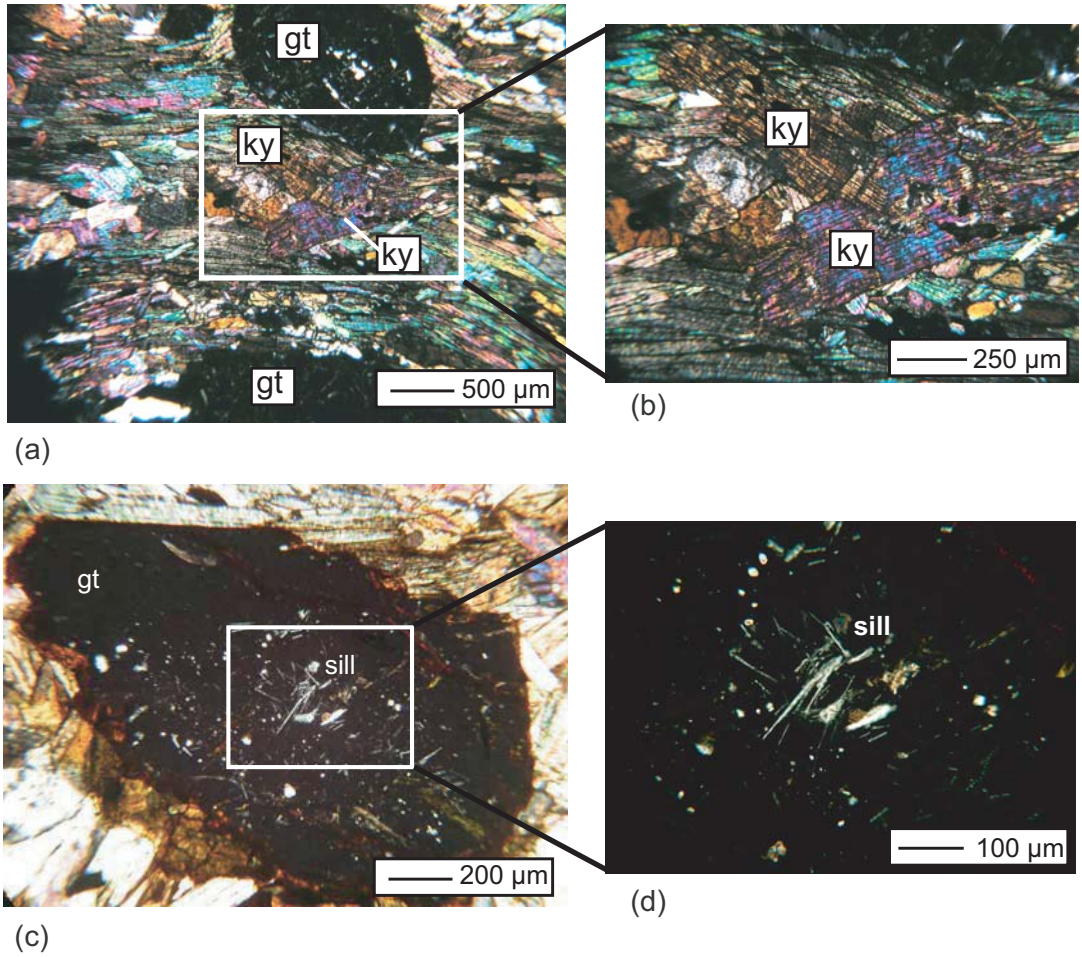


Figure 4–5. Photomicrographs of representative samples. (a) Kyanite porphyroblast crosscutting the dominant S_2 foliation in sample 588. (b) Higher magnification of kyanite porphyroblasts; sample 588. (c) Garnet porphyroblast in sample 862 displaying sillimanite (fibrolite) inclusions in the core and inner rim. (d) Higher magnification of sillimanite inclusions; sample 862. Abbreviations: gt–garnet; ky–kyanite; sill–sillimanite.

inclusions in garnets. Some matrix muscovite grains are euhedral and larger than surrounding muscovite, and possibly represent later muscovite growth.

Sample 862 (Upper Tallulah Falls)

Sample 862 is an inequigranular pelitic schist, with a medium- to fine- grained matrix of feldspar, quartz, kyanite, muscovite and biotite. Staurolite is also present and contains inclusions of feldspar (An_{14}– An_{24}), biotite, quartz, and muscovite. Fibrous sillimanite is found in several garnets (Fig. 4–5c,d). Large laths of muscovite occur throughout the sample and possibly indicate later muscovite growth. Some of the larger muscovite grains contain staurolite inclusions.

Phase Diagrams

Mineral assemblages of pelitic samples analyzed on the EMP are described using Thompson's (1957) AFM diagram. The AFM phase diagram is based on a model pelite that consists of the components SiO_2-Al_2O_3-FeO-MgO-K_2O-H_2O, and the mineral assemblage is projected through muscovite onto the plane Al_2O_3-FeO-MgO (Spear, 1993). Figures 4–6a and 4–7 represent the assemblage aluminum silicate + garnet + biotite, and include quartz, muscovite, and H_2O projected through muscovite. Minor differences are indicated for garnet rim and core compositions and biotite matrix and inclusion compositions for all pelitic samples (Fig. 4–6a and 4–7). Biotite compositions in samples 311CGt1 and 862 have greater variance in comparison to the other samples, whereas garnet compositions do not vary greatly for any of the samples.

For the calc-silicate sample CGB, the ACF diagram (modified by Pearce, 1993) is more suitable because it portrays complex rocks that contain the oxides SiO_2-Al_2O_3-MgO- FeO-CaO-Na_2O-H_2O. The ACF ternary is defined by Al_2O_3-CaO-FeO, and the mineral compositions of garnet, clinopyroxene, zoisite, and clinoamphibole are identified on the diagram (Fig. 4–6b) and representative of the mineral assemblage for sample CGB.

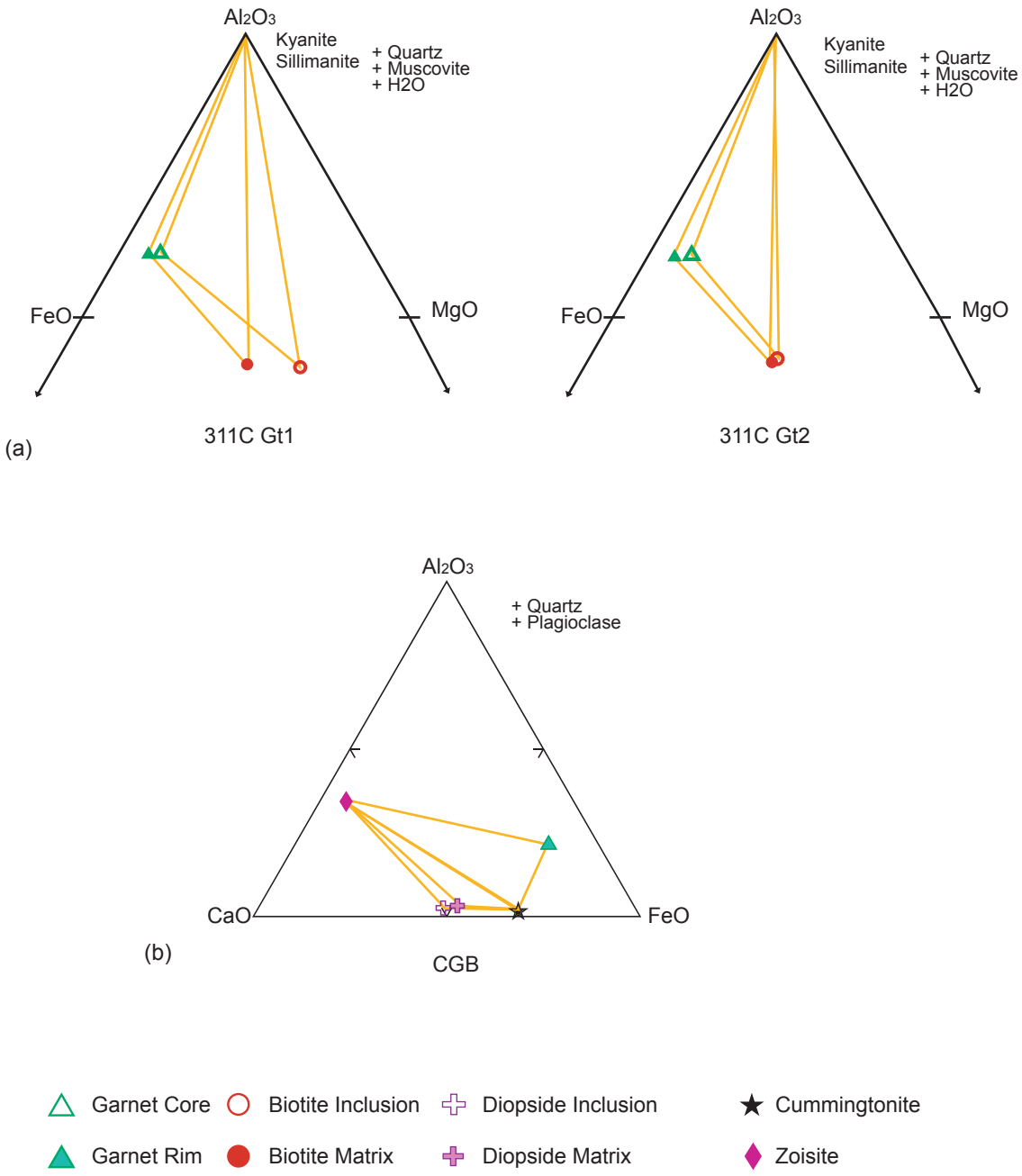


Figure 4–6. (a) Thompson (1957) AFM diagram and (b) Spear (1993) ACF diagram for Dahlonega gold belt samples.

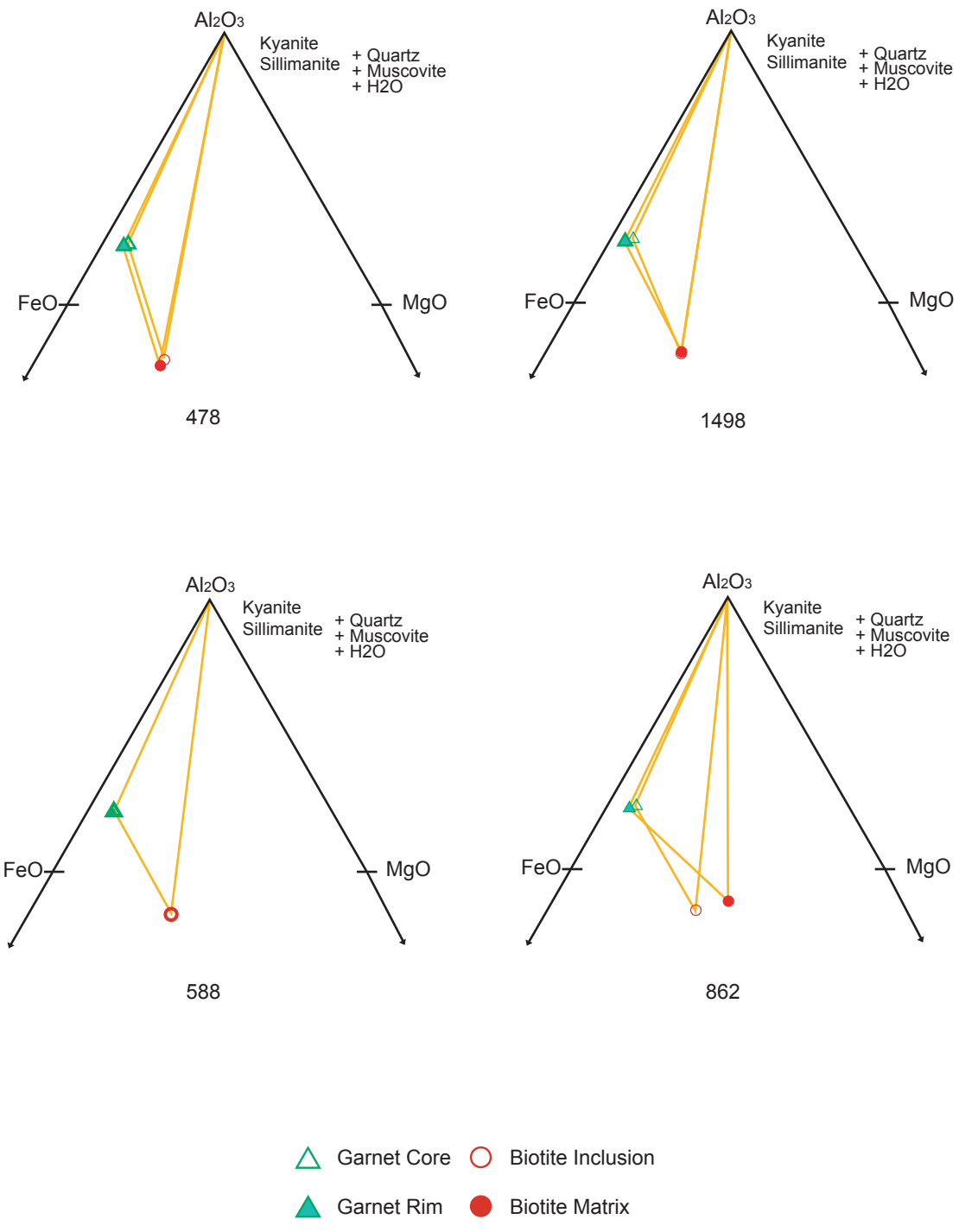


Figure 4–7. (a) Thompson (1957) AFM diagram Tugaloo terrane samples.

Mineral chemistry

Garnet porphyroblasts are anhedral to subhedral, and range from 4 to 0.5 mm. Garnets were chosen for analysis on the EMP based on how fresh the sample is, the size of the garnets, and the inclusion suite present within the garnets. Some analyzed garnets chosen for analysis are embayed with alterations of chlorite, biotite, and sericite occurring around the rim and in cracks and embayments of the garnets. All garnets analyzed are dominantly almandine (Fig. 4–8). The mafic sample, CGB, contains greater amounts of both Ca and Mg and shows the greatest range in composition when compared to the pelitic samples (Fig. 4–8), but is still almandine in composition.

Line scans were collected for all garnets analyzed for P–T estimates in order to evaluate the amount of chemical zoning present in the garnets. Garnets from all samples analyzed (Figs. 4–9 through 4–15) generally reveal weak to moderate element zoning in profiles indicating diffusion has affected the rocks in the study area. Sample 1498 displays the greatest amount of chemical zoning with relatively low spessartine and grossular compositions at the rim and increased amounts at the core and inner rim (area between the rim and core) (Fig. 4–13). The two garnets analyzed from sample 311C display a notable exchange between the Fe and Mg cations, with the pyrope component increasing at the core (Figs. 4–9 and 4–10). The higher MgO content at the core is thought to represent an earlier garnet composition, with the relative increase of FeO at the rims further indicating that some amount of diffusion has affected the garnets in the study area. The grossular content in samples 311C (garnets 1 and 2), 588, and 862 (Figs. 4–9, 4–10, 4–14, and 4–15) contain a distinct zoning pattern where the inner rim CaO content is slightly lower in comparison to the rim and core, where compositions are very similar. This pattern may represent different growth periods for the garnet, and would indicate that growth zoning was a more effective process during garnet growth instead of diffusion.

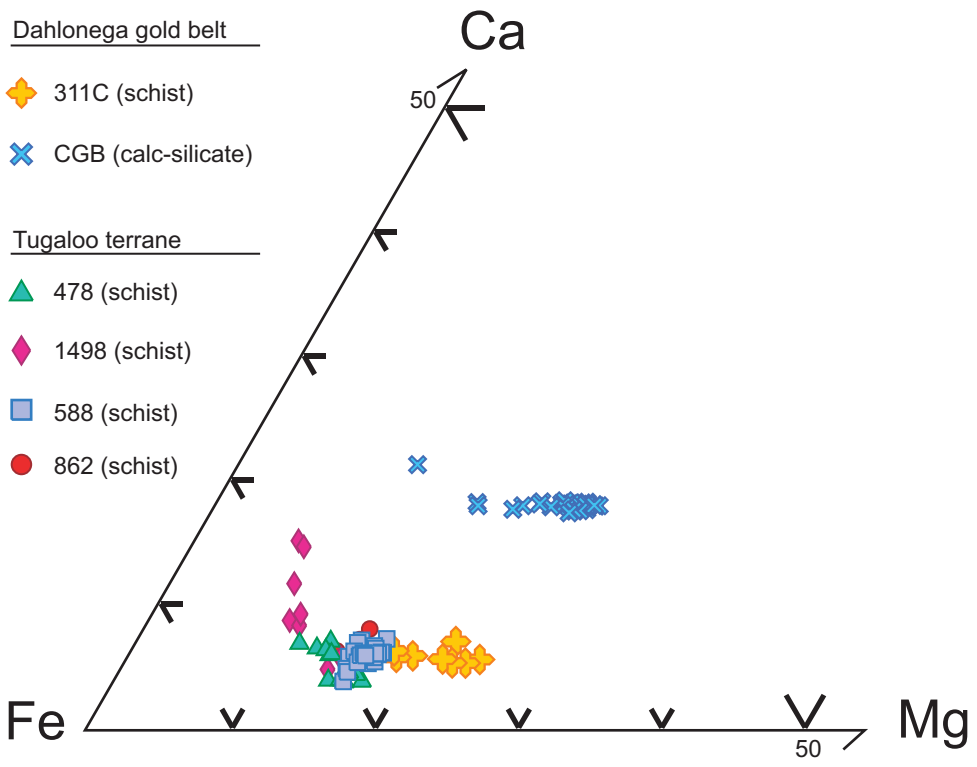


Figure 4-8. Partial ternary plot showing garnet compositions between almandine (Fe), grossular (Ca), and pyrope (Mg) end members of all samples analyzed. Tick marks indicate 10% intervals.

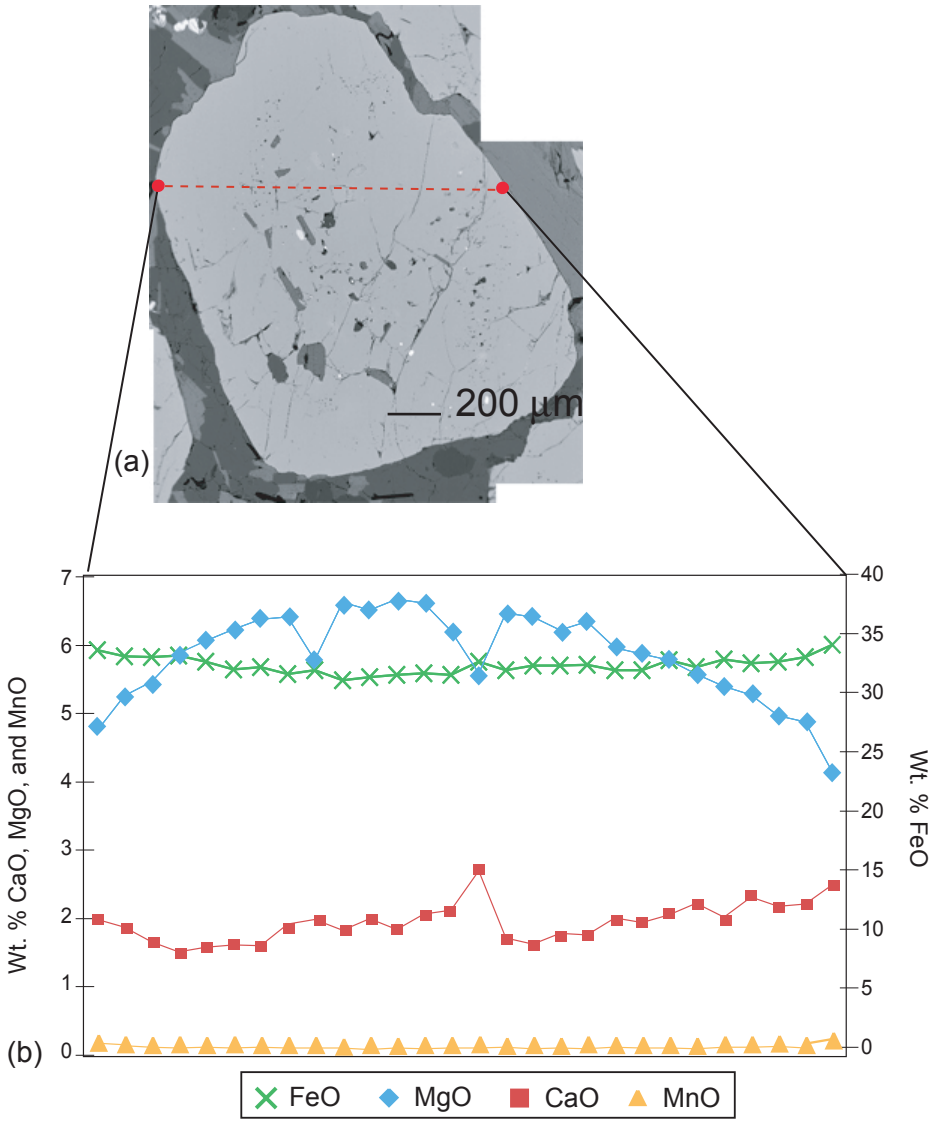


Figure 4–9. Garnet zoning profile of sample 311C garnet #1. (a) Back-scattered electron image. Line traverse is indicated by the red-dashed line. (b) Zoning profile.

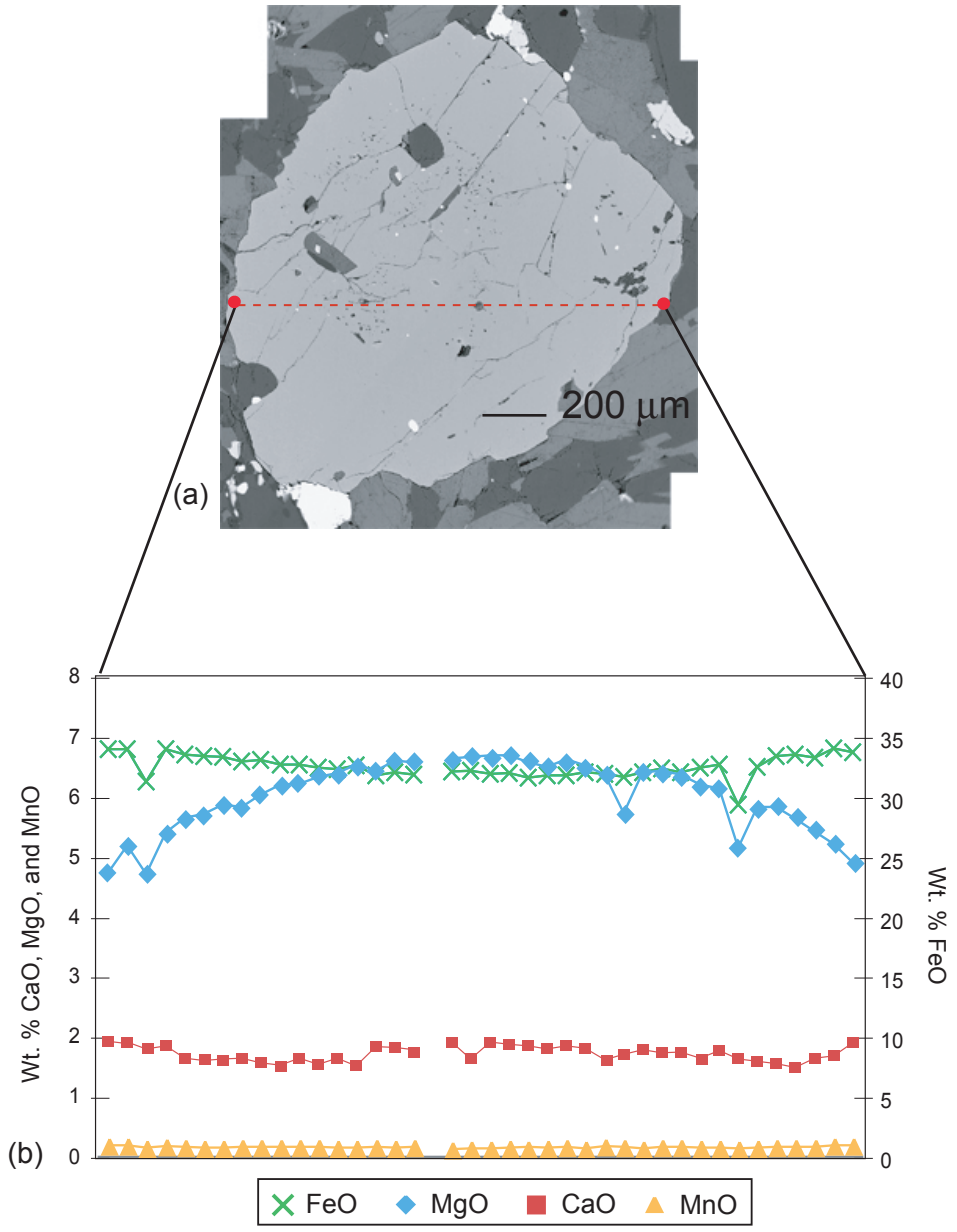


Figure 4–10. Garnet zoning profile of sample 311C garnet #2. (a) Back-scattered electron image. Line traverse is indicated by the red-dashed line. (b) Zoning profile.

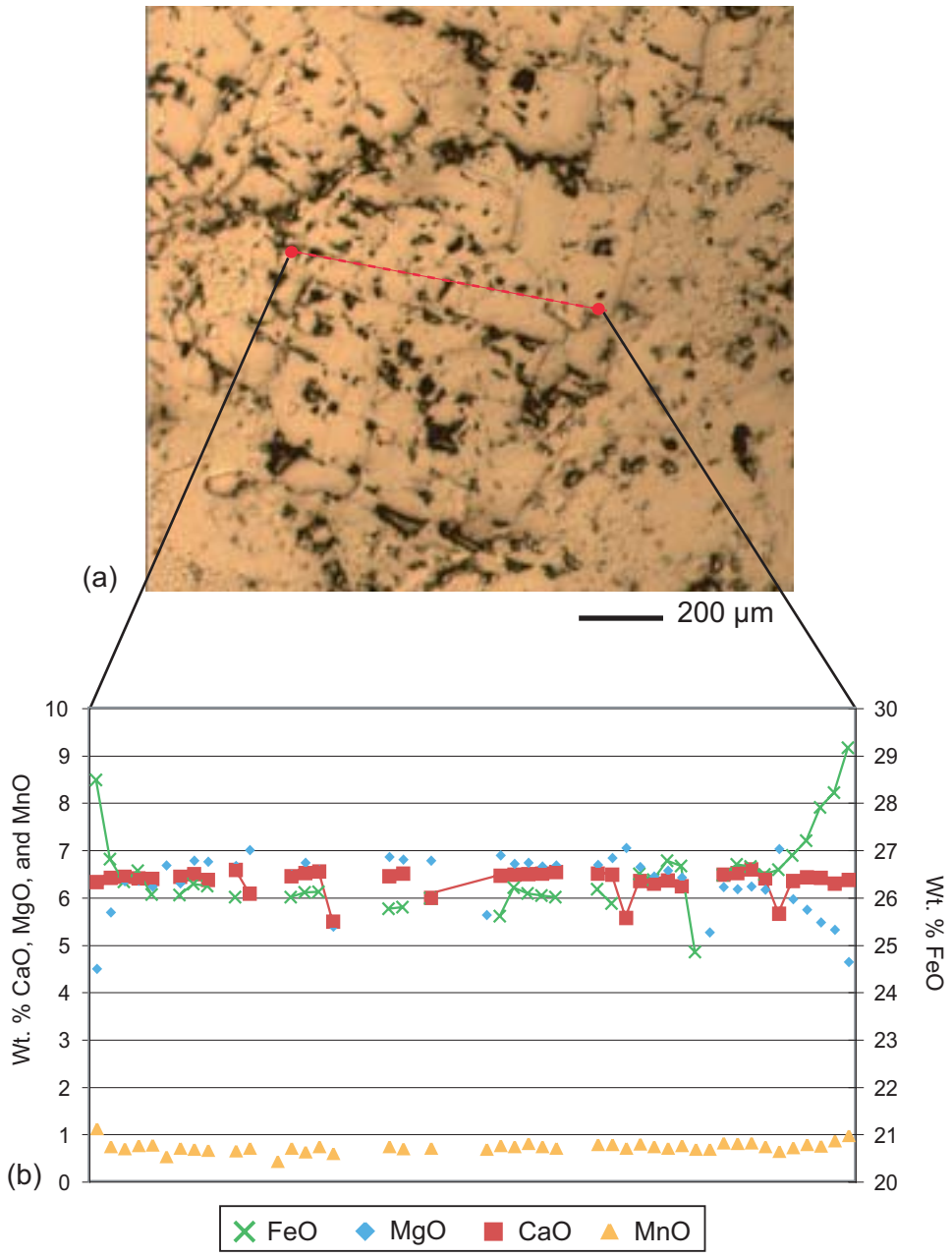


Figure 4–11. Garnet zoning profile of sample CGB garnet #3. (a) Reflected light photomicrograph. Line traverse is indicated by the red-dashed line. (b) Zoning profile.

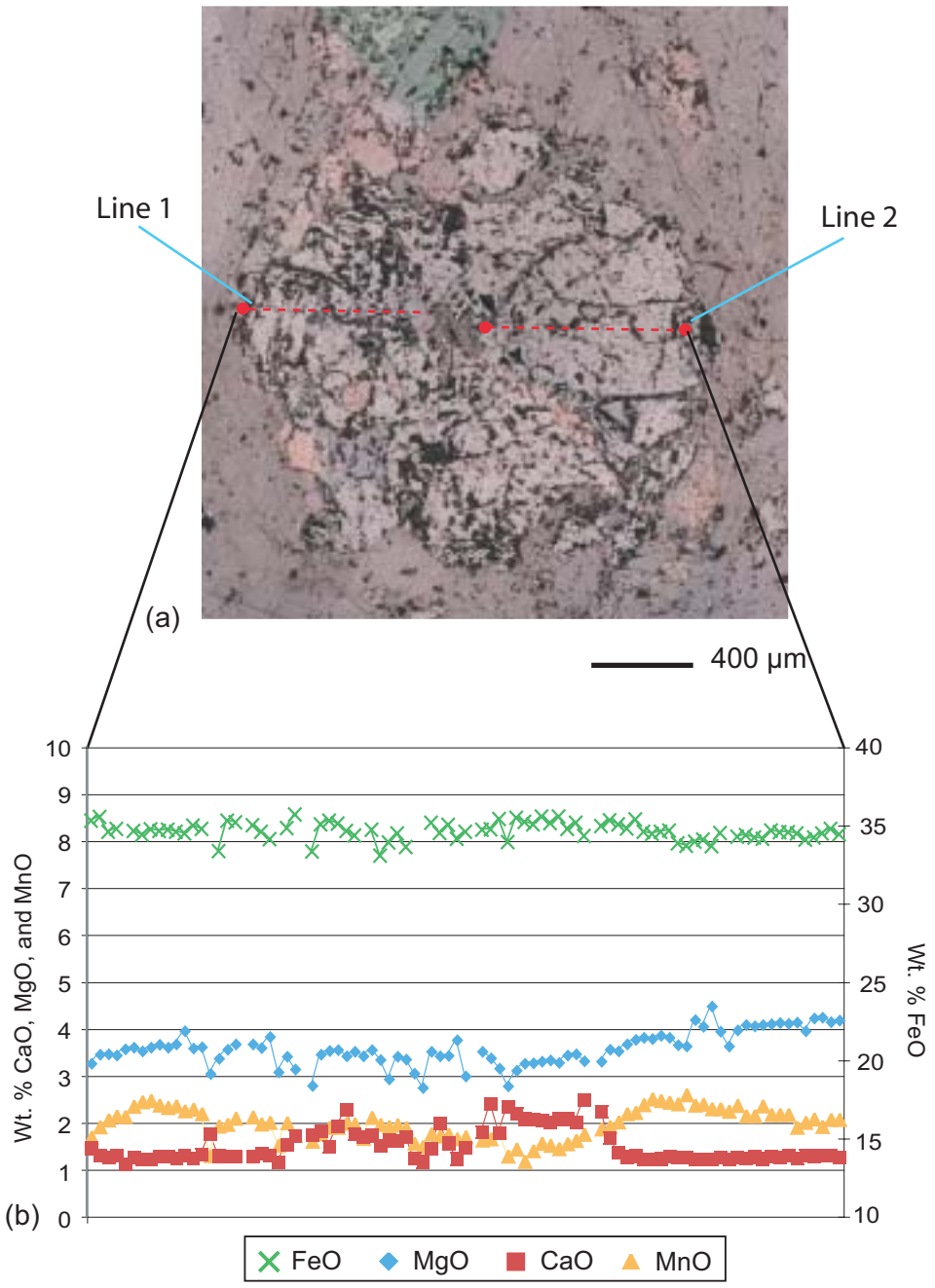


Figure 4–12. Garnet zoning profile of sample 478 garnet #5. (a) Reflected light photomicrograph. Line traverse is inidcated by the red-dashed line. (b) Zoning profile.

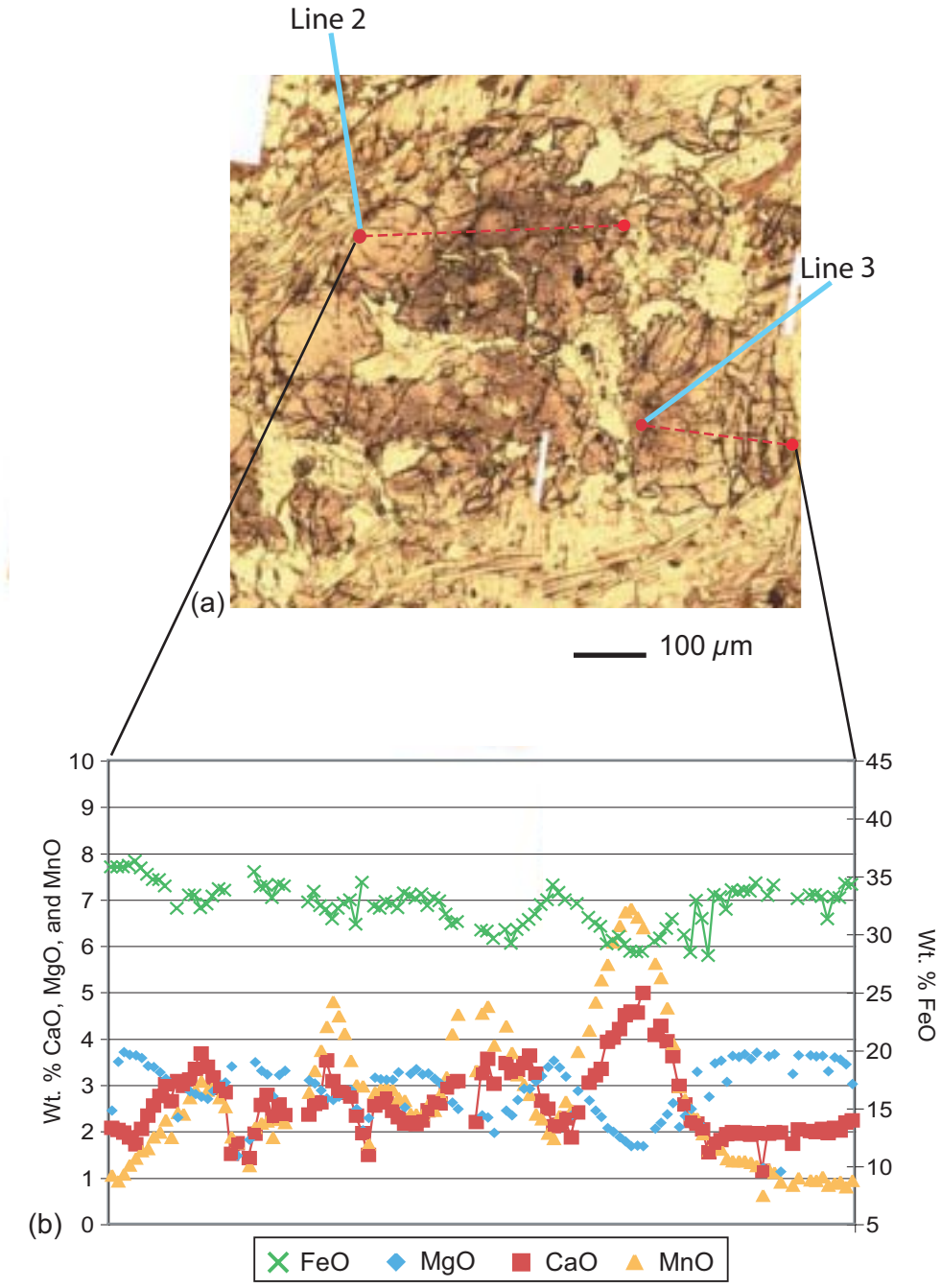


Figure 4–13. Garnet zoning profile of sample 1498 garnet #2. (a) Plane light photomicrograph. Line traverse is inidcated by the red-dashed line. (b) Zoning profile.

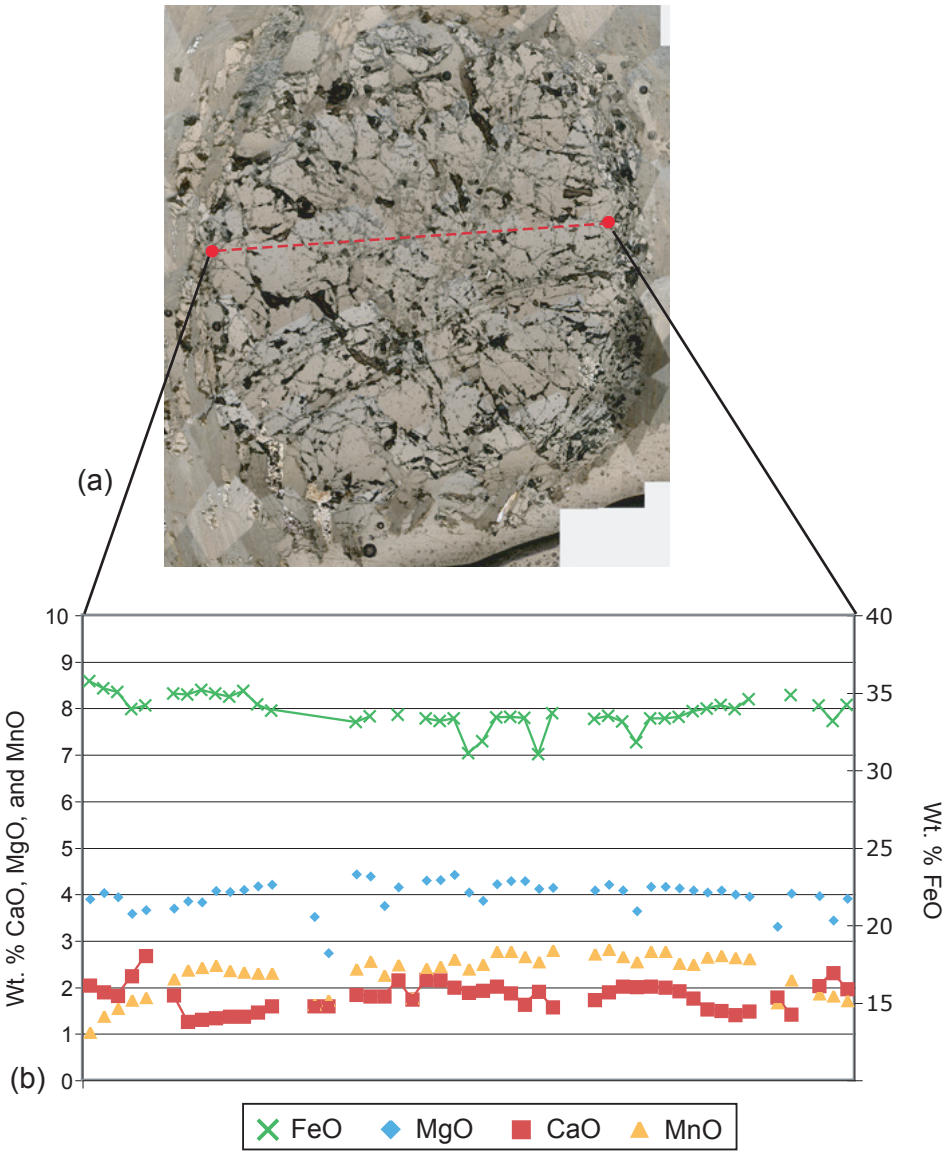


Figure 4–14. Garnet zoning profile of sample 588 garnet #1. (a) Reflected light photomicrograph. Line traverse is inidcated by the red-dashed line. (b) Zoning profile.

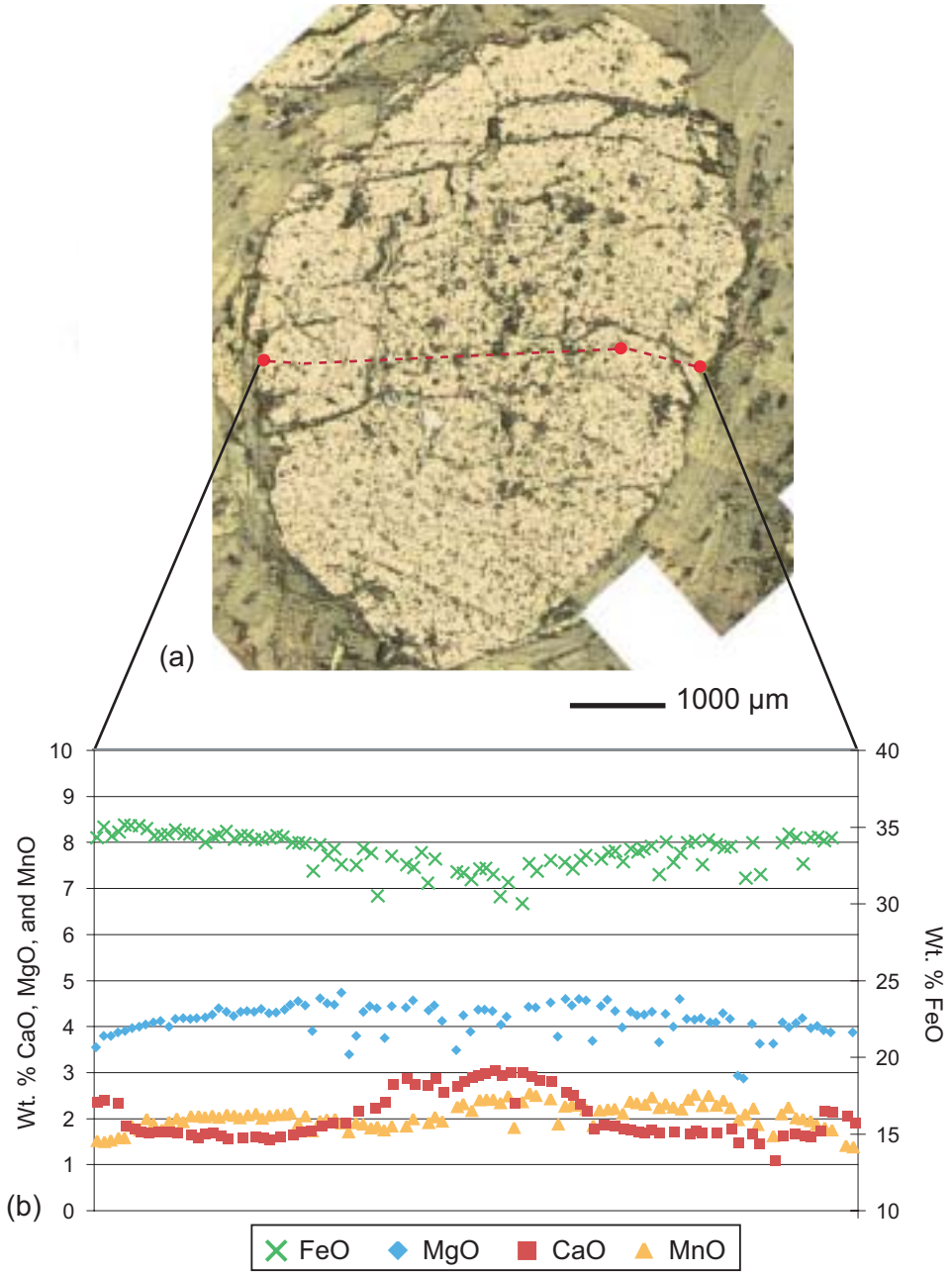


Figure 4–15. Garnet zoning profile of sample 862 garnet #1. (a) Plane light photomicrograph. Line traverse is inidcated by the red-dashed line. (b) Zoning profile.

Biotite defines the dominant S_2 foliation throughout most samples and ranges from 0.2 to 1 mm. Biotite inclusions in garnet typically have lower Fe content than matrix biotite. Analyzed biotite for all pelitic samples ranges between 0.03–0.14 formula mols Ti vs 0.2–0.71 Fe/(Fe+Mg) (Fig. 4–16a). Ilmenite compositions in pelitic samples fall between 0.0015–0.00163 formula mols Mn vs 0.0001–0.038 formula mols of Mg (Fig. 4–16b).

Fibrolitic sillimanite is found in most samples, usually as inclusions in garnet and less often in feldspar and muscovite. Matrix fibrolite is uncommon, but where present is associated with plagioclase. A minor amount of prismatic sillimanite was observed in thin section 311C. Kyanite crystals occur as euhedral and anhedral grains. Anhedral kyanite crystals are found in sample 311C, and have irregular and embayed margins, suggesting they were in disequilibrium with surrounding phases (Fig. 4–4b). Staurolite was identified in several thin sections, and contains feldspar, biotite, quartz, and muscovite inclusions.

Muscovite ranges from large (~2 mm) matrix grains to smaller laths (0.25 mm) that occur in the matrix as well as inclusions in garnets. Muscovite typically defines the dominant S_2 foliation; however, larger grains are observed in samples 1498, 588, and 862 and are discordant with S_2. Plagioclase is either untwinned or occurs as albite, pericline, and Carlsbad twins.

Geothermobarometry

In order to understand the metamorphic history of the study area, P–T estimates were calculated for each analyzed sample using inclusion suite thermobarometry of garnet porphyroblasts. Garnets are ideal for use in inclusion suite thermobarometery, because they preserve chemical zonation; ideally this record represents the evolution of elemental variation as the garnet was formed (Spear, 1993).

Two processes dominate the composition of a garnet during a metamorphic event: growth zoning and diffusion zoning. Growth zoning occurs as a garnet crystal grows, and different compositions are added to the exterior

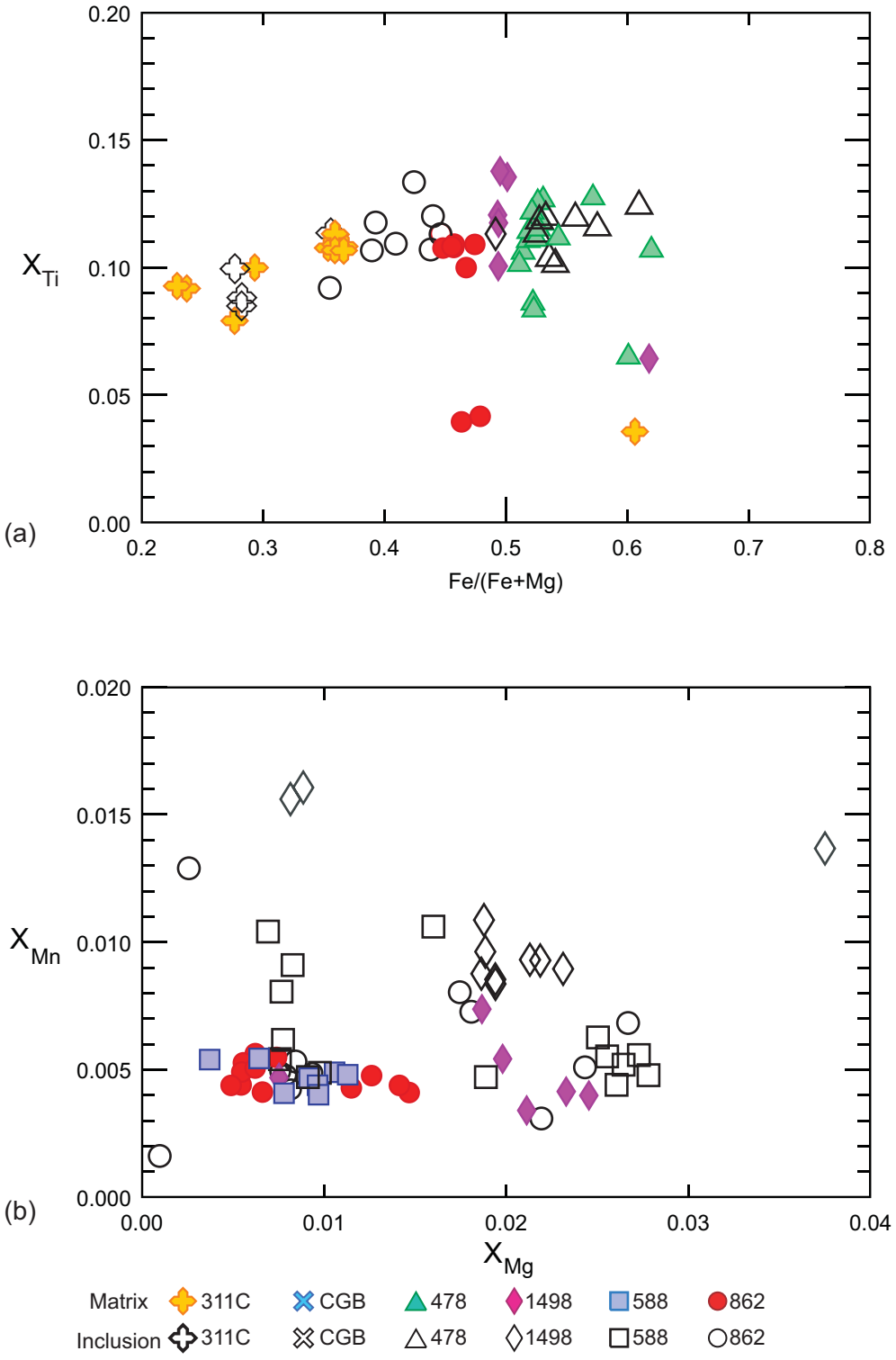


Figure 4–16. Plots of biotite and ilmenite composition. (a) Formula moles of biotite; Ti vs Fe/(Fe+Mg). (b) Formula moles for ilmenite; Mn vs formula moles of Mg.

shell of the crystal; each layer reflects changes in P–T and local bulk composition (Spear, 1993). Diffusion zoning is defined as a modification of a preexisting garnet composition through volume diffusion (Spear, 1993). Diffusion in rocks that have undergone amphibolite facies metamorphism is to be expected and previous studies in similar metamorphic terranes have shown that a change from dominantly growth zoning to dominantly diffusion zoning with increased metamorphic grade is common (Tracy et al. 1976; Anderson and Olimpio, 1977; Woodsworth, 1977; Yardley, 1977).

P–T estimates were determined using well–documented geo-thermobarometers for samples 311C, CGB, 478, 1498, 588, and 862. The garnet-biotite (Ferry and Spear, 1982), garnet-ilmenite (Pownceby et al., 1987), and garnet-pyroxene (Powell, 1985) exchange thermometers were used to determine peak metamorphic temperatures in metapelitic rocks. The garnet-aluminum silicate-quartz-plagioclase (GASP) (Hodges and Spear, 1982), and garnet-pyroxene-clinopyroxene-quartz barometer (Hodges and Spear, 1982; Powell and Holland, 1988) net transfer geobarometers were used to obtain pressure estimates for analyzed samples.

The garnet-biotite geothermometer of Hodges and Spear (1982) is based on the exchange of Fe and Mg between the garnet and biotite.

Almandine + Phlogopite = Pyrope + Annite

$Fe_3Al_2Si_3O_{12} + KMg_3AlSi_3O_{10}(OH)_2 = Mg_3Al_2\ Si_3O_{12} + KFe_3AlSi_3O_{10}(OH)_2$

However, inaccuracy in exchange in garnet-biotite geothermometers can occur due to non-ideal exchange of other elements such as Ti and Al substituting for Fe and Mg (Hoisch, 1991). The garnet-biotite thermometer was used for samples 478 and 311C.

Similarly, the garnet-ilmenite thermometer quantifies the exchange of Fe–Mg and Fe–Mn between garnet and ilmenite.

Almandine + Mn- Ilmenite = Spessartine + Fe-Ilmenite

$Fe_3Al_2Si_3O_{12} + 3MnTiO_3 = Mn_3Al_2Si_3O_{12} + 3FeTiO_3$

The garnet-ilmenite thermometer was utilized for samples 1498, 588, and 862.

The GASP barometer is based on the net-transfer exchange of Ca between the garnet and plagioclase. In this reaction grossular compositions are favored at higher pressures. Overestimation errors can occur with this barometer when Fe–Mg exchange due to diffusion affect a garnet (Hodges and Spear, 1982).

Anorthite = Grossular + Aluminum silicate + Quartz

$$3CaAl_2Si_2O_8 = Ca_3Al_2Si_3O_{12} + 2Al_2SiO_5 + SiO_2$$

The GASP barometer was utilized for samples 478, 862, 1498, 588, and 311C.

Garnet-pyroxene thermometer (Powell, 1985).

Almandine + Diopside = Pyrope + Hedenbergite

$$Fe_3Al_2Si_3O_{12} + 3CaMgSi_2O_6 = Mg_3Al_2Si_3O_{12} + 3CaFeSi_2O_6$$

Garnet-pyroxene-clinopyroxene-quartz barometer (Hodges and Spear, 1982; Powell and Holland, 1988) were used for sample CGB.

Diopside + Anorthite = Grossular + Pyrope + Quartz

$$3CaMgSi_2O_6 + 3CaAl_2Si_2O_8 = 2Ca_3Al_2Si_3O_{12} + Mg_3Al_2Si_3O_{12} + 3SiO_2$$

Results of P–T Estimates

Seven garnets were analyzed on the EMP and analyses of garnet, biotite, plagioclase, ilmenite, and muscovite were gathered to obtain P–T estimates. The program “Thermobarometry” v. 1.9 of Spear and Kohn (1989) was used to calculate the data collected from EMP analysis.

Data were collected from the core of each garnet and compared with inclusions of biotite, feldspar, ilmenite, or clinopyroxene. These P-T estimates are thought to represent peak metamorphism. Analysis of the rim of each garnet was compared to matrix biotite, feldspar, ilmenite, and clinopyroxene to determine cooling and possibly retrograde temperatures. Lastly, P-T estimates were calculated from all inclusions analyzed compared to their respective “host”

garnet. Observed diffused garnet profiles indicate that estimates of pressure and temperature from garnet cores are likely representative of peak pressure and temperature in comparison to estimates of garnet rims.

Core and rim P–T estimates for all analyzed samples are shown in Figures 4–17 through 4–23 and are also listed in Table 4–1. Figure 4–24 compares P-T estimates and locations from this study with other P–T estimates from previous work in and around the study area (Shireman, 1985; Brumback, 1990; Quinn, 1991; and Davidson, 1995).

Pressure–Temperature–time paths

Calculated P–T estimates for all samples were used to construct a partial P–T path for the Dahlonega gold belt and Tugaloo terrane. Samples were separated based on the terrane in which they were collected and plotted on two different P–T–t diagrams (Fig. 4–25). Pressure estimates for sample CGB are greater than any other samples analyzed resulting in higher peak P–T for the Dahlonega gold belt (Fig. 4–25a). The P–T–t path for the Dahlonega gold belt samples is interpreted as being clockwise. Figure 4–25b shows a possible path for the Tallulah Falls Formation; peak P–T are estimated at 690 °C followed by decompression and cooling resulting in estimates at 605 °C. Pressure estimates increase at the end of the path, suggesting retrograde effects have affected the area. The P–T path for the Tugaloo terrane has a lower peak pressure estimate, but the path has a similar clockwise pattern (Fig. 4–25).

Conclusions

Rocks in the study area contain amphibolite facies assemblages. The sillimanite–kyanite and sillimanite–kyanite–staurolite zones were observed throughout the study area. Pressure-temperature estimates generally agree with those of previous studies within the study area (Quinn, 1991; Davidson, 1995), although, some estimates from this study were slightly lower than estimates calculated by other workers in this area. These lower temperatures are likely due

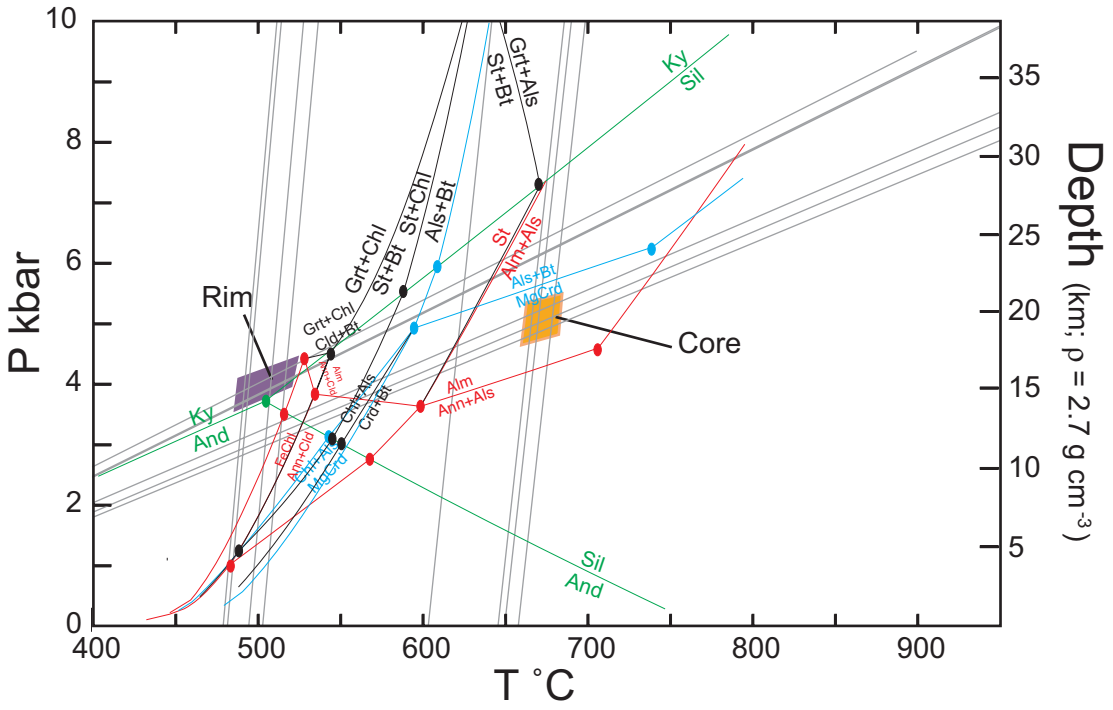


Figure 4–17. Core and rim thermobarometry results for sample SS311C, garnet 1. Reactions and invariant points are taken from the Spear and Cheney petrogenetic grid (1989). Black lines represent the KFMASH system, blue lines represent the KMASH system, and red lines represent the KFASH system. Abbreviations: Alm–almandine; Als–aluminum silicate; Annite–Fe-rich biotite; Chl–chlorite; Cld–chloritoid; Crd–Cordierite; FeChl–Fe-rich chlorite; Grt–garnet; MgCrd–Mg-rich cordierite; St–staurolite.

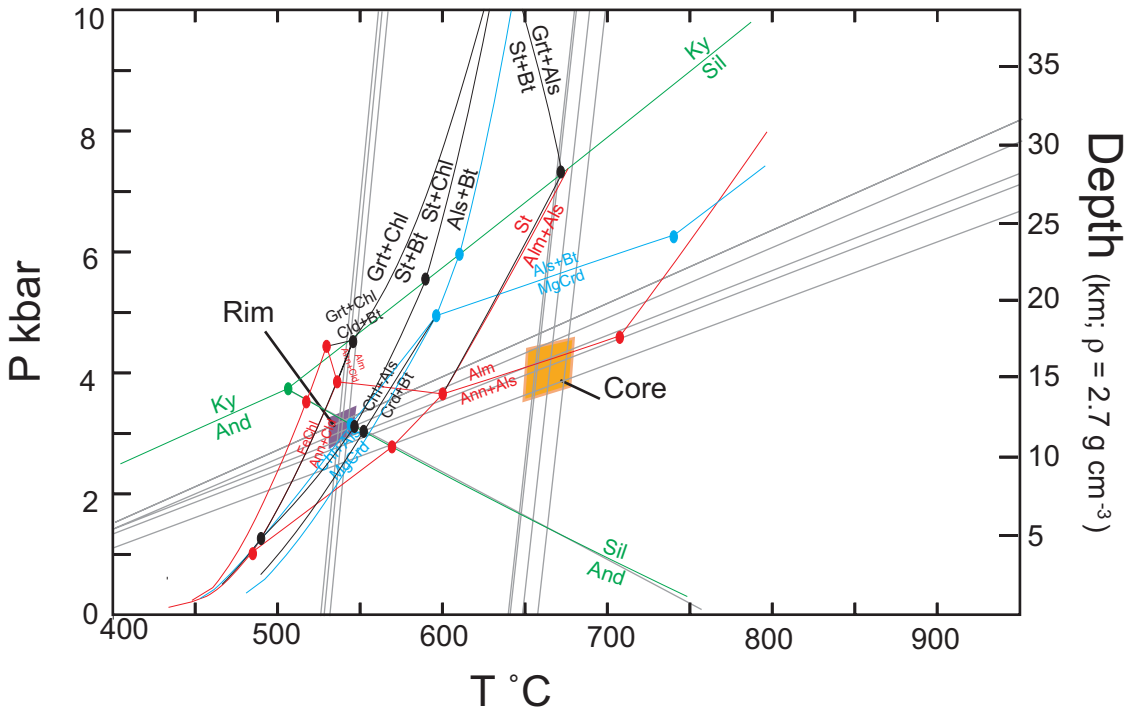


Figure 4–18. Core and rim thermobarometry results for sample SS311C, garnet 2. Reactions and invariant points are taken from the Spear and Cheney petrogenetic grid (1989). Black lines represent the KFMASH system, blue lines represent the KMASH system, and red lines represent the KFASH system. Abbreviations: Alm–almandine; Als–aluminum silicate; Annite–Fe-rich biotite; Chl–chlorite; Cld–chloritoid; Crd–Cordierite; FeChl–Fe-rich chlorite; Grt–garnet; MgCrd–Mg-rich cordierite; St–staurolite.

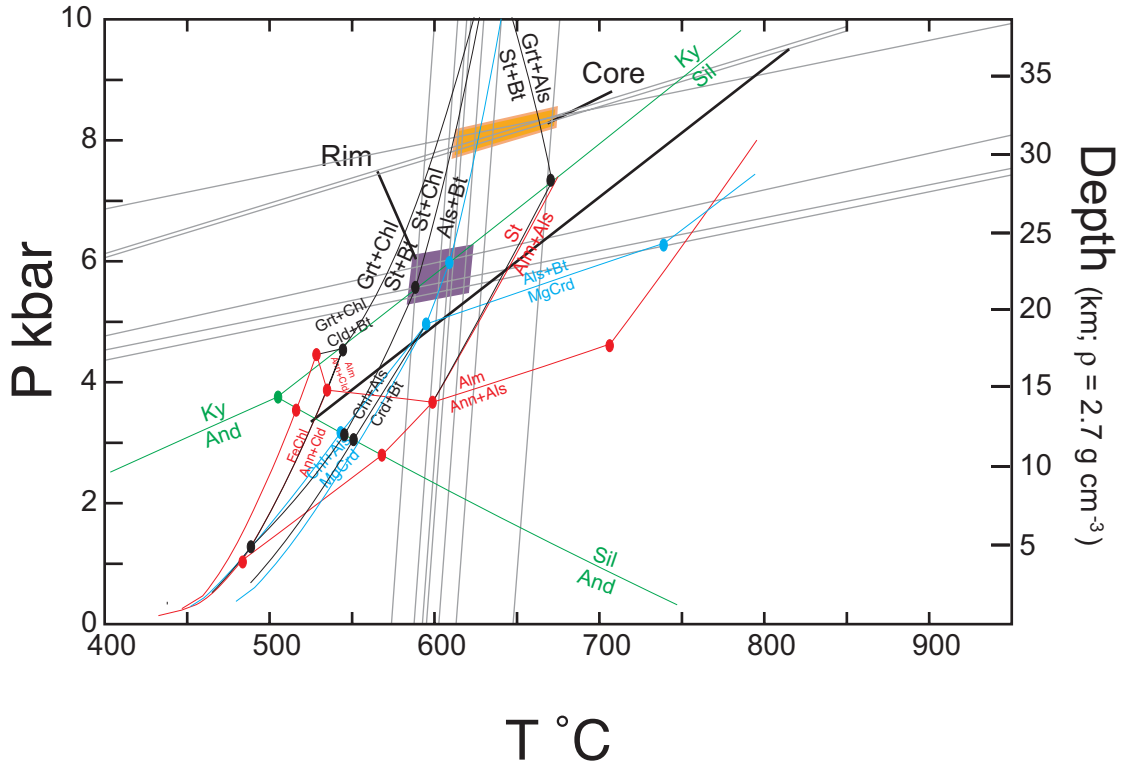


Figure 4–19. Core and rim thermobarometry results for sample CGB. Reactions and invariant points are taken from the Spear and Cheney petrogenetic grid (1989). Black lines represent the KFMASH system, blue lines represent the KMASH system, and red lines represent the KFASH system. Abbreviations: Alm–almandine; Als–aluminum silicate; Annite–Fe-rich biotite; Chl–chlorite; Cld–chloritoid; Crd–Cordierite; FeChl–Fe-rich chlorite; Grt–garnet; MgCrd–Mg-rich cordierite; St–staurolite.

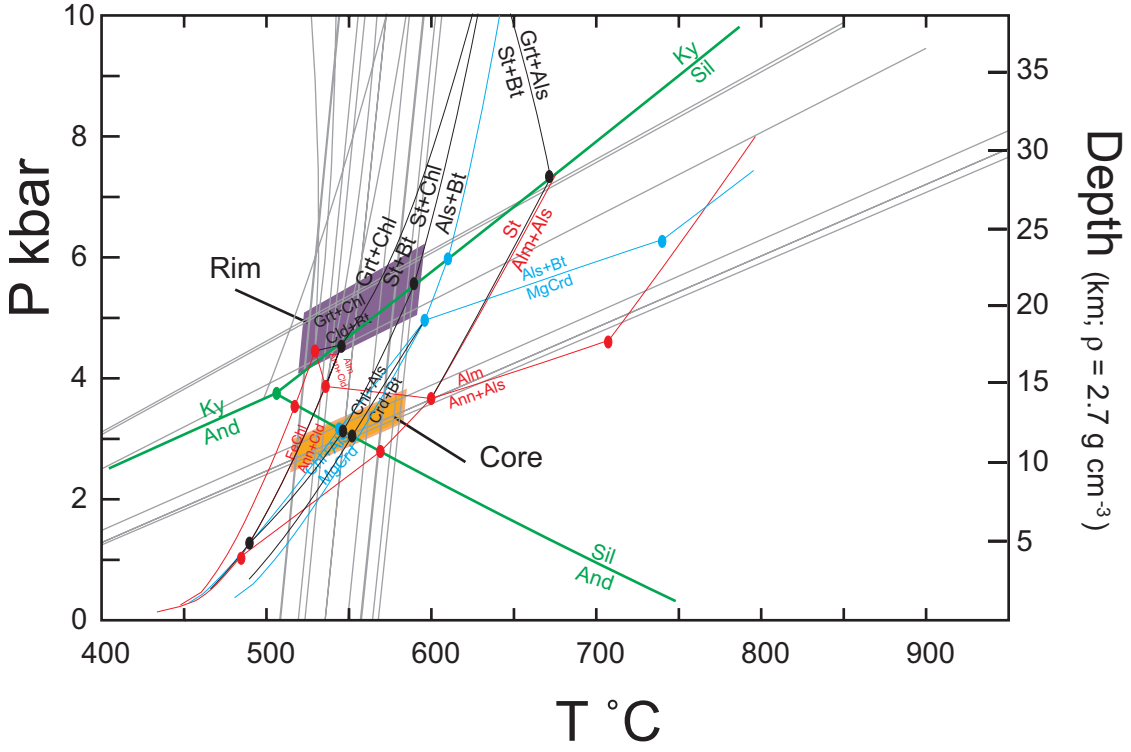


Figure 4–20. Core and rim thermobarometry results for sample 478. Reactions and invariant points are taken from the Spear and Cheney petrogenetic grid (1989). Black lines represent the KFMASH system, blue lines represent the KMASH system, and red lines represent the KFASH system. Abbreviations: Alm–almandine; Als–aluminum silicate; Annite–Fe-rich biotite; Chl–chlorite; Cld–chloritoid; Crd–Cordierite; FeChl–Fe-rich chlorite; Grt–garnet; MgCrd–Mg-rich cordierite; St–staurolite.

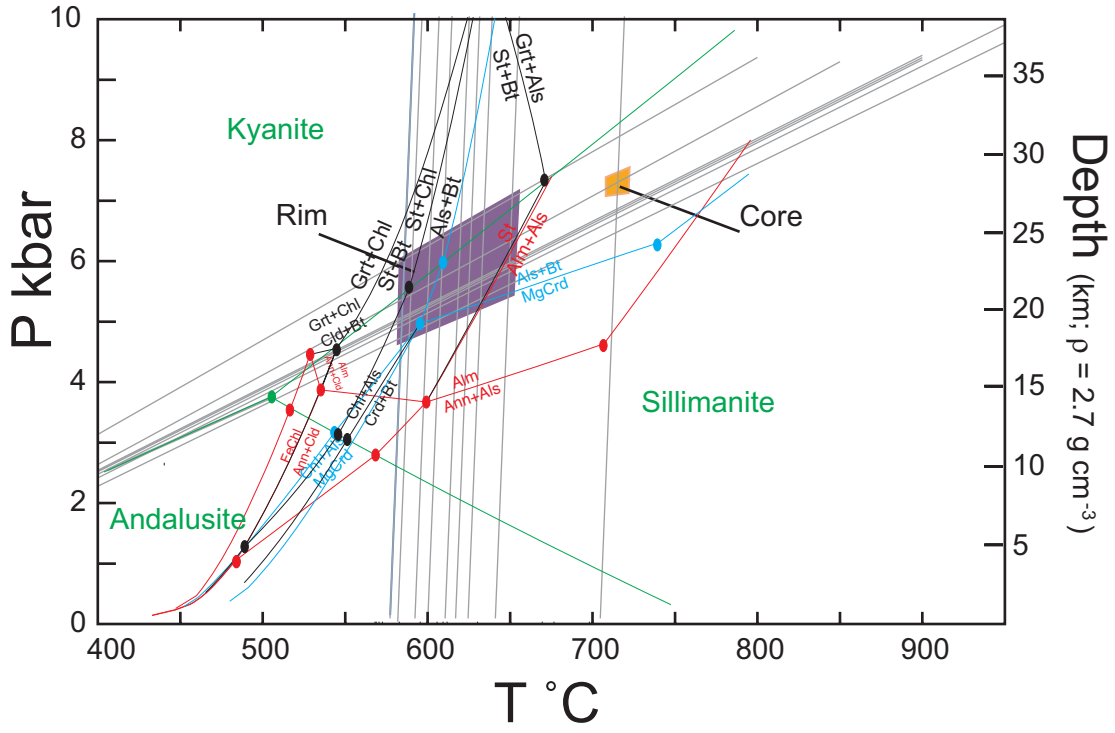


Figure 4–21. Core and rim thermobarometry results for sample 1498. Reactions and invariant points are taken from the Spear and Cheney petrogenetic grid (1989). Black lines represent the KFMASH system, blue lines represent the KMASH system, and red lines represent the KFASH system. Abbreviations: Alm–almandine; Als–aluminum silicate; Annite–Fe-rich biotite; Chl–chlorite; Cld–chloritoid; Crd–Cordierite; FeChl–Fe-rich chlorite; Grt–garnet; MgCrd–Mg-rich cordierite; St–staurolite.

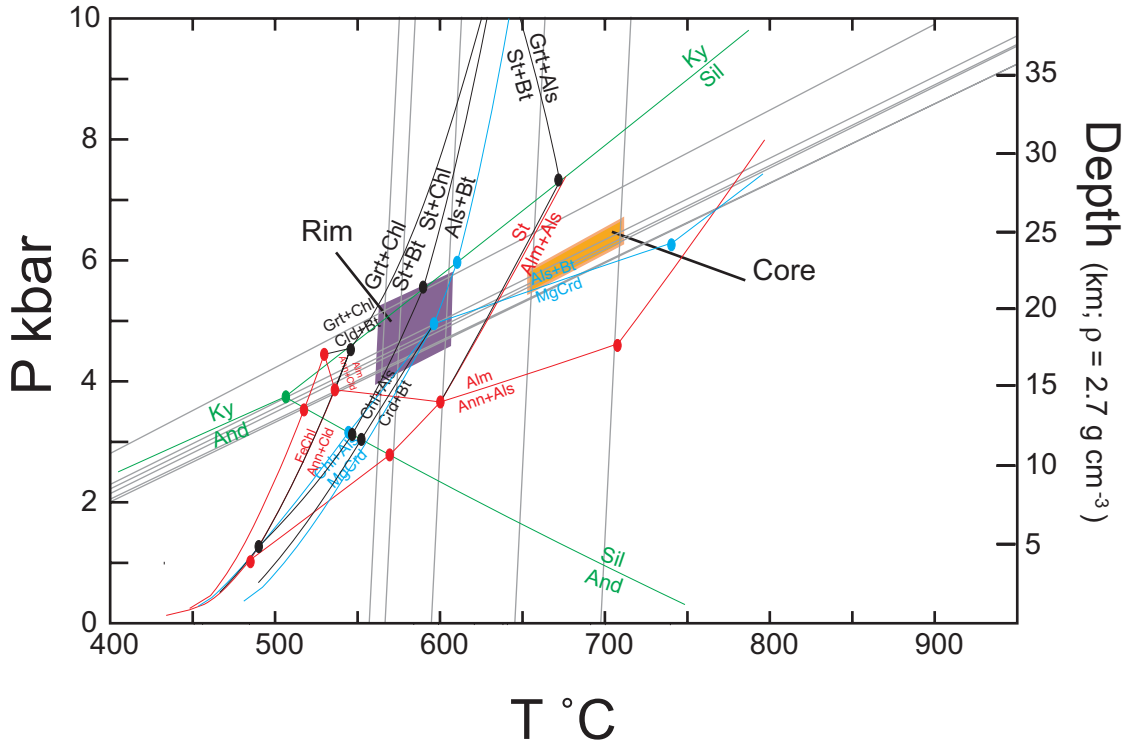


Figure 4–22. Core and rim thermobarometry results for sample 588. Reactions and invariant points are taken from the Spear and Cheney petrogenetic grid (1989). Black lines represent the KFMASH system, blue lines represent the KMASH system, and red lines represent the KFASH system. Abbreviations: Alm–almandine; Als–aluminum silicate; Annite–Fe-rich biotite; Chl–chlorite; Cld–chloritoid; Crd–Cordierite; FeChl–Fe-rich chlorite; Grt–garnet; MgCrd–Mg-rich cordierite; St–staurolite.

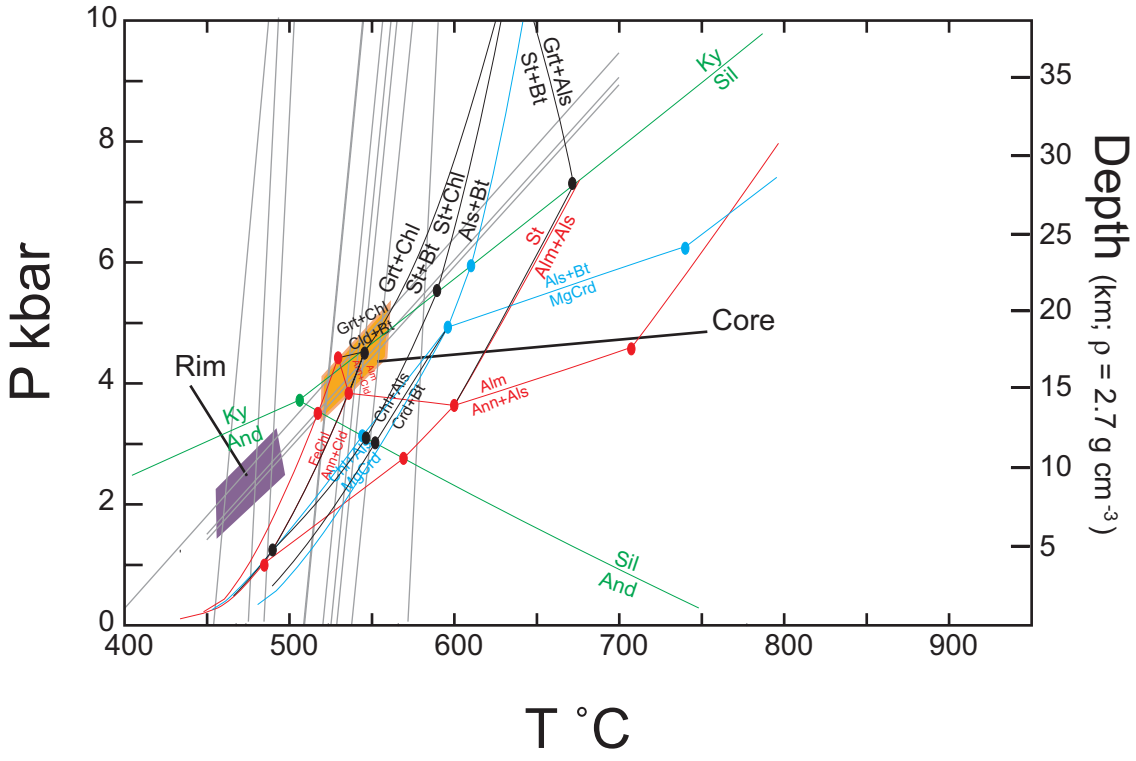


Figure 4–23. Core and rim thermobarometry results for sample 862. Reactions and invariant points are taken from the Spear and Cheney petrogenetic grid (1989). Black lines represent the KFMASH system, blue lines represent the KMASH system, and red lines represent the KFASH system. Abbreviations: Alm–almandine; Als–aluminum silicate; Annite–Fe-rich biotite; Chl–chlorite; Cld–chloritoid; Crd–Cordierite; FeChl–Fe-rich chlorite; Grt–garnet; MgCrd–Mg-rich cordierite; St–staurolite.

Table 4–1. Results of pressure–temperature calculations for Dahlonega gold belt (DGB) and Tugaloo terrane (TUG) samples. Thermometers and barometers: HP = Hodge and Powell, 1985; FS = Ferry and Spear, 1982; P = Pownceby et al., 1987; HS = Hodge and Spear, 1982.

Sample	Terrane	Core T (°C)	P (kbars)	Rim (T °C)	P (kbars)	T thermometer	B barometer
CGB	DGB	605–675	7.7–8.6	580–625	5.1–6.1	HP	PH
311C Gt1	DGB	650–675	3.6–4.5	525–550	2.7–3.5	FS	HS
311C Gt2	DGB	655–690	4.6–5.5	480–525	3.6–4.4	FS	HS
1498	TUG	705	6.6	575–645	4.3–6.6	P	HS
478	TUG	520–585	2.5–3.9	525–595	4.0–6.1	FS	HS
862	TUG	520–560	3.2–5.3	450–495	1.6–3.2	P	HS
588	TUG	650–710	5.6–6.4	555–610	3.9–5.9	P	HS

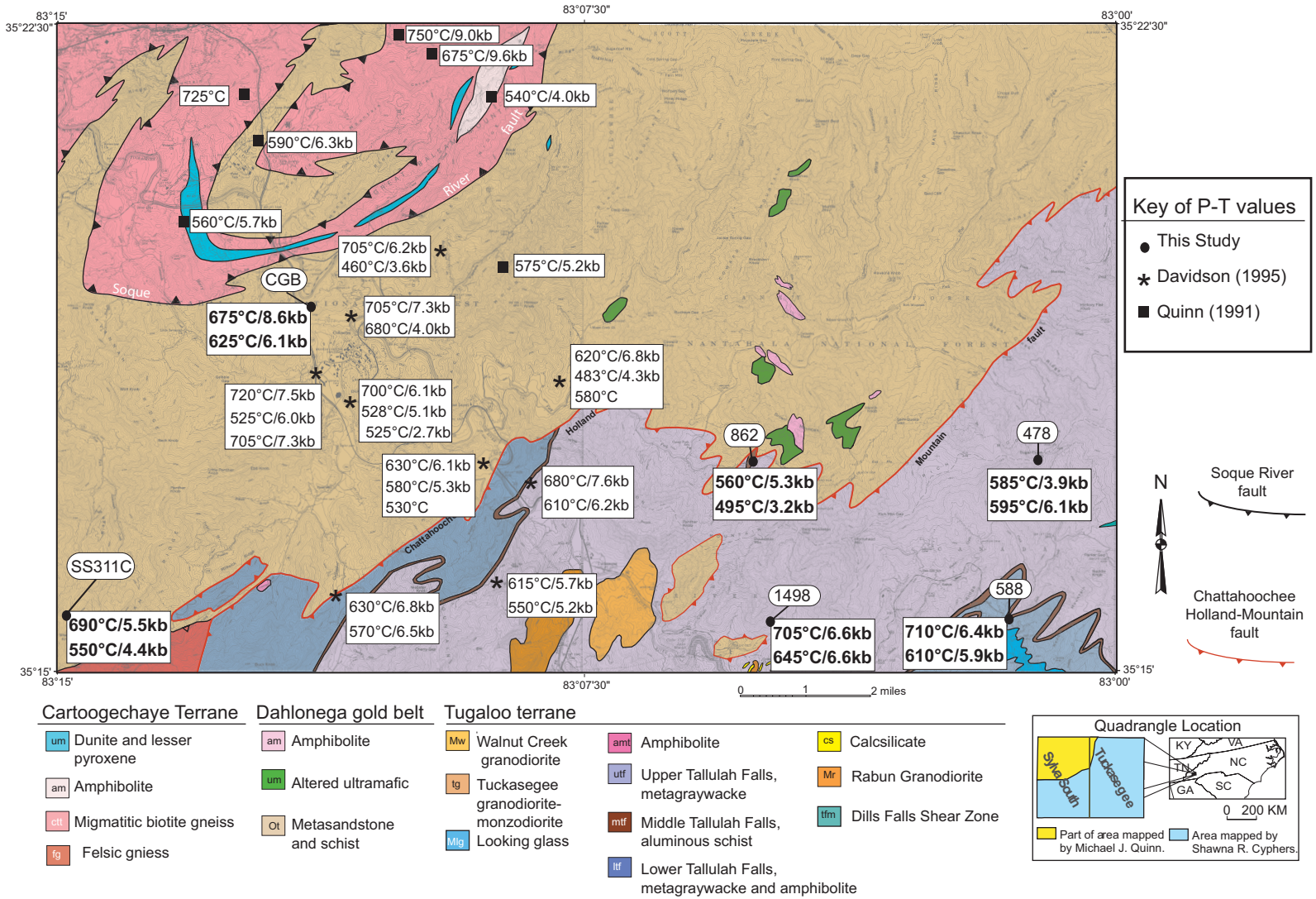


Figure 4–24. Simplified bedrock geologic map of Sylva South and Tuckaseegee quadrangles illustrating major rock units, faults, and locations of samples and P-T estimates for this study and P-T estimates from Davidson (1995) and Quinn (1991).

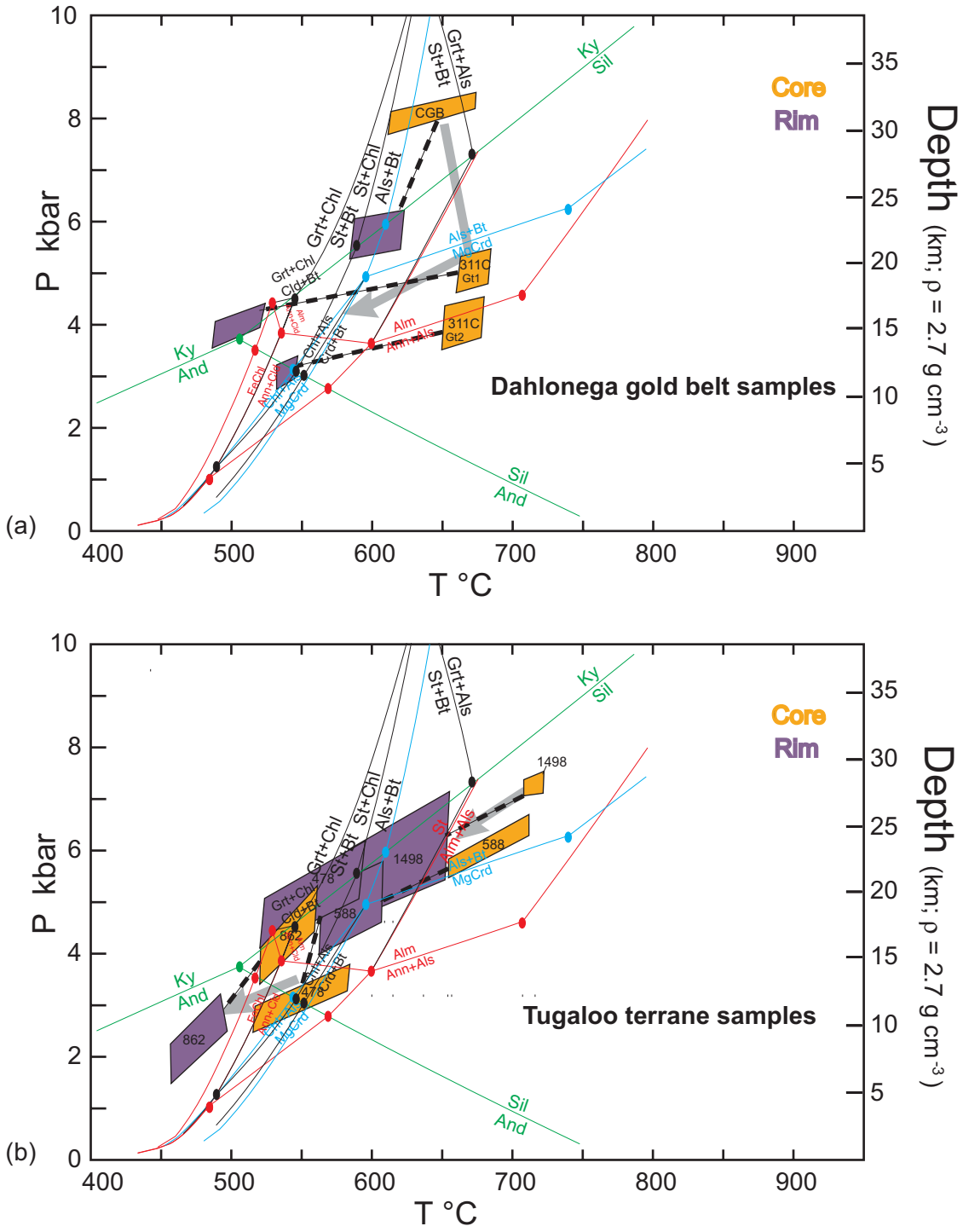


Figure 4–25. Partial P–T–t paths (gray lines) for (a) Dahlonega gold belt and (b) Tugaloo terrane samples. Dashed lines connect core and rim estimations for each reaction. Reactions and invariant points are taken from the Spear and Cheney petrogenetic grid (1989). Black lines represent the KFMASH system, blue lines represent the KMASH system, and red lines represent the KFASH system.

to diffusion, because there is evidence for both diffusion and growth zoning in the garnet profiles and inclusion data. Exchange of garnet with surrounding phases may have altered rim compositions resulting in lower P-T estimates. Diffusion may have also affected garnet compositions near inclusions, thus lowering P-T estimates.

P-T calculations fall into the range of conditions that are expected for the observed mineral assemblage. Both P–T–t paths are clockwise and the Dahlonega gold belt starts with high P and relatively high T (8.7 kbars and 675° C). Comparatively, Tallulah Falls Formation peak pressures are lower, but peak temperatures are higher than peak estimates for the Dahlonega gold belt (7.2 kbars and 725 °C). The higher temperature estimates in the Dahlonega gold belt, in comparison to the Tugaloo terrane is at odds with the migmatitc textures that are common in the Tallulah Falls Formation. This discrepancy may be due to the higher quartz content in rocks of the Dahlonega gold belt or more water may have been present in the Tallulah Falls Formation. Cooling and decompression resulted in retrograde overprinting of the amphibolite facies assemblages evidenced by chlorite observed in embayed and fractured zones of garnet porphyroblasts.

CHAPTER V Deformation and Structural Style in the Blue Ridge

Introduction

The Appalachians have undergone a complete Wilson cycle that involved three tectonothermal events; as a result, deformation in the Blue Ridge is pervasive and complex. Large westward- and SW verging thrust faults of differing ages and structural character are found in all regions of the Blue Ridge. The dominant foliation (S_2) is orogen parallel and is distinctive throughout the study area. Multiple tectonothermal events produced several generations of folds and foliations (Hatcher and Goldberg, 1991), and at least five deformational events are present throughout the region.

Interesting questions concerning the study area have come to light in recent years, because of known observations of crosscutting relationships and recent geochronologic discoveries. In particular, the truncation of the Rabun granodiorite (335 Ma) (Stahr, 2008) by the Chattahoochee-Holland Mountain Chattahoochee-Holland Mountain fault. In the past, the structural character of each Paleozoic event was broadly interpreted as follows: Taconic structures are ductile and penetrative throughout the Blue Ridge, and are overprinted by Neoacadian ductile to semi–ductile structures, and later brittle Alleghanian structures (Hatcher and Goldberg, 1991). Now an Alleghanian ductile event is considered, because of the Alleghanian age of the Chattahoochee-Holland Mountain fault.

Deciphering crosscutting structures in the field area allows correlation between structural geometries and corresponding deformational events. Detailed analysis of the structural character of this area is essential in order to piece together the tectonothermal history of the Blue Ridge.

Domains

S_0 or original (primary) stratigraphic layering is obscured by metamorphic differentiation and transposition (Quinn, 1991). An exception to this is the tripartite stratigraphy of the Tallulah Falls Formation (Tallulah Falls Formation) (see Chapter 2) composed of a lower unit of biotite–rich metasandstone with abundant interlayered amphibolite, a middle aluminous schist unit, and an upper unit of biotite–rich metasandstones and sparse amphibolite (Hatcher, 1971). The dominant foliation in the study area is S_2, which forms the regional foliation (NE–SW), and is defined by aligned micas, amphiboles, and aluminum silicates, and compositional layering. S_2 is axial planar to F_2 folds and is concordant across the Chattahoochee-Holland Mountain and SR faults (Fig. 5–1).

Approximately 1650 foliation measurements were collected in the study area. Foliation measurements were separated based on general orientation and the relationship to surrounding foliation trends. The form-line map (Fig. 5–1) displays structural trends, and three homogeneous domains are defined. The majority of foliations in the study area clearly strike NE–SW and dip moderately to steeply to the NW and SE. These foliation trends comprise Domain I. Poles to foliation were plotted and contoured on a lower hemisphere equal–area stereonet (Fig. 5–1). Folding of S_2 surfaces occurred about axes that plunge gently to the NE (18°, N44ºE) as shown by β in Figure 5–1.

Domain II is smaller than any other domain in the study area and is made up of foliation trends that strike NW–SE and dip moderately to steeply to the NE. The β axis for this foliation set plunges moderately to the NE (32°, N21ºE) (Fig. 5–1). Domain III strikes NW–SE and dips moderately to the NE. The mean foliation for this domain is oriented N35ºW, 38ºNE. This domain represents part of map scale NE plunging antiform (β axes: 28°, N8ºE) that extends NE into the Waynesville quadrangle (Merschat, pers. comm.) (Fig. 5–1).

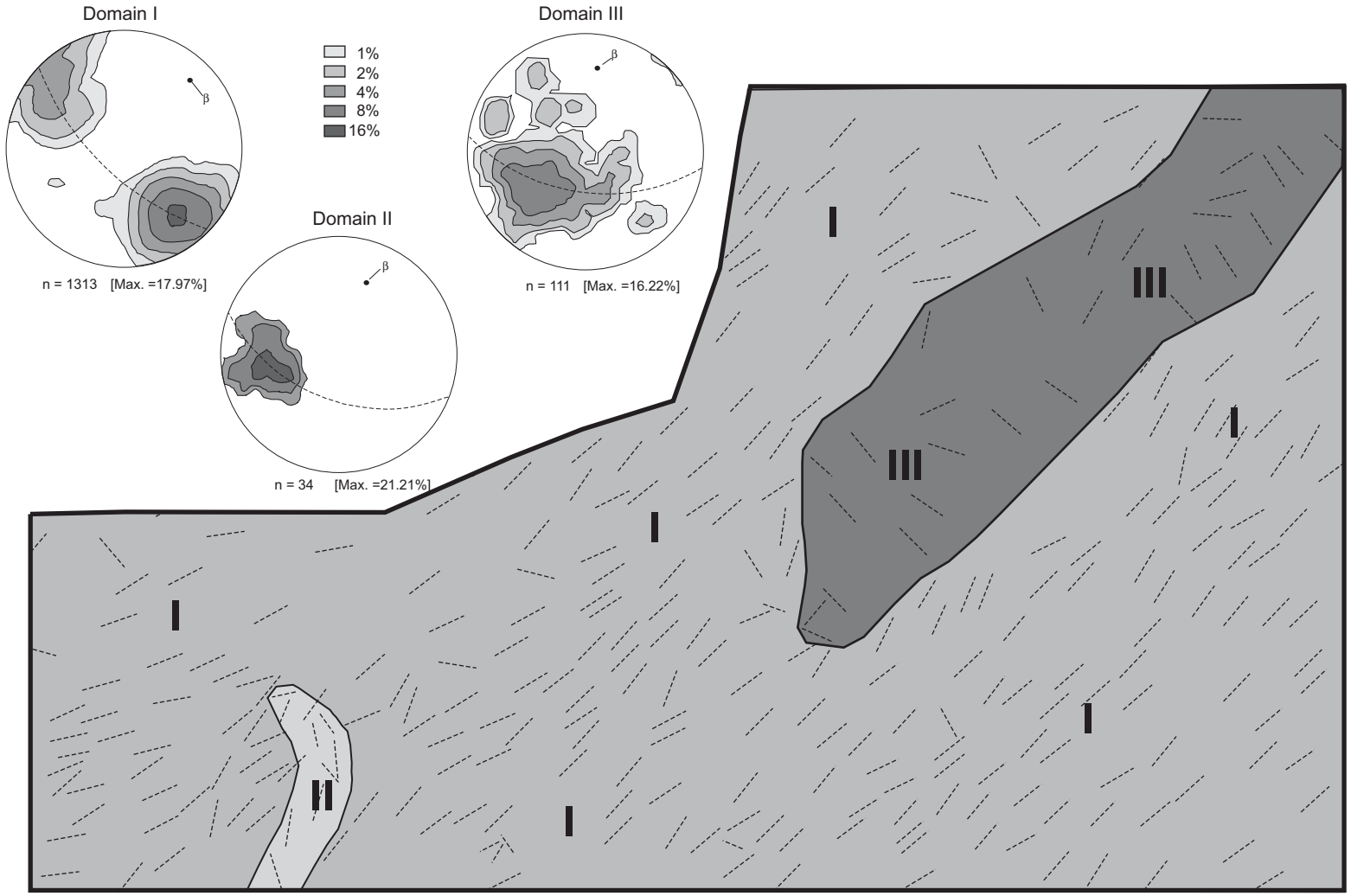


Figure 5–1. Form-line map showing generalized foliation trends, domains, and equal-area stereonet plots of foliation data. β indicates the orientation of the major fold axis and dashed great circles represent the calculated girdle.

Folds

Folding is pervasive throughout the study area, and various fold styles are present and indicative of multiple tectonothermal pulses. Hatcher and Butler (1979) suggested six possible folding/deformational events in the southern Appalachian Blue Ridge. Other workers in this area of the Blue Ridge (Hatcher, 1977; Hatcher and Butler, 1979; Eckert, 1984; Gillon, 1989; Quinn, 1991; Hopson, 1994; Settles, 2002; Stahr, 2008) observed at least five fold generations deciphered from crosscutting relationships (Table 5–1).

Folds observed in the study area were separated by morphology, and scatter plots of lower hemisphere equal-area and contoured diagrams (Fig. 5–2). All fold sets trend NE or SW except for open folds, which trend only NE. The majority of isoclinal folds plunge moderately to steeply to the NE and most verge to the SE. Tight folds also verge to the SE, but exhibit gentle to steep plunges. The closed fold set has moderate to gentle plunge and NW vergence. Open folds exhibit moderate plunge and trend to the NE. Gentle folds exhibit shallow plunge and verge to the SE.

Faults

The Chattahoochee-Holland Mountain and Soque River faults were traced through the study area. The Soque River fault separates two central Blue Ridge terranes: the Cartoogechaye terrane and the Dahlonega gold belt. The fault truncates foliation and juxtaposes terranes of different grades, and is therefore postmetamorphic (Hopson et al., 1989). SHRIMP U-Pb ages of ~455 Ma of detrital zircons collected from the Great Balsam Mountains Window indicate this terrane was metamorphosed during the Taconic orogeny (Merschat et al., 2006). The post-metamorphic Soque River fault is a bounding fault of the Dahlonega gold belt and is interpreted as a post-Taconic (Neoacadian?) structure.
The Chattahoochee-Holland Mountain fault juxtaposes migmatitic staurolite to kyanite to sillimanite grade Tugaloo terrane rocks southwestward over staurolite to kyanite to sillimanite grade rocks of the Dahlonega gold belt, and was tightly

Table 5–1. Compilation from previous studies of deformation and folding in the central and eastern and central Blue Ridge modified from Settles (2002) and Hopson (1994).

This Study	D_1 S_1 inclusion trails of quartz and sillimanite in early garnet cores.	D_2 S_2 dominant foliation and schistosity; isoclinal, axial planar folds, NW- NE - trending, D_2 structures are penetrative	D_3 F_3 - Upright tight folds, lesser crenulation and poorly developed S_3 at a low angle to S_2 foliation	D_4 F_4 - Upright closed to tight folds and crenulations, structures are non-penetrative	D_5 F_5 - Open folds upright to reclined Late isolated dome structures	Not Recognized
Stahr (2008)	D_1 S_1 inclusion trails of quartz, muscovite, and oxides in early garnet, kyanite, and staurolite porphyroblast cores.	D_2 S_2 penetrative foliation and schistosity; rootless, intrafolial, isoclinal fold hinges; F_2 tight-to-isoclinal folded gneissic layering, axial planar to S_2	D_3 F_3 - upright, open to tight (lesser isoclinal), NE - trending axes; Moderately developed axial planar foliation in hinge zones	D_4 F_4 - weak-to-moderately developed crenulation cleavage, NE-SW-plunging; chevron kink folds	D_5 F_5 - NE trending upright, open folds	Not Recognized
Hatcher (2004)	F_0 suggested that macroscopic structure of the Toxaway dome required pre-F_1 folds, thus F_0	F_1 isoclinal, E- to NE - trending fold axes, recumbent; S_1 dominant foliation	F_2 isoclinal to open, NE - trending, upright	F_3 crenulations. NE trending, upright; S_4 - crenulation cleavage	F_4 open, flexural folds, NE- trending, upright	F_5 open, flexural folds, NW-trending, upright
Hatcher and Butler (1979)	F_1 isoclinal, EW- to NE-trending axes, recumbent, observed in amphibolite boudins and as intrafolial folds	F_2 isoclinal, EW- to NW-trending fold axes, recumbent; S_1 - dominant foliation	F_3 isoclinal to open, NE - trending, upright	F_4 crenulations. NE- trending, upright; crenulation cleavage	F_5 open, NE- trending, upright	F_6 open, NW-trending, upright
Settles (2002)	D_1 Early S_1 foliation preserved with isoclinal, recumbent F_2 folded amphibolite boudins	D_2 F_2 - isoclinal with axial planar S_2 penetrative schistosity and gneissic banding (dominant)	D_3 F_3 - tight to isoclinal; S_3 - nonpenetrative axial planar cleavage	D_4 F_4 - crenulations and chevron folds; S_4 - crenulation cleavage	D_5 F_5 - open, upright folding of all previous structures	D_6 Not Recognized
Eckert (1984)	Not Recognized	F_1 isoclinal, E- to NE - trending fold axes, recumbent, upright; S_1 dominant foliation	F_2 tight to isoclinal, NE - trending, upright	F_3 open to tight folds and crenulations, NE- trending	F_4 upright, crenulations	Not Recognized
Gillon (1989)	F_1 rootless, NE- to WNW-trending fold axes, recumbent	Not Recognized	F_2 isoclinal, NE - trending, upright	F_3 crenulations; S_3 - crenulation cleavage locally observed	F_4 open upright folds produce dome and basin interference pattern	Not Recognized
Hopson (1994)	D_1 F_1 - intrafoliol folds, orientation unknown; S_1 - includes pinstriping and gneissic banding	D_2 F_2 - NE trending, recumbent to upright due to later folding by F_3; S_2 - dominant foliation, penetrative schistosity and gneissic banding	D_3 F_3 - tight to isoclinal, NE - trending, axial surfaces upright to steeply dipping; S_3 - nonpenatrative	D_4 F_4 - crenulations and chevron folds, NE- to NW- trending (orientation depends on rotation of surface folded) subhorizontal to gently dipping axial surfaces; S_4 - crenulation cleavage	D_5 F_5 - open, NE- to EW-trending, upright	D_6 F_6 - open, N to NW-trending, upright

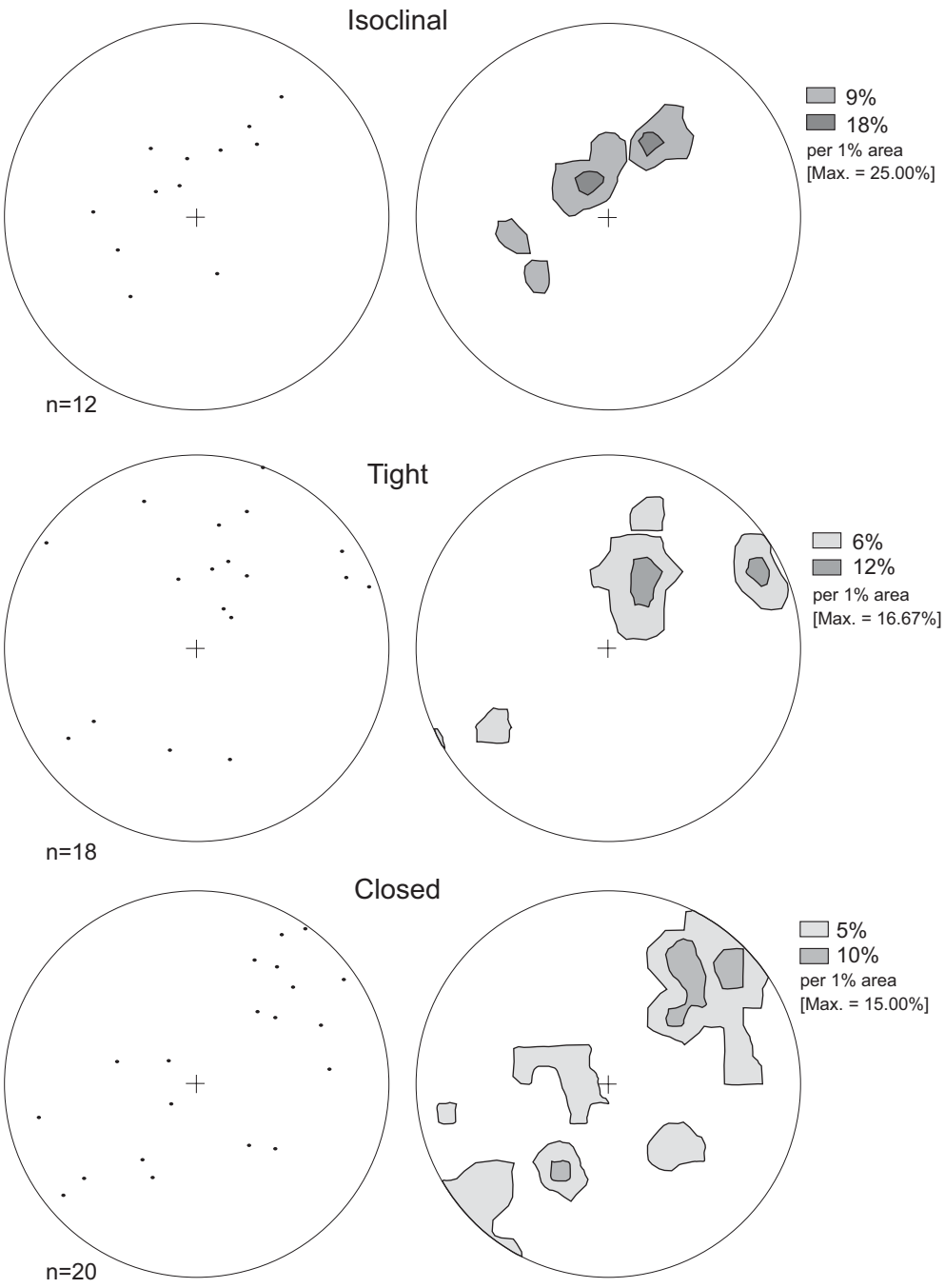


Figure 5–2. Equal-area stereonet plots of fold data. Scatter plots of fold hinges are shown on the left and lower hemisphere, equal-area contoured diagrams are shown on the right.

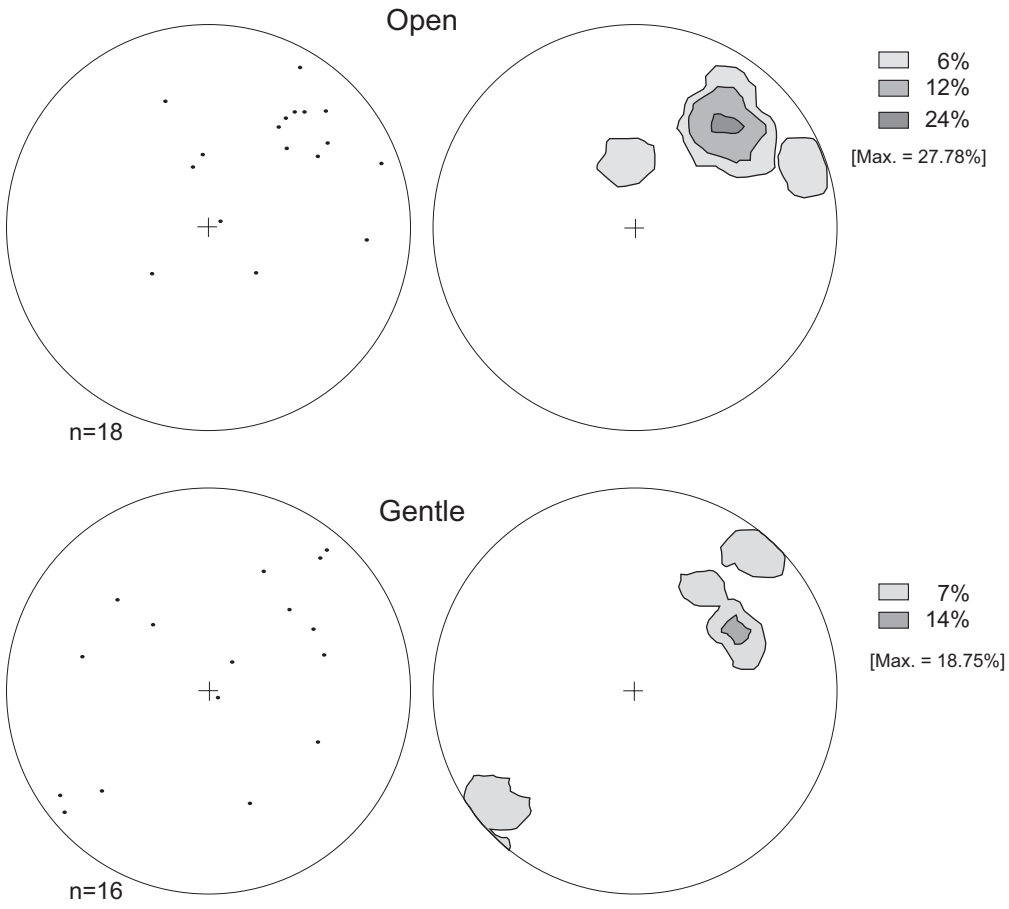


Figure 5–2 cont.

folded after emplacement. Field evidence supporting a fault contact includes truncation of lithologic units and the lithologic contrast. The Chattahoochee-Holland Mountain fault overrides the Soque River fault in the Corbin Knob quadrangle just SW of the study area (Eckert and Yurkovich, unpublished map), and the same relationship is present in the SW corner of the Sylva South quadrangle (see section below, cross section A–A').

Unraveling the history of the Chattahoochee-Holland Mountain fault is problematic; it is tightly folded, juxtaposes rocks of similar metamorphic grade, and foliation (S_2) is concordant across the fault. All of this indicates the fault is likely an early Paleozoic (Taconic?) structure; however, it also truncates the 335 Ma Rabun Granodiorite (Stahr et al., 2005; Miller et al., 2006) and therefore must be an Alleghanian fault. Small-scale shear zones were observed in the field, but were not traceable beyond single exposures (Fig. 5–3).

Map Patterns and Cross Sections

Three cross sections were constructed through the study area, each oriented normal to the regional foliation and aligned to cross major structures (Fig. 5–4). Cross section A–A' is dominated by SE-verging inclined tight folds. Truncation of the SR and Chattahoochee-Holland Mountain faults is projected above the current surface. Faults are tightly folded and indicates that the Soque River fault is a pre-Alleghanian structure. Folding styles in cross section B–B' is more variable, but is dominated by upright to inclined tight folds overprinted by later open folding. The Soque River fault exhibits closed folding exposing the Dahlonega gold belt in the core of a large antiform in the northeastern part of the cross section. The Chattahoochee-Holland Mountain fault is tightly folded and dips steeply to the NW. The easternmost cross section, C–C', contains upright to inclined tight folds (F_3) and more obvious overprinting of tight folds by later closed to open folding (F_4 and F_5). This cross section is located just east of an exposed section of the Looking Glass pluton, which is projected at depth into the



Figure 5–3. Mylonite in upper Tallulah Falls Formation located on Neddie Knob southeast part of the Tuckaseegee quadrangle.

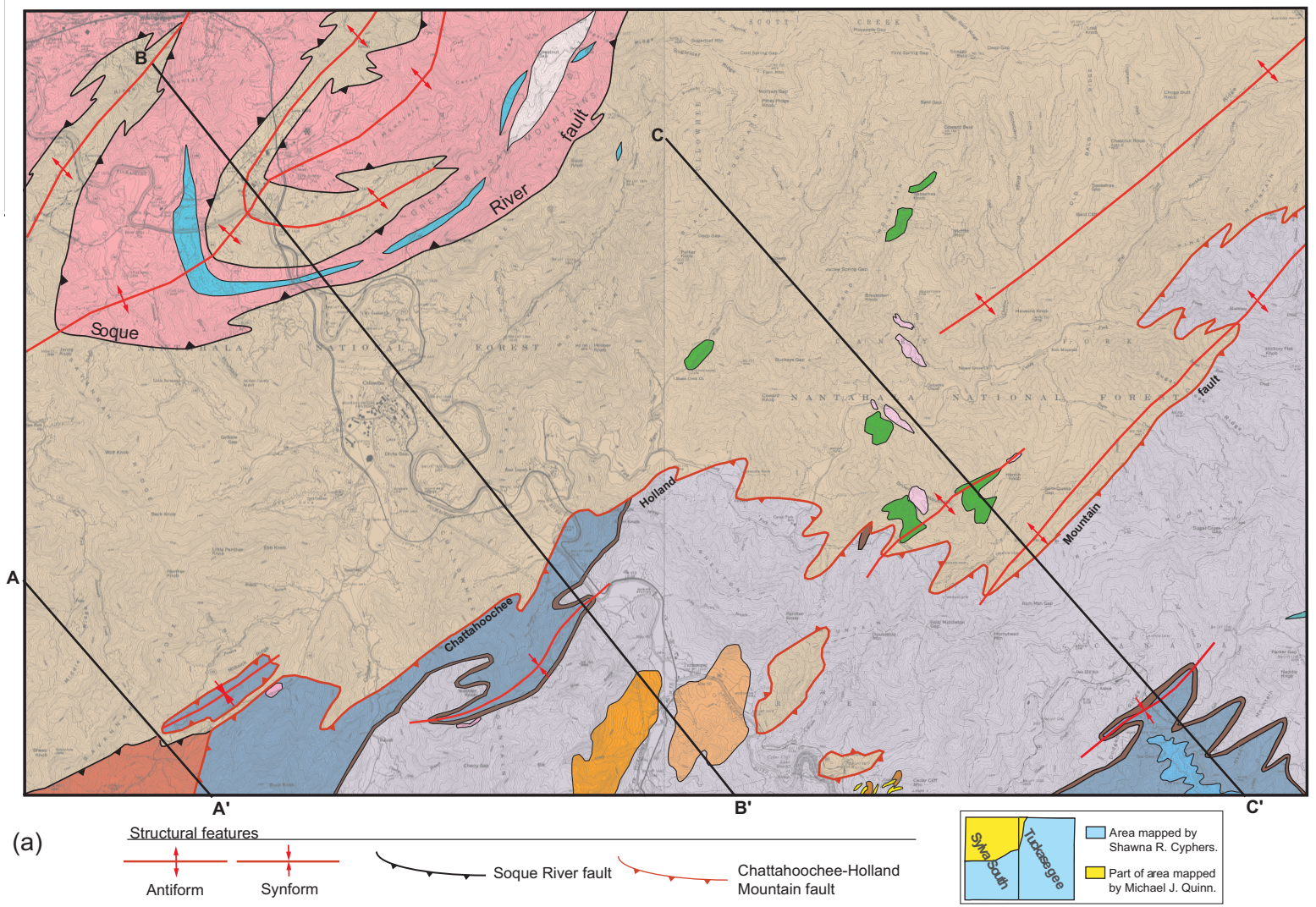


Figure 5–4. (a) Simplified bedrock geologic map of Sylva South and Tuckaseegee quadrangles illustrating major rock units, faults, topography, cross–section lines, and fold hinges. (b) Cross-section lines A-A', B-B', and C-C'. Explanation of map units on next page.

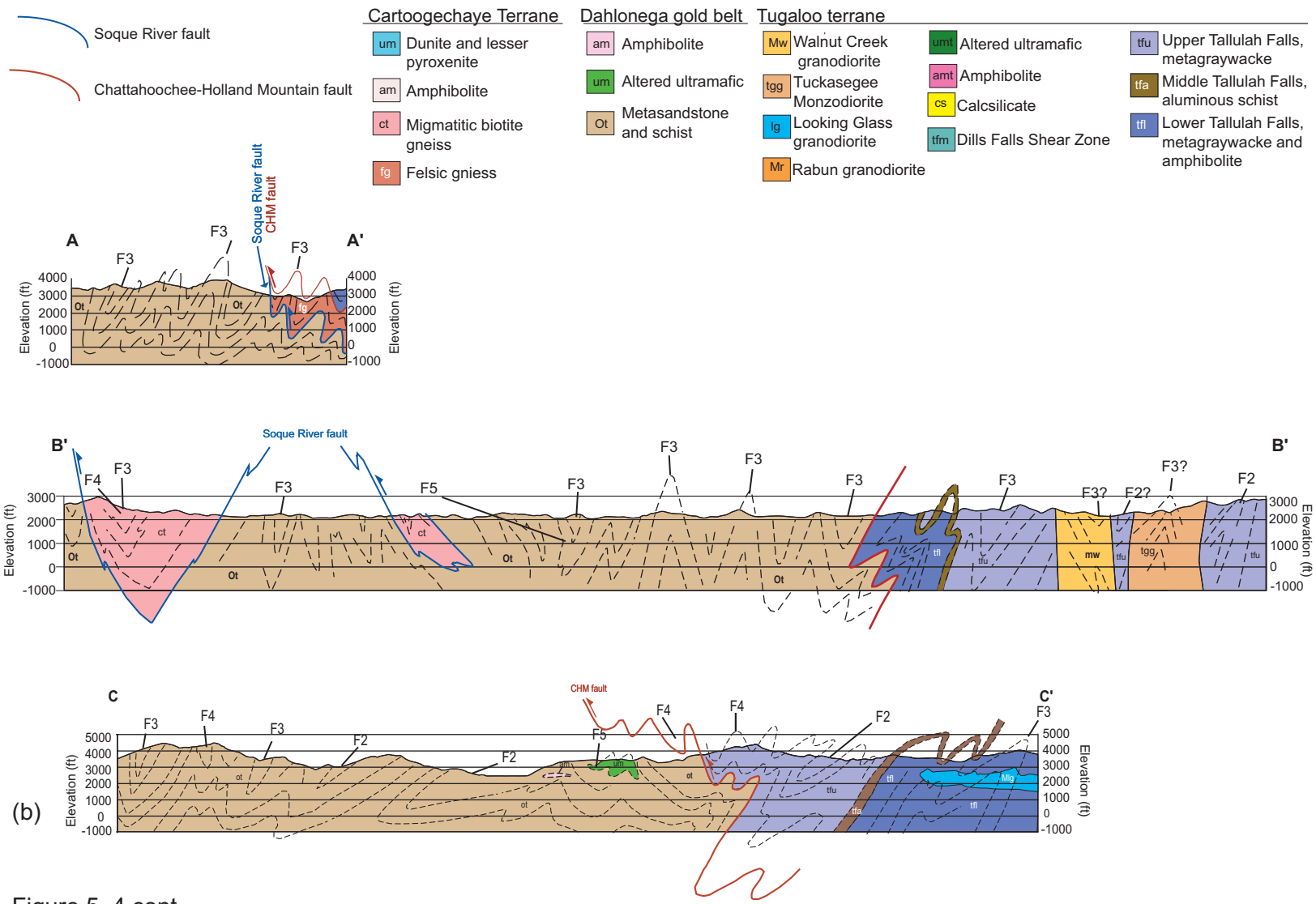


Figure 5–4 cont.

section. At the surface the Chattahoochee-Holland Mountain fault dips to the SW and is folded back to the NW at depth.

Block-in-matrix structures

Block-in-matrix structures are common and form from a range of processes, including sedimentary, igneous, diapiric, and tectonic processes (Raymond et al., 1989). These structures are found throughout the Blue Ridge province. Geochemical analysis of amphibolite blocks from the Catamount Gap and Savannah Church/Tathams Creek exposures (Chapter 3) reveal that the protolith is likely MORB. Determining how Blue Ridge block-in-matrix structures formed is complicated by multiple tectonothermal events, which transpose original textures and structure. However, multiple deformational and metamorphic events may be the processes responsible for the formation of the block-in-matrix structures in the Blue Ridge.

A description of the structural character of the Savannah Church block-in-matrix exposure is included in order to determine the origin and significance of the block-in-matrix structures in the Blue Ridge. Hatcher et al. (1984) suggested that these structures are the product of polyphase deformation involving folding, faulting, boudinage, and penetrative ductile shear. Raymond et al. (1989) interpreted the block-in-matrix units as tectonic mélanges that mark terrane sutures in the central Blue Ridge. Raymond (1984) defined mélange as, “A body of rock mappable at a scale of 1:24,000 or smaller and characterized both by the lack of internal continuity of contacts or strata and by the inclusion of fragments and blocks of all sizes, both exotic and native, embedded in a fragmented matrix of finer grained material.”

The Savannah Church and Catamount Gap block-in-matrix exposures are structurally similar. The blocks at both exposures are aligned with the dominant S_2 foliation, and are dominantly tapered (likely boudinage) with lesser sub-angular morphologies. Blocks of amphibolite, calc-silicate, and metaquartzite are present. The matrix for both exposures is composed of migmatitic gneiss,

although the matrix at the Savannah Church exposure is biotite rich whereas that at the Catamount Gap exposure contains abundant muscovite and moderate amounts of biotite. The Savannah Church exposure will be discussed further because exposure at this location has less vegetation cover than the Catamount Gap exposure.

The Savannah Church block-in-matrix structure is located along U.S. 441. Different amphibolite block morphologies are present, and range from boudinage and rounded blocks to pods with tapered ends (Fig. 5–5). Most blocks are aligned with the dominant foliation (S_2), except for rounded and angular blocks, the latter of which are found in the SW part of the exposure. Early and late-stage folds are present in the exposure and are defined based on crosscutting relationships. A tight to isoclinal fold of a leucosomal layer is present in an amphibolite pod, and is considered an F_1 fold. Early folds are isoclinal, intermediate folds are tight, and late folds are open (Fig. 5–6). Shear zones are associated with later trondhjemite dikes, which crosscut earlier structures and produce concentrated areas of greater deformation. Texturally, the rocks are migmatitic and become strongly lineated next to the shear zones.

Amphibolite blocks originated as oceanic basalt (Chapter 3), indicating that the Dahlonega gold belt sediments in this area may have been deposited near a spreading center. This would account for the elongate bands and interlayered relationship of amphibolite in the migmatitic matrix. Further evidence for the proximity of a spreading center includes the abundance of sulfides in the Dahlonega gold belt metasediments. S_1 and F_1 preserved in amphibolite blocks at Savannah Church indicate transposition of blocks after the development of an early foliation followed by an early, high-temperature deformation event that produced a new foliation (S_2), folds, and other lineations. The majority of the amphibolite blocks are concordant with the dominant foliation at the exposure (likely S_2) indicating that the blocks were likely formed during the D_2 (Taconic) event. The existence of the more angular blocks, which occur at the SW part of the exposure, is difficult to explain. It is important to note that the more angular

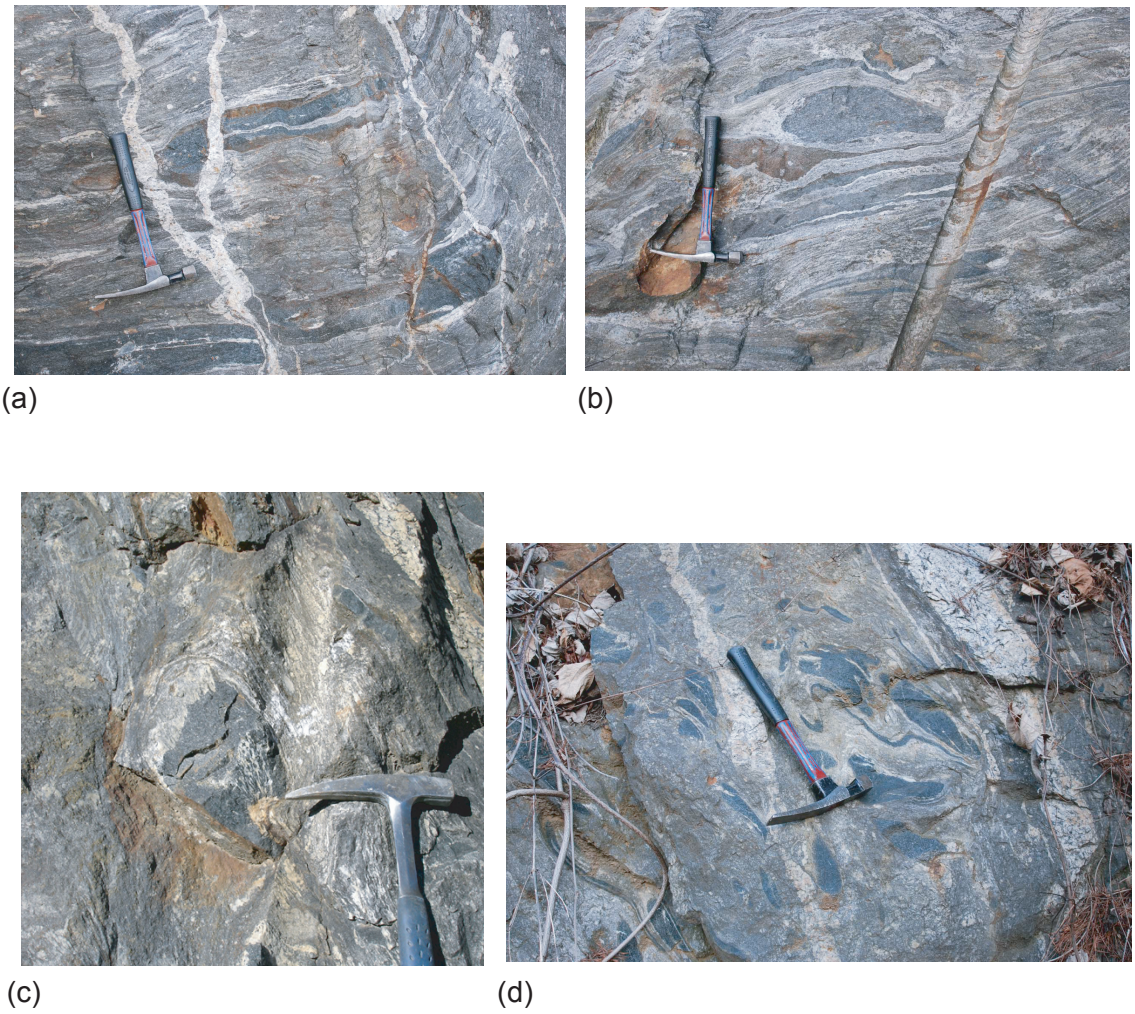


Figure 5–5. Amphibolite block morphologies at the Savannah Church block-in-matrix exposure (US441). (a) Boudinage and (b) rounded blocks are common morphologies for blocks at the Savannah Church local.(c) Pod of amphibolite with tapered end. (d) Sub-angular amphibolite blocks located at the SW part of the exposure. Photographs (a), (b), and (c) courtesy R. D. Hatcher, Jr.

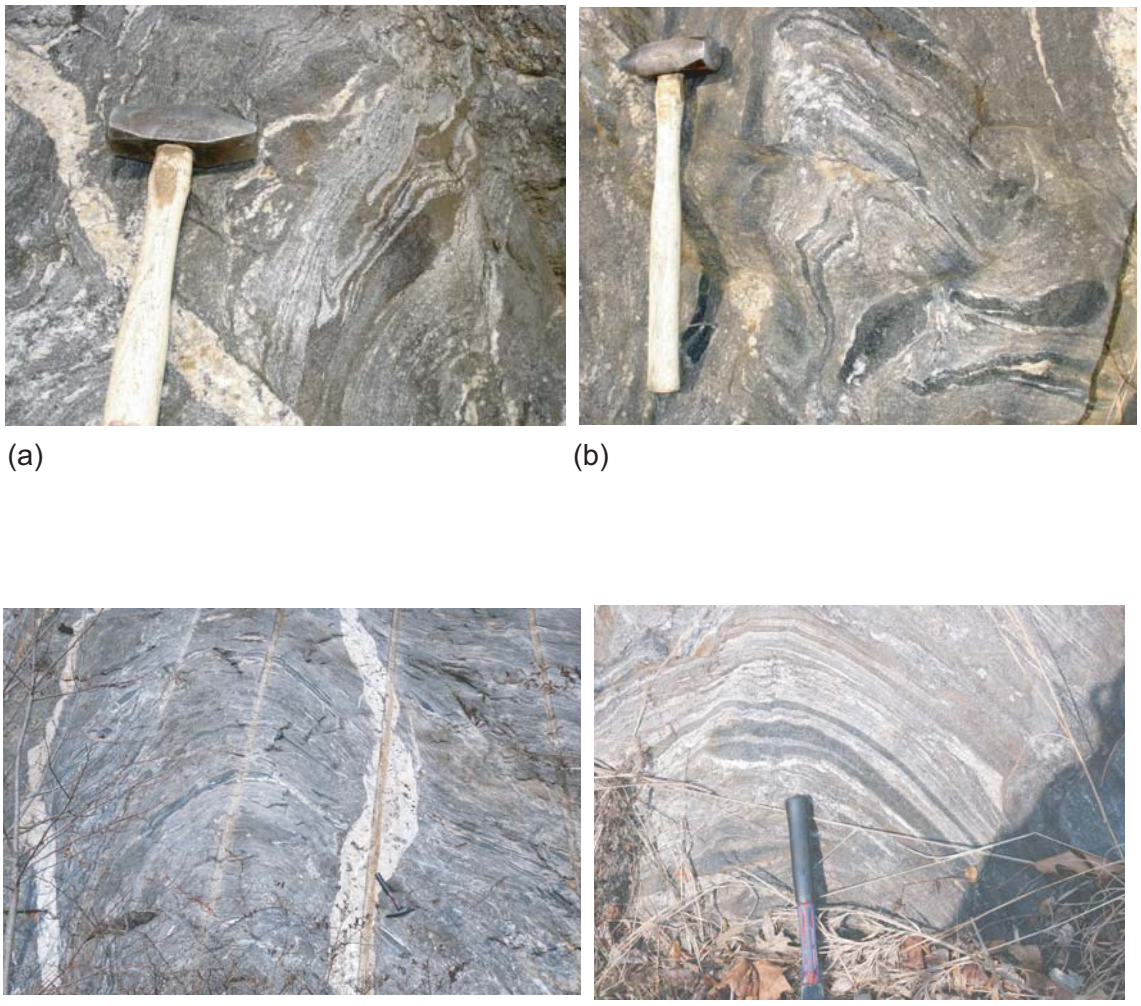


Figure 5–6. (a) Isoclinal, (b) tight, (c) closed, and (d) open folding at Savannah Church block-in-matrix structure (US 441). Photographs (c) and (d) courtesy R. D. Hatcher, Jr.

blocks are spatially isolated and are not found throughout the exposure. This may indicate that less ductile deformation was localized at this area, and resulted in the different block morphology.

Both exposures fit the basic definition of mélange by Raymond (1984), and the Savannah Church/Tathams Creek locality is located ~0.5 km from the Soque River fault, which fits the description of a tectonic mélange suggested by Raymond (1989). Conversely, the Catamount Gap exposure is not located near a terrane boundary, and the similarity of the structures and amphibolite geochemistry at the two exposures indicate components of both assemblages share a common protolith and deformational history. Crosscutting relationships of structures present at these exposures indicate that both the Savannah Church and Catamount Gap exposures are the product of polyphase deformation involving folding, faulting, boudinage, and penetrative ductile shear as suggested by Hatcher et al. (1984).

Deformation and Orogenic Events

Transposition of primary layering (S_0) into S_1, recrystallization, differentiation of lithologies, and formation of F_1 tight to isoclinal folds are products of early Taconian deformation (Quinn, 1991). Regionally, intrafolial folds and transposed foliation (S_1) are evidence for the earliest Paleozoic structures and can be found in amphibolite and calcsilicate boudins (Hatcher and Goldberg, 1991). Early structures are completely wrapped and truncated by S_2 (Hatcher and Goldberg, 1991).

In the study area, evidence for F_1 is limited to recumbent to isoclinal folds found in amphibolite boudins, and intrafolial folds, which are transposed into the regional foliation (S_2). Evidence for S_1 is present in intrafolial folds, foliation in amphibolite blocks in block-in-matrix structures, and inclusion trails of quartz and sillimanite in garnet porphyroblasts (Fig. 5–7a). Folded layers change thickness through fold hinges and into the limbs indicating F_1 folds exhibit passive flow mechanisms (Donath and Parker, 1964).

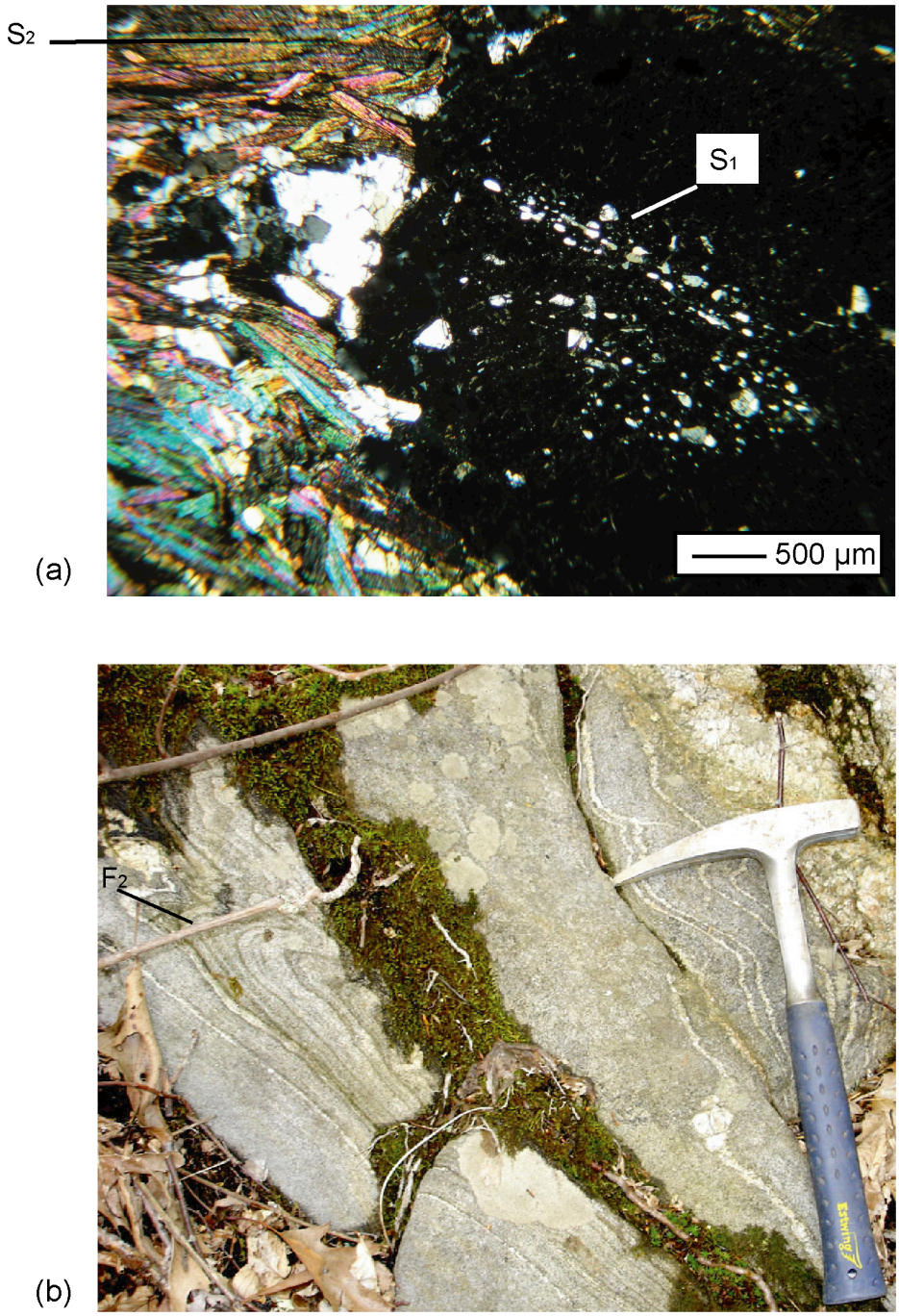


Figure 5–7. (a) Inclusion trail of quartz in garnet porphyroblast represents S_1 foliation. S_2 foliation is also indicated and wraps around the garnet porphyroblast. (b) Isoclinal F_2 folds in migmamtitic metasandstone (UTF) near Hickory Flat Knob eastern part of the Tuckaseegee quadrangle. Folds are axial planar to S_2.

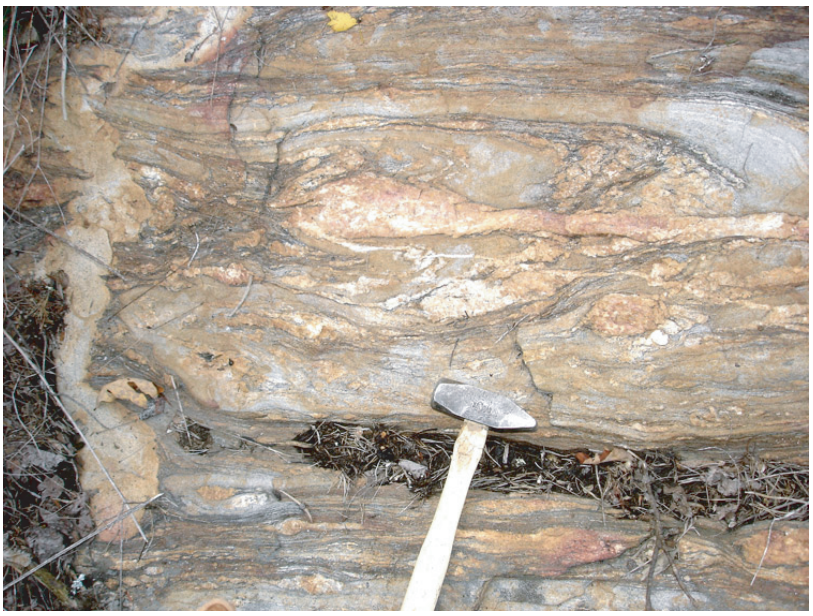
This early stage of deformation was followed by tight to isoclinal folding (F_2) overprinting F_1 and forming the dominant S_2 foliation. Axial planar, tight to isoclinal folds (F_2) are pervasive and are the most commonly observed in the study area (Fig. 5–7b). Folding style is interpreted to be passive flow, because all layers change thickness through fold hinges and into the limbs, indicating the rocks behave plastically, and rheology differences between layering plays no mechanical role in the formation of the fold (Donath and Parker, 1964).

Boudinage of more competent layers (Fig. 5–8a) is evidence of simultaneous extension in the plane of S_2 foliation (Quinn, 1991). SHRIMP U-Pb detrital zircon rim ages of 455 Ma from the Great Balsam Mountains Window (Merschat et al., 2006), and monazite and zircon rim ages from the surrounding terranes suggest D_2 is Taconic (Hatcher et al., 2007).

D_3 deformation transposed earlier D_2 structures (Fig. 5–8b) and is most readily identified by folding of the S_2 foliation; it is less commonly observed as a nonpenetrative S_3 foliation at a low angle to S_2. Tight folding is characteristic of this event and folds are upright to reclined with thickened hinges and attenuated limbs (Fig. 5–9). Quinn (1991) stated S_2 in unit 3 (Dahlonega gold belt) may not have been greatly perturbed by later folding if the layering was oriented parallel to the axial surfaces of the later fold set.

Tight folding of the Chattahoochee-Holland Mountain fault is interpreted as F_4 folds resulting from an early Alleghanian ductile event. Crenulation cleavage with tight to open morphology was also observed, commonly in schist of the Dahlonega gold belt, and is likely representative of F_4 (Fig. 5–10a). Crenulation cleavage in schistose layers likely formed by buckling and fluid induced mobility (Gray and Durney, 1979) and exhibit polyharmonic folding as a result of strain partitioning. Late-stage open cylindrical folds (Fig. 5–10b) were rarely observed in the study area and represent late Alleghanian deformation.

(a)



(b)

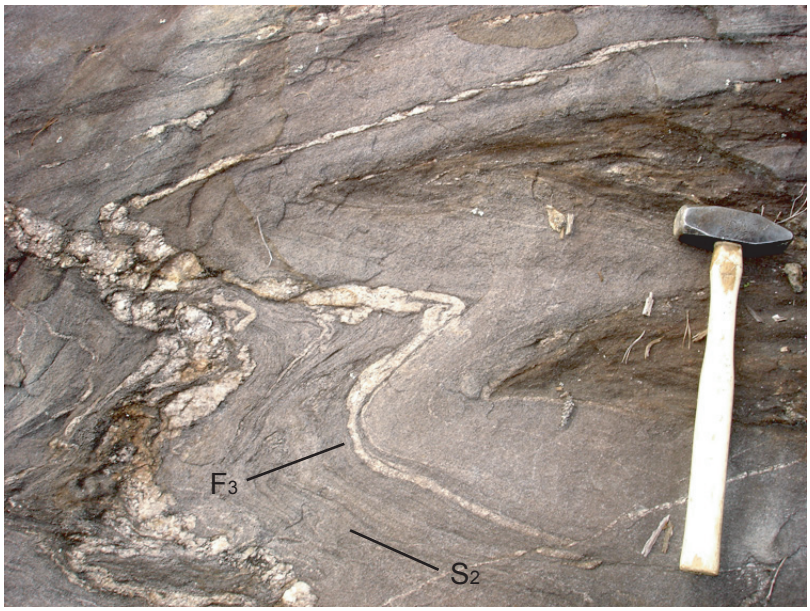
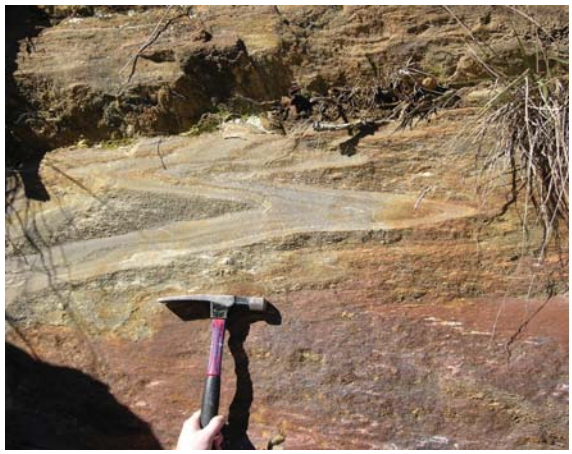


Figure 5–8. (a) Migmatitic upper Tallulah Falls Formation with isoclinal recumbent F_2 folds. Leucosomal boudins occur in the top portion of the photograph and are evidence of extension in the the plane of S_2 foliation. (b) Folding of S_2 foliation by tight flexural-flow folds (F_3). Note ptygmatically folded quartzofeldspathic layer in the lower-left portion of the photograph and asymmetric boudinage in the top of the photograph. Exposures are located near Cedar Valley Road in the southwestern part of the Tuckaseegee quadrangle.

(a)





(b)

(c)



Figure 5–9. Exposure of Otto Formation metasandstone and pelitic schist (DGB) at Speedwell Methodist Church in the town of Speedwell. (a) Tight F_3 folding of metasandstone and schist. (b) Illustration of folds in (a). (c) Same exposure showing larger view of the structures present.

(a)



(b)



Figure 5–10. (a) Crenulated schist interlayered in metasandstone, Otto Formation, southwest of Coward Knob, western part of the Tuckaseegee quadrangle. (b) Late open (F_5) fold in Otto Formation metasandstone (DGB) at Speedwell Methodist Church in the town of Speedwell.

Synthesis and Conclusions

The Taconic orogeny resulted in: high–grade Barrovian regional metamorphism in the Blue Ridge; A–type subduction of the Laurentian margin and obduction of several oceanic and arc assemblages onto the Laurentian margin with emplacement of the Cowrock, Cartoogechaye, and Tugaloo terranes; and remobilization of basement rocks (Hatcher et al., 2007). Amalgamation of old and new crust generated during the Taconic event formed a large accreted mass along the southeastern Laurentian margin. D_1 and D_2 structures likely formed during this event. These structures are penetrative and indicative of a high-grade regional event. In several areas of the Blue Ridge where Rb-Sr, K-Ar, and $^{40}Ar/^{39}Ar$ data are available, they can be interpreted as evidence for the Taconic orogeny as the dominant orogenic event (Hatcher and Goldberg, 1991). Moecher et al. (2005) suggested that D_3 is a product of a protracted Acadian event. In the study area mesoscopic and map-scale upright tight folds (Fig. 5–4) are interpreted as F_3.

Alleghanian deformation resulted in the NW transport of thrust sheets in the southern Appalachians. Blue Ridge deformation is largely associated with transport of thrust sheets, either along low–angle thrust or dextral strike–slip faults (Hatcher and Goldberg, 1991). D_4 is interpreted as an early Alleghanian, post-peak metamorphic, high temperature event. This interpretation is a re-evaluation of the deformational–tectonothermal scheme commonly used because of the high temperature structures that affected the Chattahoochee-Holland Mountain fault after its emplacement.

Previous interpretations of the Blue Ridge are still relevant and this study is in agreement with the overall deformational and metamorphic scheme suggested for this area. For example, data collected for this study concurs with other workers conclusions that D_2 structures are pervasive and that the D_2 event is the dominant tectonothermal pulse in the Blue Ridge (Hatcher, 1977; Hopson et al., 1989; Hatcher and Goldberg, 1991; Massey and Moecher, 2005). However, tight folding of the Chattahoochee-Holland Mountain fault indicates an

early ductile Alleghanian event affected the Blue Ridge. Because of this and surrounding projects in the Blue Ridge, the timing of deformational and thermal events are better constrained.

CHAPTER VI CONCLUSIONS

1) The tripartite stratigraphy of the Tallulah Falls Formation was recognized and mapped in detail in the study area.

2) The northern extent of the Walnut Creek Granodiorite, Rabun Granodiorite, and Looking Glass Granodiorite was identified and mapped in the study area building on current and previous mapping projects bordering the Sylva South and Tuckaseegee quadrangles. Additionally, a previously unmapped granitic body, the Tuckaseegee Granodiorite–Monzodiorite was described and mapped in detail in the SW part of the Tuckaseegee quadrangle.

3) The Soque River fault is recognized in the SW part of the Sylva South quadrangle and is truncated by the Chattahoochee-Holland Mountain fault.

4) Both the Walnut Creek and Tuckaseegee granitoids are similar in composition and have geochemistry that is typical of eastern Blue Ridge plutonic rocks. Minor differences between the Walnut Creek Granodiorite and the Tuckaseegee Monzodiorite exist, but are not significant. The model suggested by Miller et al., (1997) for eastern Blue Ridge plutonism of repeated intracrustal melting of accretionary wedge rocks originating from an entirely crustal derivation from a deep garnet bearing, feldspar-poor, mafic source is the best interpretation for the provenance of the Walnut Creek and Tuckaseegee granitoids,

5) Geochemical analysis of amphibolite blocks collected form the Savannah Church and Catamount Gap block-in-matrix exposures indicate increased mobility of these elements during metamorphism and evidence of crustal contamination have altered the original mineral assemblage. Despite considerable alteration all samples have a geochemical signature indicative of an igneous protolith and consistently fall in the tholeiitic basalt field with a clear affinity for a MORB protolith.

6) Rocks in the study area record amphibolite facies assemblages (sillimanite–kyanite and sillimanite–kyanite–staurolite). Some P-T estimates calculated for this study were slightly lower than estimates calculated by other workers in this area. This is likely due to diffusion as there is evidence for both diffusion and growth zoning in the garnet profiles and inclusion data. However, P-T calculations fall into the range of conditions that are expected for the observed mineral assemblages. P–T paths constructed from estimates of Dahlonega gold belt samples appear to be clockwise and have a slightly high P and relatively high T (8.7 kbars and 675° C), and peak pressures in the Tallulah Falls Formation are lower, but peak temperatures are higher than peak estimates for the Dahlonega gold belt (7.2 kbars and 725 °C).

7) Penetrative (D_2) structures are the dominant structures in the study area and are indicative of the Taconic orogeny. Evidence for the Acadian event is can be found in the study area as mesoscopic and map-scale upright tight folds. Emplacement and tight folding of the Chattahoochee-Holland Mountain fault is interpreted as an early Alleghanian (D_4) post-peak metamorphic, high temperature event because of its cross cutting relationship with the Rabun Granodiorite.

References Cited

Abbott, R. N., Jr., and Raymond, L. A., 1984, The Ashe Metamorphic Suite, northwest North Carolina; Metamorphism and observations on geologic history: American Journal of Science, v. 284, p. 350-375.

Absher, B. S., and McSween, H. Y., Jr., 1985, Granulites at Winding Stair Gap, North Carolina: the thermal axis of Paleozoic metamorphism in the southern Appalachians: Geological Society of America Bulletin, v. 96, p. 647-654.

Absher, B. S., and McSween, H. Y., Jr., 1986, Winding Stair Gap granulates: the thermal peak of Paleozoic metamorphism: Geological Society of America Centennial Field Guide SE section, p. 257-260.

Aleinikoff, J. N., Zartman, R. E., Walter, M., Rankin, D. W., Lyttle, P. T., and Burton, W. C., 1995, U-Pb ages of metarhyolites of the Catoctin and Mount Rogers Formations, central and southern Appalachians: evidence for two phases of Iapetian rifting: American Journal of Science, v. 295, p. 428-454.

Aldrich, L. T., Wetherill, G. W., Davis, G. L., and Tilton, G. R., 1958, Radioactive ages of micas from granitic rocks by Rb-Sr and K-Ar methods: American Geophysical Union Transactions, v. 39, p. 1124-1134.

Anderson, D. E., and Olimpio, J. C., 1977, Progressive homogenization of metamorphic garnets, South Morar, Scotland: evidence for volume diffusion: Canadian Mineralogist v.15, p.205-216.

Anderson, E. D., and Moecher, D. P., 2006, A comparison of retrograde eclogites along the eastern Blue Ridge-western Blue Ridge boundary, Western N.C.: plag-bearing GRT-CPX amphibolites preserve a record of high-P tectonics in the eastern Great Smoky Mountains: Geological Society of America Abstracts with Programs, v. 38, no. 3. p. 74.

Barker, F., 1979, Trondhjemite: definition, environment, and hypothesis of origin, in Barker, F., ed., Trondhjemites, Dacites, and Related rocks. Elsevier, Amsterdam.

Berquist, P. J., 2005, U–Pb geochronology and geochemistry of southern Appalachian basement: tectonic implications and constraints on age, extent, and origin [M.S. thesis]: Nashville, Tennessee, Vanderbilt University, 91 p.

Bream, B. R., 2003, Tectonic implications of geochronology and geochemistry of para- and orthogneisses from the southern Appalachian crystalline core [Ph.D. dissertation]: Knoxville, University of Tennessee, 262 p.

Bream, B. R., Hatcher, R. D. Jr., Miller, C. F., Fullagar, P. D., 2004, Detrital zircon ages and Nd isotopic data from the southern Appalachian crystalline core, Georgia, South Carolina, North Carolina, and Tennessee: new provenance constraints for part of the Laurentian margin: Geological Society of America, Memoir 197, p. 459-475.

Brewer, M. C., and Thomas, W. A., 2000, Stratigraphic evidence for Neoproterozoic-Cambrian two-phase rifting of southern Laurentia: Southeastern Geology, v. 39, p. 91-106.

Brumback, V. J., 1990, A metamorphic and structural transect in central Blue Ridge, Jackson and Macon Counties, North Carolina [M.S. thesis]: Knoxville, University of Tennessee, 103 p.

Butler, J. R., 1973, Paleozoic deformation and metamorphism in part of the Blue Ridge thrust sheet, North Carolina: American Journal of Science, v. 273-A (Cooper volume), p. 72-88.

Butler, J. R., 1991, Metamorphism, in Horton, J. W., and Zullo, V. A., eds., The geology of the Carolinas: Carolina Geological Society Fiftieth Anniversary Volume, p. 127-141.

Cabanis, B., and Lecolle, M. 1989. The La/10-Y/15-Nb/8 diagram: a tool for discriminating volcanic series and evidencing continental crust magmatic mixtures and/or contamination, Comptes Rendus - Academie des Sciences, Serie II, v. 309, Issue 20, p. 2023–2029.

Cameron, M. L., 2001, Garnet zoning, mineral inclusions, and P-T paths: Evidence for a polymetamorphic history of the Cullowhee Gneiss [M.S. thesis]: Knoxville, University of Tennessee, 240 p.

Carrigan, C. W., Bream, B. R., Miller, C. F., and Hatcher, R. D., Jr., 2001, Ion microprobe analyses of zircon rims from the eastern Blue Ridge and Inner Piedmont, NC-SC-GA: implications for the timing of Paleozoic metamorphism in the southern Appalachians: Geological Society of America Abstracts with Programs (SE section), v. 33, p. A-7.

Connelly, J. B. and Dallmeyer, R. D., 1991, Polymetamorphic evolution of the western Blue Ridge, Tennessee and North Carolina: Evidence from $^{40}Ar/^{39}Ar$ ages: Geological Society of America Abstracts with Programs, v. 23, p. 18.

Corrie, S. L., and Kohn, M. J., 2007, Resolving the timing of orogenesis in the western Blue Ridge, southern Appalachians, via in situ ID-TIMS monazite geochronology: Geology, v. 35, p. 627-630.

Cox,, K. G., Bell, J. D., and Pankhurst, R. J., 1979, The interpretation of igneous rocks: London, Allen and Unwin, 450 p.

Cronin, T. P., 1983, Petrogenesis of the Webster-Addie ultramafic body, Jackson County, North Carolina [M.S. thesis]: Knoxville, University of Tennessee, 112 p.

Dallmeyer, R. D., 1975, Incremental 40Ar/39Ar ages of biotite and hornblende from retrograded basement gneisses of the southern Blue Ridge: their bearing on the age of Paleozoic metamorphism: American Journal of Science, v. 275, p. 444-460.

Dallmeyer, R. D., 1976, $^{40}Ar/^{39}Ar$ age spectra of biotite from Grenville basement gneisses in Northwest Georgia: Geological Society of America Bulletin, v. 86, p. 1740-1744.

Dallmeyer R. D., 1988, Polymetamorphic evolution of the western Blue Ridge allochthon: Evidence from $^{40}Ar/^{39}Ar$ mineral ages, in W. J. Fritz and F. L. LaTour, eds., Geology of the Murphy Belt and Related Rocks—Georgia and North Carolina: Georgia Geological Society,
v. 8, p. 95-101.

Dallmeyer, R. D., Wright, J. W., Secor, D. T., Jr., and Snoke, A. W., 1986, Character of the Alleghanian orogeny in the southern Appalachians: part II, Geochronological constraints in the tectonothermal evolution of the eastern Piedmont in South Carolina: Geological Society of America Bulletin, v. 97, p. 1329-1344.

Davidson, G. L., 1995, The tectono-metamorphic history of a portion of the eastern Blue Ridge, Jackson County, North Carolina [M.S. thesis]: Knoxville, University of Tennessee, 157 p.

Dennis, A. J., and Wright, J. E., 1997, Middle and late Paleozoic monazite U-Pb ages, Inner Piedmont, South Carolina: Geological Society of America Abstracts with Programs, v. 29, p. 12.

Drake, A. A., Jr., Sinha, A. K., Laird, J., and Guy, R. E., 1989, The Taconic orogen, in Hatcher, R. D., Jr., Thomas, W. A., and Viele, G. W., eds., The Appalachian-Ouachita orogen in the United States: Boulder, CO, Geological Society of America, (Geology of North America, Vol. F-2) p. 101-177.

Eckert, J. O., Jr., 1984, Stratigraphy, structure, and metamorphism of the east half of the Wayah Bald quadrangle, North Carolina: evidence for Paleozoic granulite facies metamophism in the southern Appalachians [M.S. thesis]: Columbia, South Carolina, University of South Carolina, 411 p.

Eckert, J. O., Hatcher, R. D., Jr., and Mohr, D. W., 1989, The Wayah granulite-facies metamorphic core, southwestern North Carolina: high-grade culmination of Taconic metamorphism in the southern Blue Ridge: Geological Society of America Bulletin, v. 101, p. 1434-1447.

Eggers, M. R., 1983, Petrology, structure and geochemistry of the Kimsey Bald mafic complex: [unpublished M.S. thesis]:, University of South Carolina, Columbia, 72 p.

Floyd P.A. and Winchester J.A., 1975, Magma type and tectonic setting discrimination using immobile elements: Earth Planet Science Letters, v. 27, p. 211-218.

Floyd, P. A, Winchester, J. A., 1976, Petrochemical affinities of Dalradian metabasaltic rocks; a reply to C. M. Graham: Earth and Planetary Science Letters, v. 32, p. 213-214.

Force, E. R., 1976, Metamorphic source rocks of titanium placer deposits, a geochemical cycle: U.S. Geological Survey Professional Paper 959-B, 13 p.

German, J. M., 1985, The geology of the northeastern portion of the Dahlonega gold belt: Georgia Geologic Survey Bulletin, v. 100, 41 p.

Gillon, K. A., 1982, Stratigraphic, structural, and metamorphic geology of portions of the Cowrock and Helen, Georgia 7.5 minute quadrangles [M.S. thesis]: Athens, Georgia, University of Georgia, 236 p.

Gillon, K. A., 1989, Geologic compilation of a portion of the western and eastern Blue Ridge tectonic province, Georgia and North Carolina: Georgia Geological Society Guidebook, v. 9, plate 1.

Goldberg, S. A., and Dallmeyer, R. D. 1997, Chronology of Paleozoic metamorphism and deformation in the Blue Ridge thrust complex, North Carolina and Tennessee, American Journal of Science, v. 297, p. 488-526.

Gray, D., and Durney, D., 1979, Crenulation cleavage differentiation: implications of solution-deposition processes, Journal of Structural Geology, v. 1, issue 1, p. 73-80

Hadley, J. B., 1970, The Ocoee Series and its possible correlatives, in Fisher, G. W., Pettijohn, F. J., Reed, J. C., Jr., and Weaver, K. N., eds. Studies of Appalachian geology: central and southern: New York, Interscience Publishers, p. 247-259.

Hadley, J. B., and Goldsmith, R., 1963, Geology of the eastern Great Smoky Mountains, North Carolina: U.S. Geological Survey Professional Paper 349-B, 118 p.

Hadley, J. B., and Nelson, A. E., 1971, Geologic map of the Knoxville 1 x 2 degree sheet: U.S. Geological Survey Map 1-654, scale 1:250,000.

Hatcher, R. D., Jr., 1971b, Geology of Rabun and Habersham Counties, Georgia: A reconnaissance study: Georgia Geological Survey Bulletin 83, 43 p.

Hatcher, R. D., Jr., 1972, Developmental model for the southern Appalachians: Geological Society of America Bulletin, v. 83, p. 2735-2760.

Hatcher, R. D., Jr., 1973, Basement versus cover rocks in the Blue Ridge of northeast Georgia, northwestern South Carolina, and adjacent North Carolina: American Journal of Science, v. 273, p. 671-685.

Hatcher, R. D., Jr., 1974, An introduction to the Blue Ridge tectonic history of northeast Georgia: Georgia Geological Society Guidebook 13-A, 60 p.

Hatcher, R. D., Jr., 1977, Macroscopic polyphase folding illustrated by the Toxaway dome, eastern Blue Ridge, South Carolina-North Carolina: Geological Society of America Bulletin, v. 88, p. 1678-1688.

Hatcher, R. D., Jr., 1978, Tectonics of the western Piedmont and Blue Ridge, southern Appalachians: Review and speculation: American Journal of Science, v. 278, p. 276-304.

Hatcher, R. D., Jr., 1980, Geologic map and mineral resources of the Prentiss quadrangle, North Carolina: North Carolina Geological Survey, GM 167–SW, scale 1/24,000.

Hatcher, R. D., Jr., 1988, Bedrock geology and regional geologic setting of Coweeta Hydrologic Laboratory in the eastern Blue Ridge, in Swank, W. T., and Crossley, D. A., Jr., eds., Ecological Studies: Forest Hydrology and Ecology at Coweeta: Springer-Verlag, v. 66, p. 81-92.

Hatcher, R. D., Jr., 1989, Tectonic synthesis of the U.S. Appalachians, in Hatcher, R. D. Jr., Thomas, W. A., and Viele, G. W., eds., The Appalachian-Ouachita orogen in the United States: Boulder, Colorado, Geological Society of America, The geology of North America, v. F-2, p. 511-535.

Hatcher, R. D., Jr., 1990, Structural geology: Principals, concepts and problems: Columbus, Ohio, Charles E. Merrill, 531 p.

Hatcher, R. D., Jr., 2001, Rhealogical partitioning during multiple reactivation of the Paleozoic Brevard fault zone, Southern Appalachians, USA, in Holdsworth, R. E., Strachan, R. A., Macloughlin, J. F., and Knipe, R. J., eds., The Nature and Significance of Fault Zone Weakening: Geological Society [London] Special Publication 186, p. 255-269.

Hatcher, R. D., Jr., 2002, An Inner Piedmont primer, in Hatcher, R. D., Jr., and Bream, B. R., eds., Inner Piedmont geology in the South Mountains-Blue Ridge Foothills and the southwestern Brushy Mountains, central-western North Carolina: Carolina Geological Society Guidebook, p. 1-18, http://carolinageologicalsociety.org/cgscdguide.htm.

Hatcher, R.D., Jr., 2004a, Trans Appalachians Internides Geotraverse: Overview, in Hatcher, R. D. Jr., and Merschat, A. J., Trans Appalachians Internides Geotraverse: Field trip guide, 2004. p. 1-11.

Hatcher, R. D., Jr., 2004b, Trans Appalachians Internides Geotraverse: Day 2, The Neoacadian Metamorphic Core, Large ductile thrust sheets, and multiply reactivated crustal-scale shear zone, in Hatcher, R. D. Jr., and Merschat, A. J., eds., Trans Blue Ridge to Inner Piedmont geotraverse: Field trip guide, p. 29-59.

Hatcher, R. D., Jr., and Butler, J. R., 1979, Guidebook for southern Appalachian field trip in the Carolinas, Tennessee, and northeastern Georgia: International Geologic Correlation Program Project 27, University of North Carolina, Chapel Hill, 117 p.

Hatcher, R. D., Jr., Hooper, R. J., Petty, S. M., and Willis, J. D., 1984, Structure and chemical petrology of three southern Appalachian mafic-ultramafic complexes and their bearing upon the tectonics of emplacement and origin of Appalachian ultramafic bodies: American Journal of Science, v. 284, p. 484-506.

Hatcher, R. D., Jr., and Goldberg, S. A., 1991, The Blue Ridge geologic province, in Horton, J. W., and Zullo, V. A., eds., The Geology of the Carolinas: Carolina Geological Society Fiftieth Anniversay Volume. p. 11-35.

Hatcher, R. D., and Hooper, R. J., 1992, Evolution of crystalline thrust sheets in the internal parts of mountain chains, in McClay, K. R., ed., Thrust Tectonics, Chapman and Hall, New York, p. 217-233.

Hatcher, R. D., Jr., Bream, B. R., Miller, C. L., Eckert, J. O. Jr., Fullagar, P. D., and Carrigan, C. W., 2004, Paleozoic structure of southern and central Appalachian Blue Ridge Grenvillian internal basement massifs, in Tollo, R. P., Corriveau, L., McLelland, J., and Bartholomew, M. J., eds., Proterozoic evolution of the Grenville orogen in North America: Boulder, Colorado, Geological Society of America Memoir 197, p. 525-547.

Hatcher, R. D., Jr., Merschat, A. J., and Thigpen, J. R., 2005, Blue Ridge Primer, in Hatcher, R. D., Jr., and Merschat, A. J., eds., Blue Ridge geology geotraverse east of the Great Smoky Mountains National Park, western North Carolina: Carolina Geological Society Field Trip Guide, p. 1-24.

Hatcher, R. D., Jr., and Merschat, A. J., 2006, The Appalachian Inner Piedmont: An exhumed strike-parallel, tectonically forced orogneci channel, in Law, R. D., Searle, M., and Godin, L., eds., Channel flow, ductile extrusion, and exhumation of lower-mid crust in continental collision zones: Geological Society [London] Special Publication 268, p. 517-540.

Hatcher, R. D., Jr., Bream, B. R., and Merschat, A. J., 2007, Tectonic map of the southern and central Appalachians: a tale of three orogens and a complete Wilson cycle, in Hatcher, R. D., Jr., Carlson, M. P., McBride, J. H., and Martinez Catalan, J. R., eds., 4–D Framework of continental crust: Geological Society of America Memoir 200, p. 595–632.

Hess, H. H. 1955, Serpentines, orogeny and epeirogeny: Geological Society of America Special Paper, 62, p. 391-408.

Higgins, M. W., and McConnell, K. I., 1978, The Sandy Springs Group and related rocks in the Georgia Piedmont–nomenclature and stratigraphy, in Sohl, N. F., and Wright, W. B., eds., Changes in stratigraphic nomenclature by the U.S. Geological Survey, 1977: U.S. Geological Survey Bulletin 1457-A, p. A98-A105.

Higgins, M. W., Crawford, T. J., Atkins, R. L., and Crawford, R. F., 2003, Geologic map of th Atlanta 30' x50' quadrangle, Georgia: U.S. Geological Survey Geologic Investigations Series Map I-2062, scale 1:100,000.

Hodges, K. V., and Spear, F. S., 1982, Geothermometry, geobarometry and the Al_2SiO_5 triple point at Mt. Moosilauke, New Hampshire: America Mineralogist, v. 73, p. 20-47.

Hoisch, T. D., 1991, Equilibria within the mineral assemblage quartz + muscovite + biotite + garnet + platioclase, and implications for the mixing properties of octahedrally-

coordinated cations in muscovite and biotite: Contributions to Mineralogy and Petrology, v. 108, p. 43-54.

Holm, P. E., 1985, The geochemical fingerprints of different tectonomagmatic environments using hygromagmatophile element abundances of tholeiitic basalts and basaltic andesites. Chemical Geology, v. 51, p. 303-323.

Hopson, J. L., 1994, Structure of part of the Blue Ridge, northeastern Georgia and North Carolina [Ph.D. dissertation]: Knoxville, University of Tennessee, 350 p.

Hopson, J. L., and Hatcher, R. D., 1988, Structural and stratigraphic setting of the Alto allochthon, northeast Georgia: Geological Society of America Bulletin, v. 100, p. 339-350.

Hopson, J. L., Hatcher, R. D., and Stieve, A. L., 1989, Geology of the eastern Blue Ridge, northeastern Georgia and the adjacent Carolinas, in Fritz, W. J., Hatcher, R. D., and Hopson, J. L., eds., Geology of the eastern Blue Ridge, of northeast Georgia and the adjacent Carolinas: Georgia Geological Society Guidebook, v. 9, p. 1-40.

Hurst, V. J., 1955, Stratigraphy, structure, and mineral resources of the Mineral Bluff quadrangle, Georgia, Atlanta: Georgia Geological Survey Bulletin 63, 137 p.

Hurst, V. J., 1973, Geology of the southern Blue Ridge Belt: American Journal of Science, v. 273, p. 643-670.

Irvine, T. N., and Baragar, W. R. A., 1971, A guide to the chemical classification of the common volcanic rocks, Canadian Journal of Earth Science, v. 8, p. 523-548.

Jones, S. P., 1909, Second report on the gold deposits of Georgia: Georgia Geolgoical Survey Bulletin 19, 283 p.

Keith, A., 1895, Description of the Knoxville sheet (Tennessee and North Carolina): U. S. Geological Survey Geologic Atlas, Folio 16, 6p.

Keith, A., 1904, Description of the Asheville quadrangle (Tennessee and North Carolina): U.S. Geological Survey Geologic Atlas, Folio 116, 10p.

Keith, A., 1905, Description of the Mount Mitchell quadrangle, North Carolina-Tennessee, U.S. Geological Survey, Geology Atlas Folio 124.

Keith, A., 1907, Description of the Roan Mountain quadrangle (Tennessee-North Carolina): U.S. Geological Survey Geologic Atlas Folio 151, 12 p.

King, P. B., 1964, Geology of the central Great Smoky Mountains, Tennessee: U.S. Geological Survey Professional Paper 311, 36p.

King, P. B., Hadley, J. B., Neuman. R. B., Hamilton, W., 1958, Stratigraphy of the Ocoee Series, Great Smoky Mountains, Tennessee and North Carolina: Geological Society of America Bulletin, v. 69, p. 947-966.

Kish, S. A., 1982, The application of potassium-argon dating of slates to the study of the metamorphic history of the southern Appalachian Piedmont and Blue Ridge: Geological Society of America Abstracts with Programs, v. 14, p. 31.

Kish, S. A., 1991, Studies of Precambrian and Paleozoic stratigraphy in the western Blue Ridge: Carolina Geological Society Guidebook, p. 69-77.

Kish, S. A., Merschat, C. E., Mohr, D. W., and Wiener, L. S., 1975, Guide to the geology of the Blue Ridge south of the Great Smoky Mountains, North Carolina: Carolina Geological Society Guidebook, 49 p.

Kittleson, R. C., 1988, The amphibolite-to-granulite facies transition in the Franklin and Corbin Knob Quadrangles, North Carolina Blue Ridge [unpublished M.S. thesis]: Knoxville, University of Tennessee, p. 111.

Kuno, H., 1968, Differentiation of magma basalts, in Hess, H. H., and Poldervaart, A., eds., Basalts: The Poldervaart treaties on rocks of basaltic composition, v. 2, Interscience, New York, p. 623-688.

Labotka, T. C., and Shireman, J., 1991, Metamorphism in the Blue Ridge near Cullowhee, North Carolina: Geological Society of America Abstracts with Programs, v. 23, p. 55.

Lamb, D. D., 2001, Geology of the Scaly Mountain quadrangle, emphasizing the structure, timing, and emplacement mechanisms for the Rabun granodiorite, eastern Blue Ridge, southwestern north Carolina [M.S. thesis]: Knoxville, University of Tennessee, 86 p.

Larrabee, D. M., 1966, Map showing distribution of ultramafic and intrusive mafic rocks from northern New Jersey to eastern Alabama: U.S. Geologial Survey, Map I-476.

Leake, B. E., 1964, The chemical distinction between ortho- and para-amphibolites: Journal of Petrology, v. 5, p. 238-254.

Long, L. E., Kulp, J. L., and Eckelmann, F. D., 1959, Chronology of major metamorphic events in the southeastern United States: American Journal of Science, v. 257, p. 585-603.

Maniar P. O. and Piccoli, P. M., 1989, Tectonic discrimination of granitoids: Geological Society of America Bulletin, v. 101, p. 635-643.

Massey, M. A., and Moecher, D. P., 2005, Deformation and metamorphic history of the western Blue Ridge-eastern Blue Ridge terrane boundary, southern Appalachian orogen: Tectonics, v. 24, p. TC5010, 1-18.

McClellan, E. A., 1988, Geologic history of a portion of the eastern Blue Ridge, southern Appalachians: Tray Mountain and Macedonia 7 1/2' quadrangles, Georgia [unpublished M.S. thesis]: Knoxville, University of Tennessee, 179 p.

McConnell, K. I., and Abrams, C. E., 1984, Geology of the greater Atlanta region: Georgia Geological Survey Bulletin, v. 96, 127 p.

McDowell, S. M., Miller, C. F., Fullagar, P. D., Bream, B. R., and Mapes, R. W., 2002, The Persimmon Creek Gneiss, eastern Blue Ridge, North Carolina-Georgia: Evidence for the missing Taconic arc?, Southeastern Geology v. 41, p. 103-117.

Merschat, C. E., and Wiener, L. S., 1988, Geology of the Sandymush and Canton Quadrangles, North Carolina: Raleigh, North Carolina Geological Survey Bulletin 90, 1:24,000 scale, 66 p.

Merschat, A. J., Hatcher, R. D., Jr., and Davis, T. L., 2005, The northern Inner Piedmont, southern Appalachians, USA: kinematics of transpression and SW-directed mid-crustal flow: Journal of Structural Geology, v. 27, p. 1252-1281.

Merschat, A. J., Hatcher, R. D., Jr., Miller, C. F., and Wooden, J. L., 2006, Provenance of central and western Blue Ridge paragneisses, southwestern North Carolina: Geological Society of America Abstracts with Programs, v. 38, no. 3, p. 63.

Miller, B. V., and Stewart, K. G., 2002, Pluton ages in the eastern Blue Ridge province, North Carolina: Constraints on timing of tectonics and metamorphism in deep levels of an Ordovician accretionary wedge complex: Geological Society of America Abstracts with Programs, v. 34, p. 41.

Miller, B. V., Fetter, A. H., and Stewart, K. G., 2006, Plutonism in three orogenic pulses, eastern Blue Ridge Province, southern Appalachians: Geological Society of America Bulletin, v. 118, p. 171-184, doi: 10.1130/B25580.1

Miller, C. F., Fullagar, P. D., Sando, T. W., Kish, S. A., Solomon, G. C., Russell, G. S., and Wood, Steltenpohl, L. F., 1997, Low-potassium, trondhjemititic to granodioritic plutonism in the eastern Blue Ridge, southwestern North Carolina northeastern Georgia, in Sinha, A. K., Whalen, J. B., and Hogan, J. P., eds., The nature of magmatism in the Appalachian orogen: Geological Society of America Memoir 191, p. 235-254.

Miller, C. F., Hatcher, R. D., Jr., Ayers, J. C., Coath, C. D., and Hudson, T. M., 2000, Age and zircon inheritance of eastern Blue Ridge plutons, southwestern North Carolina and northeastern Georgia, with implications for magma history and evolution of the southern Appalachian orogen: American Journal of Science, v. 300, p. 142-172.

Misra, K. C., and McSween, H. Y., 1984, Mafic rocks of the southern Appalachians; a review: American Journal of Science, v. 284, p. 294-318.

Moecher, D. P., and Miller, C. F., 2000, Precise age for peak granulite facies metamorphism and melting in the eastern Blue Ridge from SHRIMP U-Pb analysis of zircon: Geological Society of America Abstracts with Programs, v. 32, no. 2, p. 63.

Moecher, D. P., Samson, S. D., and Miller, C. F., 2004, Precise time and conditions of peak Taconian granulite facies metamorphism in the southern Appalachian orogen,

USA, with implications for zircon behavior during crustal melting events: Journal of Geology, v. 112, p. 289-304.

Moecher, D. P., Massey, M. A., and Tracey, R. J., 2005, Timing and pattern of metamorphism in the western and central Blue Ridge, TN and NC: Status and outstanding problems, in Hatcher, R. D., Jr., and Merschat, A. J., eds., Blue Ridge geology geotraverse east of the Great Smoky Mountains National Park, western North Carolina: Carolina Geological Society Field trip guide, p. 57-66.

Neuman, R. B., and Nelson, W. H., 1965, Geology of the western Great Smoky Mountains, Tennessee: U.S. Geological Survey Professional Paper 349-D, 81 p.

Nelson, A. E., and Gillon, K. A., 1985, Stratigraphic nomenclature in the Richard Russell and Helen thrust sheets, Georgia and North Carolina: U.S. Geological Survey Bulletin 1605-A, p. A59-A62.

Oskarsson, G. E., Sigvaldason, G. E., and Steinthorsson, S., 1982, A dynamic model of rift zone petrogenesis and the regional petrology of Iceland: Journal Petrology ,v. 23, p. 28–74.

Pearce, J. A., 1982, Trace element characteristics of lavas from destructive plate boundaries, in Thorpe, R. S., eds., Andesites: New York, John Wiley and Sons, p. 525-548.

Pearce, J. A., 1983, Role of sub-continental lithosphere in magma genesis at active continental margins, in: Hawksworth, C. J., and Norry, M. J., eds, Continental basalts and xenoliths: Shiva, Nantwich, p. 230-249.

Pearce, J. A., and Cann, J. R., 1973, Tectonic setting of basic volcanic rocks determined using trace element analyses: Earth and Planetary Science Letters, v. 19, p. 290–300.

Pearce, J. A., and Norry, M. J., 1979, Petrogenic implications of Ti, Zr, Y, and Nb variations in volcanic rocks: Contributions to Mineralogy and Petrology, v. 69, p. 33-37.

Pearce, J. A., Harris, N. B. W., and Tindle, A. G., 1984, Trace element discrimination diagrams for the tectonic interpretation of granitic rocks: Journal of Petrology, v. 25, p. 956-983.

Pettijohn, F. J., 1954, Classification of sandstones, Journal of Geology, v. 62, p. 360-365.

Plank, M. O., Srogi, L., Schenck, W. S., and Plank, T. A., 2001, Geochemistry of the mafic rocks, Delaware Piedmont and adjacent Pennsylvania and Maryland: Confirmation of arc affinity, University of Delaware, Newark Delaware, 2001.

Pratt, J. H., and Lewis, J. V., 1905, Corundum and the peridotites of North Carolina: North Carolina Geological Survey, v. 1, 464 p.

Quinn, M. J., 1991, Stratigraphy, structure and geochemistry across two lithotectonic boundaries in western North Carolina: geologic interpretation of an area surrounding Sylva, Jackson County [M.S. thesis]: Knoxville, University of Tennessee, 223 p.

Rankin, D. W., 1970, Stratigraphy and structure of Precambrian rocks in northeastern North Carolina, *in* Fischer, G. W., Pettijohn, F. J., Reed, J. C., Jr., and Weaver, K. N., eds., Studies of Appalachian geology–central and southern: New York, Interscience, p. 227-245.

Rankin, D. W., Espenshade, G. H., and Shaw, K. W., 1973, Stratigraphy and structure of the metamorphic belt in north-western North Carolina and southwestern Virgina: a study from the Blue Ridge across the Brevard fault zone to the Sauratown Mountains anticlinorium: American Journal of Science, v. 273-A (Cooper volume), p. 1-40.

Rast, N., and Kohles, K. M., 1986, The origin of the Ocoee Supergroup: American Journal of Science, v. 286, p. 593-616.

Raymond, L. A., 1984, Classification of mélanges: Geological Society of America Special Paper, 198, p. 7-20.

Raymond, L. A., and Swanson, S. E., 1981, Deformational history of ultramafic rocks, Blue Ridge belt, correlations with Appalachian tectonic events: Geological Society of America Abstracts with Programs, v. 13, p. 535.

Raymond, L. A., Yurkovich, S. P., and McKinney, M., 1989, Block-in-matrix structures in the North Carolina Blue Ridge belt and their significance for the tectonic history of the southern Appalachian orogen: Geological Society of America Special Paper 228, p. 195-215.

Rollinson, H. R., 1993, Using geochemical data: evaluation, presentation, interpretation: Longman Group UK Limited, Singapore, 352 p.

Sando, T. W., Miller, C. G., Fullagar, P. D., Solomon, G. C., and Stein, H. J., 1983, Isotopic characteristics of Paleozoic intrusives of the northern Georgia and North Carolina Blue Ridge: Geological Society of America Abstracts with Programs, v. 15, no. 6, p. 677.

Secor, D. T., Snoke, A. W., and Dallmeyer, R. D., 1986, Character of the Alleghanian orogeny in the southern Appalachians: part III, Regional tectonic relations: Geological Society of America Bulletin, v. 97, p. 1345-1353.

Settles, D. J., 2002, Defining the Hayesville-Soque River and Allatoona faults and an Ordovician arc assemblage within the central Blue Ridge northwest of Dahlonega, Georgia [unpublished M.S. thesis]: Knoxville, University of Tennessee, 148 p.

Shaw, H. F. and Wasserburg, G. J., 1984, Isotopic constraints on the origin of Appalachian mafic complexes: American Journal of Science, v. 284, p. 319-349.

Shireman, J., Labotka, T. C., and Knapp, S., 1985, Metamorphic history of a portion of the North Carolina Blue Ridge: Geological Society of America Abstracts with Programs, v. 17, p. 135.

Spear, F. S., 1993, Metamorphic phase equilibria and pressure-temperature-time paths, Washington, D. C., Mineralogical Society of America, Monograph, 799 p.

Spear, F. S., and Cheney, J. T.,1989, A petrogenetic grid for pelitic schists in the system SiO2 - Al2O3 - FeO - MgO- K2O - H2O, Contributions to Mineral Petrology, v. 101, p. 149-164.

Spear, F. S., and Kohn, M., 1989, Thermobarometry, v. 19, computer program.

Stahr, D. W., III, 2008, Tectonometamorphic evolution of the eastern Blue Ridge: differentiating multiple Paleozoic orogenic pulses in the Glenville and Big Ridge quadrangles, southwestern North Carolina, [M.S. thesis]: Knoxville, University of Tennessee, 263 p.

Stahr, D. W., III and Hatcher, R. D. H., Jr., 2004, Emplacement of the Devonian Rabun Granodiorite, northeast Georgia and North Carolina Blue Ridge; detailed geologic mapping, and structural, and petrologic analysis, Geological Society of America, Abstracts with Programs, v. 36, no.5, p. 406.

Stahr, D. W., Miller, C. F., Hatcher, R. D., Jr., Wooden, J., and Fisher, C. M., 2005, Evidence for high-temperature ductile Alleghanian deformation in the eastern Blue Ridge: implications of new structural, petrologic, and geochronologic data from southwestern North Carolina: Geological Society of America Abstracts with Programs, v. 37, no. 7, p. 72.

Stahr, D. W., III, Hatcher, R. D., Jr., Miller, C. F., and Wooden, J. L., 2006, Alleghanian deformation in the Georgia and North Carolina eastern Blue Ridge: insights from pluton ages and fabrics: Geological Society of America Abstracts with Programs, v. 38, p. 20.

Streckeisen, A., 1976, To each plutonic rock its proper name, Earth Science Reviews, v. 12, p. 1-33.

Sun, S. S., and McDonough, W. F., 1989, Chemical and isotopic systematics of oceanic basalts: implications for mantle composition and processes, in Saunders, A. D., and Norry, M. J., eds., Magmatism in the ocean basins: London, England, Geological Society of London Special Publication 42, p. 313-345.

Taylor, S. R., and McLennan, S. M., 1985, The continental crust: its composition and evolution: Blackwell, Oxford, 312 p.

Thompson, J. B., Jr., 1957, The graphical analysis of mineral assemblages in pelitic schists, American Mineralogist, v. 42, p. 842-858.

Thompson, R. N., 1982, British Tertiary volcanic province: Scottish Journal of Geology, v. 18, p. 49-107.

Thomas, C. W., 2001, Origins of ultramafic complexes of the eastern Blue Ridge province, southern Appalachians: geochronological and geochemical constraints [M.S. thesis]: Nashville, Tennessee, Vanderbilt University, 154 p.

Tracy, R. J., Robinson, P., and Thompson, A. B., 1976, Garnet composition and zoning in the determination of temperature and pressure of metamorphism, central Massachusetts: American Mineralogist, v. 61, p. 762-775.

Twist, D., and Harmer, R. E. J., 1987, Geochemistry of contrasting siliceous magmatic suites of the Bushveld Complex: genetic aspects and implications for tectonic discrimination diagrams: Journal of Volcanic Geothermal Research, v. 32, p. 83-98.

Walter, K. A., 1990, Geochemistry and trace-element models for the petrogenesis of mafic rocks in the Hayesville thrust sheet, Georgia-North Carolina Blue Ridge, [Ph.D. dissertation]: Knoxville, University of Tennessee, 224 p.

Wilkinson, J. F. G., 1982, The genesis of mid-oceanic ridge basalt: Earth Science Research, v. 18, p. 1-57.

Winchester, J. A., and Floyd, P. A., 1976, Geochemical magma type discrimination: application to altered and metamorphosed basic igneous rocks: Earth Planetary Science Letters, v. 28, p. 259-469.

Wood, D. A., Joron, J. L., Treuil, M., Norry, M., and Tarney, J., 1979, Elemental and Sr isotope variations in basic lavas from Iceland and the surrounding ocean floor: Contributions to Mineral Petrology, v. 70, p. 319-339.

Wood, D. A., 1980, The application of the Th-Hf-Ta diagram to problems of tectonomagmatic classification and to establishing the nature of crustal contamination of basaltic lavas of the British Tertiary volcanic province: Earth and Planetary Sciences Letters, v. 50, p. 11-30.

Woodsworth, G. J., 1977, Homogenization of zoned garnets from pelitic schists: Canadian Mineralogist v. 15, p. 230-242.

Yardley, B. W. D., 1977, An empirical study of diffusion in garnet: American Mineralogist, v. 62, p. 793-800.

Yeates, W. S., McCallie, S. W., and King, F. P., 1896, A preliminary report on a part of the gold deposits of Georigia: Georgia Geological Survey Bulletin, 4-A, 542 p.

Appendix I: Electron Microprobe Analyses

Appendix IA:
Microprobe Analysis of SS311C Garnet

Oxide Wt.%	Gt1ARim1	Gt1ARim2	Gt1ARim3	Gt1ARim4	Gt1A1	Gt1A2	Gt1A3	Gt1A4	Gt1A5	Gt1A5	Gt1A6	Gt1ACore1	Gt1ACore2	Gt1ACore3
SiO_2	37.95	38.40	38.09	38.04	38.39	38.58	38.39	38.47	38.47	38.46	38.33	38.34	38.27	38.26
TiO_2	0.01	0.01	0.01	0.00	0.00	0.03	0.02	0.01	0.00	0.00	0.00	0.00	0.00	0.01
Al_2O_3	21.20	21.03	21.40	21.32	21.36	21.42	21.40	21.57	21.43	21.39	21.46	21.42	21.42	21.59
Cr_2O_3	0.04	0.00	0.02	0.00	0.00	0.00	0.03	0.00	0.00	0.03	0.04	0.03	0.01	0.02
Y_2O_3	0.00	0.06	0.00	0.01	0.00	0.00	0.03	0.05	0.01	0.03	0.02	0.03	0.01	0.01
MgO	4.34	4.20	4.55	4.62	5.78	5.82	6.11	5.79	5.71	5.63	6.19	6.47	6.61	6.59
CaO	2.63	2.60	2.22	2.64	2.07	1.87	1.83	2.19	2.09	2.24	1.74	2.01	2.10	1.87
MnO	1.00	1.12	1.00	1.02	0.72	0.78	0.79	0.82	0.87	0.82	0.80	0.89	0.72	0.78
FeO	33.50	33.44	32.92	33.05	32.23	32.55	32.09	31.75	31.94	32.13	32.19	31.15	31.00	31.67
Na_2O	0.02	0.01	0.01	0.03	0.03	0.00	0.01	0.04	0.01	0.04	0.03	0.03	0.03	0.03
Total	100.68	100.87	100.21	100.73	100.58	101.06	100.68	100.69	100.54	100.77	100.79	100.37	100.17	100.83
Cation based on 12 oxygens														
Si	3.00	3.03	3.02	3.00	3.01	3.01	3.01	3.01	3.02	3.01	3.00	3.00	3.00	2.99
Ti	0.00	0.00	0.00	0.00	0.00	0.00	0.00	0.00	0.00	0.00	0.00	0.00	0.00	0.00
Al	1.98	1.96	2.00	1.98	1.98	1.97	1.97	1.99	1.98	1.98	1.98	1.98	1.98	1.99
Cr	0.00	0.00	0.00	0.00	0.00	0.00	0.00	0.00	0.00	0.00	0.00	0.00	0.00	0.00
Y	0.00	0.00	0.00	0.00	0.00	0.00	0.00	0.00	0.00	0.00	0.00	0.00	0.00	0.00
Mg	0.51	0.49	0.54	0.54	0.68	0.68	0.71	0.68	0.67	0.66	0.72	0.76	0.77	0.77
Ca	0.22	0.22	0.19	0.22	0.17	0.16	0.15	0.18	0.18	0.19	0.15	0.17	0.18	0.16
Mn	0.07	0.08	0.07	0.07	0.05	0.05	0.05	0.06	0.06	0.06	0.05	0.06	0.05	0.05
Fe	2.22	2.21	2.18	2.18	2.11	2.13	2.10	2.08	2.09	2.11	2.11	2.04	2.03	2.07
Na	0.00	0.00	0.00	0.00	0.01	0.00	0.00	0.01	0.00	0.01	0.00	0.00	0.00	0.00
Total	8.008	7.991	7.985	8.008	8.00	8.00	8.01	8.00	7.99	8.00	8.01	8.01	8.01	8.02

Oxide Wt.%	Gt1A7	Gt1A8	Gt1a	Gt1a	Gt1a	Gt1a	Gt1a	Gt1a	Gt1a	Gt1a	Gt1a	Gt1a	Gt1a	Gt1a
SiO_2	38.51	38.24	38.08	37.79	38.25	38.07	38.45	38.38	38.49	38.64	38.33	38.61	38.52	38.29
TiO_2	0.05	0.13	0.01	0.00	0.03	0.04	0.00	0.00	0.01	0.02	0.01	0.01	0.04	0.02
Al_2O_3	21.62	21.74	21.34	21.33	21.31	21.32	21.57	21.53	21.51	21.71	21.78	21.58	21.51	21.59
Cr_2O_3	0.01	0.00	0.02	0.01	0.00	0.01	0.00	0.03	0.00	0.03	0.00	0.02	0.03	0.01
Y_2O_3	0.04	0.02	0.00	0.00	0.02	0.02	0.01	0.04	0.02	0.03	0.03	0.00	0.01	0.02
MgO	6.62	6.42	4.73	5.24	5.44	5.87	6.04	6.21	6.36	6.39	5.76	6.61	6.49	6.65
CaO	2.00	1.97	1.97	1.85	1.64	1.49	1.56	1.59	1.59	1.89	1.97	1.81	1.98	1.82
MnO	0.72	0.78	1.03	0.92	0.85	0.88	0.85	0.88	0.81	0.82	0.84	0.71	0.84	0.77
FeO	31.16	31.30	33.72	33.25	33.14	33.31	32.75	32.10	32.34	31.71	32.05	31.22	31.52	31.67
Na_2O	0.03	0.03	0.03	0.03	0.01	0.03	0.01	0.04	0.01	0.02	0.10	0.04	0.02	0.01
Total	100.75	100.62	100.92	100.42	100.70	101.03	101.24	100.78	101.13	101.25	100.87	100.60	100.95	100.83
Cation based on 12 oxygens														
Si	3.00	2.99	3.00	2.99	3.01	2.99	3.00	3.00	3.00	3.00	3.00	3.01	3.00	2.99
Ti	0.00	0.01	0.00	0.00	0.00	0.00	0.00	0.00	0.00	0.00	0.00	0.00	0.00	0.00
Al	1.99	2.00	1.98	1.99	1.98	1.97	1.98	1.98	1.98	1.99	2.01	1.98	1.98	1.99
Cr	0.00	0.00	0.00	0.00	0.00	0.00	0.00	0.00	0.00	0.00	0.00	0.00	0.00	0.00
Y	0.00	0.00	0.00	0.00	0.00	0.00	0.00	0.00	0.00	0.00	0.00	0.00	0.00	0.00
Mg	0.77	0.75	0.56	0.62	0.64	0.69	0.70	0.72	0.74	0.74	0.67	0.77	0.75	0.77
Ca	0.17	0.16	0.17	0.16	0.14	0.13	0.13	0.13	0.13	0.16	0.17	0.15	0.17	0.15
Mn	0.05	0.05	0.07	0.06	0.06	0.06	0.06	0.06	0.05	0.05	0.06	0.05	0.06	0.05
Fe	2.03	2.04	2.22	2.20	2.18	2.19	2.14	2.10	2.11	2.06	2.10	2.04	2.05	2.07
Na	0.01	0.00	0.00	0.01	0.00	0.01	0.00	0.01	0.00	0.00	0.02	0.01	0.00	0.00
Total	8.01	8.01	8.01	8.02	8.00	8.03	8.01	8.01	8.01	8.01	8.01	8.00	8.01	8.02

Appendix IA (cont.):
Microprobe Analysis of SS311C Garnet (cont.)

Oxide Wt.%	Gt1a	Gt1a
SiO_2	38.59	38.21
TiO_2	0.01	0.01
Al_2O_3	21.77	21.50
Cr_2O_3	0.00	0.01
Y_2O_3	0.05	0.03
MgO	6.59	6.19
CaO	2.05	2.10
MnO	0.84	0.85
FeO	31.78	31.67
Na_2O	0.01	0.01
Total	101.68	100.57
Cation based on 12 oxygens		
Si	2.99	2.99
Ti	0.00	0.00
Al	1.99	1.99
Cr	0.00	0.00
Y	0.00	0.00
Mg	0.76	0.72
Ca	0.17	0.18
Mn	0.06	0.06
Fe	2.06	2.08
Na	0.00	0.00
Total	8.02	8.01

Appendix IA (cont.):
Microprobe Analysis of SS311C Biotite

Oxide Wt. %	Mica(Gt1A)1	Mica(Gt1A)2	Mica(Gt1A)2a	Mica(Gt1A)3	Mica(Gt1A)incl1	Mica(Gt1A)5in	Mica(Gt1A)6in	Mica(Gt1A)7in	Mica(Gt1A)8in	mica (out)	mica 11	mica 12	mica 13	mica 14
SiO_2	37.63	36.24	37.88	37.43	38.30	37.83	35.58	39.53	39.541	37.236	37.541	37.419	37.402	37.097
TiO_2	1.64	0.45	1.65	1.55	1.29	1.43	1.13	1.37	1.38	1.55	1.57	1.62	1.53	1.53
Al_2O_3	18.41	13.06	18.40	18.38	18.58	17.45	19.23	18.07	17.62	18.11	18.09	17.91	18.03	18.41
MgO	14.08	7.58	14.36	14.18	16.25	15.97	17.25	17.72	17.94	13.86	14.02	14.00	14.12	13.78
CaO	0.04	2.59	0.04	0.06	0.04	0.05	0.04	0.03	0.01	0.01	0.00	0.02	0.00	0.01
MnO	0.04	0.62	0.05	0.00	0.00	0.03	0.00	0.01	0.01	0.02	0.00	0.01	0.04	0.00
FeO	13.86	20.81	14.39	13.83	10.72	11.82	11.77	9.84	9.51	14.34	14.05	13.99	14.11	14.22
Na_2O	0.34	0.14	0.32	0.29	0.34	0.24	0.21	0.40	0.34	0.34	0.33	0.30	0.40	0.35
K_2O	8.73	3.56	8.79	8.32	8.48	8.24	6.99	8.77	8.69	8.90	8.93	8.99	8.91	8.82
H_2O	4.06	3.56	4.09	4.04	4.10	4.03	4.01	4.19	4.17	4.02	4.04	4.02	4.03	4.02
Total	98.81	88.60	99.96	98.08	98.09	97.09	96.19	99.92	99.21	98.39	98.56	98.27	98.57	98.24
Cation based on 11 oxygens														
Si	5.56	6.10	5.55	5.56	5.60	5.63	5.32	5.66	5.69	5.55	5.58	5.58	5.56	5.54
Ti	0.18	0.06	0.18	0.17	0.14	0.16	0.13	0.15	0.15	0.17	0.18	0.18	0.17	0.17
Al	3.21	2.59	3.18	3.22	3.20	3.06	3.39	3.05	2.99	3.18	3.17	3.15	3.16	3.24
Mg	3.10	1.90	3.14	3.14	3.55	3.54	3.85	3.78	3.85	3.08	3.10	3.11	3.13	3.07
Ca	0.01	0.47	0.01	0.01	0.01	0.01	0.01	0.00	0.00	0.00	0.00	0.00	0.00	0.00
Mn	0.01	0.09	0.01	0.00	0.00	0.00	0.00	0.00	0.00	0.00	0.00	0.00	0.00	0.00
Fe	1.71	2.93	1.76	1.72	1.31	1.47	1.47	1.18	1.15	1.79	1.75	1.75	1.76	1.78
Na	0.10	0.05	0.09	0.08	0.10	0.07	0.06	0.11	0.10	0.10	0.10	0.09	0.11	0.10
K	1.65	0.76	1.64	1.58	1.58	1.56	1.33	1.60	1.60	1.69	1.69	1.71	1.69	1.68
H	0.00	0.00	0.00	0.00	0.00	0.00	0.00	0.00	0.00	0.00	0.00	0.00	0.00	0.00
Total	15.53	14.96	15.55	15.49	15.49	15.50	15.56	15.53	15.52	15.58	15.56	15.57	15.59	15.57

Oxide Wt. %	mica(Gt3)	mica(Gt3)	mica(Gt3)	mica(Gt3)	mica(Gt3)	mica(Gt3)	mica(Gt3)
SiO_2	36.51	38.51	37.87	37.61	37.79	36.29	34.95
TiO_2	0.95	1.02	1.01	1.01	1.04	1.03	0.98
Al_2O_3	18.52	18.53	18.67	18.64	18.65	18.78	19.75
MgO	14.30	15.41	15.38	15.07	15.21	14.56	13.80
CaO	0.11	0.02	0.01	0.00	0.07	0.00	0.01
MnO	0.08	0.00	0.00	0.00	0.00	0.00	0.00
FeO	13.47	12.62	12.80	12.78	12.46	12.80	12.92
Na_2O	0.34	0.35	0.35	0.36	0.36	0.38	0.41
K_2O	8.34	8.75	8.97	8.77	8.74	8.67	8.48
H_2O	3.97	4.11	4.09	4.06	4.07	3.97	3.91
Total	96.59	99.32	99.13	98.29	98.37	96.50	95.20
Cation based on 11 oxygens							
Si	5.52	5.62	5.56	5.56	5.57	5.48	5.36
Ti	0.11	0.11	0.11	0.11	0.12	0.12	0.11
Al	3.30	3.19	3.23	3.25	3.24	3.34	3.57
Mg	3.22	3.35	3.36	3.32	3.34	3.28	3.15
Ca	0.02	0.00	0.00	0.00	0.01	0.00	0.00
Mn	0.01	0.00	0.00	0.00	0.00	0.00	0.00
Fe	1.70	1.54	1.57	1.58	1.54	1.62	1.66
Na	0.10	0.10	0.10	0.10	0.10	0.11	0.12
K	1.61	1.63	1.68	1.65	1.64	1.67	1.66
H	0.00	0.00	0.00	0.00	0.00	0.00	0.00
Total	15.58	15.54	15.61	15.58	15.56	15.62	15.63

Appendix IA (cont.):
Microprobe Analysis of SS311C Feldspar

Oxide Wt.%	Feld(Gt1A)1in	Feld(Gt1A)2in	Feld(Gt1A)3in	Feld(Gt1A)4	Feld(Gt1A)5	Feld(Gt1A)6
SiO_2	60.432	60.926	60.923	58.633	58.719	59.858
Al_2O_3	23.766	24.229	24.098	25.44	24.909	24.733
CaO	6.379	6.377	6.494	8.024	7.806	7.551
FeO	0.451	0.274	0.402	0.386	0.33	0.09
Na_2O	7.892	7.921	7.931	7.187	7.049	7.336
K_2O	0.084	0.078	0.095	0.037	0.041	0.066
Total	99.004	99.805	99.943	99.707	98.854	99.634
Caton based on 8 oxygens						
Si	2.719	2.716	2.715	2.633	2.654	2.679
Al	1.26	1.273	1.266	1.346	1.327	1.305
Ca	0.308	0.305	0.31	0.386	0.378	0.362
Fe	0.017	0.01	0.015	0.014	0.012	0.003
Na	0.689	0.685	0.685	0.626	0.618	0.637
K	0.005	0.004	0.005	0.002	0.002	0.004
Total	4.998	4.993	4.996	5.007	4.991	4.99

Appendix IB:
Microprobe Analysis of CGB Garnet

Oxide Wt.%	Gt3Line1	Gt3Line1	Gt3Line1	Gt3Line1	Gt3Line1	Gt3Line1	Gt3Line1	Gt3Line1	Gt3Line1	Gt3Line1	Gt3Line1	Gt3Line1	Gt3Line1	Gt3Line1
SiO_2	37.995	38.315	38.576	38.321	38.316	37.059	39.494	37.961	38.257	60.583	38.804	38.632	43.042	56.001
TiO_2	0.047	0.067	0.046	0.051	0.046	0.017	0.045	0.068	0.097	0.066	0.039	0.084	0.041	0.077
Al_2O_3	21.104	21.217	21.35	21.362	21.249	16.779	21.206	20.846	21.182	10.946	21.52	19.568	11.069	17.778
Cr_2O_3	0.025	0.011	0.082	0.034	0.064	0.078	0.032	0.08	0.034	0.057	0	0.053	0.078	0
MgO	4.503	5.701	6.357	6.364	6.245	6.689	6.309	6.787	6.764	2.447	6.677	7.009	3.164	2.04
CaO	6.327	6.424	6.448	6.411	6.394	5.033	6.442	6.504	6.375	2.292	6.587	6.082	7.431	4.89
MnO	1.127	0.749	0.701	0.767	0.777	0.537	0.709	0.686	0.671	0.211	0.663	0.715	0.348	0.43
FeO	28.476	26.801	26.324	26.552	26.053	22.825	26.038	26.274	26.233	12.732	25.999	24.264	13.412	19.619
Na_2O	0	0.024	0.016	0.024	0.007	0.094	0.042	0	0.007	0.144	0	0.035	0.197	0.086
Total	99.604	99.309	99.9	99.886	99.151	89.111	100.317	99.206	99.62	89.478	100.289	96.442	78.782	100.921
Cation based on 12 oxygens														
Si	3.006	3.011	3.005	2.991	3.006	3.202	3.052	2.985	2.989	4.608	3.004	3.092	3.967	3.984
Ti	0.003	0.004	0.003	0.003	0.003	0.001	0.003	0.004	0.006	0.004	0.002	0.005	0.003	0.004
Al	1.968	1.965	1.96	1.965	1.965	1.709	1.931	1.932	1.951	0.981	1.963	1.846	1.202	1.491
Cr	0.002	0.001	0.005	0.002	0.004	0.005	0.002	0.005	0.002	0.003	0	0.003	0.006	0
Mg	0.531	0.668	0.738	0.74	0.73	0.862	0.727	0.796	0.788	0.278	0.77	0.836	0.435	0.216
Ca	0.536	0.541	0.538	0.536	0.537	0.466	0.533	0.548	0.534	0.187	0.546	0.522	0.734	0.373
Mn	0.076	0.05	0.046	0.051	0.052	0.039	0.046	0.046	0.044	0.014	0.043	0.048	0.027	0.026
Fe	1.884	1.761	1.715	1.733	1.709	1.649	1.683	1.728	1.714	0.81	1.683	1.624	1.034	1.167
Na	0	0.004	0.002	0.004	0.001	0.016	0.006	0	0.001	0.021	0	0.005	0.035	0.012
Total	8.006	8.005	8.012	8.025	8.007	7.949	7.983	8.044	8.029	6.906	8.011	7.981	7.443	7.273

Oxide Wt.%	Gt3Line1	Gt3Line1	Gt3Line1	Gt3Line1	Gt3Line1	Gt3Line1	Gt3Line1	Gt3Line1	Gt3Line1	Gt3Line1	Gt3Line1	Gt3Line1	Gt3Line1	Gt3Line1
SiO_2	38.79	38.313	38.314	41.815	68.231	89.139	90.213	38.41	38.561	52.839	38.023	99.812	99.931	52.651
TiO_2	0.091	0.111	0.094	0.077	0.078	0.02	0.055	0.075	0.08	0.052	0.008	0.039	0.017	0
Al_2O_3	21.562	21.495	21.474	16.091	10.308	0.34	0.327	21.601	21.455	11.62	20.948	0.029	0.021	2.882
Cr_2O_3	0.007	0.023	0.009	0.048	0	0.02	0	0.037	0.014	0.009	0.027	0.018	0	0.02
MgO	6.492	6.746	6.59	5.392	1.809	0.046	0.073	6.867	6.817	3.695	6.788	0.013	0	0.601
CaO	6.451	6.524	6.558	5.492	3.155	0.162	0.168	6.457	6.506	4.305	6	0.02	0.007	23.487
MnO	0.712	0.637	0.744	0.601	0.273	0.045	0.02	0.751	0.707	0.374	0.719	0.043	0	0.169
FeO	25.999	26.096	26.114	22.327	11.096	0.974	0.755	25.749	25.789	15.999	25.973	0.529	0.5	3.292
Na_2O	0.019	0.017	0.026	0.067	0.204	0.208	0.274	0.016	0.009	0.132	0.014	0.011	0.005	0.032
Total	100.123	99.962	99.923	91.91	95.154	90.954	91.885	99.963	99.938	89.025	98.5	100.514	100.481	83.134
Cation based on 12 oxygens														
Si	3.007	2.981	2.984	3.451	4.8	5.935	5.939	2.983	2.995	4.22	3.001	5.98	5.985	4.532
Ti	0.005	0.006	0.006	0.005	0.004	0.001	0.003	0.004	0.005	0.003	0.001	0.002	0.001	0
Al	1.97	1.971	1.971	1.565	0.855	0.027	0.025	1.977	1.964	1.094	1.949	0.002	0.001	0.292
Cr	0	0.001	0.001	0.003	0	0.001	0	0.002	0.001	0.001	0.002	0.001	0	0.001
Mg	0.75	0.782	0.765	0.663	0.19	0.005	0.007	0.795	0.789	0.44	0.799	0.001	0	0.077
Ca	0.536	0.544	0.547	0.486	0.238	0.012	0.012	0.537	0.541	0.368	0.507	0.001	0	2.166
Mn	0.047	0.042	0.049	0.042	0.016	0.003	0.001	0.049	0.047	0.025	0.048	0.002	0	0.012
Fe	1.686	1.698	1.701	1.541	0.653	0.054	0.042	1.672	1.675	1.069	1.715	0.027	0.025	0.237
Na	0.003	0.003	0.004	0.011	0.028	0.027	0.035	0.002	0.001	0.02	0.002	0.001	0.001	0.005
Total	8.004	8.028	8.028	7.767	6.784	6.065	6.064	8.021	8.018	7.24	8.024	6.017	6.013	7.322

Appendix IB:
Microprobe Analysis of CGB Garnet (cont.)

Oxide Wt.%	Gt3Line1	Gt3Line1	Gt3Line1	Gt3Line1	Gt3Line1	Gt3Line1	Gt3Line1	Gt3Line1	Gt3Line1	Gt3Line1	Gt3Line1	Gt3Line1	Gt3Line1	Gt3Line1
SiO_2	37.761	38.327	38.472	38.388	38.504	38.535	80.307	67.02	38.428	38.313	36.959	38.151	38.184	38.386
TiO_2	0.379	0.05	0.084	0.073	0.05	0.076	0	0.023	0.071	0.07	0.051	0.05	0.063	0.038
Al_2O_3	20.689	21.352	21.468	21.459	21.277	21.466	1.711	3.531	21.458	21.36	15.909	21.627	21.257	21.326
Cr_2O_3	0.051	0.06	0.023	0.032	0.039	0.059	0	0.061	0.055	0.016	0.009	0	0.034	0.005
MgO	5.637	6.906	6.723	6.748	6.668	6.69	0.612	2.381	6.701	6.841	7.062	6.654	6.457	6.578
CaO	9.156	6.461	6.487	6.496	6.509	6.539	0.69	1.773	6.507	6.49	5.57	6.35	6.297	6.362
MnO	0.69	0.768	0.752	0.816	0.746	0.708	0.081	0.215	0.788	0.786	0.714	0.798	0.752	0.711
FeO	24.05	25.598	26.202	26.08	26.034	25.996	2.907	8.615	26.168	25.867	23.641	26.488	26.361	26.765
Na_2O	0	0.025	0.026	0.029	0.011	0.026	0.218	0.224	0.007	0.029	0.053	0.002	0	0.003
Total	98.413	99.547	100.237	100.121	99.838	100.095	86.526	83.843	100.183	99.772	89.968	100.12	99.405	100.174
Cation based on 12 oxygens														
Si	2.988	2.99	2.986	2.983	2.999	2.992	5.736	5.241	2.985	2.986	3.189	2.97	2.992	2.988
Ti	0.023	0.003	0.005	0.004	0.003	0.004	0	0.001	0.004	0.004	0.003	0.003	0.004	0.002
Al	1.93	1.963	1.964	1.966	1.953	1.964	0.144	0.325	1.964	1.962	1.618	1.984	1.963	1.957
Cr	0.003	0.004	0.001	0.002	0.002	0.004	0	0.004	0.003	0.001	0.001	0	0.002	0
Mg	0.665	0.803	0.778	0.782	0.774	0.774	0.065	0.278	0.776	0.795	0.909	0.772	0.754	0.763
Ca	0.776	0.54	0.539	0.541	0.543	0.544	0.053	0.149	0.542	0.542	0.515	0.53	0.529	0.531
Mn	0.046	0.051	0.049	0.054	0.049	0.047	0.005	0.014	0.052	0.052	0.052	0.053	0.05	0.047
Fe	1.592	1.67	1.701	1.695	1.696	1.688	0.174	0.563	1.7	1.686	1.706	1.724	1.728	1.743
Na	0	0.004	0.004	0.004	0.002	0.004	0.03	0.034	0.001	0.004	0.009	0	0	0
Total	8.023	8.028	8.027	8.031	8.021	8.021	6.207	6.609	8.027	8.032	8.002	8.036	8.022	8.031

Oxide Wt.%	Gt3Line1	Gt3Line1	Gt3Line1	Gt3Line1	Gt3Line1	Gt3Line1	Gt3Line1	Gt3Line1	Gt3Line1	Gt3Line1	Gt3Line1	Gt3Line1	Gt3Line1
SiO_2	38.731	39.575	44.527	38.627	38.681	38.48	38.363	36.583	38.33	38.099	37.781	38.216	37.804
TiO_2	0.045	0.02	0.023	0.029	0.012	0.063	0.048	0.059	0.071	0.061	0.08	0.069	0.048
Al_2O_3	21.559	21.534	22.321	21.571	21.574	21.345	21.42	20.959	21.473	21.28	21.304	21.302	21.342
Cr_2O_3	0.048	0.094	0.035	0.055	0.103	0.041	0.025	0.13	0.066	0	0.032	0.07	0.082
MgO	6.429	2.978	5.275	6.235	6.183	6.238	6.175	7.032	5.974	5.747	5.487	5.329	4.652
CaO	6.245	7.877	7.842	6.484	6.517	6.603	6.406	5.664	6.355	6.437	6.418	6.299	6.378
MnO	0.767	0.695	0.686	0.83	0.81	0.827	0.75	0.651	0.723	0.786	0.755	0.872	0.984
FeO	26.657	24.836	23.816	26.465	26.69	26.64	26.477	26.577	26.878	27.196	27.891	28.203	29.148
Na_2O	0.004	0.02	0.032	0.029	0	0.001	0.049	0.023	0.011	0	0.006	0.004	0.015
Total	100.485	97.629	104.557	100.325	100.57	100.238	99.713	97.678	99.881	99.606	99.754	100.364	100.453
Cation based on 12 oxygens													
Si	3	3.132	3.231	2.998	2.998	2.995	2.997	2.93	2.994	2.992	2.975	2.991	2.975
Ti	0.003	0.001	0.001	0.002	0.001	0.004	0.003	0.004	0.004	0.004	0.005	0.004	0.003
Al	1.968	2.009	1.909	1.973	1.97	1.958	1.972	1.979	1.977	1.97	1.977	1.965	1.979
Cr	0.003	0.006	0.002	0.003	0.006	0.003	0.002	0.008	0.004	0	0.002	0.004	0.005
Mg	0.742	0.351	0.571	0.721	0.714	0.724	0.719	0.84	0.696	0.673	0.644	0.622	0.546
Ca	0.518	0.668	0.61	0.539	0.541	0.551	0.536	0.486	0.532	0.542	0.541	0.528	0.538
Mn	0.05	0.047	0.042	0.055	0.053	0.055	0.05	0.044	0.048	0.052	0.05	0.058	0.066
Fe	1.727	1.644	1.445	1.718	1.73	1.734	1.73	1.78	1.756	1.786	1.837	1.846	1.918
Na	0.001	0.003	0.005	0.004	0	0	0.007	0.004	0.002	0	0.001	0.001	0.002
Total	8.012	7.861	7.816	8.013	8.013	8.024	8.016	8.075	8.013	8.019	8.032	8.019	8.032

Appendix IB (cont.):
Microprobe Analysis of CGB Feldspar

Oxide Wt.%	fspIn1a	fspM6	fspM7	57fsp	57fsp	fspM	fspM2	fspM3	fspM4	fspM5	fspIn1	57fsp	57fsp	59fsp
SiO_2	58.052	57.759	58.328	51.016	58.509	58.167	63.243	40.277	57.734	58.143	58.52	52.281	58.235	58.52
Al_2O_3	25.46	25.725	25.448	30.084	25.556	25.023	18.188	32.355	25.681	25.611	25.555	29.951	25.473	25.854
CaO	7.762	8.182	7.64	10.88	7.816	7.494	0.209	23.91	8.045	7.895	7.599	12.549	7.716	7.87
FeO	0.329	0.321	0.106	0.354	0.094	0.121	0.234	0.222	0.31	0.046	0.516	0.326	0.128	0.154
Na_2O	7.118	6.784	6.934	3.363	7.199	7.246	0.249	0.249	6.842	7.215	6.987	4.225	7.104	7.07
K_2O	0.283	0.169	0.2	1.911	0.123	0.159	15.948	0.243	0.172	0.14	0.31	0.322	0.074	0.086
Total	99.004	98.94	98.656	97.608	99.297	98.21	98.071	97.256	98.784	99.05	99.487	99.654	98.73	99.554
Cation based on 8 oxygens														
Si	2.627	2.615	2.64	2.378	2.634	2.647	2.985	1.965	2.617	2.626	2.634	2.383	2.635	2.627
Al	1.358	1.373	1.357	1.652	1.356	1.342	1.012	1.861	1.372	1.363	1.355	1.609	1.358	1.368
Ca	0.376	0.397	0.37	0.543	0.377	0.365	0.011	1.25	0.391	0.382	0.366	0.613	0.374	0.379
Fe	0.012	0.012	0.004	0.014	0.004	0.005	0.009	0.009	0.012	0.002	0.019	0.012	0.005	0.006
Na	0.624	0.595	0.608	0.304	0.628	0.639	0.023	0.024	0.601	0.632	0.61	0.373	0.623	0.615
K	0.016	0.01	0.012	0.114	0.007	0.009	0.96	0.015	0.01	0.008	0.018	0.019	0.004	0.005
Total	5.013	5.002	4.991	5.005	5.006	5.007	5	5.124	5.003	5.013	5.002	5.009	4.999	5

Oxide Wt.%	60fsp	61fsp	62fsp
SiO_2	58.683	58.133	59.133
Al_2O_3	25.915	26.252	25.711
CaO	7.809	8.244	7.967
FeO	0.117	0	0.053
Na_2O	7.369	7.026	7.082
K_2O	0.113	0.138	0.123
Total	100.006	99.793	100.069
Cation based on 8 oxygens			
Si	2.625	2.607	2.639
Al	1.366	1.387	1.352
Ca	0.374	0.396	0.381
Fe	0.004	0	0.002
Na	0.639	0.611	0.613
K	0.006	0.008	0.007
Total	5.014	5.009	4.994

Appendix IB (cont.):
Microprobe Analysis of CGB Biotite

Oxide Wt.%	mO1a	mO2a	mO1	mO2	mIn1
SiO_2	36.52	36.962	36.204	37.002	37.999
TiO_2	2.384	2.416	2.353	2.507	2.107
Al_2O_3	16.406	16.3	16.763	16.425	17.554
MgO	13.063	13.174	12.9	13.11	16.78
CaO	0	0	0.048	0.008	0.017
MnO	0	0.069	0.09	0.11	0.056
FeO	16.128	16.187	16.268	16.209	10.757
Na_2O	0.109	0.088	0.1	0.099	0.296
K_2O	9.579	9.72	9.779	9.83	9.466
H_2O	3.947	3.977	3.949	3.99	4.105
Total	98.136	98.893	98.454	99.29	99.137
Cation based on 22 oxygens					
Si	5.548	5.574	5.498	5.561	5.551
Ti	0.272	0.274	0.269	0.283	0.231
Al	2.938	2.897	3	2.909	3.022
Mg	2.959	2.961	2.92	2.937	3.654
Ca	0	0	0.008	0.001	0.003
Mn	0	0.009	0.012	0.014	0.007
Fe	2.049	2.041	2.066	2.037	1.314
Na	0.032	0.026	0.03	0.029	0.084
K	1.857	1.87	1.894	1.885	1.764
H	0	0	0	0	0
Total	15.655	15.652	15.697	15.656	15.63

Appendix IB(cont.):
Microprobe Analysis of CGB Pyroxene

Oxide Wt.%	pxIn5	pxIn6	pxIn7	pxIn8	pxIn9	pxOut4	pxIn5	pxIn6	pxIn7	pxIn8	pxOut5	pxIn	pxIn	pxIn
SiO_2	51.885	48.728	52.477	52.763	54.547	51.527	52.659	52.39	52.34	52.484	52.738	51.773	52.489	52.948
TiO_2	0.309	0.145	0.247	0.207	0.143	0.339	0.259	0.317	0.26	0.259	0.22	0.301	0.259	0.259
Al_2O_3	2.261	5.599	1.732	1.68	1.715	2.886	2.049	2.153	1.868	2.002	3.74	2.277	1.893	1.846
Cr_2O_3	0.02	0.071	0.074	0.027	0.047	0.022	0.04	0.047	0.042	0	0.054	0.03	0.047	0.032
Fe_2O_3	1.269	2.629	1.473	0.619	0	0.734	0.373	1.271	1.587	1.07	0	1.149	0.838	0.37
MgO	13.192	12.179	14.259	13.991	14.373	13.008	13.535	13.507	13.676	13.893	15.877	13.133	13.615	13.964
CaO	22.006	19.984	22.595	22.217	23.064	20.418	22.11	23.075	22.97	22.811	12.63	22.547	22.769	22.787
MnO	0.11	0.217	0.066	0.064	0.016	0.143	0.106	0.094	0.174	0.074	0.125	0.17	0.104	0.12
FeO	7.983	9.298	6.532	7.884	6.837	9.861	8.496	7.058	6.547	6.744	11.356	7.409	7.299	7.607
Na_2O	0.543	0.338	0.433	0.415	0.351	0.553	0.462	0.461	0.494	0.471	0.321	0.496	0.464	0.373
Total	99.578	99.188	99.888	99.867	101.093	99.491	100.089	100.373	99.958	99.808	97.061	99.285	99.777	100.306
Cation based on 6 Oxygens														
Si	1.943	1.845	1.949	1.963	1.988	1.936	1.959	1.942	1.947	1.951	1.983	1.943	1.956	1.96
Ti	0.009	0.004	0.007	0.006	0.004	0.01	0.007	0.009	0.007	0.007	0.006	0.008	0.007	0.007
Al	0.1	0.25	0.076	0.074	0.074	0.128	0.09	0.094	0.082	0.088	0.166	0.101	0.083	0.081
Cr	0.001	0.002	0.002	0.001	0.001	0.001	0.001	0.001	0.001	0	0.002	0.001	0.001	0.001
Fe	0.036	0.075	0.041	0.017	0	0.021	0.01	0.035	0.044	0.03	0	0.032	0.023	0.01
Mg	0.736	0.687	0.79	0.776	0.781	0.729	0.751	0.747	0.758	0.77	0.89	0.735	0.756	0.771
Ca	0.883	0.811	0.899	0.886	0.901	0.822	0.881	0.917	0.915	0.908	0.509	0.906	0.909	0.904
Mn	0.003	0.007	0.002	0.002	0	0.005	0.003	0.003	0.005	0.002	0.004	0.005	0.003	0.004
Fe	0.25	0.294	0.203	0.245	0.208	0.31	0.264	0.219	0.204	0.21	0.357	0.232	0.227	0.236
Na	0.039	0.025	0.031	0.03	0.025	0.04	0.033	0.033	0.036	0.034	0.023	0.036	0.034	0.027
Total	4	4	4	4	3.982	4.002	3.999	4	3.999	4	3.94	3.999	3.999	4.001

Oxide Wt.%	pxOut	pxOut	pxOut	pxOut
SiO_2	37.114	37.213	52.204	53.573
TiO_2	2.46	2.576	0.238	0.128
Al_2O_3	16.859	16.867	4.111	2.612
Cr_2O_3	0.069	0.045	0.068	0.002
Fe_2O_3	0	0	0	0
MgO	13.341	13.502	16.561	17.136
CaO	0.011	0.016	12.573	12.694
MnO	0.008	0.059	0.028	0.048
FeO	16.185	16.293	11.116	10.782
Na_2O	0.145	0.17	0.364	0.22
Total	86.192	86.741	97.263	97.195
Cation based on 6 Oxygens				
Si	1.575	1.571	1.958	2.004
Ti	0.078	0.082	0.007	0.004
Al	0.843	0.839	0.182	0.115
Cr	0.002	0.002	0.002	0
Fe	0	0	0	0
Mg	0.844	0.85	0.926	0.956
Ca	0.001	0.001	0.505	0.509
Mn	0	0.002	0.001	0.002
Fe	0.574	0.575	0.349	0.337
Na	0.012	0.014	0.026	0.016
Total	3.929	3.936	3.956	3.943

Appendix IB(cont.):
Microprobe Analysis of CGB Pyroxene (cont.)

Oxide Wt.%	69Op	70Op	71Op	72Op	73Op	74Op	75Op	76Op	77Op	78Op (Zircon)
SiO_2	0.016	0.012	0.577	30.291	0.349	0.219	0.072	38.481	0.094	37.091
TiO_2	52.095	98.789	51.401	38.887	50.807	52.033	52.043	0.015	51.869	0
Al_2O_3	0	0.013	0.038	1.066	0.021	0.033	0.003	11.032	0.001	1.054
Cr_2O_3	0.007	0.151	0.072	0.035	0	0.007	0	0	0	0.047
MgO	0.038	0.012	0.436	0	0.08	0.049	0.095	2.811	0.615	0.353
CaO	0.136	0.209	0.24	28.318	0.38	0.317	0.157	3.37	0.254	0.46
MnO	0.933	0	0.716	0	0.993	0.561	0.836	0.356	0.653	0.076
FeO	46.026	0.639	45.449	0.531	46.095	46.147	45.985	12.586	45.313	3.03
Na_2O	0	0.017	0.031	0.038	0.004	0.007	0.004	0	0.053	0
Total	99.251	99.842	98.96	99.166	98.729	99.373	99.195	68.651	98.852	42.111
Cation based on 12 oxygens										
Si	0.002	0.001	0.059	2.394	0.036	0.022	0.007	4.011	0.01	5.583
Ti	3.988	5.959	3.925	2.312	3.916	3.971	3.983	0.001	3.97	0
Al	0	0.001	0.005	0.099	0.003	0.004	0	1.355	0	0.187
Cr	0.001	0.01	0.006	0.002	0	0.001	0	0	0	0.006
Mg	0.006	0.001	0.066	0	0.012	0.007	0.014	0.437	0.093	0.079
Ca	0.015	0.018	0.026	2.398	0.042	0.034	0.017	0.376	0.028	0.074
Mn	0.08	0	0.062	0	0.086	0.048	0.072	0.031	0.056	0.01
Fe	3.919	0.043	3.86	0.035	3.951	3.916	3.914	1.097	3.857	0.381
Na	0	0.003	0.006	0.006	0.001	0.001	0.001	0	0.01	0
Total	8.011	6.036	8.015	7.246	8.047	8.004	8.008	7.308	8.024	6.32

Appendix IB (cont.):
Microprobe Analysis of CGB Amphibole

Oxide Wt.%	amph1a	amph2a	amphIn1	amphIn2
SiO_2	54.338	55.575	54.944	49.848
TiO_2	0.082	0.05	0.082	0.232
Al_2O_3	1.253	1.224	2.538	8.336
Cr_2O_3	0.028	0.027	0.02	0.098
MgO	18.898	19.342	19.526	15.48
CaO	2.29	12.682	13.47	13.042
MnO	0.251	0.054	0.032	0.016
FeO	20.507	8.588	6.526	9.984
Na_2O	0.113	0.125	0.172	0.673
K_2O	0.03	0.07	0	0.016
H_2O	2.075	2.128	2.134	2.099
Total	99.865	99.865	99.444	99.824
Cation based on 23 oxygens				
Si	7.852	7.83	7.719	7.122
Ti	0.009	0.005	0.009	0.025
Al	0.213	0.203	0.42	1.404
Cr	0.003	0.003	0.002	0.011
Mg	4.071	4.063	4.089	3.297
Ca	0.355	1.914	2.027	1.997
Mn	0.031	0.006	0.004	0.002
Fe	2.478	1.012	0.767	1.193
Na	0.032	0.034	0.047	0.187
K	0.006	0.013	0	0.003
H	0	0	0	0
Total	15.05	15.083	15.084	15.241

Appendix IB (cont.):
Microprobe Analysis of CGB Epidote

Oxide Wt.%	EpM3	EpM4	EpM5	EpM6	65Ep	66Ep	67Ep	68Ep
SiO_2	38.513	38.657	38.666	38.667	38.542	48.893	38.458	40.202
TiO_2	0.103	0.047	0.159	0.134	0.01	0.342	0.022	0.097
Al_2O_3	28.601	28.485	28.706	29.249	29.23	7.53	28.865	25.763
Cr_2O_3	0	0	0	0	0	0.022	0	0.012
Fe_2O_3	6.102	6.181	5.86	5.503	5.341	14.604	6.155	7.123
MgO	0.03	0.051	0.068	0.048	0.038	13.541	0.041	1.7
CaO	24.387	24.41	24.257	24.586	24.337	12.387	24.332	22.694
MnO	0.05	0.054	0.046	0.012	0.036	0.087	0.078	0.066
Na_2O	0	0.006	0	0	0	0.631	0.001	0.05
H_2O	1.929	1.931	1.932	1.941	1.931	1.946	1.932	1.932
Total	99.715	99.822	99.694	100.14	99.465	99.983	99.884	99.639
Cation based on 25 oxygens								
Si	5.986	6.003	6.002	5.972	5.986	7.533	5.967	6.239
Ti	0.012	0.005	0.019	0.016	0.001	0.04	0.003	0.011
Al	5.239	5.213	5.251	5.324	5.351	1.367	5.278	4.712
Cr	0	0	0	0	0	0.003	0	0.002
Fe	0.714	0.722	0.684	0.64	0.624	1.693	0.719	0.832
Mg	0.007	0.012	0.016	0.011	0.009	3.11	0.01	0.393
Ca	4.061	4.061	4.034	4.068	4.05	2.045	4.045	3.773
Mn	0.007	0.007	0.006	0.002	0.005	0.011	0.01	0.009
Na	0	0.002	0	0	0	0.189	0	0.015
H	0.021	0.021	0.021	0.021	0	0	0	0
Total	16.047	16.046	16.033	16.054	16.026	15.991	16.032	15.986

Appendix IC:
Microprobe Analysis of 478 Garnet

Oxide Wt. %	T478GtRim1	T478GtRim2	T478GtRim3	T478GtRim5	T478GtCor1	T478GtCor2	T478GtCor3	T478Gt5Line1	T478Gt5Line1	T478Gt5Line1	T478Gt5Line1	T478Gt5Line1	T478Gt5Line1	T478Gt5Line1
SiO_2	36.816	36.84	36.882	36.949	36.777	36.436	37.273	37.215	37.035	37.679	38.116	39.17	36.854	36.505
TiO_2	0.018	0.019	0	0	0.034	0.042	0.024	0	0.004	0	0	0	0.028	0.014
Al_2O_3	21.185	20.488	21.06	21.141	21.231	21.148	20.981	20.748	21.057	20.488	20.913	15.131	20.967	20.322
MgO	3.591	3.247	3.255	3.451	3.773	3.725	4.241	3.268	3.46	3.47	3.445	3.576	3.608	3.532
CaO	1.303	2.123	2.361	2.058	1.345	1.275	1.501	1.465	1.316	1.258	1.302	1.125	1.267	1.222
MnO	1.954	1.394	1.435	1.433	1.91	1.794	1.932	1.7	1.915	2.067	2.146	2.135	2.36	2.454
FeO	35.277	34.749	34.561	35.394	35.169	35.589	34.073	35.294	35.534	34.576	34.764	29.652	34.628	34.401
Na_2O	0.027	0	0.015	0.003	0.019	0.014	0.013	0.002	0.009	0.023	0.048	0.062	0.003	0.03
Total	100.171	98.86	99.569	100.429	100.258	100.023	100.038	99.692	100.33	99.561	100.734	90.851	99.715	98.48
Cations based on 12 oxygens														
Si	2.964	3.002	2.98	2.967	2.957	2.944	2.987	3.007	2.978	3.039	3.036	3.399	2.978	2.992
Ti	0.001	0.001	0	0	0.002	0.003	0.001	0	0	0	0	0	0.002	0.001
Al	2.01	1.967	2.006	2.001	2.012	2.014	1.982	1.976	1.996	1.947	1.963	1.547	1.997	1.963
Mg	0.431	0.394	0.392	0.413	0.452	0.449	0.507	0.394	0.415	0.417	0.409	0.463	0.435	0.432
Ca	0.112	0.185	0.204	0.177	0.116	0.11	0.129	0.127	0.113	0.109	0.111	0.105	0.11	0.107
Mn	0.133	0.096	0.098	0.097	0.13	0.123	0.131	0.116	0.13	0.141	0.145	0.157	0.162	0.17
Fe	2.375	2.368	2.335	2.377	2.365	2.404	2.283	2.385	2.39	2.332	2.315	2.152	2.34	2.358
Na	0.004	0	0.002	0	0.003	0.002	0.002	0	0.001	0.004	0.007	0.01	0	0.005
Total	8.03	8.013	8.017	8.032	8.037	8.049	8.022	8.005	8.023	7.989	7.986	7.833	8.024	8.028

Oxide Wt. %	T478Gt5Line1	T478Gt5Line1	T478Gt5Line1	T478Gt5Line1	T478Gt5Line1	T478Gt5Line1	T478Gt5Line1	T478Gt5Line1	T478Gt5Line1	T478Gt5Line1	T478Gt5Line1	T478Gt5Line1	T478Gt5Line1	T478Gt5Line1
SiO_2	37.208	37.053	37.109	36.852	36.2	36.854	36.505	37.208	37.053	37.109	36.852	36.2	37.132	36.761
TiO_2	0	0.041	0.028	0.015	0.014	0.028	0.014	0	0.041	0.028	0.015	0.014	0.005	0.007
Al_2O_3	21.108	21.16	21.001	21.175	20.582	20.967	20.322	21.108	21.16	21.001	21.175	20.582	21.106	20.973
MgO	3.615	3.672	3.615	3.681	3.965	3.608	3.532	3.615	3.672	3.615	3.681	3.965	3.596	3.624
CaO	1.225	1.285	1.29	1.255	1.317	1.267	1.222	1.225	1.285	1.29	1.255	1.317	1.257	1.326
MnO	2.476	2.383	2.329	2.366	2.264	2.36	2.454	2.476	2.383	2.329	2.366	2.264	2.296	2.199
FeO	34.743	34.641	34.72	34.581	34.473	34.628	34.401	34.743	34.641	34.72	34.581	34.473	34.979	34.773
Na_2O	0.011	0.023	0	0	0.013	0.003	0.03	0.011	0.023	0	0	0.013	0	0.011
Total	100.386	100.258	100.092	99.925	98.828	99.715	98.48	100.386	100.258	100.092	99.925	98.828	100.371	99.674
Cations based on 12 oxygens														
Si	2.985	2.975	2.985	2.97	2.957	2.978	2.992	2.985	2.975	2.985	2.97	2.957	2.981	2.973
Ti	0	0.002	0.002	0.001	0.001	0.002	0.001	0	0.002	0.002	0.001	0.001	0	0
Al	1.996	2.003	1.991	2.011	1.982	1.997	1.963	1.996	2.003	1.991	2.011	1.982	1.997	1.999
Mg	0.432	0.44	0.434	0.442	0.483	0.435	0.432	0.432	0.44	0.434	0.442	0.483	0.43	0.437
Ca	0.105	0.111	0.111	0.108	0.115	0.11	0.107	0.105	0.111	0.111	0.108	0.115	0.108	0.115
Mn	0.168	0.162	0.159	0.161	0.157	0.162	0.17	0.168	0.162	0.159	0.161	0.157	0.156	0.151
Fe	2.331	2.326	2.336	2.33	2.355	2.34	2.358	2.331	2.326	2.336	2.33	2.355	2.348	2.352
Na	0.002	0.004	0	0	0.002	0	0.005	0.002	0.004	0	0	0.002	0	0.002
Total	8.019	8.023	8.018	8.023	8.052	8.024	8.028	8.019	8.023	8.018	8.023	8.052	8.02	8.029

Oxide Wt. %	T478Gt5Line1	T478Gt5Line1	T478Gt5Line1	T478Gt5Line1	T478Gt5Line1	T478Gt5Line1	T478Gt5Line1	T478Gt5Line1	T478Gt5Line1	T478Gt5Line1	T478Gt5Line1	T478Gt5Line1	T478Gt5Line1	T478Gt5Line1
SiO_2	36.286	37.667	37.018	36.811	43.091	36.955	36.848	38.572	47.536	37.121	37.038	10.832	79.393	39.511
TiO_2	0.14	0.028	0.005	0.003	0.039	0.004	0.007	0	0.012	0.026	0	0.01	0.026	0.021
Al_2O_3	17.351	20.106	21.22	21.007	7.76	21.179	21.045	20.969	17.621	20.914	21.034	4.517	3.93	19.821
MgO	3.051	3.372	3.57	3.685	2.18	3.684	3.598	3.842	3.084	3.416	3.148	2.188	0.291	2.794
CaO	1.771	1.295	1.291	1.299	0.923	1.292	1.348	1.313	1.163	1.542	1.725	0.875	0.348	1.745
MnO	1.304	1.935	1.973	2.107	1.247	2.132	1.984	2.012	1.527	2.008	1.743	0.916	0.135	1.614
FeO	22.726	33.358	35.3	35.197	23.012	35.005	34.594	34.121	27.925	34.829	35.692	17.937	4.583	33.318
Na_2O	0.83	0.025	0.024	0	0.182	0.005	0.007	0.013	0.099	0.03	0.003	0.592	0.094	0.043
Total	83.459	97.786	100.401	100.109	78.434	100.256	99.431	100.842	98.967	99.886	100.383	37.867	88.8	98.867
Cations based on 12 oxygens														
Si	3.329	3.077	2.972	2.967	4.148	2.97	2.981	3.053	3.637	2.993	2.98	2.589	5.584	3.174
Ti	0.01	0.002	0	0	0.003	0	0	0	0.001	0.002	0	0.002	0.001	0.001
Al	1.876	1.936	2.008	1.996	0.88	2.006	2.006	1.956	1.589	1.987	1.995	1.272	0.326	1.876
Mg	0.417	0.411	0.427	0.443	0.313	0.441	0.434	0.453	0.352	0.411	0.378	0.779	0.031	0.335
Ca	0.174	0.113	0.111	0.112	0.095	0.111	0.117	0.111	0.095	0.133	0.149	0.224	0.026	0.15
Mn	0.101	0.134	0.134	0.144	0.102	0.145	0.136	0.135	0.099	0.137	0.119	0.185	0.008	0.11
Fe	1.743	2.279	2.37	2.373	1.852	2.353	2.34	2.259	1.787	2.348	2.402	3.585	0.27	2.238
Na	0.148	0.004	0.004	0	0.034	0.001	0.001	0.002	0.015	0.005	0	0.274	0.013	0.007
Total	7.798	7.956	8.026	8.035	7.427	8.027	8.015	7.969	7.575	8.016	8.023	8.91	6.259	7.891

Appendix IC (cont.):
Microprobe Analysis of 478 Garnet (cont.)

Oxide Wt. %	T478Gt5Line1	T478Gt5Line1	T478Gt5Line1	T478Gt5Line1	T478Gt5Line1	T478Gt5Line1	T478Gt5Line1	T478Gt5Line1	T478Gt5Line1	T478Gt5Line1	T478Gt5Line1	T478Gt5Line1	T478Gt5Line1	T478Gt5Line1
SiO_2	37.191	37.006	36.909	36.934	37.237	44.265	36.732	34.213	39.928	37.323	36.426	42.535	47.547	36.56
TiO_2	0	0	0	0.021	0	0	0.014	0	0.008	0	0.002	0.005	0	0
Al_2O_3	21.053	21.088	21.219	21.302	21.292	19.147	21.009	16.946	22.23	21.251	20.036	16.214	18.692	21.251
MgO	3.462	3.544	3.558	3.426	3.525	3.429	3.562	3.351	2.933	3.418	3.354	3.058	2.754	3.522
CaO	1.831	1.5	1.933	2.287	1.773	1.698	1.738	1.514	1.626	1.617	1.707	1.242	1.173	1.45
MnO	1.773	1.912	1.914	1.995	1.982	1.678	2.121	1.972	1.93	1.966	1.9	1.566	1.5	1.77
FeO	35.06	35.284	35.121	34.64	34.35	30.657	34.718	33.066	33.911	34.491	33.608	28.796	28.633	35.17
Na_2O	0.03	0.02	0.014	0.023	0.009	0.084	0.021	0.047	0.01	0.025	0.034	0.077	0.059	0.007
Total	100.4	100.354	100.668	100.628	100.168	100.958	99.915	91.109	102.576	100.091	97.067	93.493	100.358	99.73
Cations based on 12 oxygens														
Si	2.984	2.974	2.958	2.959	2.985	3.395	2.965	3.055	3.085	2.994	3.018	3.517	3.594	2.956
Ti	0	0	0	0.001	0	0	0.001	0	0	0	0	0	0	0
Al	1.991	1.997	2.005	2.011	2.012	1.731	1.999	1.784	2.025	2.009	1.956	1.58	1.665	2.025
Mg	0.414	0.425	0.425	0.409	0.421	0.392	0.429	0.446	0.338	0.409	0.414	0.377	0.31	0.425
Ca	0.157	0.129	0.166	0.196	0.152	0.14	0.15	0.145	0.135	0.139	0.152	0.11	0.095	0.126
Mn	0.12	0.13	0.13	0.135	0.135	0.109	0.145	0.149	0.126	0.134	0.133	0.11	0.096	0.121
Fe	2.352	2.371	2.354	2.321	2.303	1.966	2.344	2.47	2.192	2.314	2.328	1.991	1.81	2.378
Na	0.005	0.003	0.002	0.004	0.001	0.012	0.003	0.008	0.001	0.004	0.005	0.012	0.009	0.001
Total	8.023	8.029	8.04	8.036	8.009	7.745	8.036	8.057	7.902	8.003	8.006	7.697	7.579	8.032

Oxide Wt. %	T478Gt5Line1	T478Gt5Line1	T478Gt5Line1	T478Gt5Line1	T478Gt5Line1	T478Gt5Line1	T478Gt5Line1	T478Gt5Line1	T478Gt5Line2	T478Gt5Line2	T478Gt5Line2	T478Gt5Line2	T478Gt5Line2	T478Gt5Line2
SiO_2	36.39	36.738	33.282	21.572	73.979	35.975	35.994	35.959	36.877	37.031	37.016	37.198	37.028	46.913
TiO_2	0	0.013	0	0.008	0.024	0.021	0.063	0.441	0.111	0.061	0.014	0.02	0.012	0.036
Al_2O_3	21.13	21.417	17.799	11.675	5.962	21.324	21.124	20.779	20.716	21.074	21.142	21.059	21.006	17.838
MgO	3.428	3.435	3.77	2.995	0.873	3.519	3.387	3.163	3.081	3.648	3.624	3.759	3.733	1.477
CaO	1.999	1.568	1.24	1.476	0.268	1.804	2.41	1.791	1.983	1.425	1.743	1.341	1.39	1.397
MnO	1.727	1.76	1.664	1.712	0.341	1.639	1.669	1.815	1.624	1.657	1.728	1.86	1.822	1.292
FeO	34.501	35.038	34.133	34.572	7.118	34.726	34.737	35.394	34.945	35.174	34.34	35.048	35.048	26.231
Na_2O	0.013	0	0.017	0.043	0.276	0.004	0.04	0.008	0.036	0.013	0.015	0.008	0	0.049
Total	99.188	99.969	91.905	74.053	88.841	99.012	99.424	99.35	99.373	100.083	99.622	100.293	100.039	95.233
Cations based on 12 oxygens														
Si	2.956	2.96	2.959	2.582	5.328	2.931	2.927	2.934	2.992	2.978	2.983	2.984	2.98	3.699
Ti	0	0.001	0	0.001	0.001	0.001	0.004	0.027	0.007	0.004	0.001	0.001	0.001	0.002
Al	2.023	2.034	1.865	1.647	0.506	2.048	2.025	1.998	1.981	1.998	2.008	1.991	1.992	1.658
Mg	0.415	0.413	0.5	0.534	0.094	0.427	0.411	0.385	0.373	0.437	0.435	0.45	0.448	0.174
Ca	0.174	0.135	0.118	0.189	0.021	0.157	0.21	0.157	0.172	0.123	0.151	0.115	0.12	0.118
Mn	0.119	0.12	0.125	0.174	0.021	0.113	0.115	0.125	0.112	0.113	0.118	0.126	0.124	0.086
Fe	2.344	2.361	2.538	3.461	0.429	2.366	2.362	2.415	2.371	2.366	2.314	2.351	2.359	1.73
Na	0.002	0	0.003	0.01	0.038	0.001	0.006	0.001	0.006	0.002	0.002	0.001	0	0.007
Total	8.033	8.024	8.108	8.598	6.438	8.044	8.06	8.042	8.014	8.021	8.012	8.019	8.024	7.474

Oxide Wt. %	T478Gt5Line2	T478Gt5Line2	T478Gt5Line2	T478Gt5Line2	T478Gt5Line2	T478Gt5Line2	T478Gt5Line2	T478Gt5Line2	T478Gt5Line2	T478Gt5Line2	T478Gt5Line2	T478Gt5Line2	T478Gt5Line2	T478Gt5Line2
SiO_2	99.454	37.148	50.015	98.708	38.136	33.964	65.262	37.212	37.331	37.275	99.496	99.825	99.604	37.094
TiO_2	0.026	0.014	0.023	0.016	2.014	0	0.128	0.021	0.022	0.023	0.016	0.01	0	0.008
Al_2O_3	0.178	21.154	16.428	0.054	19.568	18.559	0.532	20.977	21.065	21.025	0.018	0.002	0.004	21.187
MgO	0.028	3.844	2.706	0.023	12.007	3.908	0.352	3.905	3.97	3.881	0	0.001	0	4.051
CaO	0.033	1.309	1.765	0.035	0.036	1.301	0.236	1.431	1.308	1.339	0.018	0	0.014	1.452
MnO	0.046	1.762	1.36	0.02	0.052	1.696	0.133	1.528	1.713	1.675	0.028	0.028	0.096	1.794
FeO	1.059	34.926	28.685	0.626	15.215	34.929	2.722	34.745	34.603	34.764	0.528	0.51	0.631	34.809
Na_2O	0.004	0.007	0.033	0.032	0.339	0.014	0.274	0.039	0.012	0.007	0	0	0.012	0.02
Total	100.828	100.164	101.015	99.514	87.367	94.371	69.639	99.858	100.024	99.989	100.104	100.376	100.361	100.415
Cations based on 12 oxygens														
Si	5.959	2.981	3.746	5.977	3.158	2.94	5.797	2.991	2.993	2.992	5.984	5.986	5.981	2.969
Ti	0.001	0.001	0.001	0.001	0.125	0	0.009	0.001	0.001	0.001	0.001	0	0	0
Al	0.013	2	1.45	0.004	1.91	1.894	0.056	1.987	1.991	1.989	0.001	0	0	1.999
Mg	0.003	0.46	0.302	0.002	1.482	0.504	0.047	0.468	0.475	0.464	0	0	0	0.483
Ca	0.002	0.112	0.142	0.002	0.003	0.121	0.022	0.123	0.112	0.115	0.001	0	0.001	0.125
Mn	0.002	0.12	0.086	0.001	0.004	0.124	0.01	0.104	0.116	0.114	0.001	0.001	0.005	0.122
Fe	0.053	2.344	1.797	0.032	1.054	2.529	0.202	2.336	2.32	2.334	0.027	0.026	0.032	2.33
Na	0	0.001	0.005	0.004	0.054	0.002	0.047	0.006	0.002	0.001	0	0	0.001	0.003
Total	6.033	8.019	7.529	6.023	7.79	8.114	6.19	8.016	8.01	8.01	6.015	6.013	6.02	8.031

Appendix IC (cont.):
Microprobe Analysis of 478 Garnet (cont.)

Oxide Wt. %	T478Gt5Line2	T478Gt5Line2	T478Gt5Line2	T478Gt5Line2	T478Gt5Line2	T478Gt5Line2	T478Gt5Line2	T478Gt5Line2	T478Gt5Line2	T478Gt5Line2	T478Gt5Line2	T478Gt5Line2	T478Gt5Line2	T478Gt5Line2
SiO_2	37.549	93.318	36.07	36.91	37.688	37.418	38.45	36.854	36.957	37.191	40.545	59.534	39.722	24.033
TiO_2	0.004	0.015	0	0	0.015	0	0.019	0.027	0	0.025	0.012	0.039	0	0.007
Al_2O_3	21.363	2.527	21.059	21.074	19.501	20.934	20.997	21.014	21.098	21.218	20.556	4.719	8.057	10.611
MgO	3.948	0.479	4.065	4.001	4.483	3.956	3.374	4.181	4.188	4.13	3.676	1.242	2.258	4.028
CaO	1.399	0.263	1.293	1.351	1.39	1.307	1.401	1.35	1.327	1.322	1.332	0.57	0.951	1.204
MnO	1.816	0.205	1.631	1.82	1.775	1.733	1.679	1.833	1.781	1.689	1.628	0.506	1.398	1.634
FeO	34.363	4.555	35	34.563	33.113	34.681	33.423	34.899	34.736	34.499	32.935	11.013	24.809	32.942
Na_2O	0	0	0.017	0	0.038	0.025	0.036	0.009	0.013	0.014	0.047	0.214	0.149	0.011
Total	100.442	101.362	99.135	99.719	98.003	100.054	99.379	100.167	100.1	100.088	100.731	77.837	77.344	74.47
Cations based on 12 oxygens														
Si	2.993	5.71	2.935	2.974	3.071	3.001	3.076	2.962	2.968	2.979	3.173	5.111	3.967	2.798
Ti	0	0.001	0	0	0.001	0	0.001	0.002	0	0.002	0.001	0.003	0	0.001
Al	2.007	0.182	2.019	2.001	1.873	1.979	1.98	1.99	1.997	2.003	1.896	0.477	0.948	1.456
Mg	0.469	0.044	0.493	0.481	0.545	0.473	0.402	0.501	0.501	0.493	0.429	0.159	0.336	0.699
Ca	0.119	0.017	0.113	0.117	0.121	0.112	0.12	0.116	0.114	0.113	0.112	0.052	0.102	0.15
Mn	0.123	0.011	0.112	0.124	0.122	0.118	0.114	0.125	0.121	0.115	0.108	0.037	0.118	0.161
Fe	2.291	0.233	2.382	2.329	2.256	2.326	2.236	2.345	2.333	2.311	2.156	0.791	2.072	3.207
Na	0	0	0.003	0	0.006	0.004	0.006	0.001	0.002	0.002	0.007	0.036	0.029	0.002
Total	8.002	6.198	8.057	8.026	7.995	8.013	7.935	8.042	8.036	8.018	7.882	6.666	7.572	8.474

Oxide Wt. %	T478Gt5Line2	T478Gt5Line2	T478Gt5Line2	T478Gt5Line2	T478Gt5Line2	T478Gt5Line2	T478Gt5Line2	T478Gt5Line2	T478Gt5Line2	T478Gt5Line2	T478Gt5Line2	T478Gt5Line2	T478Gt5Line2	T478Gt5Line2
SiO_2	39.15	38.813	28.344	49.723	37.931	38.297	36.849	37.508	36.962	36.887	36.6	35.972	37.208	36.833
TiO_2	0.018	0.036	0.007	0	0.018	0.038	0.011	0	0	0.008	0	0.006	0.003	0.004
Al_2O_3	21.79	22.035	12.416	20.597	21.749	20.874	21.553	21.662	21.506	21.322	21.295	19.845	21.548	21.386
MgO	3.317	4.336	3.96	2.877	4.052	3.858	4.182	4.365	4.188	4.303	4.364	3.876	4.289	4.247
CaO	1.322	1.229	1.023	1.2	1.289	1.265	1.304	1.294	1.267	1.294	1.261	1.261	1.37	1.289
MnO	1.523	1.789	1.434	1.408	1.767	1.809	1.851	1.832	1.916	1.807	1.762	1.871	1.987	1.79
FeO	33.834	34.008	29.275	28.769	34.327	33.388	34.491	35.128	34.378	33.813	34.73	33.652	34.511	34.1
Na_2O	0.032	0.015	0.1	0.075	0.014	0.05	0.009	0.004	0.016	0.016	0	0.019	0.022	0
Total	100.986	102.261	76.559	104.649	101.147	99.579	100.25	101.793	100.233	99.45	100.012	96.502	100.938	99.649
Cations based on 12 oxygens														
Si	3.074	3.017	3.052	3.578	2.995	3.06	2.95	2.958	2.958	2.969	2.943	3	2.958	2.962
Ti	0.001	0.002	0.001	0	0.001	0.002	0.001	0	0	0	0	0	0	0
Al	2.017	2.019	1.576	1.747	2.024	1.966	2.034	2.014	2.029	2.022	2.018	1.95	2.019	2.027
Mg	0.388	0.502	0.636	0.309	0.477	0.46	0.499	0.513	0.5	0.516	0.523	0.482	0.508	0.509
Ca	0.111	0.102	0.118	0.093	0.109	0.108	0.112	0.109	0.109	0.112	0.109	0.113	0.117	0.111
Mn	0.101	0.118	0.131	0.086	0.118	0.122	0.126	0.122	0.13	0.123	0.12	0.132	0.134	0.122
Fe	2.222	2.211	2.636	1.731	2.267	2.231	2.31	2.317	2.301	2.276	2.335	2.347	2.295	2.293
Na	0.005	0.002	0.021	0.01	0.002	0.008	0.001	0.001	0.002	0.002	0	0.003	0.003	0
Total	7.919	7.973	8.171	7.554	7.993	7.957	8.033	8.034	8.029	8.02	8.048	8.027	8.034	8.024

Oxide Wt. %	T478Gt5Line2	T478Gt5Line2	T478Gt5Line2	T478Gt5Line2	T478Gt5Line2	T478Gt5Line2	T478Gt5Line2B	T478Gt5Line2B	T478Gt5Line2B	T478Gt5Line2B	T478Gt5Line2B	T478Gt5Line2B	T478Gt5Line2B	T478Gt5Line2B
SiO_2	36.638	37.256	36.677	36.582	37.5	36.824	36.341	36.758	37.083	37.041	36.963	36.888	37.025	36.961
TiO_2	0	0.016	0.016	0.021	0.01	0.007	0.02	0.024	0.017	0	0.015	0.008	0.01	0.035
Al_2O_3	21.434	21.335	21.474	21.315	21.334	21.385	19.954	21.295	21.066	21.184	21.166	21.069	21.274	21.262
MgO	4.271	4.196	4.27	4.236	4.337	4.275	2.787	3.118	3.271	3.274	3.311	3.343	3.286	3.445
CaO	1.269	1.263	1.286	1.267	1.305	1.32	2.348	2.202	2.088	2.078	2.05	2.005	2.083	2.082
MnO	1.836	1.871	1.984	1.879	1.917	2.061	1.293	1.449	1.181	1.411	1.568	1.528	1.457	1.564
FeO	34.05	34.578	34.413	34.216	33.995	34.388	33.919	35.476	35.223	35.046	35.547	35.133	35.559	34.777
Na_2O	0.011	0.012	0.027	0	0.015	0.006	0.044	0.023	0.034	0.017	0	0.004	0.004	0
Total	99.509	100.527	100.147	99.516	100.413	100.266	96.706	100.345	99.963	100.051	100.62	99.978	100.698	100.126
Cations based on 12 oxygens														
Si	2.952	2.973	2.943	2.951	2.987	2.951	3.025	2.958	2.986	2.98	2.966	2.974	2.966	2.97
Ti	0	0.001	0.001	0.001	0.001	0	0.001	0.001	0.001	0	0.001	0	0.001	0.002
Al	2.035	2.007	2.031	2.026	2.003	2.02	1.958	2.02	1.999	2.009	2.002	2.002	2.009	2.014
Mg	0.513	0.499	0.511	0.509	0.515	0.511	0.346	0.374	0.393	0.393	0.396	0.402	0.392	0.413
Ca	0.11	0.108	0.111	0.11	0.111	0.113	0.209	0.19	0.18	0.179	0.176	0.173	0.179	0.179
Mn	0.125	0.126	0.135	0.128	0.129	0.14	0.091	0.099	0.081	0.096	0.107	0.104	0.099	0.106
Fe	2.294	2.308	2.309	2.308	2.264	2.304	2.361	2.387	2.372	2.358	2.385	2.369	2.383	2.337
Na	0.002	0.002	0.004	0	0.002	0.001	0.007	0.004	0.005	0.003	0	0.001	0.001	0
Total	8.031	8.024	8.045	8.033	8.012	8.04	7.998	8.033	8.017	8.018	8.033	8.025	8.03	8.021

Appendix IC (cont.):
Microprobe Analysis of 478 Garnet (cont.)

Oxide Wt. %	T478Gt5Line2B	T478Gt5Line2B	T478Gt5Line2B	T478Gt5Line2B	T478Gt5Line2B	T478Gt5Line2B	T478Gt5Line2B	T478Gt5Line2B	T478Gt5Line2B	T478Gt5Line2B	T478Gt5Line2B	T478Gt5Line2B	T478Gt5Line2B	T478Gt5Line2B
SiO_2	36.888	36.844	27.538	37.094	36.65	36.704	36.08	36.997	36.41	36.571	36.842	36.826	37.102	37.744
TiO_2	0.007	0.013	0.015	0	0.041	0	0.008	0	0.004	0.019	0.007	0.001	0.029	0.005
Al_2O_3	21.261	21.077	8.749	20.997	21.1	21.146	20.769	21.323	21.092	21.22	21.196	21.222	21.194	21.149
MgO	3.475	3.319	1.543	3.313	3.571	3.53	3.679	3.778	3.817	3.793	3.867	3.821	3.667	3.639
CaO	2.014	2.486	1.932	2.233	1.677	1.363	1.277	1.296	1.222	1.231	1.237	1.284	1.263	1.264
MnO	1.628	1.761	1.208	1.873	1.931	2.025	2.199	2.229	2.395	2.514	2.481	2.449	2.413	2.599
FeO	35.173	34.319	26.664	34.956	35.318	35.06	34.801	35.364	34.592	34.456	34.596	34.67	33.86	33.678
Na_2O	0.028	0.039	0.086	0.02	0.002	0.043	0.031	0.006	0.018	0	0.028	0.035	0	0.046
Total	100.474	99.858	67.735	100.486	100.29	99.871	98.844	100.993	99.55	99.804	100.254	100.308	99.528	100.124
Cations based on 12 oxygens														
Si	2.96	2.971	3.36	2.978	2.953	2.964	2.951	2.956	2.95	2.953	2.961	2.959	2.99	3.018
Ti	0	0.001	0.001	0	0.002	0	0	0	0	0.001	0	0	0.002	0
Al	2.011	2.003	1.258	1.987	2.003	2.013	2.002	2.008	2.014	2.02	2.008	2.01	2.013	1.993
Mg	0.416	0.399	0.281	0.396	0.429	0.425	0.448	0.45	0.461	0.457	0.463	0.458	0.441	0.434
Ca	0.173	0.215	0.253	0.192	0.145	0.118	0.112	0.111	0.106	0.106	0.107	0.111	0.109	0.108
Mn	0.111	0.12	0.125	0.127	0.132	0.139	0.152	0.151	0.164	0.172	0.169	0.167	0.165	0.176
Fe	2.361	2.314	2.721	2.347	2.379	2.368	2.38	2.363	2.344	2.327	2.325	2.33	2.282	2.252
Na	0.004	0.006	0.02	0.003	0	0.007	0.005	0.001	0.003	0	0.004	0.005	0	0.007
Total	8.036	8.029	8.019	8.03	8.043	8.034	8.05	8.04	8.042	8.036	8.037	8.04	8.002	7.988

Oxide Wt. %	T478Gt5Line2B	T478Gt5Line2B	T478Gt5Line2B	T478Gt5Line2B	T478Gt5Line2B	T478Gt5Line2B	T478Gt5Line2B	T478Gt5Line2B	T478Gt5Line2B	T478Gt5Line2B	T478Gt5Line2B	T478Gt5Line2B	T478Gt5Line2B	T478Gt5Line2B
SiO_2	36.284	36.647	36.091	36.389	38.596	37.145	36.787	36.874	36.794	36.685	36.605	36.77	36.907	37.674
TiO_2	0.019	0	0.016	0.016	0.011	0.02	0.009	0.017	0	0.008	0.031	0.025	0.013	0
Al_2O_3	20.59	21.024	20.196	20.536	18.848	21.187	21.14	21.232	21.214	21.148	21.098	21.227	21.377	21.559
MgO	4.195	4.056	4.485	3.949	3.638	3.982	4.093	4.065	4.092	4.11	4.139	4.118	4.145	3.958
CaO	1.231	1.224	1.224	1.263	1.23	1.272	1.246	1.277	1.238	1.287	1.269	1.305	1.256	1.316
MnO	2.383	2.402	2.309	2.309	2.256	2.377	2.157	2.158	2.362	2.182	2.184	2.185	1.907	2.017
FeO	33.947	34.086	33.656	34.517	31.561	34.261	34.377	34.212	34.14	34.656	34.56	34.567	34.471	34.092
Na_2O	0.045	0.027	0.02	0.011	0.067	0.015	0.038	0.031	0.011	0.01	0.034	0.005	0	0.02
Total	98.694	99.466	97.997	98.99	96.207	100.259	99.847	99.866	99.851	100.086	99.92	100.202	100.076	100.636
Cations based on 12 oxygens														
Si	2.962	2.964	2.966	2.967	3.18	2.976	2.963	2.966	2.962	2.952	2.951	2.953	2.961	2.994
Ti	0.001	0	0.001	0.001	0.001	0.001	0.001	0.001	0	0	0.002	0.001	0.001	0
Al	1.981	2.004	1.956	1.973	1.83	2.001	2.006	2.013	2.013	2.006	2.004	2.009	2.021	2.019
Mg	0.51	0.489	0.549	0.48	0.447	0.476	0.491	0.487	0.491	0.493	0.497	0.493	0.496	0.469
Ca	0.108	0.106	0.108	0.11	0.109	0.109	0.107	0.11	0.107	0.111	0.11	0.112	0.108	0.112
Mn	0.165	0.165	0.161	0.159	0.157	0.161	0.147	0.147	0.161	0.149	0.149	0.149	0.13	0.136
Fe	2.317	2.305	2.313	2.354	2.175	2.296	2.315	2.301	2.298	2.332	2.33	2.322	2.313	2.266
Na	0.007	0.004	0.003	0.002	0.011	0.002	0.006	0.005	0.002	0.002	0.005	0.001	0	0.003
Total	8.051	8.037	8.057	8.046	7.91	8.022	8.036	8.03	8.034	8.045	8.048	8.04	8.03	7.999

Oxide Wt. %	T478Gt5Line2B	T478Gt5Line2B	T478Gt5Line2B	T478Gt5Line2B	T478Gt4Line1B	T478Gt4Line1B	T478Gt4Line1B	T478Gt4Line1B	T478Gt4Line1B	T478Gt4Line1B	T478Gt4Line1B	T478Gt4Line1B	T478Gt4Line1B	T478Gt4Line1B
SiO_2	36.903	36.731	37.079	37.068	36.452	28.891	36.821	36.554	36.682	36.346	36.651	36.525	36.806	36.693
TiO_2	0.007	0.013	0.008	0	0.059	0.418	0.058	0.032	0.037	0.046	0.042	0.026	0.064	0.029
Al_2O_3	21.411	21.177	21.359	21.42	20.998	13.143	21.084	20.843	20.968	21.002	20.995	21.062	21.111	21.093
MgO	4.235	4.251	4.151	4.19	3.423	3.94	3.394	3.439	3.42	3.42	3.544	3.523	3.467	3.517
CaO	1.301	1.309	1.311	1.274	2.034	1.69	2.072	2.31	2.347	2.446	1.95	1.956	1.77	1.765
MnO	2.09	1.929	2.075	2.08	1.469	1.353	1.54	1.456	1.602	1.651	1.735	1.693	1.915	1.9
FeO	34.218	34.478	34.758	34.421	35.406	31.325	35.056	34.77	34.734	35.058	34.634	34.471	34.91	34.667
Na_2O	0.028	0	0.027	0.015	0.034	0.181	0.038	0.03	0.03	0.041	0.023	0.025	0.011	0
Total	100.193	99.888	100.768	100.468	99.875	80.941	100.063	99.434	99.82	100.01	99.574	99.281	100.054	99.664
Cations based on 12 oxygens														
Si	2.956	2.956	2.959	2.962	2.95	2.967	2.967	2.965	2.963	2.94	2.966	2.962	2.966	2.966
Ti	0	0.001	0	0	0.004	0.032	0.003	0.002	0.002	0.003	0.003	0.002	0.004	0.002
Al	2.022	2.008	2.009	2.017	2.003	1.591	2.002	1.992	1.997	2.002	2.002	2.013	2.005	2.009
Mg	0.506	0.51	0.494	0.499	0.413	0.603	0.408	0.416	0.412	0.412	0.427	0.426	0.417	0.424
Ca	0.112	0.113	0.112	0.109	0.176	0.186	0.179	0.201	0.203	0.212	0.169	0.17	0.153	0.153
Mn	0.142	0.131	0.14	0.141	0.101	0.118	0.105	0.1	0.11	0.113	0.119	0.116	0.131	0.13
Fe	2.293	2.32	2.32	2.3	2.396	2.69	2.362	2.359	2.347	2.371	2.344	2.338	2.353	2.343
Na	0.004	0	0.004	0.002	0.005	0.036	0.006	0.005	0.005	0.006	0.004	0.004	0.002	0
Total	8.035	8.039	8.038	8.03	8.048	8.223	8.032	8.04	8.039	8.059	8.034	8.031	8.031	8.027

Appendix IC (cont.):
Microprobe Analysis of 478 Garnet (cont.)

Oxide Wt. %	T478Gt4Line1B	T478Gt4Line1B	T478Gt4Line1B	T478Gt4Line1B	T478Gt4Line1B	T478Gt4Line1B	T478Gt4Line1B	T478Gt4Line1B	T478Gt4Line1B	T478Gt4Line1B	T478Gt4Line1B	T478Gt4Line1B	T478Gt4Line1B	T478Gt4Line1B
SiO_2	36.768	39.568	35.909	36.129	36.298	36.401	36.537	36.723	36.914	36.311	36.27	36.403	36.373	36.772
TiO_2	0.038	0.004	0	0.016	0.015	0	0.041	0.011	0.027	0.032	0	0.003	0.001	0.013
Al_2O_3	21.261	17.385	20.754	21.153	21.02	20.929	21.267	21.071	20.988	21.232	21.111	20.966	21.058	21.026
MgO	3.547	1.715	2.759	3.61	3.589	3.655	3.673	3.685	3.627	3.675	3.721	3.753	3.803	3.836
CaO	1.644	1.429	1.365	1.318	1.222	1.273	1.36	1.283	1.28	1.255	1.323	1.28	1.276	1.314
MnO	2.009	1.909	2.312	2.275	2.565	2.441	2.486	2.552	2.541	2.628	2.686	2.545	2.447	2.541
FeO	35.085	30.683	34.997	34.452	34.583	34.929	34.895	34.395	34.292	34.796	34.548	34.495	34.468	34.386
Na_2O	0.039	0.149	0.011	0.009	0.02	0.026	0.014	0.035	0.004	0.018	0.004	0.006	0.038	0.009
Total	100.391	92.842	98.107	98.962	99.312	99.654	100.273	99.755	99.673	99.947	99.663	99.451	99.464	99.897
Cations based on 12 oxygens														
Si	2.955	3.358	2.965	2.945	2.952	2.953	2.943	2.967	2.981	2.937	2.941	2.955	2.95	2.966
Ti	0.002	0	0	0.001	0.001	0	0.002	0.001	0.002	0.002	0	0	0	0.001
Al	2.014	1.739	2.02	2.032	2.015	2.001	2.019	2.006	1.998	2.024	2.017	2.006	2.013	1.999
Mg	0.425	0.217	0.34	0.439	0.435	0.442	0.441	0.444	0.437	0.443	0.45	0.454	0.46	0.461
Ca	0.142	0.13	0.121	0.115	0.107	0.111	0.117	0.111	0.111	0.109	0.115	0.111	0.111	0.114
Mn	0.137	0.137	0.162	0.157	0.177	0.168	0.17	0.175	0.174	0.18	0.184	0.175	0.168	0.174
Fe	2.358	2.178	2.417	2.349	2.352	2.37	2.351	2.324	2.316	2.354	2.343	2.341	2.338	2.319
Na	0.006	0.024	0.002	0.001	0.003	0.004	0.002	0.005	0.001	0.003	0.001	0.001	0.006	0.001
Total	8.039	7.783	8.027	8.039	8.042	8.049	8.045	8.033	8.02	8.052	8.051	8.043	8.046	8.035

Oxide Wt. %	T478Gt4Line1B	T478Gt4Line1B	T478Gt4Line1B	T478Gt4Line1B	T478Gt4Line1B	T478Gt4Line1B	T478Gt4Line1B	T478Gt4Line1B	T478Gt4Line1B	T478Gt4Line1B	T478Gt4Line1B	T478Gt4Line1B	T478Gt4Line1B	T478Gt4Line1B
SiO_2	36.609	31.376	36.258	36.463	35.969	37.046	38.929	36.968	35.598	33.843	36.708	36.818	37.098	52.082
TiO_2	0.018	0.001	0.008	0.029	0.014	0.026	0.034	0.023	0.008	0	0	0.017	0	0.037
Al_2O_3	20.94	16.934	20.973	21.054	20.091	20.94	18.742	20.966	20.138	18.008	21.217	21.27	21.394	16.05
MgO	3.766	4.606	3.906	3.855	3.961	3.913	1.687	4.058	4.555	2.66	4.064	4.178	4.124	3.036
CaO	1.222	1.184	1.269	1.317	1.3	1.293	1.284	1.328	1.3	1.327	1.386	1.385	1.369	1.067
MnO	2.56	2.334	2.562	2.519	2.377	2.45	2.102	2.337	2.236	2.183	2.224	2.158	2.135	1.492
FeO	34.555	33.947	34.436	34.233	33.424	34.018	31.367	33.99	33.956	33.978	33.983	34.008	34.209	24.781
Na_2O	0.037	0.031	0.01	0.02	0.055	0.034	0.041	0	0.015	0.041	0.054	0.014	0.001	0.205
Total	99.707	90.413	99.422	99.49	97.191	99.72	94.186	99.67	97.806	92.04	99.636	99.848	100.33	98.75
Cations based on 12 oxygens														
Si	2.963	2.869	2.945	2.954	2.981	2.985	3.267	2.979	2.94	3.004	2.96	2.96	2.967	3.895
Ti	0.001	0	0	0.002	0.001	0.002	0.002	0.001	0.001	0	0	0.001	0	0.002
Al	1.997	1.825	2.007	2.01	1.962	1.989	1.854	1.991	1.96	1.884	2.016	2.015	2.016	1.415
Mg	0.454	0.628	0.473	0.466	0.489	0.47	0.211	0.487	0.561	0.352	0.489	0.501	0.492	0.338
Ca	0.106	0.116	0.11	0.114	0.115	0.112	0.115	0.115	0.115	0.126	0.12	0.119	0.117	0.085
Mn	0.175	0.181	0.176	0.173	0.167	0.167	0.149	0.16	0.156	0.164	0.152	0.147	0.145	0.095
Fe	2.339	2.596	2.339	2.319	2.317	2.292	2.202	2.291	2.345	2.522	2.292	2.287	2.288	1.55
Na	0.006	0.006	0.002	0.003	0.009	0.005	0.007	0	0.002	0.007	0.008	0.002	0	0.03
Total	8.041	8.221	8.052	8.041	8.041	8.022	7.807	8.024	8.08	8.059	8.037	8.032	8.025	7.41

Oxide Wt. %	T478Gt4Line1B	T478Gt4Line1B	T478Gt4Line1B	T478Gt4Line1B	T478Gt4Line1B	T478Gt4Line1B	T478Gt4Line1B	T478Gt4Line1B	T478Gt4Line1B	T478Gt4Line1B	T478Gt4Line1B	T478Gt4Line1B	T478Gt4Line2B	T478Gt4Line2B
SiO_2	40.814	36.617	36.711	36.548	36.678	36.884	36.897	37.244	37.146	36.745	36.944	36.57	35.535	37.015
TiO_2	0.039	0	0.019	0.01	0	0.037	0	0.003	0.035	0.004	0	0	0.04	0.003
Al_2O_3	21.619	21.058	21.016	21.138	21.112	21.291	21.087	21.135	21.292	21.011	18.468	21.229	13.985	21.469
MgO	4.374	4.402	4.281	4.295	4.423	4.446	4.406	4.457	4.353	4.52	3.545	4.484	3.223	4.606
CaO	1.243	1.395	1.355	1.343	1.313	1.369	1.334	1.346	1.386	1.319	1.514	1.397	1.111	1.424
MnO	1.916	2.025	1.974	2.003	2.027	1.957	1.89	1.822	1.892	1.996	1.543	1.827	1.487	1.724
FeO	32.734	34.275	34.292	33.988	34.004	34.029	33.896	33.882	34.322	33.727	30.69	33.83	28.986	34.04
Na_2O	0.093	0.026	0.026	0	0.004	0.008	0.013	0	0.041	0.017	0.102	0	0.123	0.027
Total	102.832	99.798	99.674	99.325	99.561	100.021	99.523	99.889	100.467	99.339	92.806	99.337	84.49	100.308
Cations based on 12 oxygens														
Si	3.123	2.951	2.96	2.955	2.957	2.957	2.971	2.983	2.966	2.965	3.155	2.951	3.345	2.955
Ti	0.002	0	0.001	0.001	0	0.002	0	0	0.002	0	0	0	0.003	0
Al	1.949	2	1.997	2.014	2.006	2.012	2.001	1.995	2.003	1.998	1.859	2.019	1.552	2.02
Mg	0.499	0.529	0.515	0.518	0.532	0.531	0.529	0.532	0.518	0.544	0.451	0.539	0.452	0.548
Ca	0.102	0.12	0.117	0.116	0.113	0.118	0.115	0.115	0.119	0.114	0.139	0.121	0.112	0.122
Mn	0.124	0.138	0.135	0.137	0.138	0.133	0.129	0.124	0.128	0.136	0.112	0.125	0.119	0.117
Fe	2.094	2.31	2.313	2.298	2.293	2.282	2.283	2.27	2.292	2.276	2.192	2.283	2.282	2.272
Na	0.014	0.004	0.004	0	0.001	0.001	0.002	0	0.006	0.003	0.017	0	0.023	0.004
Total	7.907	8.052	8.042	8.039	8.04	8.036	8.03	8.019	8.034	8.036	7.925	8.038	7.888	8.038

Appendix IC (cont.):
Microprobe Analysis of 478 Garnet (cont.)

Oxide Wt. %	T478Gt4Line2B	T478Gt4Line2B	T478Gt4Line2B	T478Gt4Line2B	T478Gt4Line2B	T478Gt4Line2B	T478Gt4Line2B	T478Gt4Line2B	T478Gt4Line2B	T478Gt4Line2B	T478Gt4Line2B	T478Gt4Line2B	T478Gt4Line2B	T478Gt4Line2B
SiO_2	37.18	36.625	36.681	37.122	36.641	39.603	36.903	36.885	36.496	37.045	34.84	36.881	41.169	36.862
TiO_2	0	0	0.006	0	0	0	0	0.034	0.022	0.014	0.02	0.017	0.029	0.008
Al_2O_3	21.256	20.744	21.068	21.498	21	20.08	21.024	21.12	20.833	21.189	17.737	21.206	18.708	20.983
MgO	4.61	4.99	4.688	4.787	4.786	4.583	4.63	4.672	3.9	4.548	5.078	4.392	3.501	4.331
CaO	1.432	1.387	1.444	1.46	1.469	1.505	1.703	1.708	1.704	1.877	1.73	1.893	1.684	1.804
MnO	1.668	1.73	1.65	1.553	1.661	1.382	1.631	1.597	1.629	1.524	1.568	1.677	1.474	1.722
FeO	33.939	33.325	33.639	33.868	33.537	31.831	33.599	33.446	34.156	33.605	31.665	33.918	29.455	34.614
Na_2O	0	0.035	0.02	0.009	0	0.051	0.013	0	0.033	0.027	0.048	0.017	0.177	0.032
Total	100.085	98.836	99.196	100.297	99.094	99.035	99.503	99.462	98.773	99.829	92.686	100.001	96.197	100.356
Cations based on 12 oxygens														
Si	2.972	2.965	2.96	2.958	2.96	3.147	2.968	2.965	2.97	2.968	3.022	2.957	3.326	2.956
Ti	0	0	0	0	0	0	0	0.002	0.001	0.001	0.001	0.001	0.002	0
Al	2.002	1.979	2.004	2.019	1.999	1.881	1.993	2.001	1.998	2.001	1.813	2.004	1.781	1.983
Mg	0.549	0.602	0.564	0.569	0.576	0.543	0.555	0.56	0.473	0.543	0.657	0.525	0.422	0.518
Ca	0.123	0.12	0.125	0.125	0.127	0.128	0.147	0.147	0.149	0.161	0.161	0.163	0.146	0.155
Mn	0.113	0.119	0.113	0.105	0.114	0.093	0.111	0.109	0.112	0.103	0.115	0.114	0.101	0.117
Fe	2.269	2.256	2.27	2.257	2.265	2.116	2.26	2.248	2.324	2.252	2.297	2.274	1.99	2.321
Na	0	0.005	0.003	0.001	0	0.008	0.002	0	0.005	0.004	0.008	0.003	0.028	0.005
Total	8.028	8.046	8.039	8.034	8.041	7.916	8.036	8.032	8.032	8.033	8.074	8.041	7.796	8.055

Oxide Wt. %	T478Gt4Line2B	T478Gt4Line2B	T478Gt4Line2B	T478Gt4Line2B	T478Gt4Line2B	T478Gt4Line2B	T478Gt4Line2B	T478Gt4Line2B	T478Gt4Line2B	T478Gt4Line2B	T478Gt4Line2B	T478Gt4Line2B	T478Gt4Line2B	T478Gt4Line2B
SiO_2	31.085	39.02	36.814	28.981	35.233	34.087	98.859	98.277	36.368	36.861	31.371	36.776	36.783	36.568
TiO_2	0.035	0.003	0.031	0.02	0.974	0.026	0.013	0.083	0.003	0	0	0.022	0.028	0.01
Al_2O_3	13.854	21.923	21.02	7.044	22.208	19.574	0.064	0.003	20.761	21.012	17.227	20.989	20.916	20.769
MgO	4.181	1.179	4.087	1.25	8.572	2.644	0.002	0.012	3.455	3.639	4.022	3.739	3.844	3.786
CaO	1.521	1.608	1.473	0.889	0.455	1.594	0.049	0.01	1.425	1.525	1.389	1.386	1.388	1.436
MnO	1.611	1.534	1.868	0.563	0.148	1.77	0.036	0.018	1.769	1.76	1.724	1.69	1.758	1.813
FeO	30.744	33.585	34.823	10.763	15.492	34.231	0.495	0.373	35.239	34.874	35.141	35.399	35.039	34.868
Na_2O	0.072	0	0.013	0.098	0.294	0.003	0.002	0	0.026	0.001	0.018	0.02	0	0
Total	83.103	98.852	100.129	49.608	83.376	93.929	99.52	98.776	99.046	99.672	90.892	100.021	99.756	99.25
Cations based on 12 oxygens														
Si	3.065	3.129	2.96	4.198	3.068	2.951	5.981	5.985	2.966	2.977	2.862	2.966	2.97	2.97
Ti	0.003	0	0.002	0.002	0.064	0.002	0.001	0.004	0	0	0	0.001	0.002	0.001
Al	1.61	2.072	1.992	1.203	2.279	1.997	0.005	0	1.996	2	1.852	1.995	1.991	1.988
Mg	0.614	0.141	0.49	0.27	1.113	0.341	0	0.001	0.42	0.438	0.547	0.449	0.463	0.458
Ca	0.161	0.138	0.127	0.138	0.042	0.148	0.003	0.001	0.125	0.132	0.136	0.12	0.12	0.125
Mn	0.135	0.104	0.127	0.069	0.011	0.13	0.002	0.001	0.122	0.12	0.133	0.115	0.12	0.125
Fe	2.535	2.252	2.342	1.304	1.128	2.479	0.025	0.019	2.404	2.355	2.681	2.387	2.366	2.368
Na	0.014	0	0.002	0.028	0.05	0	0	0	0.004	0	0.003	0.003	0	0
Total	8.137	7.836	8.042	7.212	7.755	8.048	6.017	6.011	8.037	8.022	8.214	8.036	8.032	8.035

Oxide Wt. %	T478Gt4Line2B	T478Gt4Line2B	T478Gt4Line2B	T478Gt4Line2B	T478Gt4Line2B	T478Gt4Line2B	T478Gt4Line2B	T478Gt4Line2B	T478Gt4Line2B	T478Gt4Line2B	T478Gt4Line2B	T478Gt4Line2B	T478Gt4Line2B	T478Gt4Line2B
SiO_2	36.898	15.103	34.961	22.161	36.433	37.22	36.558	32.216	36.966	36.665	46.867	37.027	36.909	44.02
TiO_2	0	0.026	0.027	0	0	0.009	0	0.033	0.007	0.015	0.75	1.595	1.602	0
Al_2O_3	21.243	3.121	18.059	10.195	21.047	21.286	18.982	19.114	21.672	20.535	34.931	19.288	19.042	14.681
MgO	3.879	4.899	2.729	5.096	3.882	4.038	0.788	3.263	3.937	4.376	0.694	12.209	12.209	3.578
CaO	1.409	0.881	1.43	1.343	1.505	1.464	1.492	0.986	1.408	1.235	0.017	0	0.026	1.092
MnO	1.829	1.439	1.524	1.595	1.836	1.83	1.648	1.551	1.822	1.893	0.079	0	0.052	1.569
FeO	35.061	30.042	32.336	32.814	34.603	34.552	32.726	31.041	34.681	34.027	1.574	16.192	15.989	28.261
Na_2O	0.005	0.079	0.056	0.061	0.012	0.004	0.004	1.024	0	0.044	1.478	0.425	0.456	0.14
Total	100.324	55.59	91.122	73.265	99.318	100.403	92.198	89.228	100.493	98.79	86.39	86.736	86.285	93.341
Cations based on 12 oxygens														
Si	2.961	2.573	3.088	2.653	2.954	2.975	3.174	2.919	2.954	2.981	3.504	3.114	3.12	3.628
Ti	0	0.003	0.002	0	0	0.001	0	0.002	0	0.001	0.042	0.101	0.102	0
Al	2.009	0.627	1.88	1.439	2.012	2.005	1.942	2.041	2.041	1.968	3.078	1.912	1.897	1.426
Mg	0.464	1.244	0.359	0.91	0.469	0.481	0.102	0.441	0.469	0.53	0.077	1.531	1.538	0.44
Ca	0.121	0.161	0.135	0.172	0.131	0.125	0.139	0.096	0.121	0.108	0.001	0	0.002	0.096
Mn	0.124	0.208	0.114	0.162	0.126	0.124	0.121	0.119	0.123	0.13	0.005	0	0.004	0.11
Fe	2.353	4.281	2.388	3.285	2.347	2.31	2.376	2.352	2.317	2.313	0.098	1.139	1.13	1.948
Na	0.001	0.026	0.01	0.014	0.002	0.001	0.001	0.18	0	0.007	0.214	0.069	0.075	0.022
Total	8.033	9.123	7.976	8.635	8.041	8.022	7.855	8.15	8.025	8.038	7.019	7.866	7.868	7.67

Appendix IC (cont.):
Microprobe Analysis of 478 Garnet (cont.)

Oxide Wt. %	T478Gt4Line2B	T478Gt4Line2B	T478Gt4Line2B	T478Gt4Line2B	T478Gt4Line2B	T478Gt4Line2B	T478Gt4Line3B	T478Gt4Line3B	T478Gt4Line3B	T478Gt4Line3B	T478Gt4Line3B	T478Gt4Line3B	T478Gt4Line3B	T478Gt4Line3B
SiO_2	39.661	41.386	36.397	36.515	28.108	36.179	36.491	36.667	37.517	35	34.566	40.459	36.574	35.272
TiO_2	0	0.029	0.044	0.011	0.057	0.007	0.074	0.028	0.003	0.028	0.037	0.008	0	0.013
Al_2O_3	22.039	23.083	20.791	21.177	24.55	21.165	20.672	18.221	21.43	19.107	17.209	19.368	21.072	18.86
MgO	3.722	3.093	3.527	3.411	11.179	3.257	2.755	3.207	3.388	3.315	3.481	3.511	3.372	3.197
CaO	1.42	1.313	1.385	1.273	0.046	1.426	1.46	1.473	1.291	1.23	1.132	1.195	1.321	1.282
MnO	1.859	2.077	1.872	1.761	0.09	1.793	1.532	1.622	1.829	1.797	1.657	1.644	1.923	1.722
FeO	33.849	33.852	35.184	35.487	27.674	35.994	32.013	31.166	35.478	34.926	34.444	32.927	35.7	35.177
Na_2O	0.062	0.012	0.014	0	0.034	0.023	0.087	0.139	0.027	0.036	0.045	0.052	0.007	0.049
Total	102.612	104.845	99.214	99.635	91.738	99.844	95.084	92.523	100.963	95.439	92.571	99.164	99.969	95.572
Cations based on 12 oxygens														
Si	3.065	3.109	2.964	2.959	2.415	2.937	3.052	3.154	2.989	2.982	3.044	3.222	2.959	3.003
Ti	0	0.002	0.003	0.001	0.004	0	0.005	0.002	0	0.002	0.002	0	0	0.001
Al	2.007	2.044	1.995	2.022	2.486	2.025	2.038	1.847	2.012	1.919	1.786	1.818	2.009	1.892
Mg	0.429	0.346	0.428	0.412	1.432	0.394	0.344	0.411	0.402	0.421	0.457	0.417	0.407	0.406
Ca	0.118	0.106	0.121	0.111	0.004	0.124	0.131	0.136	0.11	0.112	0.107	0.102	0.114	0.117
Mn	0.122	0.132	0.129	0.121	0.007	0.123	0.109	0.118	0.123	0.13	0.124	0.111	0.132	0.124
Fe	2.187	2.127	2.396	2.405	1.988	2.444	2.239	2.242	2.364	2.489	2.537	2.193	2.415	2.504
Na	0.009	0.002	0.002	0	0.006	0.004	0.014	0.023	0.004	0.006	0.008	0.008	0.001	0.008
Total	7.937	7.868	8.038	8.031	8.342	8.051	7.932	7.933	8.004	8.061	8.065	7.871	8.037	8.055

Oxide Wt. %	T478Gt4Line3B	T478Gt4Line3B	T478Gt4Line3B	T478Gt4Line3B	T478Gt4Line3B	T478Gt4Line3B	T478Gt4Line3B	T478Gt4Line3B	T478Gt4Line3B	T478Gt4Line3B	T478Gt4Line3B	T478Gt4Line3B	T478Gt4Line3B	T478Gt4Line3B
SiO_2	36.837	37.052	36.923	37.963	47.423	36.687	36.93	51.05	18.692	36.486	36.488	36.518	36.635	36.669
TiO_2	0.013	0.005	0.004	0	0.008	0.002	0	0.058	0.001	0	0.024	0	0.009	0
Al_2O_3	21.204	21.279	21.254	21.593	20.616	21.182	21.071	18.353	11.607	20.853	21.078	21.036	20.938	21.075
MgO	3.325	3.263	3.228	3.16	1.558	2.955	2.822	2.142	0.192	3.144	3.376	3.355	3.429	3.399
CaO	1.312	1.336	1.383	1.529	1.56	2.001	2.008	1.511	1.088	1.434	1.442	1.654	1.746	2.058
MnO	1.67	1.611	1.537	1.676	1.359	1.527	1.643	1.198	0.841	1.41	1.417	1.524	1.502	1.448
FeO	35.757	35.747	35.563	36.228	30.481	35.453	35.776	25.207	39.499	36.287	35.726	35.353	34.876	35.065
Na_2O	0.015	0.014	0.031	0.036	0.095	0.025	0.01	0.154	0.026	0.01	0.053	0.018	0.005	0.022
Total	100.133	100.307	99.923	102.185	103.1	99.832	100.26	99.673	71.946	99.624	99.604	99.458	99.14	99.736
Cations based on 12 oxygens														
Si	2.969	2.978	2.978	2.993	3.512	2.968	2.978	3.789	2.409	2.966	2.959	2.964	2.976	2.964
Ti	0.001	0	0	0	0	0	0	0.003	0	0	0.001	0	0.001	0
Al	2.014	2.016	2.02	2.006	1.799	2.019	2.003	1.605	1.763	1.998	2.014	2.012	2.005	2.008
Mg	0.4	0.391	0.388	0.371	0.172	0.356	0.339	0.237	0.037	0.381	0.408	0.406	0.415	0.41
Ca	0.113	0.115	0.119	0.129	0.124	0.173	0.174	0.12	0.15	0.125	0.125	0.144	0.152	0.178
Mn	0.114	0.11	0.105	0.112	0.085	0.105	0.112	0.075	0.092	0.097	0.097	0.105	0.103	0.099
Fe	2.41	2.403	2.399	2.389	1.888	2.398	2.413	1.565	4.257	2.467	2.423	2.399	2.369	2.371
Na	0.002	0.002	0.005	0.005	0.014	0.004	0.001	0.022	0.006	0.002	0.008	0.003	0.001	0.003
Total	8.023	8.015	8.014	8.005	7.594	8.023	8.02	7.416	8.714	8.036	8.035	8.033	8.022	8.033

Oxide Wt. %	T478Gt4Line3B	T478Gt4Line3B	T478Gt4Line3B	T478Gt4Line3B	T478Gt4Line3B	T478Gt4Line3B	T478Gt4Line3B	T478Gt4Line3B	T478Gt5Frg2
SiO_2	37.06	30.108	31.653	41.55	29.273	6.514	37.718	37.586	36.638
TiO_2	0	0.003	0.012	0.047	0.054	42.051	0	0	0
Al_2O_3	21.28	15.913	16.473	20.166	15.299	3.825	20.958	19.702	20.897
MgO	3.425	4.411	3.019	3.196	2.04	1.223	2.649	3.123	3.648
CaO	2.06	1.723	2.041	1.855	1.987	0.428	2.22	2.091	1.234
MnO	1.553	1.533	1.552	1.394	1.342	0.588	1.722	1.6	2.124
FeO	34.839	33.541	33.015	31.532	33.121	44.295	34.319	32.931	35.128
Na_2O	0	0.008	0.026	0.033	0.035	0.015	0.018	0.069	0.042
Total	100.217	87.24	87.791	99.773	83.151	98.939	99.604	97.102	99.711
Cations based on 12 oxygens	2.975	2.864	2.966	3.255	2.934	0.636	3.038	3.092	2.967
Si	0	0	0.001	0.003	0.004	3.088	0	0	0
Ti	2.013	1.784	1.819	1.862	1.807	0.44	1.989	1.91	1.994
Al	0.41	0.626	0.422	0.373	0.305	0.178	0.318	0.383	0.44
Mg	0.177	0.176	0.205	0.156	0.213	0.045	0.192	0.184	0.107
Ca	0.106	0.124	0.123	0.092	0.114	0.049	0.118	0.112	0.146
Mn	2.339	2.669	2.587	2.066	2.777	3.618	2.312	2.266	2.379
Fe	0	0.002	0.005	0.005	0.007	0.003	0.003	0.011	0.007
Na	8.02	8.245	8.128	7.812	8.161	8.057	7.97	7.958	8.04
Total									

Appendix IC (cont.):
Microprobe Analysis of 478 Feldspar

Oxide Wt. %	T478FeldIn1	T478FeldIn2	T478FeldOut1	T478FeldOut2	T478FeldOut3	T478FeldOut4	T478Feld2.1	T478Gt4feldtch1	T478Gt4feldtch2	T478Gt4feldtch3	T478Gt5feldM1	T478Gt5feldM2	T478Gt5FeldM5	T478Gt5FeldM6
SiO2	60.904	60.279	60.342	60.526	61.468	60.591	58.913	45.389	44.662	45.226	61.167	60.926	45.253	44.15
Al2O3	24.216	23.112	24.157	24.153	24.197	24.229	24.315	34.729	34.275	32.155	23.746	23.571	34.424	32.294
CaO	5.377	5.207	5.722	5.601	5.716	5.805	6.711	0.021	0.039	0.049	5.481	5.329	0.051	0.029
FeO	0.507	0.482	0.23	0.385	0.435	0.418	0.321	1.723	1.761	1.732	0.07	0.059	1.028	3.824
Na2O	8.694	9.333	8.663	8.646	8.424	8.428	7.747	1.141	1.138	1.219	8.715	8.658	1.207	1.069
K2O	0.074	0.083	0.094	0.074	0.071	0.101	0.036	9.839	9.549	9.123	0.085	0.118	9.729	9.746
Total	99.772	98.496	99.208	99.385	100.311	99.572	98.043	92.842	91.424	89.504	99.264	98.661	91.692	91.112
Cations based on 8 oxygens														
Si	2.718	2.732	2.709	2.713	2.726	2.711	2.681	2.255	2.252	2.322	2.738	2.742	2.268	2.266
Al	1.274	1.235	1.278	1.276	1.265	1.277	1.304	2.034	2.037	1.946	1.253	1.25	2.033	1.953
Ca	0.257	0.253	0.275	0.269	0.272	0.278	0.327	0.001	0.002	0.003	0.263	0.257	0.003	0.002
Fe	0.019	0.018	0.009	0.014	0.016	0.016	0.012	0.072	0.074	0.074	0.003	0.002	0.043	0.164
Na	0.752	0.82	0.754	0.751	0.724	0.731	0.684	0.11	0.111	0.121	0.756	0.756	0.117	0.106
K	0.004	0.005	0.005	0.004	0.004	0.006	0.002	0.624	0.614	0.598	0.005	0.007	0.622	0.638
Total	5.024	5.063	5.03	5.027	5.007	5.019	5.01	5.096	5.09	5.064	5.018	5.014	5.086	5.129

Oxide Wt. %	T478Gt4Feldtch4	T478Gt4Feldtch5
SiO2	64.336	63.797
Al2O3	20.689	20.672
CaO	2.175	2.149
FeO	0.715	0.646
Na2O	10.455	10.446
K2O	0.071	0.099
Total	98.441	97.809
Cations based on 8 oxygens		
Si	2.886	2.881
Al	1.094	1.1
Ca	0.105	0.104
Fe	0.027	0.024
Na	0.909	0.914
K	0.004	0.006
Total	5.025	5.029

Appendix IC (cont.):
Microprobe Analysis of 478 Biotite

Oxide Wt. %	T478MicaIn1	T478BiIn2	T478BiOut1	T478BiOut2	T478BiOut3	T478mica2.1in	T478mica2.2in	T478Gt4micain1	T478Gt4micain2	T478Gt4micain3	T478Gt4micaout1	T478Gt4micaout2	T478Gt4micaout3	T478Gt4micaout4
SiO2	35.485	36.266	35.416	35.745	35.249	36.404	25.978	34.423	35.202	35.568	35.452	35.507	35.769	34.398
TiO2	1.613	1.387	1.194	1.774	1.618	1.372	0.11	1.686	1.596	1.661	1.471	1.542	1.592	1.501
Al2O3	18.34	16.778	18.559	18.497	17.713	20.756	22.23	17.882	18.042	18.447	18.39	18.701	18.456	17.948
MgO	10.135	9.722	10.06	9.77	9.963	13.065	16.114	8.065	8.92	9.159	10.115	9.995	9.997	9.677
CaO	0	0.132	0.051	0.03	0.086	0.567	0.018	0.034	0.005	0.029	0.074	0.005	0.009	0.009
MnO	0.016	0.039	0.06	0.104	0.033	0.054	0.114	0.027	0.075	0.092	0.075	0.012	0.048	0.019
FeO	19.742	20.424	19.615	19.703	20.011	13.843	22.352	22.459	21.548	20.55	19.101	19.191	19.228	19.074
Na2O	0.174	0.189	0.208	0.199	0.18	0.362	0.061	0.189	0.218	0.25	0.176	0.187	0.182	0.155
K2O	9.531	7.885	9.492	9.818	9.335	5.463	0.523	9.405	9.446	9.306	9.526	9.735	9.499	9.414
H2O	3.917	3.85	3.903	3.938	3.873	4.01	3.67	3.817	3.879	3.908	3.9	3.918	3.921	3.798
Total	98.953	96.672	98.558	99.578	98.061	95.896	91.17	97.987	98.931	98.97	98.28	98.793	98.701	95.993
Cation based on 22 oxygens														
Si	5.433	5.649	5.441	5.443	5.458	5.444	4.245	5.408	5.441	5.458	5.451	5.434	5.471	5.431
Ti	0.186	0.162	0.138	0.203	0.188	0.154	0.013	0.199	0.186	0.192	0.17	0.177	0.183	0.178
Al	3.309	3.08	3.36	3.32	3.232	3.658	4.281	3.311	3.287	3.336	3.333	3.373	3.327	3.34
Mg	2.313	2.258	2.304	2.218	2.3	2.913	3.925	1.889	2.056	2.095	2.319	2.28	2.28	2.278
Ca	0	0.022	0.008	0.005	0.014	0.091	0.003	0.006	0.001	0.005	0.012	0.001	0.001	0.002
Mn	0.002	0.005	0.008	0.013	0.004	0.007	0.016	0.004	0.01	0.012	0.01	0.001	0.006	0.003
Fe	2.528	2.66	2.52	2.509	2.591	1.731	3.054	2.951	2.786	2.637	2.456	2.456	2.46	2.519
Na	0.052	0.057	0.062	0.059	0.054	0.105	0.019	0.058	0.065	0.074	0.052	0.055	0.054	0.048
K	1.862	1.567	1.86	1.907	1.844	1.042	0.109	1.885	1.863	1.822	1.869	1.901	1.854	1.896
H	0	0	0	0	0	0	0	0	0	0	0	0	0	0
Total	15.685	15.46	15.701	15.677	15.685	15.145	15.665	15.711	15.695	15.631	15.672	15.678	15.636	15.695

Oxide Wt. %	T478Gt4micaM1	T478Gt4micaM2	T478Gt4muscM1	T478Gt4muscM2	T478Gt5BiM8	T478Gt5BiM9	T478Gt5MuscM4	T478Gt5MuscM5	T478Gt5Chl4	T478Gt5Chl3	T478Gt5Chl2	T478Gt5BiM1	T478Gt5BiM2	T478Gt5BiIn5
SiO2	35.39	35.169	45.133	45.352	35.415	35.556	45.33	45.506	26.102	25.31	25.043	35.579	35.955	35.839
TiO2	1.741	1.664	0.542	0.646	1.688	1.607	0.647	0.535	0.175	0.087	0.055	1.156	1.647	1.659
Al2O3	18.12	18.171	35.105	34.642	18.112	18.21	35.056	35.12	21.29	20.863	21.805	18.372	18.12	18.065
MgO	9.919	10.007	0.722	0.788	10.025	10.07	0.831	0.86	13.998	14.212	14.868	10.054	9.73	9.552
CaO	0.03	0.023	0.014	0.014	0.045	0.034	0.026	0.045	0.053	0.054	0.022	0.05	0.038	0.072
MnO	0.075	0.05	0	0	0.062	0.09	0.038	0.028	0.073	0.132	0.17	0	0.077	0.013
FeO	19.651	19.613	1.237	1.202	19.486	20.003	1.156	1.251	24.972	24.665	25.382	19.657	19.371	19.429
Na2O	0.211	0.156	1.241	1.208	0.195	0.183	1.142	1.213	0.044	0.055	0.033	0.188	0.205	0.234
K2O	9.491	9.667	9.725	9.906	9.372	9.664	9.866	9.832	0.588	0.313	0.15	9.411	9.462	9.198
H2O	3.898	3.889	4.434	4.432	3.895	3.923	4.45	4.464	3.609	3.54	3.609	3.899	3.911	3.892
Total	98.526	98.409	98.153	98.19	98.295	99.34	98.542	98.854	90.904	89.231	91.137	98.366	98.516	97.953
Cation based on 22 oxygens														
Si	5.444	5.423	6.104	6.136	5.452	5.435	6.108	6.114	4.337	4.288	4.161	5.472	5.514	5.522
Ti	0.201	0.193	0.055	0.066	0.195	0.185	0.066	0.054	0.022	0.011	0.007	0.134	0.19	0.192
Al	3.285	3.302	5.595	5.524	3.286	3.281	5.567	5.561	4.169	4.165	4.27	3.33	3.275	3.281
Mg	2.275	2.3	0.146	0.159	2.301	2.295	0.167	0.172	3.468	3.589	3.683	2.305	2.224	2.194
Ca	0.005	0.004	0.002	0.002	0.008	0.006	0.004	0.007	0.009	0.01	0.004	0.008	0.006	0.012
Mn	0.01	0.007	0	0	0.008	0.012	0.004	0.003	0.01	0.019	0.024	0	0.01	0.002
Fe	2.528	2.529	0.14	0.136	2.509	2.557	0.13	0.141	3.47	3.494	3.527	2.528	2.484	2.504
Na	0.063	0.047	0.325	0.317	0.058	0.054	0.298	0.316	0.014	0.018	0.011	0.056	0.061	0.07
K	1.863	1.902	1.678	1.71	1.841	1.885	1.696	1.685	0.125	0.068	0.032	1.846	1.851	1.808
H	0	0	0	0	0	0	0	0	0	0	0	0	0	0
Total	15.674	15.707	14.045	14.05	15.658	15.71	14.04	14.053	15.624	15.662	15.719	15.679	15.615	15.585

Appendix IC (cont.):
Microprobe Analysis of 478 Biotite (cont.)

Oxide Wt. %	T478Gt5Biln6	T478Gt5Biln7	T478Gt4Bith5	T478Gt4Bith6	T478Gt4Bith7	T478Gt4Bith8	T478Gt4Bith9
SiO2	35.556	34.998	33.001	34.992	33.001	31.217	35.466
TiO2	1.577	1.436	0.859	1.536	1.706	1.389	1.404
Al2O3	18.678	19.342	19.381	18.069	17.689	17.562	18.692
MgO	9.811	9.462	8.371	9.638	9.317	8.528	10.047
CaO	0.053	0.104	0.184	0.085	0.009	0.094	0.033
MnO	0.077	0.066	0.033	0.058	0.033	0.035	0.056
FeO	19.374	19.466	22.48	20.431	22.18	24.804	18.741
Na2O	0.214	0.197	0.266	0.151	0.163	0.17	0.188
K2O	9.435	9.148	5.276	9.217	8.701	7.504	9.556
H2O	3.916	3.896	3.726	3.867	3.762	3.656	3.901
Total	98.691	98.115	93.577	98.044	96.561	94.959	98.084
Cation based on 22 oxygens							
Si	5.444	5.387	5.312	5.427	5.26	5.121	5.453
Ti	0.182	0.166	0.104	0.179	0.204	0.171	0.162
Al	3.371	3.509	3.676	3.303	3.323	3.396	3.387
Mg	2.239	2.171	2.009	2.228	2.214	2.086	2.303
Ca	0.009	0.017	0.032	0.014	0.001	0.017	0.005
Mn	0.01	0.009	0.004	0.008	0.004	0.005	0.007
Fe	2.481	2.506	3.026	2.65	2.956	3.403	2.409
Na	0.064	0.059	0.083	0.045	0.05	0.054	0.056
K	1.843	1.796	1.083	1.824	1.769	1.57	1.874
H	0	0	0	0	0	0	0
Total	15.643	15.62	15.329	15.678	15.781	15.823	15.656

Appendix ID:
Microprobe Analysis of 1498 Garnet

Oxide Wt.%	Gt9cor	Gt910	Gt11	Gt12	Gt13	Gt14	Gt15	Gt16	Gt18	Gt18	Gt19	Gt20	Gt21	Gt1Line1
SiO_2	35.954	36.002	36.31	36.617	37.128	36.569	36.147	36.872	36.629	36.436	36.177	36.667	36.648	36.236
TiO_2	0.002	0	0	0	0.02	0.013	0	0.001	0.177	0.107	0.435	0.261	0.284	0
Al_2O_3	20.948	20.706	21.058	21.054	21.238	20.955	21.091	21.137	21.031	20.824	20.892	20.791	20.802	21.012
MgO	2.583	2.521	3.571	3.428	3.196	3.315	3.34	3.383	2.842	1.666	1.646	2.491	2.464	3.583
CaO	2.006	2.749	1.993	1.905	2.05	1.941	2.048	2.102	1.917	3.872	4.077	2.471	2.564	1.86
MnO	4.362	4.281	1.145	1.852	1.199	2.139	0.867	1.041	1.197	6.74	6.697	4.417	4.358	1.555
FeO	33.19	32.768	35.397	34.671	35.211	33.669	35.846	33.874	36.493	29.82	29.356	31.736	31.618	34.463
Na_2O	0.046	0.015	0	0	0.027	0.027	0.016	0.02	0.012	0.017	0.043	0.03	0.022	0.022
Total	99.091	99.042	99.474	99.527	100.069	98.628	99.355	98.43	100.298	99.482	99.323	98.864	98.76	98.731
Cation based on 12 oxygens														
Si	2.946	2.952	2.946	2.966	2.985	2.981	2.941	2.997	2.959	2.971	2.953	2.99	2.99	2.956
Ti	0	0	0	0	0.001	0.001	0	0	0.011	0.007	0.027	0.016	0.017	0
Al	2.023	2.001	2.014	2.01	2.012	2.013	2.023	2.025	2.002	2.002	2.01	1.998	2	2.02
Mg	0.316	0.308	0.432	0.414	0.383	0.403	0.405	0.41	0.342	0.203	0.2	0.303	0.3	0.436
Ca	0.176	0.241	0.173	0.165	0.177	0.17	0.179	0.183	0.166	0.338	0.357	0.216	0.224	0.163
Mn	0.303	0.297	0.079	0.127	0.082	0.148	0.06	0.072	0.082	0.466	0.463	0.305	0.301	0.107
Fe	2.275	2.247	2.402	2.348	2.367	2.295	2.439	2.303	2.466	2.034	2.004	2.164	2.157	2.351
Na	0.007	0.002	0	0	0.004	0.004	0.003	0.003	0.002	0.003	0.007	0.005	0.004	0.003
Total	8.046	8.048	8.046	8.03	8.011	8.015	8.05	7.993	8.03	8.024	8.021	7.997	7.993	8.036

Oxide Wt.%	Gt1Line1	Gt1Line1	Gt1Line1	Gt1Line1	Gt1Line1	Gt1Line1	Gt1Line1	Gt1Line1	Gt1Line1	Gt1Line1	Gt1Line1	Gt1Line1	Gt1Line1	Gt1Line1
SiO_2	36.402	36.511	36.183	35.969	36.581	35.045	43.688	36.006	36.385	98.144	39.912	36.074	35.642	36.1
TiO_2	0	0.027	0	0	0.04	0.038	0.012	0.01	0.003	0.012	0	0	0.01	0.025
Al_2O_3	21.16	20.698	20.849	20.848	20.67	20.144	19.03	20.743	20.69	0.011	11.414	20.776	20.675	20.706
MgO	3.441	3.359	3.225	3.154	3.057	3.007	2.148	2.91	2.853	0.003	2.168	2.497	2.518	2.423
CaO	1.979	2.551	2.585	2.397	2.426	2.327	1.971	2.41	2.245	0.021	2.438	2.955	2.981	2.928
MnO	1.806	2.098	2.627	2.911	3.135	3.542	3.789	3.818	3.948	0.05	3.36	4.741	4.879	4.93
FeO	34.272	33.656	33.282	33.922	34.266	34.42	29.212	33.581	33.353	0.5	24.423	32.381	31.986	32.289
Na_2O	0.01	0.01	0.002	0	0.005	0.026	0.075	0.015	0.025	0	0.203	0.012	0.028	0.007
Total	99.07	98.91	98.753	99.201	100.18	98.549	99.925	99.493	99.502	98.741	83.918	99.436	98.719	99.408
Cation based on 12 oxygens														
Si	2.958	2.974	2.957	2.938	2.961	2.909	3.403	2.94	2.965	5.984	3.704	2.947	2.935	2.951
Ti	0	0.002	0	0	0.002	0.002	0.001	0.001	0	0.001	0	0	0.001	0.002
Al	2.027	1.987	2.008	2.007	1.972	1.971	1.747	1.996	1.987	0.001	1.248	2.001	2.007	1.995
Mg	0.417	0.408	0.393	0.384	0.369	0.372	0.249	0.354	0.347	0	0.3	0.304	0.309	0.295
Ca	0.172	0.223	0.226	0.21	0.21	0.207	0.164	0.211	0.196	0.001	0.242	0.259	0.263	0.257
Mn	0.124	0.145	0.182	0.201	0.215	0.249	0.25	0.264	0.272	0.003	0.264	0.328	0.34	0.341
Fe	2.329	2.293	2.274	2.317	2.32	2.39	1.903	2.293	2.273	0.025	1.895	2.213	2.203	2.208
Na	0.002	0.002	0	0	0.001	0.004	0.011	0.002	0.004	0	0.037	0.002	0.004	0.001
Total	8.029	8.034	8.04	8.057	8.05	8.104	7.728	8.061	8.044	6.015	7.69	8.054	8.062	8.05

Oxide Wt.%	Gt1Line1	Gt1Line1	Gt1Line1	Gt1Line1	Gt1Line1	Gt1Line1	Gt1Line1	Gt1Line1	Gt1Line1	Gt1Line1	Gt1Line1	Gt1Line1	Gt1Line1	Gt1Line1
SiO_2	97.71	36.282	35.537	37.838	50.114	36.195	35.948	37.239	35.616	36.474	36.252	36.654	35.97	36.31
TiO_2	0	0	0.009	0.003	0.017	0.023	0	0	0	0.052	0.001	0.034	0.016	0.004
Al_2O_3	0	20.511	20.748	21.146	15.988	20.523	20.461	20.419	20.257	20.752	20.634	20.923	20.29	20.807
MgO	0	2.554	2.476	2.276	1.64	2.416	2.478	2.301	2.215	2.214	2.223	2.232	2.351	2.25
CaO	0.01	2.732	2.607	2.685	2.196	2.753	2.671	2.716	3.695	3.357	3.036	2.881	3.031	2.709
MnO	0.091	5.112	5.021	5.05	3.763	5.238	5.083	5.383	5.634	5.417	5.091	5.187	5.095	5.371
FeO	0.506	32.384	32.767	31.555	24.337	32.48	32.8	32.408	31.081	31.594	32.716	32.32	32.443	32.451
Na_2O	0.012	0.027	0.025	0.011	0.109	0.011	0.003	0	0.007	0.008	0.015	0.007	0.012	0
Total	98.329	99.602	99.19	100.564	98.164	99.639	99.444	100.466	98.505	99.868	99.968	100.238	99.208	99.902
Cation based on 12 oxygens														
Si	5.984	2.962	2.922	3.027	3.831	2.957	2.947	3.008	2.946	2.965	2.955	2.968	2.956	2.957
Ti	0	0	0.001	0	0.001	0.001	0	0	0	0.003	0	0.002	0.001	0
Al	0	1.973	2.011	1.994	1.441	1.976	1.977	1.944	1.975	1.988	1.982	1.997	1.965	1.997
Mg	0	0.311	0.304	0.271	0.187	0.294	0.303	0.277	0.273	0.268	0.27	0.269	0.288	0.273
Ca	0.001	0.239	0.23	0.23	0.18	0.241	0.235	0.235	0.327	0.292	0.265	0.25	0.267	0.236
Mn	0.005	0.353	0.35	0.342	0.244	0.362	0.353	0.368	0.395	0.373	0.351	0.356	0.355	0.37
Fe	0.026	2.211	2.253	2.111	1.556	2.219	2.249	2.189	2.15	2.148	2.23	2.189	2.229	2.21
Na	0.001	0.004	0.004	0.002	0.016	0.002	0	0	0.001	0.001	0.002	0.001	0.002	0
Total	6.017	8.053	8.075	7.977	7.456	8.052	8.064	8.021	8.067	8.038	8.055	8.032	8.063	8.043

Appendix ID (cont.):
Microprobe Analysis of 1498 Garnet (cont.)

Oxide Wt.%	Gt1Line1	Gt1Line1	Gt1Line1	Gt1Line1	Gt1Line1	Gt1Line1	Gt1Line1	Gt1Line1	Gt1Line1	Gt1Line1	Gt1Line1	Gt1Line1	Gt1Line1	Gt1Line1
SiO_2	36.307	36.282	35.85	35.932	35.638	36.071	36.316	42.206	36.139	35.763	36.464	36.156	36.588	36.13
TiO_2	0.032	0.026	0.009	0	0	0.023	0.031	0.035	0.025	0.045	0.043	0	0.1	0.022
Al_2O_3	20.781	20.559	19.992	20.884	20.743	20.663	20.706	19.36	20.63	20.43	20.811	20.791	21.191	20.952
MgO	2.237	2.262	2.45	2.213	2.259	2.286	2.138	1.498	2.015	2.075	2.139	2.224	2.313	2.377
CaO	2.935	2.95	2.912	3.138	2.742	3.026	3.434	3.124	3.544	3.419	3.619	3.34	2.844	2.817
MnO	5.282	5.336	5.272	5.234	5.085	5.22	5.448	4.909	5.351	5.421	5.326	5.094	4.95	4.894
FeO	33.108	32.777	32.591	32.576	33.124	32.005	32.398	29.101	31.982	32.364	32.803	32.871	33.295	33.749
Na_2O	0	0	0.019	0	0.017	0	0.016	0.047	0.024	0.004	0	0	0.006	0
Total	100.682	100.192	99.095	99.977	99.608	99.294	100.487	100.28	99.71	99.521	101.205	100.476	101.287	100.941
Cation based on 12 oxygens														
Si	2.943	2.953	2.955	2.931	2.924	2.954	2.947	3.314	2.952	2.937	2.941	2.936	2.94	2.924
Ti	0.002	0.002	0.001	0	0	0.001	0.002	0.002	0.002	0.003	0.003	0	0.006	0.001
Al	1.985	1.972	1.942	2.008	2.006	1.994	1.98	1.792	1.986	1.977	1.978	1.99	2.007	1.999
Mg	0.27	0.274	0.301	0.269	0.276	0.279	0.259	0.175	0.245	0.254	0.257	0.269	0.277	0.287
Ca	0.255	0.257	0.257	0.274	0.241	0.265	0.299	0.263	0.31	0.301	0.313	0.291	0.245	0.244
Mn	0.363	0.368	0.368	0.362	0.353	0.362	0.374	0.327	0.37	0.377	0.364	0.35	0.337	0.336
Fe	2.244	2.231	2.247	2.222	2.273	2.192	2.199	1.911	2.185	2.223	2.212	2.232	2.238	2.284
Na	0	0	0.003	0	0.003	0	0.003	0.007	0.004	0.001	0	0	0.001	0
Total	8.062	8.057	8.074	8.066	8.076	8.047	8.063	7.791	8.054	8.073	8.068	8.068	8.051	8.075

Oxide Wt.%	Gt1Line1	Gt1Line1	Gt1Line1	Gt1Line1	Gt1Line1	Gt1Line1	Gt1Line1	Gt1Line1	Gt1Line1	Gt1Line1	Gt1Line1	Gt1Line1	Gt1Line1	Gt1Line1
SiO_2	35.96	36.238	36.204	36.418	36.208	36.24	36.234	36.156	99.06	36.256	36.516	36.618	36.455	37.586
TiO_2	0.038	0	0.026	0	0.007	0.013	0.014	0.018	0.01	0.021	0.003	0.023	0.05	0.046
Al_2O_3	20.915	21.048	20.869	20.652	20.947	20.679	21.071	20.83	0.007	21.161	20.639	20.852	20.919	19.708
MgO	2.373	2.467	2.522	2.484	2.476	2.439	2.446	2.442	0	2.434	2.362	2.442	2.179	1.855
CaO	3.053	2.715	2.73	2.748	2.944	3.007	3.311	2.842	0.005	2.73	2.734	2.754	3.454	3.837
MnO	4.767	4.524	4.561	4.536	4.624	4.545	4.54	4.583	0.058	4.468	4.485	4.681	4.91	4.829
FeO	33.063	33.578	33.715	33.456	33.718	32.583	32.611	33.166	0.382	33.117	33.336	32.893	32.526	30.611
Na_2O	0.044	0.009	0.019	0	0.01	0.016	0	0	0	0.032	0.005	0.001	0.011	0.05
Total	100.213	100.579	100.646	100.294	100.934	99.522	100.227	100.037	99.522	100.219	100.08	100.264	100.504	98.522
Cation based on 12 oxygens														
Si	2.926	2.934	2.933	2.956	2.927	2.958	2.937	2.942	5.988	2.939	2.968	2.965	2.95	3.075
Ti	0.002	0	0.002	0	0	0.001	0.001	0.001	0	0.001	0	0.001	0.003	0.003
Al	2.006	2.009	1.993	1.976	1.996	1.989	2.013	1.998	0.001	2.022	1.977	1.99	1.995	1.9
Mg	0.288	0.298	0.305	0.301	0.298	0.297	0.296	0.296	0	0.294	0.286	0.295	0.263	0.226
Ca	0.266	0.236	0.237	0.239	0.255	0.263	0.288	0.248	0	0.237	0.238	0.239	0.3	0.336
Mn	0.329	0.31	0.313	0.312	0.317	0.314	0.312	0.316	0.003	0.307	0.309	0.321	0.337	0.335
Fe	2.25	2.274	2.285	2.271	2.28	2.224	2.211	2.257	0.019	2.245	2.266	2.227	2.201	2.094
Na	0.007	0.001	0.003	0	0.002	0.003	0	0	0	0.005	0.001	0	0.002	0.008
Total	8.074	8.062	8.071	8.055	8.075	8.049	8.058	8.058	6.011	8.05	8.045	8.038	8.051	7.977

Oxide Wt.%	Gt1Line1	Gt1Line1	Gt1Line1	Gt1Line1	Gt1Line1	Gt1Line1	Gt1Line1	Gt1Line1	Gt1Line1	Gt1Line1	Gt1Line1	Gt1Line1	Gt1Line1	Gt1Line1
SiO_2	36.469	36.526	36.331	36.677	36.965	37.889	36.752	36.464	36.689	36.718	36.23	36.713	36.854	36.647
TiO_2	0.021	0.03	0.036	0.138	0.046	0.007	0.064	0.143	0.018	0.02	0.021	0	0	0.032
Al_2O_3	20.91	20.709	20.625	20.748	20.727	20.963	20.766	20.901	20.964	20.719	20.934	20.994	20.877	20.839
MgO	2.24	2.244	2.306	2.207	2.191	2.228	2.429	2.409	2.413	2.506	2.561	2.589	2.558	2.581
CaO	3.536	3.043	2.87	2.868	3.276	2.942	2.63	3.044	3.185	2.961	2.718	2.825	2.886	2.694
MnO	4.858	4.956	5.317	5.422	5.371	5.164	4.758	4.799	4.705	4.704	4.391	4.495	4.58	4.274
FeO	32.561	32.689	32.326	31.913	31.433	31.514	32.442	32.228	31.908	32.177	32.138	32.413	32.969	32.871
Na_2O	0.014	0.004	0.001	0.01	0.006	0.016	0.011	0.012	0.016	0.013	0.008	0	0	0.011
Total	100.609	100.201	99.812	99.983	100.015	100.723	99.852	100	99.898	99.818	99.001	100.029	100.724	99.949
Cation based on 12 oxygens														
Si	2.949	2.965	2.961	2.976	2.992	3.03	2.981	2.957	2.972	2.979	2.961	2.97	2.969	2.971
Ti	0.001	0.002	0.002	0.008	0.003	0	0.004	0.009	0.001	0.001	0.001	0	0	0.002
Al	1.992	1.981	1.981	1.984	1.977	1.976	1.985	1.998	2.001	1.981	2.016	2.002	1.982	1.991
Mg	0.27	0.271	0.28	0.267	0.264	0.266	0.294	0.291	0.291	0.303	0.312	0.312	0.307	0.312
Ca	0.306	0.265	0.251	0.249	0.284	0.252	0.229	0.264	0.276	0.257	0.238	0.245	0.249	0.234
Mn	0.333	0.341	0.367	0.373	0.368	0.35	0.327	0.33	0.323	0.323	0.304	0.308	0.313	0.293
Fe	2.202	2.219	2.203	2.165	2.128	2.107	2.201	2.186	2.161	2.183	2.196	2.193	2.221	2.228
Na	0.002	0.001	0	0.002	0.001	0.002	0.002	0.002	0.002	0.002	0.001	0	0	0.002
Total	8.055	8.045	8.045	8.024	8.017	7.983	8.023	8.037	8.027	8.029	8.029	8.03	8.041	8.033

Appendix ID (cont.):
Microprobe Analysis of 1498 Garnet (cont.)

Oxide Wt.%	Gt1Line1	Gt1Line1	Gt1Line1	Gt1Line1	Gt1Line1	Gt1Line1	Gt1Line1	Gt1Line1	Gt1Line1	Gt2Line2	Gt2Line2	Gt2Line2	Gt2Line2	Gt2Line2
SiO_2	37.037	36.591	36.661	36.815	36.51	36.006	37.104	37.033	36.8	36.177	36.871	36.719	37.086	36.527
TiO_2	0.004	0.103	0.032	0.036	0.002	0.007	0.003	0	0.023	0.024	0	0.002	0	0.008
Al_2O_3	21.099	20.877	20.833	20.847	20.262	20.773	21.216	21.137	20.965	21.257	21.116	21.068	21.236	21.244
MgO	2.654	2.713	2.859	2.956	2.767	2.962	3.147	3.308	3.523	2.465	3.522	3.727	3.669	3.65
CaO	2.546	2.472	2.373	2.294	2.37	2.728	2.97	2.321	1.791	2.085	2.041	1.977	1.878	1.728
MnO	4.332	4.193	3.867	3.626	3.666	2.938	2.581	2.113	1.821	1.064	0.944	1.091	1.284	1.432
FeO	33.288	33.057	32.919	33.559	32.552	33.923	33.431	34.145	34.686	35.799	35.792	35.794	35.907	36.275
Na_2O	0	0	0	0.025	0.033	0.101	0.014	0.019	0	0.12	0.009	0	0.009	0.033
Total	100.96	100.006	99.544	100.158	98.162	99.438	100.466	100.076	99.609	98.991	100.295	100.378	101.069	100.897
Cation based on 12 oxygens														
Si	2.971	2.964	2.976	2.974	3.004	2.938	2.973	2.978	2.975	2.957	2.965	2.953	2.961	2.932
Ti	0	0.006	0.002	0.002	0	0	0	0	0.001	0.001	0	0	0	0
Al	1.995	1.993	1.993	1.985	1.964	1.998	2.004	2.003	1.998	2.047	2.001	1.997	1.998	2.01
Mg	0.317	0.328	0.346	0.356	0.339	0.36	0.376	0.397	0.425	0.3	0.422	0.447	0.437	0.437
Ca	0.219	0.215	0.206	0.199	0.209	0.239	0.255	0.2	0.155	0.183	0.176	0.17	0.161	0.149
Mn	0.294	0.288	0.266	0.248	0.255	0.203	0.175	0.144	0.125	0.074	0.064	0.074	0.087	0.097
Fe	2.233	2.24	2.235	2.267	2.24	2.315	2.24	2.296	2.345	2.447	2.407	2.407	2.397	2.435
Na	0	0	0	0.004	0.005	0.016	0.002	0.003	0	0.019	0.001	0	0.001	0.005
Total	8.029	8.034	8.024	8.035	8.016	8.069	8.025	8.021	8.024	8.028	8.036	8.048	8.042	8.065

Oxide Wt.%	Gt2Line2	Gt2Line2	Gt2Line2	Gt2Line2	Gt2Line2	Gt2Line2	Gt2Line2	Gt2Line2	Gt2Line2	Gt2Line2	Gt2Line2	Gt2Line2	Gt2Line2	Gt2Line2
SiO_2	36.793	36.781	36.66	36.661	37.185	50.713	36.789	36.503	37.068	36.485	36.766	36.76	36.897	49.373
TiO_2	0	0.002	0	0	0	0.007	0.179	0.027	0.003	0.132	0.001	0.02	0	0.011
Al_2O_3	20.997	21.247	20.986	21.112	20.976	19.889	21.113	21.005	20.858	20.903	21.055	21.177	21.004	18.801
MgO	3.602	3.425	3.405	3.283	3.147	0.373	2.88	2.814	2.766	2.716	2.891	3.022	3.066	1.489
CaO	2.061	2.35	2.564	2.774	3.02	2.657	3.13	3.356	3.693	3.397	3.171	2.94	2.855	1.748
MnO	1.593	1.636	1.888	1.989	2.255	1.882	2.736	2.91	3.088	2.896	2.993	2.734	2.543	1.768
FeO	35.721	35.127	34.71	34.695	34.146	25.555	33.344	33.343	32.274	32.603	33.259	33.916	33.77	28.305
Na_2O	0.017	0.005	0	0.028	0.007	0.04	0.005	0.014	0.005	0.014	0.001	0	0.019	0.066
Total	100.784	100.573	100.213	100.542	100.736	101.116	100.176	99.972	99.755	99.146	100.137	100.569	100.154	101.561
Cation based on 12 oxygens														
Si	2.953	2.952	2.955	2.948	2.978	3.733	2.962	2.953	2.991	2.967	2.965	2.954	2.972	3.673
Ti	0	0	0	0	0	0	0.011	0.002	0	0.008	0	0.001	0	0.001
Al	1.986	2.01	1.994	2.001	1.98	1.726	2.004	2.003	1.984	2.004	2.001	2.006	1.994	1.648
Mg	0.431	0.41	0.409	0.394	0.376	0.041	0.346	0.339	0.333	0.329	0.347	0.362	0.368	0.165
Ca	0.177	0.202	0.221	0.239	0.259	0.21	0.27	0.291	0.319	0.296	0.274	0.253	0.246	0.139
Mn	0.108	0.111	0.129	0.135	0.153	0.117	0.187	0.199	0.211	0.199	0.204	0.186	0.173	0.111
Fe	2.397	2.358	2.34	2.333	2.287	1.573	2.245	2.256	2.178	2.218	2.243	2.279	2.275	1.761
Na	0.003	0.001	0	0.004	0.001	0.006	0.001	0.002	0.001	0.002	0	0	0.003	0.01
Total	8.055	8.044	8.048	8.054	8.034	7.406	8.026	8.045	8.017	8.023	8.034	8.041	8.031	7.508

Oxide Wt.%	Gt2Line2	Gt2Line2	Gt2Line2	Gt2Line2	Gt2Line2	Gt2Line2	Gt2Line2	Gt2Line2	Gt2Line2	Gt2Line2	Gt2Line2	Gt2Line2	Gt2Line2	Gt2Line2
SiO_2	97.529	36.562	37.016	36.316	36.304	36.711	0.012	0.801	36.712	36.528	36.05	36.576	36.681	36.625
TiO_2	0.026	0.012	0.008	0	0.018	0.09	53.079	52.116	1.746	0.05	0.811	0.071	0.034	0.051
Al_2O_3	0.165	21.202	21.098	21.147	20.787	20.838	0.02	0.025	20.629	20.752	20.369	20.698	20.88	20.693
MgO	0	3.503	3.323	3.247	3.228	3.324	0.615	0.667	3.115	3.046	2.897	2.725	2.69	2.762
CaO	0.012	1.961	2.578	2.797	2.588	2.358	0.027	0.029	2.369	2.602	2.637	3.539	3.094	2.856
MnO	0.039	2.091	2.184	2.235	2.272	2.201	0.458	0.462	2.848	3.326	3.76	4.278	4.811	4.502
FeO	1.215	35.387	34.084	34.175	34.271	34.132	45.579	44.339	32.789	33.666	32.466	32.119	31.289	32.225
Na_2O	0.03	0.014	0.006	0.009	0.012	0	0.023	0.018	0	0	0.157	0.038	0	0.005
Total	99.016	100.732	100.297	99.926	99.48	99.654	99.813	98.457	100.208	99.97	99.147	100.044	99.479	99.719
Cation based on 12 oxygens														
Si	5.957	2.938	2.973	2.938	2.952	2.971	0.001	0.081	2.946	2.959	2.944	2.961	2.976	2.972
Ti	0.001	0.001	0	0	0.001	0.005	4.013	3.967	0.105	0.003	0.05	0.004	0.002	0.003
Al	0.012	2.008	1.997	2.016	1.992	1.987	0.002	0.003	1.951	1.981	1.96	1.975	1.997	1.979
Mg	0	0.42	0.398	0.392	0.391	0.401	0.092	0.101	0.373	0.368	0.353	0.329	0.325	0.334
Ca	0.001	0.169	0.222	0.242	0.226	0.204	0.003	0.003	0.204	0.226	0.231	0.307	0.269	0.248
Mn	0.002	0.142	0.149	0.153	0.157	0.151	0.039	0.04	0.194	0.228	0.26	0.293	0.331	0.31
Fe	0.062	2.378	2.289	2.312	2.331	2.31	3.832	3.754	2.201	2.281	2.217	2.175	2.123	2.187
Na	0.004	0.002	0.001	0.001	0.002	0	0.004	0.003	0	0	0.025	0.006	0	0.001
Total	6.039	8.058	8.029	8.054	8.052	8.029	7.986	7.952	7.974	8.046	8.04	8.05	8.023	8.034

Appendix ID (cont.):
Microprobe Analysis of 1498 Garnet (cont.)

Oxide Wt.%	Gt2Line2	Gt2Line2	Gt2Line2	Gt2Line2	Gt2Line2	Gt2Line2	Gt2Line2	Gt2Line2	Gt2Line2	Gt2Line2	Gt2Line2	Gt2Line2	Gt2Line2	Gt2Line2
SiO_2	36.688	36.223	36.243	36.937	36.991	37.064	37.125	36.527	36.681	36.906	37.032	36.964	36.684	36.818
TiO_2	0.013	0.013	0.036	0.004	0.029	0.023	0.015	0.009	0.043	0	0.028	0.018	0.161	0.019
Al_2O_3	21.002	20.944	20.804	20.739	20.964	20.772	20.842	20.569	20.791	21.067	20.9	20.894	20.861	20.814
MgO	2.824	2.911	3.174	3.135	3.122	3.125	3.289	2.536	3.249	3.358	3.244	3.261	3.148	3.051
CaO	2.841	2.755	2.571	2.634	2.748	2.451	2.315	2.176	2.228	2.164	2.25	2.462	2.647	2.612
MnO	4.123	3.541	2.848	2.921	2.967	2.904	2.732	2.675	2.392	2.382	2.371	2.586	2.462	2.822
FeO	32.682	32.945	32.411	32.22	32.834	32.638	32.285	33.527	33.32	33.101	33.459	32.462	33.15	32.849
Na_2O	0	0	0.001	0	0.006	0.011	0.017	0.004	0	0.005	0.004	0	0.009	0.027
Total	100.173	99.332	98.088	98.59	99.661	98.988	98.62	98.023	98.704	98.983	99.288	98.647	99.122	99.012
Cation based on 12 oxygens														
Si	2.963	2.95	2.972	3.006	2.986	3.007	3.014	3.005	2.988	2.991	2.997	3.003	2.978	2.991
Ti	0.001	0.001	0.002	0	0.002	0.001	0.001	0.001	0.003	0	0.002	0.001	0.01	0.001
Al	1.999	2.01	2.011	1.989	1.994	1.986	1.994	1.994	1.996	2.012	1.993	2	1.996	1.993
Mg	0.34	0.353	0.388	0.38	0.376	0.378	0.398	0.311	0.395	0.406	0.391	0.395	0.381	0.37
Ca	0.246	0.24	0.226	0.23	0.238	0.213	0.201	0.192	0.194	0.188	0.195	0.214	0.23	0.227
Mn	0.282	0.244	0.198	0.201	0.203	0.2	0.188	0.186	0.165	0.164	0.163	0.178	0.169	0.194
Fe	2.207	2.244	2.223	2.193	2.216	2.214	2.192	2.307	2.27	2.243	2.264	2.205	2.25	2.232
Na	0	0	0	0	0.001	0.002	0.003	0.001	0	0.001	0.001	0	0.001	0.004
Total	8.038	8.042	8.02	7.999	8.016	8.001	7.991	7.997	8.011	8.005	8.006	7.996	8.015	8.012

Oxide Wt.%	Gt2Line2	Gt2Line2	Gt2Line2	Gt2Line2	Gt2Line2	Gt2Line2	Gt2Line2	Gt2Line2	Gt2Line2	Gt2Line2	Gt2Line2	Gt2Line3	Gt2Line3	Gt2Line3
SiO_2	37.168	36.8	36.999	36.949	61.189	36.846	41.849	36.985	37.334	37.081	37.129	37.061	36.905	36.882
TiO_2	0.041	0.035	0.015	0.038	0	0.05	0.004	0.022	0.024	0.033	0.031	0.025	0.007	0.003
Al_2O_3	20.916	20.639	20.757	20.838	24.75	20.75	20.753	20.724	20.941	20.957	21.036	21.096	21.028	21.137
MgO	2.63	2.493	2.358	2.314	0.01	2.46	2.359	2.927	3.208	3.401	3.538	3.396	3.198	2.882
CaO	3.082	3.088	3.265	3.578	6.196	3.481	3.264	3.646	2.664	2.494	2.116	2.151	2.29	2.419
MnO	4.117	4.541	4.555	4.706	0.109	4.28	3.711	2.811	2.284	1.972	1.85	2.345	2.662	3.733
FeO	30.897	31.059	30.353	30.236	0.489	30.367	29.175	31.241	32.515	32.934	34.254	33.59	32.97	32.648
Na_2O	0	0.011	0.019	0.011	8.035	0.015	0.022	0.014	0.067	0.024	0.032	0.012	0	0.012
Total	98.851	98.666	98.321	98.67	100.778	98.249	101.137	98.37	99.037	98.896	99.986	99.676	99.06	99.716
Cation based on 12 oxygens														
Si	3.015	3.004	3.021	3.009	4.055	3.01	3.241	3.01	3.016	3.002	2.985	2.987	2.991	2.98
Ti	0.002	0.002	0.001	0.002	0	0.003	0	0.001	0.001	0.002	0.002	0.002	0	0
Al	2	1.986	1.997	2	1.933	1.998	1.894	1.988	1.994	1.999	1.993	2.004	2.009	2.013
Mg	0.318	0.303	0.287	0.281	0.001	0.3	0.272	0.355	0.386	0.41	0.424	0.408	0.386	0.347
Ca	0.268	0.27	0.286	0.312	0.44	0.305	0.271	0.318	0.231	0.216	0.182	0.186	0.199	0.209
Mn	0.283	0.314	0.315	0.325	0.006	0.296	0.243	0.194	0.156	0.135	0.126	0.16	0.183	0.256
Fe	2.096	2.12	2.072	2.059	0.027	2.075	1.889	2.127	2.197	2.23	2.303	2.264	2.235	2.206
Na	0	0.002	0.003	0.002	1.032	0.002	0.003	0.002	0.011	0.004	0.005	0.002	0	0.002
Total	7.982	8.001	7.982	7.99	7.494	7.989	7.813	7.995	7.992	7.998	8.02	8.013	8.003	8.013

Oxide Wt.%	Gt2Line3	Gt2Line3	Gt2Line3	Gt2Line3	Gt2Line3	Gt2Line3	Gt2Line3	Gt2Line3	Gt2Line3	Gt2Line3	Gt2Line3	Gt2Line3	Gt2Line3	Gt2Line3
SiO_2	37.314	36.703	36.447	36.645	36.216	36.797	36.385	36.484	36.576	36.357	36.652	36.665	36.376	36.28
TiO_2	0.032	0.046	0.04	0.022	0.036	0.04	0.113	0.059	0.022	0.088	0	0.117	0.006	0.009
Al_2O_3	20.907	20.683	20.638	20.537	20.619	20.764	20.729	20.599	20.558	20.837	20.936	20.648	20.701	20.34
MgO	2.675	2.462	2.331	2.09	2.007	1.892	1.796	1.695	1.703	1.692	2.073	2.203	2.381	2.618
CaO	3.061	3.224	3.361	3.939	4.03	4.21	4.517	4.596	4.574	4.992	4.086	4.283	3.956	3.633
MnO	4.198	4.8	5.278	5.614	6.092	6.451	6.744	6.816	6.635	6.401	5.641	5.321	4.669	3.903
FeO	31.415	30.948	30.652	29.137	29.469	29.794	29.087	28.498	28.464	28.506	29.362	29.636	30.475	31.311
Na_2O	0.04	0.035	0.045	0.034	0	0.03	0.003	0.022	0.006	0.028	0	0	0	0
Total	99.642	98.901	98.792	98.018	98.469	99.978	99.374	98.769	98.538	98.901	98.75	98.873	98.564	98.094
Cation based on 12 oxygens														
Si	3.01	2.993	2.982	3.009	2.976	2.981	2.967	2.987	2.998	2.971	2.99	2.99	2.978	2.986
Ti	0.002	0.003	0.002	0.001	0.002	0.002	0.007	0.004	0.001	0.005	0	0.007	0	0.001
Al	1.988	1.988	1.99	1.988	1.997	1.983	1.992	1.988	1.986	2.007	2.013	1.984	1.997	1.973
Mg	0.322	0.299	0.284	0.256	0.246	0.229	0.218	0.207	0.208	0.206	0.252	0.268	0.291	0.321
Ca	0.265	0.282	0.295	0.347	0.355	0.365	0.395	0.403	0.402	0.437	0.357	0.374	0.347	0.32
Mn	0.287	0.332	0.366	0.391	0.424	0.443	0.466	0.473	0.461	0.443	0.39	0.368	0.324	0.272
Fe	2.119	2.111	2.097	2.001	2.025	2.019	1.984	1.951	1.951	1.948	2.003	2.021	2.086	2.155
Na	0.006	0.005	0.007	0.005	0	0.005	0	0.003	0.001	0.004	0	0	0	0
Total	7.999	8.013	8.023	7.998	8.025	8.027	8.029	8.016	8.008	8.021	8.005	8.012	8.023	8.028

Appendix ID (cont.):
Microprobe Analysis of 1498 Garnet (cont.)

Oxide Wt.%	Gt2Line3	Gt2Line3	Gt2Line3	Gt2Line3	Gt2Line3	Gt2Line3	Gt2Line3	Gt2Line3	Gt2Line3	Gt2Line3	Gt2Line3	Gt2Line3	Gt2Line3	Gt2Line3
SiO_2	42	37.298	45.883	37.304	37.514	40.554	37.27	37.031	37.086	36.971	37.061	37.145	36.924	43.986
TiO_2	0.041	0.028	0.042	0.01	0.032	0.002	0.039	0.025	0.001	0	0.002	0	0	0
Al_2O_3	18.549	21.09	18.552	20.907	20.979	22.084	21.274	20.927	20.969	21.149	20.994	21.033	20.994	23.681
MgO	2.353	3.295	2.762	3.485	3.544	3.083	3.637	3.617	3.679	3.572	3.711	3.628	3.677	1.146
CaO	2.592	2.179	1.56	1.737	1.827	1.948	1.992	1.96	1.987	1.931	1.974	1.958	1.991	1.983
MnO	2.709	2.292	1.605	1.689	1.628	1.42	1.369	1.369	1.38	1.344	1.272	1.189	1.128	0.916
FeO	29.924	32.916	28.136	33.395	33.24	32.104	33.836	33.626	33.769	33.684	34.422	33.315	34.219	29.806
Na_2O	0.042	0.019	0.118	0.006	0.011	0.029	0.033	0.041	0.06	0.044	0.042	0.029	0.037	0.009
Total	98.21	99.117	98.658	98.533	98.775	101.224	99.45	98.596	98.931	98.695	99.478	98.297	98.97	101.527
Cation based on 12 oxygens														
Si	3.349	3.011	3.543	3.025	3.03	3.141	2.997	3.004	3	2.996	2.989	3.014	2.99	3.312
Ti	0.002	0.002	0.002	0.001	0.002	0	0.002	0.002	0	0	0	0	0	0
Al	1.743	2.006	1.688	1.998	1.997	2.016	2.016	2.001	1.999	2.02	1.996	2.012	2.004	2.101
Mg	0.28	0.397	0.318	0.421	0.427	0.356	0.436	0.437	0.444	0.432	0.446	0.439	0.444	0.129
Ca	0.221	0.188	0.129	0.151	0.158	0.162	0.172	0.17	0.172	0.168	0.171	0.17	0.173	0.16
Mn	0.183	0.157	0.105	0.116	0.111	0.093	0.093	0.094	0.095	0.092	0.087	0.082	0.077	0.058
Fe	1.995	2.222	1.817	2.264	2.245	2.08	2.275	2.282	2.285	2.283	2.322	2.261	2.317	1.877
Na	0.007	0.003	0.018	0.001	0.002	0.004	0.005	0.006	0.009	0.007	0.007	0.005	0.006	0.001
Total	7.78	7.986	7.62	7.977	7.972	7.852	7.996	7.996	8.004	7.998	8.018	7.983	8.011	7.638

Oxide Wt.%	Gt2Line3	Gt2Line3	Gt2Line3	Gt2Line3	Gt2Line3	Gt2Line3	Gt2Line3	Gt1	Gt2	Gt3	Gt4	Gt5rim	G6rim	Gt7
SiO_2	45.227	37.366	71.853	37.42	37.233	37.166	37.014	36.274	37.002	36.952	36.888	37.104	36.485	36.787
TiO_2	0	0	0.02	0.019	0.007	0	0.007	0.952	0.223	0.02	0.032	0.012	0.001	0.054
Al_2O_3	20.282	21.151	10.637	21.125	21.022	20.93	20.989	20.784	20.893	21.01	20.909	21.104	21.223	20.773
MgO	3.255	3.655	1.537	3.654	3.628	3.647	3.464	2.222	2.45	1.911	2.275	3.53	3.554	1.536
CaO	1.739	2.046	1.007	2.017	1.996	2.061	2.195	2.774	2.674	3.641	2.851	1.63	1.884	4.565
MnO	0.849	1.006	0.379	0.964	0.952	1.031	0.814	3.759	3.562	5.246	4.944	1.126	1.551	6.562
FeO	29.306	33.061	13.363	33.343	33.397	33.223	34.358	33.54	33.706	32.011	32.153	35.731	34.254	30.232
Na_2O	0.068	0.016	0.201	0	0.003	0.025	0.014	0.005	0.021	0	0.01	0.022	0	0
Total	100.726	98.301	98.997	98.542	98.238	98.083	98.855	100.31	100.531	100.791	100.062	100.259	98.952	100.509
Cation based on 12 oxygens			4.855	3.023	3.02	3.02	2.999	2.936	2.98	2.975	2.984	2.98	2.963	2.975
Si	3.428	3.024	0.001	0.001	0	0	0	0.058	0.014	0.001	0.002	0.001	0	0.003
Ti	0	0	0.847	2.012	2.01	2.005	2.004	1.983	1.983	1.994	1.998	2.031	1.98	
Al	1.812	2.017	0.155	0.44	0.439	0.442	0.418	0.268	0.294	0.229	0.274	0.423	0.43	0.185
Mg	0.368	0.441	0.073	0.175	0.174	0.179	0.191	0.241	0.231	0.314	0.247	0.14	0.164	0.396
Ca	0.141	0.177	0.022	0.066	0.065	0.071	0.056	0.258	0.243	0.358	0.339	0.077	0.107	0.449
Mn	0.055	0.069	0.755	2.253	2.266	2.258	2.328	2.271	2.27	2.155	2.175	2.4	2.326	2.044
Fe	1.858	2.238	0.026	0	0	0.004	0.002	0.001	0.003	0	0.002	0.003	0	0
Na	0.01	0.002	6.734	7.97	7.974	7.979	7.998	8.016	8.018	8.026	8.017	8.022	8.021	8.032
Total	7.672	7.968												

Oxide Wt.%	Gt8	Gt22	Gt23	Gt24	Gt25	Gt26	Gt27	Gt28	Gt29	Gt30	Gt31	Gt32	Gt33	Gt34
SiO_2	36.667	37.647	36.782	36.866	37.321	36.691	36.908	36.633	37.042	37.077	37.188	35.972	36.872	36.996
TiO_2	0	0.205	0.595	0.505	0.559	0.318	0.513	0.457	0.32	0.203	0.323	1.216	0.394	0
Al_2O_3	20.63	21.474	20.575	21.019	21.006	20.767	21.199	21.005	21.098	21.044	20.751	20.81	20.918	21.232
MgO	1.662	3.216	3.256	3.339	3.371	3.295	3.267	3.233	3.522	3.583	3.496	3.276	3.382	3.14
CaO	4.408	2.614	2.298	2.196	2.068	2.309	2.091	2.409	1.718	1.717	1.901	1.976	1.909	2.086
MnO	6.166	2.399	2.352	2.489	2.404	2.536	2.67	2.469	1.634	1.632	1.184	1.072	0.962	3.03
FeO	30.093	32.586	33.087	32.589	33.632	33.274	32.411	32.558	33.962	34.672	34.199	34.377	34.219	32.097
Na_2O	0.011	0	0.001	0.024	0.004	0.002	0.014	0.017	0.021	0.034	0.03	0.022	0.002	0.011
Total	99.637	100.141	98.946	99.027	100.365	99.192	99.073	98.781	99.317	99.962	99.072	98.721	98.658	98.592
Cation based on 12 oxygens														
Si	2.985	3.003	2.986	2.982	2.985	2.976	2.981	2.974	2.988	2.981	3.007	2.932	2.993	3.002
Ti	0	0.012	0.036	0.031	0.034	0.019	0.031	0.028	0.019	0.012	0.02	0.075	0.024	0
Al	1.979	2.019	1.969	2.004	1.98	1.985	2.018	2.01	2.006	1.994	1.977	1.999	2.001	2.031
Mg	0.202	0.382	0.394	0.403	0.402	0.398	0.393	0.391	0.424	0.429	0.421	0.398	0.409	0.38
Ca	0.385	0.223	0.2	0.19	0.177	0.201	0.181	0.21	0.148	0.148	0.165	0.173	0.166	0.181
Mn	0.425	0.162	0.162	0.171	0.163	0.174	0.183	0.17	0.112	0.111	0.081	0.074	0.066	0.208
Fe	2.049	2.174	2.246	2.204	2.25	2.257	2.19	2.21	2.291	2.331	2.312	2.343	2.323	2.178
Na	0.002	0	0	0.004	0.001	0	0.002	0.003	0.003	0.005	0.005	0.003	0	0.002
Total	8.027	7.975	7.993	7.989	7.992	8.01	7.979	7.996	7.991	8.011	7.988	7.997	7.982	7.982

Appendix ID (cont.):
Microprobe Analysis of 1498 Garnet (cont.)

Oxide Wt.%	Gt35	Gt36	Gt37	Gt38	Gt39	Gt40	Gt41	Gt42	Gt43	Gt44	Gt45	Gt46
SiO_2	36.972	36.878	36.784	36.84	36.853	37.009	37.049	36.899	36.81	36.781	36.97	37.12
TiO_2	0.012	0.024	0.016	0.005	0.012	0.011	0.005	0.004	0	0.017	0.007	0.008
Al_2O_3	21.058	20.942	20.825	20.768	20.688	20.696	20.741	20.897	20.983	21.09	21.043	21.085
MgO	3.09	3.23	2.354	2.508	2.416	3.532	3.64	3.274	3.304	3.547	3.249	3.242
CaO	2.298	2.111	2.922	3.125	3.177	1.724	1.955	1.983	2.017	1.93	2.206	2.285
MnO	3.148	3.052	4.71	4.767	4.729	1.134	1.2	0.963	0.955	1.019	1.032	0.901
FeO	32.926	32.674	31.335	31.382	30.853	34.969	34.461	34.714	34.553	34.433	34.94	34.546
Na_2O	0.019	0.021	0	0.015	0	0.028	0.024	0.031	0.02	0.029	0	0
Total	99.523	98.932	98.946	99.41	98.728	99.103	99.075	98.765	98.642	98.846	99.447	99.187
Cation based on 12 oxygens												
Si	2.988	2.994	2.998	2.991	3.006	3.001	3.001	2.999	2.994	2.984	2.988	3
Ti	0.001	0.001	0.001	0	0.001	0.001	0	0	0	0.001	0	0
Al	2.006	2.004	2	1.987	1.989	1.978	1.98	2.002	2.012	2.016	2.005	2.009
Mg	0.372	0.391	0.286	0.304	0.294	0.427	0.44	0.397	0.401	0.429	0.392	0.391
Ca	0.199	0.184	0.255	0.272	0.278	0.15	0.17	0.173	0.176	0.168	0.191	0.198
Mn	0.215	0.21	0.325	0.328	0.327	0.078	0.082	0.066	0.066	0.07	0.071	0.062
Fe	2.225	2.218	2.136	2.131	2.105	2.372	2.334	2.36	2.35	2.336	2.362	2.335
Na	0.003	0.003	0	0.002	0	0.004	0.004	0.005	0.003	0.005	0	0
Total	8.009	8.005	8.001	8.015	8	8.011	8.011	8.002	8.002	8.009	8.009	7.995

Appendix 1D:
Microprobe Analysis of 1498 Feldspar

Oxide Wt.%	fsp5in	fsp6in	fsp7	fsp8	fsp9	fsp10	fsp1out	fsp2out	fsp3in	fsp4in	fsp11in	fsp12in	fsp13in	fsp14in
SiO_2	59.524	59.92	58.139	59.728	57.992	61.36	60.294	60.719	59.035	15.31	59.547	65.089	59.063	66.015
Al_2O_3	24.427	24.543	23.959	23.204	22.658	23.549	24.162	24.201	25.404	7.385	24.592	20.685	24.157	19.638
CaO	6.205	6.344	6.135	5.415	5.135	5.49	5.949	5.62	7.162	2.507	6.401	2.104	7.023	1.419
FeO	0.165	0.064	0	0.014	0.683	0.078	0	0.064	0.125	14.547	0.41	0.772	0.657	0.407
Na_2O	8.112	7.871	8.165	8.309	7.934	8.46	8.452	8.366	7.664	0.586	7.912	10.771	7.554	10.906
K_2O	0.069	0.078	0.087	0.06	0.073	0.037	0.068	0.066	0.064	0	0.121	0.054	0.112	0.056
Total	98.502	98.82	96.485	96.73	94.475	98.974	98.925	99.036	99.454	40.335	98.983	99.475	98.566	98.441
Cation based on 8 oxygens														
Si	2.691	2.697	2.686	2.74	2.731	2.75	2.711	2.722	2.65	2.073	2.684	2.891	2.68	2.947
Al	1.302	1.302	1.304	1.255	1.258	1.244	1.28	1.279	1.344	1.178	1.306	1.083	1.292	1.033
Ca	0.301	0.306	0.304	0.266	0.259	0.264	0.287	0.27	0.344	0.364	0.309	0.1	0.341	0.068
Fe	0.006	0.002	0	0.001	0.027	0.003	0	0.002	0.005	1.647	0.015	0.029	0.025	0.015
Na	0.711	0.687	0.731	0.739	0.725	0.735	0.737	0.727	0.667	0.154	0.691	0.928	0.665	0.944
K	0.004	0.004	0.005	0.003	0.004	0.002	0.004	0.004	0.004	0	0.007	0.003	0.006	0.003
Total	5.015	4.998	5.03	5.004	5.004	4.998	5.019	5.004	5.014	5.416	5.012	5.034	5.009	5.01

Oxide Wt.%	fsp15	fsp16	fsp17	fsp18	fspM1	fspM2	fspM3	fspM4
SiO_2	60.619	59.792	60.759	60.341	60.679	60.83	55.852	61.022
Al_2O_3	23.238	23.042	23.423	23.75	23.723	23.177	22.336	23.279
CaO	6.11	6.059	5.713	5.815	5.544	5.489	5.071	5.501
FeO	0.352	0.091	0.589	0.424	0.206	0.091	1.6	0.123
Na_2O	7.944	8.233	8.257	8.366	8.374	8.351	7.666	8.311
K_2O	0.061	0.043	0.04	0.025	0.064	0.071	0.054	0.09
Total	98.324	97.26	98.781	98.721	98.59	98.009	92.579	98.326
Cation based on 8 oxygens								
Si	2.741	2.735	2.737	2.721	2.734	2.754	2.701	2.753
Al	1.239	1.242	1.244	1.262	1.26	1.237	1.273	1.238
Ca	0.296	0.297	0.276	0.281	0.268	0.266	0.263	0.266
Fe	0.013	0.003	0.022	0.016	0.008	0.003	0.065	0.005
Na	0.697	0.73	0.721	0.732	0.731	0.733	0.719	0.727
K	0.004	0.003	0.002	0.001	0.004	0.004	0.003	0.005
Total	4.99	5.01	5.002	5.013	5.005	4.997	5.024	4.994

Appendix 1D (cont.):
Microprobe Analysis of 1498 Biotite

Oxide Wt.%	MicaIn1	bi1tch	bi2tch	bi3	bi4M	bi5M	bi6M	bi7M
SiO_2	27.267	35.301	35.386	35.324	35.508	7.786	35.541	35.632
TiO_2	0.858	1.669	1.627	1.561	1.404	0.209	1.896	1.928
Al_2O_3	52.852	18.354	18.175	18.096	18.744	6.921	18.138	18.265
MgO	2.11	10.526	10.576	10.569	10.671	0.734	10.656	10.701
CaO	0.027	0.008	0.015	0.002	0.011	0.196	0.01	0
MnO	0.165	0.064	0.044	0	0.072	0	0.046	0.022
FeO	13.332	18.273	18.409	18.223	18.555	2.115	19.092	18.72
Na_2O	0.037	0.256	0.234	0.227	0.269	1.06	0.295	0.284
K_2O	0	8.957	9.227	9.272	9.36	2.084	9.324	9.033
H_2O	4.464	3.886	3.889	3.874	3.925	0.914	3.929	3.928
Total	101.112	97.294	97.582	97.148	98.519	22.019	98.927	98.513
Cation based on 22 oxygens								
Si	3.663	5.448	5.456	5.468	5.425	5.106	5.425	5.439
Ti	0.087	0.194	0.189	0.182	0.161	0.103	0.218	0.221
Al	8.368	3.338	3.303	3.302	3.375	5.349	3.263	3.286
Mg	0.423	2.422	2.431	2.439	2.43	0.717	2.425	2.435
Ca	0.004	0.001	0.003	0	0.002	0.137	0.002	0
Mn	0.019	0.008	0.006	0	0.009	0	0.006	0.003
Fe	1.498	2.358	2.374	2.359	2.371	1.16	2.437	2.39
Na	0.01	0.077	0.07	0.068	0.08	1.348	0.087	0.084
K	0	1.764	1.815	1.831	1.824	1.744	1.816	1.759
H	0	0	0	0	0	0	0	0
Total	14.072	15.61	15.647	15.649	15.677	15.664	15.679	15.617

Appendix 1D (cont.):
Microprobe Analysis of 1498 Ilmenite

Oxide Wt.%	Il4	Il5	Il6	Il7	Il8tch	Il9tch	Il10in	Il11in	Il12in	Il13in	Illin1	Illin2	Illin3	Il14in
SiO_2	0.063	0.052	0.027	0.088	0.073	1.026	0.045	0.051	0.168	0.589	0.202	1.959	0.067	0.029
TiO_2	52.487	52.571	51.777	51.575	52.209	51.279	52.473	52.398	52.798	52.612	51.397	49.299	50.808	52.286
Al_2O_3	0.008	0.01	0.035	0.045	0.041	0.604	0.016	0.038	0.005	0.002	0.019	0.965	0.001	0.007
MgO	0.242	0.19	0.433	0.429	0.035	0.063	0.125	0.162	0.033	0.019	0.251	1.182	0.269	0.579
CaO	0.013	0.014	0.007	0.011	0.039	0.063	0.019	0.072	0.032	0.035	0.098	0.085	0.08	0.034
MnO	0.219	0.239	0.217	0.248	0.511	0.479	1.638	1.698	2.5	2.521	0.844	0.758	0.857	0.589
FeO	43.885	43.393	44.445	44.733	45.453	43.707	44.351	44.178	42.232	41.556	46.818	45.913	46.335	45.431
Na_2O	0.004	0.028	0.029	0	0.004	0.004	0.017	0.007	0	0.019	0.004	0	0	0
Total	96.921	96.497	96.97	97.129	98.365	97.225	98.684	98.604	97.768	97.353	99.633	100.161	98.417	98.955
Cation based on 12 oxygens														
Si	0.007	0.005	0.003	0.009	0.007	0.105	0.005	0.005	0.017	0.06	0.021	0.195	0.007	0.003
Ti	4.071	4.09	4.027	4.009	4.017	3.943	4.022	4.018	4.063	4.048	3.928	3.687	3.935	3.995
Al	0.001	0.001	0.004	0.006	0.005	0.073	0.002	0.005	0.001	0	0.002	0.113	0	0.001
Mg	0.037	0.029	0.067	0.066	0.005	0.01	0.019	0.025	0.005	0.003	0.038	0.175	0.041	0.088
Ca	0.001	0.002	0.001	0.001	0.004	0.007	0.002	0.008	0.004	0.004	0.011	0.009	0.009	0.004
Mn	0.019	0.021	0.019	0.022	0.044	0.041	0.141	0.147	0.217	0.218	0.073	0.064	0.075	0.051
Fe	3.785	3.754	3.844	3.867	3.889	3.737	3.78	3.767	3.614	3.556	3.979	3.819	3.991	3.86
Na	0.001	0.006	0.006	0	0.001	0.001	0.003	0.001	0	0.004	0.001	0	0	0
Total	7.922	7.908	7.971	7.98	7.972	7.917	7.974	7.976	7.921	7.893	8.053	8.062	8.058	8.002

Oxide Wt.%	Il15in	Il16in	Il17in	Il18in	Il18inB	Il19in	Il20in	Il21	Il22	Il23	Il24	Il25	IlM
SiO_2	0.008	0.061	0.651	1.026	0.012	0.018	0.002	0.06	0.064	2.864	0.051	0.1	0.031
TiO_2	52.807	52.765	52.781	49.787	52.704	52.616	52.792	52.143	52.433	51.309	52.707	52.744	53.887
Al_2O_3	0.02	0.006	0.006	0.876	0.07	0.017	0.007	0	0.005	0.045	0.001	0.038	0.006
MgO	0.602	0.603	0.578	0.705	0.579	0.653	0.67	0.604	0.57	0.649	0.752	0.716	0.234
CaO	0.033	0.04	0.022	0.11	0.019	0.02	0.02	0.033	0.006	0.106	0.041	0.027	0.019
MnO	0.466	0.457	0.478	0.48	0.52	0.502	0.5	0.291	0.396	0.184	0.215	0.224	0.256
FeO	45.414	45.642	43.965	42.93	43.757	43.72	43.241	44.169	43.64	40.248	43.548	43.736	44.049
Na_2O	0	0	0.002	0.022	0	0	0	0.013	0.038	0.035	0.008	0.01	0.002
Total	99.35	99.574	98.483	95.936	97.661	97.546	97.232	97.313	97.152	95.44	97.323	97.595	98.484
Cation based on 12 oxygens													
Si	0.001	0.006	0.066	0.106	0.001	0.002	0	0.006	0.007	0.291	0.005	0.01	0.003
Ti	4.012	4.002	4.011	3.874	4.053	4.052	4.071	4.033	4.054	3.927	4.06	4.052	4.102
Al	0.002	0.001	0.001	0.107	0.008	0.002	0.001	0	0.001	0.005	0	0.005	0.001
Mg	0.091	0.091	0.087	0.109	0.088	0.1	0.102	0.093	0.087	0.099	0.115	0.109	0.035
Ca	0.004	0.004	0.002	0.012	0.002	0.002	0.002	0.004	0.001	0.012	0.005	0.003	0.002
Mn	0.04	0.039	0.041	0.042	0.045	0.044	0.043	0.025	0.035	0.016	0.019	0.019	0.022
Fe	3.837	3.849	3.715	3.715	3.743	3.744	3.708	3.799	3.752	3.426	3.731	3.737	3.729
Na	0	0	0	0.004	0	0	0	0.003	0.008	0.007	0.002	0.002	0
Total	7.987	7.992	7.923	7.969	7.94	7.946	7.927	7.963	7.945	7.783	7.937	7.937	7.894

Appendix 1D (cont.):
Microprobe Analysis of 1498 Staurolite

Oxide Wt.%	St2	St3
SiO_2	24.243	26.957
TiO_2	0.127	0.784
Al_2O_3	21.625	51.762
MgO	15.786	1.755
CaO	0.065	0.004
MnO	0.039	0.04
FeO	23.714	12.336
Na_2O	0.021	0.053
Total	85.62	93.691
Cation based on 12 oxygens		
Si	2.231	2.027
Ti	0.009	0.044
Al	2.345	4.586
Mg	2.166	0.197
Ca	0.006	0
Mn	0.003	0.003
Fe	1.825	0.776
Na	0.004	0.008
Total	8.589	7.641

Appendix IE:
Microprobe Analysis of 588 Garnet

Oxide Wt.%	GtRim1	GtRim2	GtRim5	GtRim6	GtCore1	GtCore2	GtCore3	GtCore4	Gt1	Gt2	588Gt12line1	588Gt12line1	588Gt12line1	588Gt12line1
SiO_2	37.883	37.783	37.788	37.331	37.845	37.669	37.825	37.848	37.515	37.859	37.991	37.866	37.897	60.939
TiO_2	0.007	0.019	0.021	0.019	0.02	0	0.035	0.041	0	0.023	0.131	0	0	0.021
Al_2O_3	21.192	21.234	20.978	21.018	21.267	21.288	21.134	21.281	21.001	21.143	21.287	21.254	21.247	14.562
MgO	3.977	4.011	3.921	3.963	4.234	4.168	4.282	4.181	4.007	4.04	3.856	4.079	4.22	2.306
CaO	2.074	2.06	1.999	1.822	2.062	1.8	2.056	2.43	2.223	2.141	2.03	2.022	1.961	1.336
MnO	1.527	1.114	1.826	2.641	2.444	2.668	2.206	2.44	2.452	2.381	0.906	1.046	1.149	0.946
FeO	34.277	34.401	34.147	34.569	33.314	33.339	33.363	32.856	33.04	32.918	35.679	34.595	34.75	22.173
Na_2O	0.038	0.004	0.018	0.01	0.013	0.025	0.011	0.011	0.02	0.013	0.015	0.039	0.025	0.21
Total	100.975	100.626	100.698	101.373	101.199	100.957	100.912	101.088	100.258	100.518	101.895	100.901	101.249	102.493
Cation based on 12 Oxygens														
Si	3.003	3.002	3.007	2.969	2.992	2.988	2.997	2.992	2.996	3.009	2.992	3.001	2.996	4.25
Ti	0	0.001	0.001	0.001	0.001	0	0.002	0.002	0	0.001	0.008	0	0	0.001
Al	1.98	1.988	1.967	1.97	1.982	1.99	1.974	1.983	1.977	1.98	1.976	1.985	1.979	1.197
Mg	0.47	0.475	0.465	0.47	0.499	0.493	0.506	0.493	0.477	0.479	0.453	0.482	0.497	0.24
Ca	0.176	0.175	0.17	0.155	0.175	0.153	0.175	0.206	0.19	0.182	0.171	0.172	0.166	0.1
Mn	0.103	0.075	0.123	0.178	0.164	0.179	0.148	0.163	0.166	0.16	0.06	0.07	0.077	0.056
Fe	2.272	2.286	2.272	2.3	2.203	2.212	2.211	2.173	2.207	2.188	2.35	2.293	2.297	1.293
Na	0.006	0.001	0.003	0.002	0.002	0.004	0.002	0.002	0.003	0.002	0.002	0.006	0.004	0.028
Total	8.01	8.003	8.008	8.045	8.018	8.019	8.015	8.014	8.016	8.001	8.012	8.009	8.016	7.165

Oxide Wt.%	588Gt12line1	588Gt12line1	588Gt12line1	588Gt12line1	588Gt12line1	588Gt12line1	588Gt12line1	588Gt12line1	588Gt12line1	588Gt12line1	588Gt12line1	588Gt12line1	588Gt12line1	588Gt12line1
SiO_2	37.736	37.87	37.608	37.576	37.963	37.485	37.991	35.368	96.596	37.682	37.533	60.783	67.256	62.034
TiO_2	0.003	0	0.024	0.001	0	0	0	0.001	0.028	0.017	0.042	0	0.01	0.001
Al_2O_3	21.308	21.145	21.202	20.968	21.055	20.973	20.562	20.338	0.298	21.068	21.018	24.805	21.795	23.601
MgO	4.061	3.928	3.782	3.875	3.806	3.755	3.93	2.864	0.067	3.818	3.808	0.003	0.021	0.002
CaO	1.733	1.993	2.143	2.232	1.73	1.862	1.729	1.719	0.231	1.721	1.889	6.741	5.887	5.512
MnO	1.758	1.839	1.897	2.129	2.238	2.329	2.484	2.731	0.04	2.522	2.469	0	0	0
FeO	34.398	34.282	33.551	33.752	34.058	33.832	34.043	35.086	0.838	34.651	34.207	0.37	0.274	0.292
Na_2O	0.02	0.048	0.041	0.012	0.014	0.019	0.021	0.055	0.225	0.035	0.004	7.814	6.47	8.619
Total	101.017	101.105	100.248	100.545	100.864	100.255	100.76	98.162	98.323	101.514	100.97	100.516	101.713	100.061
Cation based on 12 Oxygens														
Si	2.992	3.002	3.001	2.998	3.016	3	3.026	2.937	5.943	2.988	2.989	4.04	4.342	4.129
Ti	0	0	0.001	0	0	0	0	0	0.001	0.001	0.002	0	0	0
Al	1.991	1.975	1.994	1.971	1.971	1.978	1.931	1.99	0.022	1.969	1.973	1.943	1.658	1.851
Mg	0.48	0.464	0.45	0.461	0.451	0.448	0.467	0.355	0.006	0.451	0.452	0	0.002	0
Ca	0.147	0.169	0.183	0.191	0.147	0.16	0.148	0.153	0.015	0.146	0.161	0.48	0.407	0.393
Mn	0.118	0.123	0.128	0.144	0.151	0.158	0.168	0.192	0.002	0.169	0.167	0	0	0
Fe	2.281	2.273	2.239	2.252	2.262	2.265	2.268	2.437	0.043	2.298	2.278	0.021	0.015	0.016
Na	0.003	0.007	0.006	0.002	0.002	0.003	0.003	0.009	0.027	0.005	0.001	1.007	0.81	1.112
Total	8.012	8.013	8.002	8.019	8	8.012	8.011	8.073	6.059	8.027	8.023	7.491	7.234	7.501

Oxide Wt.%	588Gt12line1	588Gt12line1	588Gt12line1	588Gt12line1	588Gt12line1	588Gt12line1	588Gt12line1	588Gt12line1	588Gt12line1	588Gt12line1	588Gt12line1	588Gt12line1	588Gt12line1	588Gt12line1
SiO_2	83.252	73.022	37.796	37.318	37.752	37.776	37.494	37.321	37.312	37.609	40.687	71.913	37.824	37.499
TiO_2	0	0.005	0.02	0.031	0.005	0.028	0.063	0	0.004	0	0.007	0.013	0	0.023
Al_2O_3	9.464	10.565	21.279	20.961	21.015	20.802	21.041	21.087	20.734	21.187	20.398	9.832	21.345	21.188
MgO	0.114	0.94	3.854	3.845	3.751	3.761	3.756	3.787	3.801	3.768	3.417	1.599	3.902	3.429
CaO	2.279	1.062	1.935	2.058	2.34	2.384	2.095	1.615	1.506	1.436	1.381	1.061	1.845	1.986
MnO	0.038	0.945	2.333	2.32	2.335	2.255	2.298	2.568	2.535	2.361	2.008	0.65	1.245	1.108
FeO	0.761	13.86	33.974	33.642	34.037	33.546	34.109	34.545	34.258	34.499	33.136	15.973	34.572	35.459
Na_2O	2.988	0.274	0.027	0.017	0.01	0.012	0	0.044	0.033	0	0.1	0.372	0.009	0.024
Total	98.896	100.673	101.218	100.192	101.245	100.564	100.856	100.967	100.183	100.86	101.134	101.413	100.742	100.716
Cation based on 12 Oxygens														
Si	5.274	4.87	2.994	2.99	2.996	3.012	2.988	2.978	2.997	2.995	3.18	4.821	3.003	2.993
Ti	0	0	0.001	0.002	0	0.002	0.004	0	0	0	0	0.001	0	0.001
Al	0.707	0.83	1.987	1.979	1.965	1.955	1.976	1.983	1.963	1.989	1.879	0.777	1.997	1.993
Mg	0.011	0.093	0.455	0.459	0.444	0.447	0.446	0.45	0.455	0.447	0.398	0.16	0.462	0.408
Ca	0.155	0.076	0.164	0.177	0.199	0.204	0.179	0.138	0.13	0.123	0.116	0.076	0.157	0.17
Mn	0.002	0.053	0.157	0.157	0.157	0.152	0.155	0.174	0.172	0.159	0.133	0.037	0.084	0.075
Fe	0.04	0.773	2.251	2.254	2.259	2.237	2.273	2.305	2.301	2.298	2.166	0.895	2.295	2.367
Na	0.367	0.035	0.004	0.003	0.002	0.002	0	0.007	0.005	0	0.015	0.048	0.001	0.004
Total	6.556	6.73	8.013	8.021	8.022	8.011	8.021	8.035	8.023	8.011	7.887	6.815	7.999	8.011

Appendix IE (cont.):
Microprobe Analysis of 588 Garnet (cont.)

Oxide Wt.%	588Gt1line1	588Gt1line1	588Gt1line1	588Gt1line1	588Gt1line1	588Gt1line1	588Gt1line1	588Gt1line1	588Gt1line1	588Gt1line1	588Gt1line1	588Gt1line1	588Gt1line1	588Gt1line1
SiO_2	37.728	37.716	37.742	37.75	37.621	37.769	37.731	37.592	37.858	37.886	37.839	97.655	52.566	37.678
TiO_2	0.008	0	0.038	0	0	0.005	0.003	0	0.004	0.021	0.008	0.033	0.034	0
Al_2O_3	21.345	21.022	21.191	21.315	21.118	21.265	21.078	21.198	21.103	21.28	21.251	0.449	16.771	21.15
MgO	3.899	4.032	3.95	3.673	3.854	3.835	4.082	4.062	4.1	4.18	4.217	0.124	2.748	4.442
CaO	2.037	1.896	1.813	2.677	1.264	1.308	1.335	1.373	1.368	1.459	1.589	0.254	1.598	1.842
MnO	1.037	1.379	1.554	1.788	2.379	2.435	2.476	2.366	2.326	2.307	2.312	0.04	1.723	2.394
FeO	35.709	35.236	35.004	34.16	34.857	35.157	34.908	34.725	35.077	34.212	33.816	1.323	25.893	33.078
Na_2O	0.011	0.03	0.022	0.045	0.009	0.004	0.014	0.02	0.025	0	0.037	0.352	0.264	0.009
Total	101.774	101.311	101.314	101.408	101.102	101.778	101.627	101.336	101.861	101.345	101.069	100.23	101.597	100.593
Cation based on 12 Oxygens														
Si	2.979	2.991	2.991	2.987	2.993	2.987	2.988	2.982	2.99	2.995	2.997	5.916	3.846	2.993
Ti	0	0	0.002	0	0	0	0	0	0	0.001	0	0.001	0.002	0
Al	1.987	1.965	1.979	1.988	1.98	1.982	1.967	1.982	1.964	1.983	1.984	0.032	1.446	1.98
Mg	0.459	0.477	0.467	0.433	0.457	0.452	0.482	0.48	0.483	0.493	0.498	0.011	0.3	0.526
Ca	0.172	0.161	0.154	0.227	0.108	0.111	0.113	0.117	0.116	0.124	0.135	0.016	0.125	0.157
Mn	0.069	0.093	0.104	0.12	0.16	0.163	0.166	0.159	0.156	0.154	0.155	0.002	0.107	0.161
Fe	2.358	2.337	2.32	2.261	2.319	2.325	2.312	2.304	2.317	2.262	2.24	0.067	1.584	2.198
Na	0.002	0.005	0.003	0.007	0.001	0.001	0.002	0.003	0.004	0	0.006	0.041	0.037	0.001
Total	8.026	8.029	8.02	8.023	8.018	8.021	8.03	8.027	8.03	8.012	8.015	6.086	7.447	8.016

Oxide Wt.%	588Gt1line1	588Gt1line1	588Gt1line1	588Gt1line1	588Gt1line1	588Gt1line1	588Gt1line1	588Gt1line1	588Gt1line1	588Gt1line1	588Gt1line1	588Gt1line1	588Gt1line1	588Gt1line1
SiO_2	38.068	38.116	37.899	37.82	41.785	38.23	37.866	37.738	37.811	96.269	38.171	37.594	37.841	41.552
TiO_2	0	0.001	0.035	0	0	0.035	0.038	0	0	0.008	0.02	0.018	0	0.007
Al_2O_3	21.185	21.156	21.215	21.176	19.868	21.249	21.01	21.195	21.111	0.679	21.241	20.87	21.072	20.26
MgO	4.387	4.306	4.313	4.431	3.874	4.229	4.289	4.293	4.152	0.128	4.09	4.219	4.088	3.648
CaO	1.802	2.165	2.147	1.999	1.93	2.019	1.869	1.632	1.573	0.38	1.728	1.896	2.016	2.007
MnO	2.559	2.411	2.456	2.604	2.502	2.781	2.776	2.669	2.801	0.063	2.725	2.818	2.662	2.553
FeO	33.459	33.325	33.153	33.309	31.836	33.375	33.407	33.334	33.63	1.337	33.272	33.481	33.111	31.756
Na_2O	0.024	0.017	0.003	0.042	0.021	0.001	0.017	0.001	0.056	0.49	0.019	0.019	0.023	0.057
Total	101.484	101.497	101.221	101.381	101.816	101.919	101.272	100.862	101.134	99.354	101.266	100.915	100.813	101.84
Cation based on 12 Oxygens														
Si	3.001	3.003	2.994	2.987	3.229	3.002	2.997	2.994	2.998	5.894	3.013	2.991	3.004	3.211
Ti	0	0	0.002	0	0	0.002	0.002	0	0	0	0.001	0.001	0	0
Al	1.968	1.965	1.975	1.971	1.809	1.967	1.96	1.982	1.972	0.049	1.976	1.957	1.972	1.845
Mg	0.516	0.506	0.508	0.522	0.446	0.495	0.506	0.508	0.491	0.012	0.481	0.5	0.484	0.42
Ca	0.152	0.183	0.182	0.169	0.16	0.17	0.158	0.139	0.134	0.025	0.146	0.162	0.171	0.166
Mn	0.171	0.161	0.164	0.174	0.164	0.185	0.186	0.179	0.188	0.003	0.182	0.19	0.179	0.167
Fe	2.206	2.196	2.19	2.2	2.057	2.192	2.211	2.212	2.23	0.068	2.196	2.228	2.198	2.052
Na	0.004	0.003	0	0.006	0.003	0	0.003	0	0.009	0.058	0.003	0.003	0.004	0.009
Total	8.018	8.017	8.015	8.029	7.868	8.013	8.023	8.014	8.022	6.109	7.998	8.032	8.012	7.87

Oxide Wt.%	588Gt1line1	588Gt1line1	588Gt1line1	588Gt1line1	588Gt1line1	588Gt1line1	588Gt1line1	588Gt1line1	588Gt1line1	588Gt1line1	588Gt1line1	588Gt1line1	Gt1(4)	Gt1(6)
SiO_2	37.715	37.754	37.697	37.744	37.693	37.539	37.697	37.894	91.474	37.634	39.484	37.707	37.654	37.886
TiO_2	0.028	0	0.029	0.007	0	0.008	0.01	0.011	0.002	0	0	0.004	0.032	0.017
Al_2O_3	21.168	21.143	21.147	21.249	21.332	21.176	21.25	21.261	3.197	21.183	21.581	21.069	21.084	21.251
MgO	4.173	4.168	4.132	4.095	4.044	4.088	3.954	4.022	0.388	3.972	3.449	3.914	4.117	4.205
CaO	2.015	2	1.915	1.758	1.528	1.493	1.483	1.421	0.341	2.027	2.312	1.961	2.038	2.232
MnO	2.781	2.771	2.515	2.497	2.651	2.692	2.615	2.158	0.193	1.867	1.82	1.717	0.856	2.301
FeO	33.304	33.304	33.401	33.777	33.934	34.186	34.548	34.819	3.63	34.157	33.152	34.185	34.9	33.555
Na_2O	0.038	0.007	0.014	0.016	0.023	0.029	0.013	0	0.355	0.05	0.024	0.03	0	0.019
Total	101.222	101.147	100.85	101.143	101.205	101.211	101.57	101.586	99.58	100.89	101.822	100.587	100.681	101.466
Cation based on 12 Oxygens														
Si	2.987	2.991	2.994	2.991	2.987	2.981	2.984	2.994	5.685	2.991	3.076	3.003	2.995	2.99
Ti	0.002	0	0.002	0	0	0	0.001	0.001	0	0	0	0	0.002	0.001
Al	1.976	1.974	1.979	1.985	1.993	1.982	1.983	1.98	0.234	1.984	1.982	1.978	1.977	1.977
Mg	0.493	0.492	0.489	0.484	0.478	0.484	0.467	0.474	0.036	0.471	0.401	0.465	0.488	0.495
Ca	0.171	0.17	0.163	0.149	0.13	0.127	0.126	0.12	0.023	0.173	0.193	0.167	0.174	0.189
Mn	0.187	0.186	0.169	0.168	0.178	0.181	0.175	0.144	0.01	0.126	0.12	0.116	0.058	0.154
Fe	2.206	2.207	2.218	2.238	2.249	2.27	2.287	2.301	0.189	2.27	2.16	2.277	2.322	2.215
Na	0.006	0.001	0.002	0.002	0.004	0.004	0.002	0	0.043	0.008	0.004	0.005	0	0.003
Total	8.028	8.021	8.016	8.017	8.019	8.029	8.025	8.014	6.22	8.023	7.936	8.011	8.016	8.024

Appendix IE (cont.):
Microprobe Analysis of 588 Garnet (cont.)

Oxide Wt.%	Gt1(7)	Gt1(8)	Gt1(9)	Gt1(10)	Gt1(11)	Gt1(12)	Gt1(13)	GRim1	GRim2	Gt3	Gt4	Gt5	Gt6	Gt7
SiO_2	36.871	37.445	37.858	37.076	37.769	37.771	37.747	37.795	37.666	37.301	36.954	37.058	37.719	36.929
TiO_2	0.02	0	0.004	0	0.007	0.02	0.009	0.026	0.029	0.095	0.08	0.063	0.268	0.276
Al_2O_3	20.829	21.046	21.096	21.017	20.88	21.214	21.268	21.258	21.105	20.72	20.475	20.788	21.033	20.699
MgO	4.083	4.086	4.072	4.011	4.065	4.362	4.304	3.615	3.827	3.793	3.825	3.908	3.68	3.649
CaO	2.106	2.248	1.788	1.89	1.859	1.866	1.796	2.15	2.039	2.113	2.012	2.13	2.102	2.517
MnO	2.416	2.569	2.276	2.314	2.545	2.463	2.485	0.826	0.99	0.958	0.98	0.954	0.976	1.144
FeO	32.87	32.898	34.06	33.307	34.393	33.288	33.57	34.616	34.765	35.203	34.543	34.988	34.542	34.726
Na_2O	0.008	0.013	0.054	0.031	0.003	0.022	0	0.029	0	0.006	0.043	0.041	0	0
Total	99.203	100.305	101.208	99.646	101.521	101.006	101.179	100.421	99.263	100.189	98.912	99.93	100.32	99.94
Cation based on 12 Oxygens														
Si	2.98	2.99	2.999	2.983	2.993	2.991	2.987	3.012	3.003	2.993	2.999	2.981	3.008	2.974
Ti	0.001	0	0	0	0	0.001	0.001	0.002	0.002	0.006	0.005	0.004	0.016	0.017
Al	1.984	1.98	1.97	1.993	1.95	1.98	1.984	1.997	1.983	1.959	1.959	1.971	1.977	1.965
Mg	0.492	0.486	0.481	0.481	0.48	0.515	0.508	0.429	0.455	0.454	0.463	0.469	0.438	0.438
Ca	0.182	0.192	0.152	0.163	0.158	0.158	0.152	0.184	0.174	0.182	0.175	0.184	0.18	0.217
Mn	0.165	0.174	0.153	0.158	0.171	0.165	0.167	0.056	0.067	0.065	0.067	0.065	0.066	0.078
Fe	2.222	2.197	2.257	2.241	2.279	2.205	2.222	2.307	2.318	2.362	2.345	2.354	2.304	2.339
Na	0.001	0.002	0.008	0.005	0	0.003	0	0.005	0	0.001	0.007	0.006	0	0
Total	8.027	8.021	8.02	8.024	8.031	8.018	8.021	7.992	8.002	8.022	8.02	8.034	7.989	8.028

Oxide Wt.%	Gt8	Gt9	Gt10	Gt11	Gt12	Gt13	Gt15	Gt16	Gt17	Gt18	Gt19	Gt20	588Gt4line1	588Gt4line1
SiO_2	37.342	36.992	36.885	36.971	36.559	37.361	37.523	38.182	37.408	37.313	37.385	37.012	38.39	37.991
TiO_2	0.038	0.438	0.489	0.006	0.007	0	0	0.034	0	0.019	0.036	0.005	0	0
Al_2O_3	20.984	20.723	20.763	20.861	20.561	21.076	20.785	21.288	20.866	20.579	20.603	20.653	21.484	21.063
MgO	3.79	3.716	3.748	3.907	3.79	3.876	3.755	3.66	3.751	3.76	3.587	3.812	3.924	4.157
CaO	2.068	2.153	2.113	1.565	1.453	2.048	2.005	2.072	1.889	1.697	2.089	2.109	1.961	1.946
MnO	1.279	2.389	2.325	2.491	2.427	0.999	2.313	0.996	1.816	1.941	1.039	1.048	1.029	1.224
FeO	35.155	33.945	34.016	34.365	34.068	34.66	34.052	35.273	34.847	34.862	35.026	34.956	34.528	34.502
Na_2O	0.016	0	0.004	0	0.009	0	0.033	0.021	0.017	0.002	0.029	0.031	0.009	0.016
Total	100.672	100.356	100.343	100.166	98.874	100.02	100.466	101.526	100.594	100.173	99.794	99.626	101.325	100.899
Cation based on 12 Oxygens														
Si	2.983	2.969	2.961	2.974	2.98	2.993	3.002	3.013	2.992	3	3.01	2.988	3.021	3.011
Ti	0.002	0.026	0.029	0	0	0	0	0.002	0	0.001	0.002	0	0	0
Al	1.976	1.96	1.964	1.978	1.975	1.99	1.96	1.98	1.967	1.95	1.955	1.965	1.993	1.967
Mg	0.451	0.445	0.448	0.468	0.46	0.463	0.448	0.431	0.447	0.451	0.431	0.459	0.46	0.491
Ca	0.177	0.185	0.182	0.135	0.127	0.176	0.172	0.175	0.162	0.146	0.18	0.182	0.165	0.165
Mn	0.087	0.162	0.158	0.17	0.168	0.068	0.157	0.067	0.123	0.132	0.071	0.072	0.069	0.082
Fe	2.349	2.278	2.284	2.312	2.322	2.322	2.278	2.327	2.331	2.344	2.359	2.36	2.273	2.287
Na	0.002	0	0.001	0	0.001	0	0.005	0.003	0.003	0	0.005	0.005	0.001	0.003
Total	8.027	8.025	8.027	8.037	8.033	8.012	8.022	7.998	8.025	8.024	8.013	8.031	7.982	8.006

Oxide Wt.%	588Gt4line1	588Gt4line1	588Gt4line1	588Gt4line1	588Gt4line1	588Gt4line1	588Gt4line1	588Gt4line1	588Gt4line1	588Gt4line1	588Gt4line1	588Gt4line1	588Gt4line1	588Gt4line1
SiO_2	38.003	38.252	37.832	37.726	37.621	38.194	38.29	37.665	46.292	38.003	37.534	37.745	37.76	40.484
TiO_2	0.016	0.001	0	0.004	0	0.009	0.015	0.014	0	0.022	0.003	0.035	0.018	0.017
Al_2O_3	21.106	21.228	21.05	20.827	20.897	21.058	21.153	20.864	17.185	20.914	21.022	20.966	20.891	19.34
MgO	4	4.08	3.967	3.902	3.928	3.947	3.957	3.955	3.477	3.843	3.842	3.737	3.771	3.225
CaO	1.912	1.996	2.174	1.997	2.077	2.006	1.493	1.58	1.43	1.648	1.698	1.695	1.731	1.786
MnO	1.196	1.23	1.389	1.498	1.628	1.571	1.892	1.905	1.719	1.998	2.082	1.871	2.126	1.957
FeO	34.863	33.992	33.94	34.138	33.941	34.558	34.26	34.624	29.138	34.283	34.433	34.535	34.448	32.467
Na_2O	0.025	0.004	0.038	0.026	0.055	0.02	0.034	0.006	0.123	0.026	0.008	0.034	0.026	0.098
Total	101.121	100.783	100.39	100.118	100.147	101.363	101.094	100.613	99.364	100.737	100.622	100.618	100.771	99.374
Cation based on 12 Oxygens														
Si	3.009	3.025	3.012	3.017	3.008	3.017	3.027	3.005	3.57	3.022	2.996	3.01	3.009	3.221
Ti	0.001	0	0	0	0	0.001	0.001	0.001	0	0.001	0	0.002	0.001	0.001
Al	1.97	1.979	1.975	1.963	1.969	1.96	1.971	1.962	1.562	1.96	1.977	1.97	1.962	1.814
Mg	0.472	0.481	0.471	0.465	0.468	0.465	0.466	0.47	0.4	0.456	0.457	0.444	0.448	0.383
Ca	0.162	0.169	0.185	0.171	0.178	0.17	0.126	0.135	0.118	0.14	0.145	0.145	0.148	0.152
Mn	0.08	0.082	0.094	0.101	0.11	0.105	0.127	0.129	0.112	0.135	0.141	0.126	0.144	0.132
Fe	2.309	2.248	2.26	2.283	2.27	2.283	2.265	2.31	1.879	2.28	2.298	2.303	2.296	2.161
Na	0.004	0.001	0.006	0.004	0.008	0.003	0.005	0.001	0.018	0.004	0.001	0.005	0.004	0.015
Total	8.007	7.985	8.003	8.004	8.011	8.004	7.988	8.013	7.659	7.998	8.015	8.005	8.012	7.879

Appendix IE (cont.):
Microprobe Analysis of 588 Garnet (cont.)

Oxide Wt.%	588Gt4line1	588Gt4line1	588Gt4line1	588Gt4line1	588Gt4line1	588Gt4line1	588Gt4line1	588Gt4line1	588Gt4line1	588Gt4line1	588Gt4line1	588Gt4line1	588Gt4line1	588Gt4line1
SiO_2	37.663	37.653	37.002	54.928	41.209	37.93	37.51	37.316	40.534	37.537	37.571	37.613	37.529	37.431
TiO_2	0.04	0.011	0.013	0.007	0.018	0	0.017	0	0.007	0.002	0.006	0.014	0	0.033
Al_2O_3	20.838	20.773	20.755	15.274	19.231	20.786	20.888	20.846	19.418	20.801	20.639	20.812	20.705	20.653
MgO	3.759	3.628	2.208	3.097	3.829	3.803	3.654	3.651	3.224	3.712	3.776	3.704	3.676	3.734
CaO	1.916	1.924	1.976	1.47	1.872	1.968	2.001	1.985	1.845	1.949	2.046	1.975	2.046	1.949
MnO	2.136	2.034	2.282	1.442	1.772	2.017	1.92	1.935	1.691	1.949	1.879	1.886	1.847	1.84
FeO	33.885	34.43	36.032	25.065	31.976	34.517	34.388	34.578	32.69	35.046	34.527	35.055	34.391	34.856
Na_2O	0	0.021	0.018	0.192	0.057	0.019	0.018	0.014	0.052	0.021	0.021	0.003	0.014	0.009
Total	100.237	100.474	100.286	101.475	99.964	101.04	100.396	100.325	99.461	101.017	100.465	101.062	100.208	100.505
Cation based on 12 Oxygens														
Si	3.012	3.011	2.996	3.984	3.244	3.015	3.001	2.993	3.221	2.994	3.007	2.997	3.009	2.999
Ti	0.002	0.001	0.001	0	0.001	0	0.001	0	0	0	0	0.001	0	0.002
Al	1.964	1.958	1.981	1.306	1.784	1.947	1.97	1.97	1.819	1.955	1.947	1.955	1.956	1.95
Mg	0.448	0.433	0.267	0.335	0.449	0.451	0.436	0.437	0.382	0.441	0.45	0.44	0.439	0.446
Ca	0.164	0.165	0.171	0.114	0.158	0.168	0.172	0.171	0.157	0.167	0.175	0.169	0.176	0.167
Mn	0.145	0.138	0.156	0.089	0.118	0.136	0.13	0.131	0.114	0.132	0.127	0.127	0.125	0.125
Fe	2.267	2.303	2.44	1.521	2.105	2.294	2.301	2.319	2.172	2.338	2.311	2.336	2.306	2.335
Na	0	0.003	0.003	0.027	0.009	0.003	0.003	0.002	0.008	0.003	0.003	0	0.002	0.001
Total	8.002	8.012	8.015	7.376	7.868	8.014	8.014	8.023	7.873	8.03	8.02	8.025	8.013	8.025

Oxide Wt.%	588Gt4line1	588Gt4line1	588Gt4line1	588Gt4line1	588Gt4line1	588Gt4line1	588Gt4line1	588Gt4line1	588Gt4line1	588Gt4line1	588Gt4line1	588Gt4line1	588Gt4line1	588Gt4line1
SiO_2	37.253	37.139	37.42	36.908	37.499	38.078	37.161	36.541	37.014	36.731	37.069	36.919	36.776	36.577
TiO_2	0	0	0.045	0.038	0.003	0.026	0	0.022	0.045	0	0	0.006	0	0.01
Al_2O_3	20.636	20.473	20.776	20.825	20.725	21.054	20.58	20.381	20.618	20.475	20.566	20.657	20.676	20.737
MgO	3.751	3.741	3.756	3.686	3.731	3.697	3.747	3.717	3.765	3.76	3.844	3.797	3.777	3.789
CaO	1.849	1.864	1.822	1.847	1.902	1.871	2.033	1.861	1.787	1.958	1.886	1.679	1.744	1.785
MnO	1.904	1.912	1.974	1.921	1.898	1.92	1.912	1.918	1.91	1.95	1.838	1.971	1.984	2.086
FeO	34.392	34.595	34.608	34.752	34.553	34.596	34.235	34.205	34.357	34.008	34.289	34.661	34.733	34.945
Na_2O	0.031	0.027	0.021	0.031	0.019	0.015	0.035	0.036	0.015	0.019	0	0.014	0.025	0.014
Total	99.816	99.751	100.422	100.008	100.33	101.257	99.703	98.681	99.511	98.901	99.492	99.704	99.715	99.943
Cation based on 12 Oxygens														
Si	3.001	2.999	2.997	2.975	3.005	3.016	2.998	2.984	2.992	2.989	2.996	2.983	2.975	2.958
Ti	0	0	0.003	0.002	0	0.002	0	0.001	0.003	0	0	0	0	0.001
Al	1.959	1.948	1.961	1.978	1.957	1.965	1.957	1.962	1.964	1.964	1.959	1.967	1.971	1.976
Mg	0.45	0.45	0.448	0.443	0.446	0.436	0.451	0.452	0.454	0.456	0.463	0.457	0.455	0.457
Ca	0.16	0.161	0.156	0.159	0.163	0.159	0.176	0.163	0.155	0.171	0.163	0.145	0.151	0.155
Mn	0.13	0.131	0.134	0.131	0.129	0.129	0.131	0.133	0.131	0.134	0.126	0.135	0.136	0.143
Fe	2.317	2.336	2.318	2.342	2.315	2.292	2.31	2.336	2.323	2.314	2.318	2.342	2.35	2.363
Na	0.005	0.004	0.003	0.005	0.003	0.002	0.005	0.006	0.002	0.003	0	0.002	0.004	0.002
Total	8.022	8.029	8.02	8.035	8.018	8.001	8.028	8.037	8.024	8.031	8.025	8.031	8.042	8.055

Oxide Wt.%	588Gt4line1	588Gt4line1	588Gt4line1	588Gt4line1	588Gt4line1	588Gt4line1	588Gt4line1	588Gt4line1	588Gt4line1	588Gt4line1	588Gt4line1	588Gt4line1	588Gt4line1	588Gt4line1
SiO_2	37.208	37.45	36.91	37.534	36.593	37.13	36.688	36.91	37.058	36.963	37.689	37.72	37.218	37.583
TiO_2	0.034	0.012	0	0	0.031	0.007	0	0.022	0.023	0.027	0.015	0.016	0.004	0
Al_2O_3	20.853	20.571	20.705	20.713	20.791	20.923	20.71	20.594	20.63	20.476	20.959	20.883	20.932	20.91
MgO	3.824	3.837	3.81	3.754	3.78	3.749	3.804	3.75	3.911	4.035	4.048	3.943	4.049	4.068
CaO	1.7	1.792	1.671	1.656	1.614	1.666	1.676	1.588	1.574	1.479	1.545	1.929	1.633	1.919
MnO	2.084	2.025	1.901	1.898	2.114	2.051	1.915	1.784	1.775	1.768	1.609	1.523	1.353	1.164
FeO	34.49	34.217	34.195	34.506	34.298	34.247	34.143	34.493	34.84	34.491	34.851	34.733	34.742	35.163
Na_2O	0.028	0.023	0.035	0.005	0.016	0.008	0.009	0.009	0.012	0.012	0.013	0.009	0.026	0.019
Total	100.221	99.927	99.227	100.066	99.237	99.781	98.945	99.15	99.823	99.251	100.729	100.756	99.957	100.826
Cation based on 12 Oxygens														
Si	2.987	3.011	2.99	3.012	2.97	2.99	2.982	2.994	2.989	2.995	3.002	3.004	2.988	2.993
Ti	0.002	0.001	0	0	0.002	0	0	0.001	0.001	0.002	0.001	0.001	0	0
Al	1.973	1.949	1.977	1.959	1.989	1.986	1.984	1.969	1.961	1.955	1.967	1.96	1.981	1.963
Mg	0.458	0.46	0.46	0.449	0.457	0.45	0.461	0.454	0.47	0.487	0.481	0.468	0.485	0.483
Ca	0.146	0.154	0.145	0.142	0.14	0.144	0.146	0.138	0.136	0.128	0.132	0.165	0.14	0.164
Mn	0.142	0.138	0.13	0.129	0.145	0.14	0.132	0.123	0.121	0.121	0.109	0.103	0.092	0.079
Fe	2.315	2.3	2.317	2.316	2.328	2.306	2.321	2.34	2.35	2.337	2.321	2.313	2.333	2.342
Na	0.004	0.004	0.005	0.001	0.003	0.001	0.001	0.001	0.002	0.002	0.002	0.001	0.004	0.003
Total	8.027	8.017	8.024	8.008	8.034	8.017	8.027	8.02	8.03	8.027	8.015	8.015	8.023	8.027

Appendix IE (cont.):
Microprobe Analysis of 588 Garnet (cont.)

Oxide Wt.%	588Gt4line1	588Gt4line1	588Gt4line1	588Gt4line1	588Gt4line1	588Gt4line1	588Gt4line1	588Gt4line1	588Gt4line1	588Gt4line1	588Gt4line1
SiO_2	37.199	37.5	37.115	37.263	37.511	37.688	37.511	37.574	37.291	37.794	37.73
TiO_2	0	0	0.024	0.021	0	0.013	0	0.004	0	0.007	0.003
Al_2O_3	20.724	21.047	20.838	21.129	21.076	20.904	21.097	20.432	21.067	20.553	21.082
MgO	3.66	4.1	4.031	4.177	4.19	4.083	4.148	4.066	4.026	4.113	3.723
CaO	2.064	2.033	1.833	1.576	1.711	1.912	1.879	1.854	1.992	2.16	2.084
MnO	1.11	1.164	1.092	1.086	1.075	1.077	1.048	0.955	0.901	0.965	0.942
FeO	35.438	34.704	34.971	34.297	35.137	34.817	34.791	34.575	35.097	34.436	35.158
Na_2O	0.006	0.044	0.036	0.008	0	0.008	0.009	0.065	0.012	0.003	0.016
Total	100.201	100.592	99.94	99.557	100.7	100.502	100.483	99.525	100.386	100.031	100.738
Cation based on 12 Oxygens											
Si	2.99	2.989	2.983	2.992	2.988	3.005	2.991	3.024	2.982	3.024	3.004
Ti	0	0	0.001	0.001	0	0.001	0	0	0	0	0
Al	1.963	1.977	1.974	2	1.979	1.964	1.982	1.938	1.985	1.938	1.978
Mg	0.439	0.487	0.483	0.5	0.498	0.485	0.493	0.488	0.48	0.491	0.442
Ca	0.178	0.174	0.158	0.136	0.146	0.163	0.16	0.16	0.171	0.185	0.178
Mn	0.076	0.079	0.074	0.074	0.073	0.073	0.071	0.065	0.061	0.065	0.064
Fe	2.382	2.313	2.351	2.303	2.341	2.321	2.32	2.327	2.347	2.304	2.341
Na	0.001	0.007	0.006	0.001	0	0.001	0.001	0.01	0.002	0	0.003
Total	8.029	8.026	8.03	8.007	8.025	8.013	8.018	8.012	8.028	8.007	8.01

Appendix IE (cont.):
Microprobe Analysis of 588 Feldspar

Oxide Wt.%	Feldin1	Feldin2	Feldin3	Feldin4	Feldin5	Feldin6	Feldin7	Feldin8	Feldin9	Feldin10	FeldRim1	FeldRim2
SiO2	59.879	62.336	59.876	62.543	61.472	60.224	100.598	79.219	61.907	63.318	100.106	100.538
Al2O3	24.762	23.801	25.041	23.364	23.619	24.391	0.015	6.648	23.363	22.173	0.011	0.005
CaO	6.997	5.487	7.114	3.937	5.721	6.12	0.013	1.883	6.378	5.852	0.03	0.014
FeO	0.343	0.35	0.297	0.856	0.198	0.453	0.345	0.547	0.507	0.522	0.161	0.315
Na2O	7.883	8.635	7.813	8.347	8.533	8.338	0	1.745	7.681	7.375	0	0.034
K2O	0.062	0.094	0.047	0.797	0.114	0.073	0.008	0.285	0.189	0.156	0	0
Total	99.926	100.703	100.188	99.844	99.657	99.599	100.979	90.327	100.025	99.396	100.308	100.906
Cation based on 8 oxygens												
Si	2.676	2.75	2.669	2.781	2.742	2.697	3.993	3.631	2.752	2.817	3.996	3.994
Al	1.304	1.237	1.315	1.224	1.242	1.287	0.001	0.359	1.224	1.163	0.001	0
Ca	0.335	0.259	0.34	0.188	0.273	0.294	0.001	0.092	0.304	0.279	0.001	0.001
Fe	0.013	0.013	0.011	0.032	0.007	0.017	0.011	0.021	0.019	0.019	0.005	0.01
Na	0.683	0.739	0.675	0.72	0.738	0.724	0	0.155	0.662	0.636	0	0.003
K	0.004	0.005	0.003	0.045	0.006	0.004	0	0.017	0.011	0.009	0	0
Total	5.015	5.003	5.013	4.99	5.008	5.023	4.006	4.275	4.972	4.923	4.003	4.008

Appendix IE (cont.):
Microprobe Analysis of 588 Biotite

Oxide Wt.%	Mrim2	Mrim3	Mrim4
SiO_2	36.881	36.584	36.559
TiO_2	2.039	1.923	1.907
Al_2O_3	19.264	18.679	19.046
MgO	11.201	11.415	11.607
CaO	0.036	0.074	0.046
MnO	0.049	0.031	0.018
FeO	17.206	17.58	17.157
Na_2O	0.359	0.415	0.301
K_2O	8.94	8.969	9.006
H_2O	4.037	4.008	4.018
Total	100.012	99.678	99.665
Cation based on 22 oxygens			
Si	5.478	5.474	5.456
Ti	0.228	0.216	0.214
Al	3.373	3.294	3.35
Mg	2.48	2.546	2.582
Ca	0.006	0.012	0.007
Mn	0.006	0.004	0.002
Fe	2.137	2.2	2.141
Na	0.104	0.12	0.087
K	1.694	1.712	1.715
H	0	0	0
Total	15.506	15.578	15.554

Appendix IE (cont.):
Microprobe Analysis of 588 Ilmenite

Oxide Wt.%	Il1	Il2	Il3	Il4	Il5	Il6	Il7	Il8	Il9	Il10	Il11	Il12	Il13	Il14
SiO2	0.061	0.031	0.552	0.059	0.08	0.222	0.244	0.306	0.13	0.058	0.099	0.126	0.097	0.099
TiO2	52.434	53.015	51.508	52.878	52.634	52.876	52.878	51.622	52.386	52.693	52.54	51.932	52.165	52.425
Al2O3	0.02	0.045	0.095	0.056	0.017	0.017	0.023	0.008	0.081	0.018	0.081	0.079	0.041	0.02
MgO	0.807	0.827	0.494	0.797	0.784	0.854	0.869	0.254	0.328	0.242	0.352	0.115	0.586	0.302
CaO	0.011	0.016	0.069	0.004	0.027	0.012	0.026	0.069	0.01	0	0	0	0	0.002
MnO	0.24	0.286	0.576	0.303	0.345	0.307	0.263	0.491	0.267	0.222	0.263	0.293	0.257	0.265
FeO	45.666	45.919	45.838	45.731	46.923	45.983	45.578	46.074	46.308	46.234	46.778	46.95	46.869	46.078
Na2O	0.024	0.004	0.021	0.034	0.025	0.004	0	0	0.002	0	0.021	0.027	0	0.004
Total	99.817	100.143	99.153	99.862	100.835	100.275	99.881	98.824	99.512	99.467	100.134	99.522	100.015	99.195
Cation based on 12 oxygens														
Si	0.006	0.003	0.056	0.006	0.008	0.022	0.024	0.031	0.013	0.006	0.01	0.013	0.01	0.01
Ti	3.988	3.994	3.926	3.994	3.955	3.976	3.986	3.959	3.984	4.009	3.976	3.965	3.955	3.999
Al	0.002	0.005	0.011	0.007	0.002	0.002	0.003	0.001	0.01	0.002	0.01	0.009	0.005	0.002
Mg	0.122	0.124	0.075	0.119	0.117	0.127	0.13	0.039	0.049	0.036	0.053	0.017	0.088	0.046
Ca	0.001	0.002	0.007	0	0.003	0.001	0.003	0.008	0.001	0	0	0	0	0
Mn	0.021	0.024	0.049	0.026	0.029	0.026	0.022	0.042	0.023	0.019	0.022	0.025	0.022	0.023
Fe	3.862	3.847	3.885	3.841	3.921	3.845	3.821	3.93	3.917	3.912	3.937	3.986	3.952	3.909
Na	0.005	0.001	0.004	0.007	0.005	0.001	0	0	0	0	0.004	0.005	0	0.001
Total	8.007	8	8.013	8	8.04	8	7.989	8.01	7.997	7.984	8.012	8.02	8.032	7.99

Oxide Wt.%	Il15	Il16	Il17	Il18	Il19	Il20	Il21	Il22	Il23
SiO2	0.178	2.609	0.228	0.093	0.058	0.038	0.021	0.226	0.067
TiO2	52.451	50.865	51.676	52.051	52.625	52.49	52.873	52.424	52.462
Al2O3	0.007	0.107	0.055	0.086	0.039	0.02	0.012	0.041	0.117
MgO	0.285	0.218	0.236	0.235	0.241	0.2	0.301	0.302	0.283
CaO	0.015	0.06	0.085	0.01	0.019	0	0.026	0.028	0.011
MnO	0.255	0.576	0.436	0.295	0.337	0.297	0.241	0.22	0.257
FeO	46.71	45.865	46.476	47.132	46.636	47.007	46.948	46.862	46.45
Na2O	0.004	0.049	0.013	0.013	0.015	0.011	0	0.015	0
Total	99.905	100.349	99.205	99.915	99.97	100.063	100.422	100.118	99.647
Cation based on 12 oxygens									
Si	0.018	0.258	0.023	0.009	0.006	0.004	0.002	0.023	0.007
Ti	3.978	3.788	3.953	3.958	3.99	3.983	3.992	3.967	3.987
Al	0.001	0.012	0.007	0.01	0.005	0.002	0.001	0.005	0.014
Mg	0.043	0.032	0.036	0.035	0.036	0.03	0.045	0.045	0.043
Ca	0.002	0.006	0.009	0.001	0.002	0	0.003	0.003	0.001
Mn	0.022	0.048	0.038	0.025	0.029	0.025	0.021	0.019	0.022
Fe	3.94	3.798	3.954	3.986	3.932	3.967	3.942	3.944	3.926
Na	0.001	0.009	0.003	0.003	0.003	0.002	0	0.003	0
Total	8.005	7.951	8.023	8.027	8.003	8.013	8.006	8.009	8

Appendix IF:
Microprobe Analysis of 862 Garnet

Oxide Wt.%	Gt4ll1in	Gt4llin	Gt4ll3in	Gt4ll4in	Gt4ll5in	Gt4ll6tch	Gt4ll7tch	Gt4ll8tch	Gt4l9tch	Gt4l11out	Gt4line1	Gt4line1	Gt4line1	Gt4line1
SiO_2	0.03	0.07	0.363	0.015	4.1	0.049	0.448	0.028	0.076	2.246	37.104	36.762	36.897	36.87
TiO_2	51.232	51.302	50.702	50.785	48.816	50.557	50.577	50.303	50.98	49.417	0.01	0	0.005	0.017
Al_2O_3	0.024	0.011	0.038	0	0.103	0.052	0.034	0.011	0.014	0.167	21.191	21.329	20.661	21.422
MgO	0.553	0.079	0.232	0.285	0.682	0.445	0.431	0.382	0.167	0.227	3.469	3.78	3.769	3.952
CaO	0.022	0.019	0.053	0.027	0.11	0.009	0.021	0.026	0.008	0.04	2.106	2.435	1.852	1.553
MnO	0.391	0.692	0.264	0.261	0.169	0.219	0.235	0.254	0.263	0.296	1.494	1.597	1.739	1.932
FeO	46.645	46.698	47.239	47.534	44.264	47.033	46.84	47.629	47.224	45.93	34.681	34.082	34.096	34.976
Na_2O	0	0	0.025	0	0.188	0	0.033	0.011	0	0.056	0.029	0.011	0.023	0.004
Total	98.897	98.871	98.916	98.907	98.432	98.364	98.619	98.644	98.732	98.379	100.084	99.996	99.042	100.726
Cation based on 12 oxygens														
Si	0.003	0.007	0.037	0.002	0.409	0.005	0.046	0.003	0.008	0.228	2.98	2.954	2.993	2.948
Ti	3.94	3.954	3.904	3.922	3.662	3.919	3.898	3.9	3.938	3.773	0.001	0	0	0.001
Al	0.003	0.001	0.005	0	0.012	0.006	0.004	0.001	0.002	0.02	2.006	2.02	1.975	2.019
Mg	0.084	0.012	0.035	0.044	0.101	0.068	0.066	0.059	0.026	0.034	0.415	0.453	0.456	0.471
Ca	0.002	0.002	0.006	0.003	0.012	0.001	0.002	0.003	0.001	0.004	0.181	0.21	0.161	0.133
Mn	0.034	0.06	0.023	0.023	0.014	0.019	0.02	0.022	0.023	0.025	0.102	0.109	0.119	0.131
Fe	3.989	4.002	4.045	4.083	3.693	4.054	4.014	4.107	4.057	3.899	2.329	2.29	2.313	2.339
Na	0	0	0.005	0	0.036	0	0.007	0.002	0	0.011	0.005	0.002	0.004	0.001
Total	8.055	8.038	8.06	8.077	7.939	8.072	8.057	8.097	8.055	7.994	8.019	8.038	8.021	8.043

Oxide Wt.%	Gt4line1	Gt4line1	Gt4line1	Gt4line1	Gt4line1	Gt4line1	Gt4line1	Gt4line1	Gt4line1	Gt4line1	Gt4line1	Gt4line1	Gt4line1	Gt4line1
SiO_2	37.223	37.053	37.085	36.684	36.617	39.311	36.648	36.856	36.868	37.012	37.274	46.34	37.193	37.213
TiO_2	0.003	0	0	0	0.025	0.004	0.001	0.028	0	0.03	0.015	0.025	0.006	0
Al_2O_3	21.455	21.286	21.232	21.13	21.072	18.666	21.211	21.105	21.338	21.369	21.439	20.755	21.33	21.556
MgO	3.852	3.835	3.984	3.985	4.02	3.824	3.968	4.009	3.893	3.896	3.887	2.927	3.901	3.89
CaO	1.607	1.705	1.668	1.61	1.619	1.53	1.525	1.554	1.614	1.573	1.616	1.523	1.629	1.685
MnO	1.916	1.914	2.038	1.97	2.129	2.01	2.155	2.245	2.274	2.203	2.261	2.069	2.254	2.279
FeO	34.655	33.791	33.93	34.231	34.273	32.899	33.82	34.202	33.659	34.076	34.483	29.784	33.803	34.044
Na_2O	0.028	0	0.005	0.017	0.011	0.11	0.01	0.043	0.012	0.022	0.029	0.07	0.021	0.04
Total	100.739	99.584	99.942	99.627	99.766	98.354	99.338	100.042	99.658	100.181	101.004	103.493	100.137	100.707
Cation based on 12 oxygens														
Si	2.968	2.981	2.976	2.96	2.954	3.181	2.962	2.963	2.968	2.966	2.966	3.43	2.978	2.966
Ti	0	0	0	0	0.002	0	0	0.002	0	0.002	0.001	0.001	0	0
Al	2.017	2.018	2.008	2.01	2.004	1.78	2.021	2	2.024	2.019	2.011	1.81	2.013	2.025
Mg	0.458	0.46	0.477	0.479	0.484	0.461	0.478	0.481	0.467	0.466	0.461	0.323	0.466	0.462
Ca	0.137	0.147	0.143	0.139	0.14	0.133	0.132	0.134	0.139	0.135	0.138	0.121	0.14	0.144
Mn	0.129	0.13	0.139	0.135	0.146	0.138	0.148	0.153	0.155	0.15	0.152	0.13	0.153	0.154
Fe	2.311	2.273	2.277	2.31	2.313	2.226	2.286	2.3	2.266	2.284	2.295	1.844	2.264	2.269
Na	0.004	0	0.001	0.003	0.002	0.017	0.002	0.007	0.002	0.003	0.004	0.01	0.003	0.006
Total	8.024	8.009	8.021	8.036	8.045	7.936	8.029	8.04	8.021	8.025	8.028	7.669	8.017	8.026

Oxide Wt.%	Gt4line1	Gt4line1	Gt4line1	Gt4line1	Gt4line1	Gt4line1	Gt4line1	Gt4line1	Gt4line1	Gt4line1	Gt4line1	Gt4line1	Gt4line1	Gt4line1
SiO_2	37.032	37.089	37.707	37.198	36.925	37.246	36.968	36.871	36.97	36.973	37.078	36.758	36.966	37.082
TiO_2	0.009	0.022	0.015	0	0.022	0.027	0.01	0.016	0.004	0.02	0.03	0.012	0.023	0.015
Al_2O_3	21.355	21.161	20.703	20.977	21.307	21.476	21.032	21.334	21.248	21.137	21.045	20.924	21.181	21.22
MgO	3.855	3.852	3.681	3.798	3.973	3.829	3.954	3.939	3.93	4.029	3.866	4.087	3.935	3.947
CaO	1.676	1.752	1.696	1.741	1.808	1.856	1.846	1.858	1.895	1.86	1.905	1.913	1.995	1.987
MnO	2.415	2.382	2.277	2.247	2.322	2.293	2.351	2.314	2.272	2.164	2.221	2.249	2.212	2.21
FeO	33.778	33.107	33.164	33.449	33.807	33.765	33.742	33.781	34.245	33.668	33.759	33.588	33.633	33.589
Na_2O	0.002	0.001	0.031	0.069	0.023	0.018	0.011	0.025	0.026	0.029	0.006	0.018	0.001	0.024
Total	100.122	99.366	99.274	99.479	100.187	100.51	99.914	100.138	100.59	99.88	99.91	99.549	99.946	100.074
Cation based on 12 oxygens														
Si	2.969	2.988	3.036	2.997	2.96	2.972	2.973	2.958	2.958	2.97	2.98	2.967	2.969	2.973
Ti	0.001	0.001	0.001	0	0.001	0.002	0.001	0.001	0	0.001	0.002	0.001	0.001	0.001
Al	2.018	2.009	1.965	1.992	2.013	2.02	1.993	2.017	2.004	2.001	1.993	1.99	2.005	2.005
Mg	0.461	0.463	0.442	0.456	0.475	0.455	0.474	0.471	0.469	0.483	0.463	0.492	0.471	0.472
Ca	0.144	0.151	0.146	0.15	0.155	0.159	0.159	0.16	0.162	0.16	0.164	0.165	0.172	0.171
Mn	0.164	0.163	0.155	0.153	0.158	0.155	0.16	0.157	0.154	0.147	0.151	0.154	0.15	0.15
Fe	2.265	2.231	2.233	2.254	2.267	2.253	2.269	2.266	2.291	2.262	2.269	2.267	2.259	2.252
Na	0	0	0.005	0.011	0.004	0.003	0.002	0.004	0.004	0.005	0.001	0.003	0	0.004
Total	8.022	8.006	7.983	8.013	8.033	8.019	8.031	8.034	8.042	8.029	8.023	8.039	8.027	8.028

Appendix IF (cont.):
Microprobe Analysis of 862 Garnet (cont.)

Oxide Wt.%	Gt4line1	Gt4line1	Gt4line1	Gt4line1	Gt4line1	Gt4line1	Gt4line1	Gt4line1	Gt4line1	Gt4line1	Gt4line1	Gt4line1	Gt4line1	Gt4line1
SiO_2	37.35	37.258	37.16	37.238	36.876	36.673	36.799	36.49	36.812	36.826	36.93	37.199	37.251	37.236
TiO_2	0.002	0.016	0.028	0.05	0.013	0.049	0.028	0.481	0.003	0.022	0.005	0.015	0	0.005
Al_2O_3	21.14	21.264	21.366	21.232	21.175	21.244	21.174	21.008	21.287	21.075	21.145	21.154	21.187	21.168
MgO	3.978	4.003	4.054	4.008	4.033	3.978	3.988	3.941	4.001	3.949	3.982	3.892	3.941	3.879
CaO	1.95	2.008	2.045	1.943	1.995	2.003	1.988	1.972	1.998	2.001	1.996	2.156	2.146	2.148
MnO	2.232	2.253	2.255	2.219	2.149	2.048	2.201	2.096	2.216	2.088	2.113	2.126	2.048	2.12
FeO	33.633	33.863	33.702	33.757	33.655	33.44	33.68	33.33	33.772	33.725	34.073	33.579	33.598	33.778
Na_2O	0.011	0.022	0.026	0.021	0.013	0.013	0.016	0.032	0.017	0.02	0.033	0	0	0.028
Total	100.296	100.687	100.636	100.468	99.909	99.448	99.874	99.35	100.106	99.706	100.277	100.121	100.171	100.362
Cation based on 12 oxygens														
Si	2.986	2.971	2.963	2.974	2.963	2.958	2.96	2.948	2.955	2.967	2.961	2.98	2.981	2.978
Ti	0	0.001	0.002	0.003	0.001	0.003	0.002	0.029	0	0.001	0	0.001	0	0
Al	1.992	1.998	2.008	1.998	2.005	2.02	2.007	2.001	2.014	2.001	1.998	1.997	1.998	1.995
Mg	0.474	0.476	0.482	0.477	0.483	0.478	0.478	0.475	0.479	0.474	0.476	0.465	0.47	0.462
Ca	0.167	0.172	0.175	0.166	0.172	0.173	0.171	0.171	0.172	0.173	0.171	0.185	0.184	0.184
Mn	0.151	0.152	0.152	0.15	0.146	0.14	0.15	0.143	0.151	0.142	0.144	0.144	0.139	0.144
Fe	2.248	2.258	2.247	2.254	2.262	2.256	2.265	2.252	2.267	2.272	2.285	2.249	2.248	2.259
Na	0.002	0.003	0.004	0.003	0.002	0.002	0.003	0.005	0.003	0.003	0.005	0	0	0.004
Total	8.02	8.031	8.033	8.025	8.034	8.03	8.036	8.024	8.041	8.033	8.04	8.021	8.02	8.026

Oxide Wt.%	Gt4line1	Gt4line1	Gt4line1	Gt4line1	Gt4line1	Gt4line1	Gt4line1	Gt4line1	Gt4line1	Gt4line1	Gt4line1	862Gt6line1	862Gt6line1	862Gt6line1
SiO_2	36.93	37.199	37.251	37.236	37.263	36.846	36.832	36.617	36.988	37.011	39.117	37.219	37.332	37.385
TiO_2	0.005	0.015	0	0.005	0.018	0.023	0.002	0	0	0.005	0.115	0.006	0.01	0.016
Al_2O_3	21.145	21.154	21.187	21.168	21.271	21.25	21.211	20.829	21.328	21.208	21.631	21.07	21.067	21.167
MgO	3.982	3.892	3.941	3.879	3.928	3.998	4.104	3.84	4	3.979	3.55	4.042	4.008	4.024
CaO	1.996	2.156	2.146	2.148	2.207	2.133	2.102	2.072	2.124	2.096	2.529	1.977	1.938	1.999
MnO	2.113	2.126	2.048	2.12	2.065	2.059	2.053	2.046	2.083	2.059	1.84	2.042	2.066	2.188
FeO	34.073	33.579	33.598	33.778	33.555	33.131	33.19	33.256	33.574	33.801	31.033	33.955	33.712	33.757
Na_2O	0.033	0	0	0.028	0.037	0.001	0.02	0.077	0.017	0.014	0.183	0.018	0.054	0.005
Total	100.277	100.121	100.171	100.362	100.344	99.441	99.514	98.737	100.114	100.173	99.998	100.329	100.187	100.541
Cation based on 12 oxygens														
Si	2.961	2.98	2.981	2.978	2.977	2.968	2.965	2.977	2.963	2.966	3.081	2.978	2.987	2.982
Ti	0	0.001	0	0	0.001	0.001	0	0	0	0	0.007	0	0.001	0.001
Al	1.998	1.997	1.998	1.995	2.003	2.017	2.013	1.996	2.014	2.003	2.008	1.987	1.987	1.99
Mg	0.476	0.465	0.47	0.462	0.468	0.48	0.493	0.465	0.478	0.475	0.417	0.482	0.478	0.478
Ca	0.171	0.185	0.184	0.184	0.189	0.184	0.181	0.18	0.182	0.18	0.213	0.169	0.166	0.171
Mn	0.144	0.144	0.139	0.144	0.14	0.14	0.14	0.141	0.141	0.14	0.123	0.138	0.14	0.148
Fe	2.285	2.249	2.248	2.259	2.242	2.232	2.235	2.261	2.25	2.266	2.044	2.272	2.256	2.252
Na	0.005	0	0	0.004	0.006	0	0.003	0.012	0.003	0.002	0.028	0.003	0.008	0.001
Total	8.04	8.021	8.02	8.026	8.026	8.022	8.03	8.032	8.031	8.032	7.921	8.029	8.023	8.023

Oxide Wt.%	862Gt6line1	862Gt6line1	862Gt6line1	862Gt6line1	862Gt6line1	862Gt6line1	862Gt6line1	862Gt6line1	862Gt6line1	862Gt6line1	862Gt6line1	862Gt6line1	862Gt6line1	862Gt6line1
SiO_2	37.241	36.554	37.158	37.21	37.133	37.057	39.351	37.174	36.922	36.973	36.678	37.169	37.296	37.195
TiO_2	0.036	0.006	0	0.121	0.014	0.01	0.007	0.017	0	0.024	0.039	0.008	0.015	0.055
Al_2O_3	20.97	20.39	21.043	21.143	21.099	21.144	21.043	21.236	21.265	21.177	20.762	21.267	21.168	21.201
MgO	4.004	3.982	4.087	4.026	4.053	4.071	4.333	4.055	4.088	4.034	3.94	4.027	3.981	3.976
CaO	1.951	1.967	2.044	1.944	1.978	1.964	1.879	1.959	1.938	2.01	2.028	1.964	2.015	1.913
MnO	2.155	2.056	2.108	2.067	2.057	2.084	2.018	2.025	2.122	2.153	2.175	2.156	2.121	1.978
FeO	33.538	33.651	33.965	34.254	33.816	34.436	32.451	34.392	33.874	34.147	34.131	33.835	34.455	34.183
Na_2O	0	0.089	0.009	0.02	0.018	0.018	0.101	0.031	0.015	0.009	0.032	0.029	0.007	0.007
Total	99.895	98.695	100.414	100.785	100.168	100.784	101.183	100.889	100.224	100.527	99.785	100.455	101.058	100.508
Cation based on 12 oxygens														
Si	2.988	2.98	2.973	2.967	2.975	2.959	3.08	2.963	2.959	2.958	2.962	2.969	2.969	2.972
Ti	0.002	0	0	0.007	0.001	0.001	0	0.001	0	0.001	0.002	0	0.001	0.003
Al	1.983	1.959	1.984	1.987	1.992	1.99	1.941	1.995	2.008	1.997	1.976	2.002	1.986	1.996
Mg	0.479	0.484	0.487	0.479	0.484	0.485	0.506	0.482	0.488	0.481	0.474	0.48	0.472	0.474
Ca	0.168	0.172	0.175	0.166	0.17	0.168	0.158	0.167	0.166	0.172	0.175	0.168	0.172	0.164
Mn	0.146	0.142	0.143	0.14	0.14	0.141	0.134	0.137	0.144	0.146	0.149	0.146	0.143	0.134
Fe	2.251	2.295	2.272	2.284	2.266	2.3	2.124	2.292	2.27	2.285	2.305	2.261	2.294	2.284
Na	0	0.014	0.001	0.003	0.003	0.003	0.015	0.005	0.002	0.001	0.005	0.004	0.001	0.001
Total	8.017	8.046	8.035	8.033	8.031	8.047	7.958	8.042	8.037	8.041	8.048	8.03	8.038	8.028

Appendix IF (cont.):
Microprobe Analysis of 862 Garnet (cont.)

Oxide Wt.%	862Gt6line1	862Gt6line1	862Gt6line1	862Gt6line1	862Gt6line1	862Gt6line1	862Gt6line1	862Gt6line1	862Gt6line1	862Gt6line1	862Gt6line1	862Gt6line1	862Gt6line1	862Gt6line1
SiO_2	37.237	37.103	36.976	36.718	37.134	37.031	36.837	37.007	37.064	36.919	36.856	37.094	36.746	36.706
TiO_2	0.035	0.001	0.211	0.007	0.03	0.044	0.015	0.059	0.018	0	0.02	0.009	0.027	0.068
Al_2O_3	21.088	21.151	21.302	21.022	21.177	21.329	21.132	21.129	21.108	21.097	21.165	21.253	21.209	21.278
MgO	4.056	4.027	4.07	3.646	4.076	3.966	4.008	4.024	4.087	4.16	4.045	3.857	4.152	4.081
CaO	1.978	1.912	1.949	2.013	2.015	1.963	1.928	1.934	1.938	1.951	1.989	1.948	1.925	1.834
MnO	2.02	2.002	2.096	2.062	1.923	2.106	2.031	2.1	2.144	2.092	2.072	1.975	2.099	2.226
FeO	34.209	33.852	34.423	33.898	33.907	34.115	34.005	34.226	34	33.942	34.36	33.882	34.184	34.123
Na_2O	0.018	0.012	0.024	0.021	0.016	0.001	0.045	0.012	0.017	0.017	0.004	0.002	0.02	0.004
Total	100.641	100.06	101.051	99.387	100.278	100.555	100.001	100.491	100.376	100.178	100.511	100.02	100.362	100.32
Cation based on 12 oxygens														
Si	2.973	2.975	2.945	2.971	2.971	2.959	2.961	2.962	2.967	2.961	2.952	2.975	2.946	2.944
Ti	0.002	0	0.013	0	0.002	0.003	0.001	0.004	0.001	0	0.001	0.001	0.002	0.004
Al	1.984	1.999	2	2.005	1.997	2.009	2.002	1.993	1.991	1.994	1.998	2.009	2.004	2.011
Mg	0.483	0.481	0.483	0.44	0.486	0.473	0.48	0.48	0.488	0.497	0.483	0.461	0.496	0.488
Ca	0.169	0.164	0.166	0.174	0.173	0.168	0.166	0.166	0.166	0.168	0.171	0.167	0.165	0.158
Mn	0.137	0.136	0.141	0.141	0.13	0.143	0.138	0.142	0.145	0.142	0.141	0.134	0.143	0.151
Fe	2.284	2.27	2.293	2.294	2.269	2.28	2.286	2.291	2.276	2.277	2.302	2.273	2.292	2.289
Na	0.003	0.002	0.004	0.003	0.002	0	0.007	0.002	0.003	0.003	0.001	0	0.003	0.001
Total	8.035	8.027	8.045	8.028	8.03	8.035	8.041	8.04	8.037	8.042	8.049	8.02	8.051	8.046

Oxide Wt.%	862Gt6line1	862Gt6line1	862Gt6line1	862Gt6line1	862Gt6line1	862Gt6line1	862Gt6line1	862Gt6line1	862Gt6line1	862Gt6line1	862Gt6line1	862Gt6line1	862Gt6line1	862Gt6line1
SiO_2	36.823	36.835	35.858	36.529	37.11	36.836	36.245	36.432	36.295	36.258	37.117	36.6	35.419	36.396
TiO_2	0.004	0.013	3.028	0.043	0.01	0.006	0.015	0.203	0.015	0.015	0.031	0.103	0.219	0.092
Al_2O_3	21.098	21.166	20.681	21.305	21.369	21.297	21.152	21.049	21.231	21.227	21.545	21.232	20.662	21.317
MgO	4.105	4.057	3.977	4.117	4.091	4.175	4.176	4.087	4.069	4.107	4.085	4.013	3.998	3.803
CaO	1.842	1.891	1.833	1.817	1.854	1.773	1.831	1.832	1.841	1.8	1.775	1.734	1.842	2.241
MnO	2.138	2.051	1.989	2.069	2.106	2.043	2.003	2.121	2.094	2.152	2.118	1.982	2.148	2.005
FeO	34.076	34.358	33.138	34.276	34.214	34.417	34.274	34.005	33.995	33.999	34.265	34.49	33.997	33.94
Na_2O	0	0.018	0.036	0.031	0.002	0.004	0.005	0.038	0.026	0.048	0.002	0.002	0.015	0.034
Total	100.086	100.389	100.54	100.187	100.756	100.551	99.701	99.767	99.566	99.606	100.938	100.156	98.3	99.828
Cation based on 12 oxygens														
Si	2.959	2.953	2.866	2.936	2.959	2.947	2.93	2.94	2.935	2.932	2.953	2.943	2.913	2.935
Ti	0	0.001	0.182	0.003	0.001	0	0.001	0.012	0.001	0.001	0.002	0.006	0.014	0.006
Al	1.998	2	1.948	2.018	2.008	2.008	2.015	2.002	2.023	2.023	2.02	2.012	2.003	2.026
Mg	0.492	0.485	0.474	0.493	0.486	0.498	0.503	0.492	0.491	0.495	0.485	0.481	0.49	0.457
Ca	0.159	0.162	0.157	0.156	0.158	0.152	0.159	0.158	0.159	0.156	0.151	0.149	0.162	0.194
Mn	0.146	0.139	0.135	0.141	0.142	0.138	0.137	0.145	0.143	0.147	0.143	0.135	0.15	0.137
Fe	2.29	2.304	2.215	2.304	2.282	2.303	2.317	2.295	2.299	2.299	2.28	2.319	2.339	2.289
Na	0	0.003	0.006	0.005	0	0.001	0.001	0.006	0.004	0.007	0	0	0.002	0.005
Total	8.044	8.047	7.983	8.056	8.036	8.047	8.063	8.05	8.055	8.06	8.034	8.045	8.073	8.049

Oxide Wt.%	862Gt6line1	862Gt6line1	862Gt6line1	862Gt6line1	862Gt6line1	862Gt6line1	862Gt6line1	862Gt6line1	862Gt6line1	862Gt6line1	862Gt6line1	862Gt6line1	862Gt6line1	862Gt6line1
SiO_2	35.604	35.978	35.706	35.948	36.637	35.76	36.25	36.194	36.391	36.065	36.505	39.716	36.471	36.588
TiO_2	0.037	0.025	0.013	0.02	0.018	0.015	0.009	0.003	0.042	0.023	0.036	0.019	0.004	0.016
Al_2O_3	20.708	21.231	20.658	21.418	21.179	21.454	21.386	21.387	21.374	21.319	21.077	20.292	21.532	21.376
MgO	4.325	4.198	4.204	4.199	3.971	4.225	4.174	4.156	4.143	4.076	4.11	3.491	4.108	4.104
CaO	1.819	1.739	1.717	1.653	1.615	1.588	1.563	1.592	1.524	1.608	1.561	1.6	1.53	1.487
MnO	2.175	2.165	2.146	2.319	2.255	2.226	2.402	2.166	2.211	2.267	2.182	2.114	2.443	2.463
FeO	34.2	34.048	33.781	34.22	33.797	34.236	34.286	33.985	34.016	34.067	34.347	30.975	34.027	33.977
Na_2O	0.008	0.008	0.014	0.012	0.031	0.032	0.015	0.04	0.012	0.004	0.025	0.115	0.028	0.023
Total	98.876	99.392	98.239	99.789	99.503	99.536	100.085	99.523	99.713	99.429	99.843	98.322	100.143	100.034
Cation based on 12 oxygens														
Si	2.912	2.918	2.932	2.907	2.959	2.899	2.921	2.927	2.935	2.923	2.945	3.176	2.931	2.942
Ti	0.002	0.002	0.001	0.001	0.001	0.001	0.001	0	0.003	0.001	0.002	0.001	0	0.001
Al	1.996	2.029	1.999	2.041	2.016	2.05	2.031	2.038	2.032	2.036	2.004	1.913	2.039	2.026
Mg	0.527	0.508	0.515	0.506	0.478	0.511	0.501	0.501	0.498	0.492	0.494	0.416	0.492	0.492
Ca	0.159	0.151	0.151	0.143	0.14	0.138	0.135	0.138	0.132	0.14	0.135	0.137	0.132	0.128
Mn	0.151	0.149	0.149	0.159	0.154	0.153	0.164	0.148	0.151	0.156	0.149	0.143	0.166	0.168
Fe	2.339	2.309	2.32	2.314	2.283	2.321	2.31	2.298	2.295	2.309	2.318	2.072	2.287	2.285
Na	0.001	0.001	0.002	0.002	0.005	0.005	0.002	0.006	0.002	0.001	0.004	0.018	0.004	0.004
Total	8.087	8.067	8.069	8.073	8.036	8.078	8.065	8.056	8.048	8.058	8.051	7.876	8.051	8.046

Appendix IF (cont.):
Microprobe Analysis of 862 Garnet (cont.)

Oxide Wt.%	862Gt6line1	862Gt6line1	862Gt6line1	862Gt6line1	862Gt6line1	862Gt6line1	862Gt6line1	862Gt6line1	862Gt6line1	862Gt6line1	862Gt6line1	862Gt6line1	862Gt6line1	862Gt6line1
SiO_2	36.671	36.483	36.632	36.535	36.272	36.069	36.059	36.317	36.323	36.249	36.034	36.506	36.157	36.276
TiO_2	0.004	0	0	0.003	0.013	0.01	0	0.02	0	0	0.012	0	0.009	0
Al_2O_3	21.494	21.352	21.334	21.319	21.15	21.118	21.264	21.313	21.239	21.322	21.517	21.268	21.396	21.335
MgO	3.961	4.003	4.052	4.066	4.101	4.079	4.065	3.858	3.971	3.989	4.071	4.016	3.974	4.057
CaO	1.525	1.493	1.479	1.496	1.521	1.487	1.527	1.546	1.485	1.551	1.499	1.549	1.526	1.538
MnO	2.343	2.374	2.315	2.47	2.306	2.361	2.237	2.426	2.406	2.333	2.204	2.251	2.226	2.349
FeO	33.557	34.329	34.105	33.236	34.271	34.075	34.131	33.59	34.066	33.969	34.438	34.239	34.738	34.54
Na_2O	0	0.046	0.031	0.023	0.014	0.023	0.017	0.004	0.008	0.024	0.026	0.041	0.031	0.022
Total	99.555	100.08	99.948	99.148	99.648	99.222	99.3	99.074	99.498	99.437	99.801	99.87	100.057	100.117
Cation based on 12 oxygens														
Si	2.955	2.937	2.948	2.956	2.935	2.931	2.926	2.947	2.94	2.935	2.912	2.943	2.918	2.924
Ti	0	0	0	0	0.001	0.001	0	0.001	0	0	0.001	0	0.001	0
Al	2.041	2.026	2.023	2.033	2.017	2.022	2.034	2.038	2.026	2.035	2.049	2.021	2.035	2.027
Mg	0.476	0.48	0.486	0.49	0.495	0.494	0.492	0.467	0.479	0.481	0.49	0.483	0.478	0.488
Ca	0.132	0.129	0.128	0.13	0.132	0.129	0.133	0.134	0.129	0.135	0.13	0.134	0.132	0.133
Mn	0.16	0.162	0.158	0.169	0.158	0.162	0.154	0.167	0.165	0.16	0.151	0.154	0.152	0.16
Fe	2.261	2.311	2.295	2.249	2.319	2.316	2.317	2.279	2.306	2.3	2.327	2.309	2.345	2.329
Na	0	0.007	0.005	0.004	0.002	0.004	0.003	0.001	0.001	0.004	0.004	0.006	0.005	0.003
Total	8.025	8.052	8.043	8.031	8.059	8.059	8.059	8.034	8.046	8.05	8.064	8.05	8.066	8.064

Oxide Wt.%	862Gt6line1	862Gt6line1	862Gt6line1	862Gt6line1	862Gt6line1	862Gt6line1	862Gt6line1	862Gt6line1	862Gt6line1	862Gt6line1	862Gt6line1	862Gt1line1	862Gt1line1	862Gt1line1
SiO_2	36.417	36.48	35.989	36.15	36.092	36.592	37.007	36.478	37.043	37.017	36.45	36.724	37.263	37.897
TiO_2	0.001	0.002	0.011	0	0	0	0	0.042	0.006	0.051	0.021	0.009	0	0.053
Al_2O_3	21.461	21.239	21.328	21.257	21.064	21.361	21.278	21.257	21.441	21.354	20.803	21.17	21.181	21.355
MgO	3.981	3.907	3.828	3.793	3.781	3.934	3.768	3.789	3.784	3.644	3.525	3.534	3.794	3.77
CaO	1.623	1.833	2.394	2.346	2.828	2.402	2.322	2.385	2.399	2.424	2.44	2.338	2.392	2.29
MnO	2.153	2.226	1.989	1.923	1.838	1.748	1.606	1.439	1.459	1.39	1.348	1.479	1.468	1.515
FeO	34.257	34.217	33.96	34.11	33.606	34.112	34.289	34.574	35.098	34.613	34.449	34.227	34.954	34.321
Na_2O	0.026	0.011	0.01	0.01	0.026	0.018	0.018	0.038	0.025	0.031	0.043	0	0.019	0.036
Total	99.919	99.915	99.509	99.589	99.235	100.167	100.288	100.002	101.255	100.524	99.079	99.481	101.071	101.237
Cation based on 12 oxygens														
Si	2.934	2.942	2.917	2.927	2.931	2.939	2.965	2.938	2.947	2.96	2.964	2.967	2.968	2.997
Ti	0	0	0.001	0	0	0	0	0.003	0	0.003	0.001	0.001	0	0.003
Al	2.038	2.019	2.037	2.028	2.016	2.022	2.009	2.018	2.011	2.013	1.994	2.016	1.988	1.991
Mg	0.478	0.47	0.462	0.458	0.458	0.471	0.45	0.455	0.449	0.435	0.427	0.426	0.45	0.445
Ca	0.14	0.158	0.208	0.203	0.246	0.207	0.199	0.206	0.204	0.208	0.213	0.202	0.204	0.194
Mn	0.147	0.152	0.137	0.132	0.126	0.119	0.109	0.098	0.098	0.094	0.093	0.101	0.099	0.101
Fe	2.308	2.308	2.302	2.31	2.282	2.291	2.297	2.329	2.335	2.315	2.343	2.312	2.328	2.27
Na	0.004	0.002	0.002	0.002	0.004	0.003	0.003	0.006	0.004	0.005	0.007	0	0.003	0.006
Total	8.049	8.051	8.066	8.06	8.063	8.052	8.032	8.053	8.048	8.033	8.042	8.025	8.04	8.007

Oxide Wt.%	862Gt1line1	862Gt1line1	862Gt1line1	862Gt1line1	862Gt1line1	862Gt1line1	862Gt1line1	862Gt1line1	862Gt1line1	862Gt1line1	862Gt1line1	862Gt1line1	862Gt1line1	862Gt1line1
SiO_2	37.14	36.94	37.181	37.182	37.167	38.136	37.646	37.315	37.093	36.784	37.058	37.022	37.082	36.946
TiO_2	0	0	0.015	0	0.002	0.022	0.007	0.027	0.029	0	0.002	0.01	0.001	0
Al_2O_3	21.322	21.375	21.471	21.453	21.116	21.737	21.375	21.418	21.374	21.434	21.258	21.299	21.355	21.189
MgO	3.868	3.883	3.96	3.968	4.022	4.07	4.097	3.968	4.135	4.174	4.131	4.167	4.172	4.214
CaO	2.321	1.831	1.765	1.709	1.661	1.716	1.744	1.689	1.674	1.697	1.617	1.607	1.651	1.671
MnO	1.555	1.557	1.817	1.724	1.971	1.882	1.762	1.922	1.976	1.923	2.021	2.033	2.023	2.037
FeO	34.631	35.035	34.978	35.065	34.866	34.361	34.421	34.485	34.702	34.504	34.514	34.418	33.954	34.279
Na_2O	0.012	0.017	0	0.018	0.031	0.041	0.042	0.034	0	0	0.021	0.037	0	0.048
Total	100.849	100.638	101.187	101.119	100.836	101.965	101.094	100.858	100.983	100.516	100.622	100.593	100.238	100.384
Cation based on 12 oxygens														
Si	2.961	2.954	2.956	2.958	2.967	2.991	2.984	2.97	2.954	2.943	2.961	2.958	2.966	2.958
Ti	0	0	0.001	0	0	0.001	0	0.002	0.002	0	0	0.001	0	0
Al	2.003	2.015	2.012	2.011	1.987	2.009	1.997	2.009	2.006	2.021	2.002	2.006	2.013	2
Mg	0.46	0.463	0.469	0.471	0.479	0.476	0.484	0.471	0.491	0.498	0.492	0.496	0.497	0.503
Ca	0.198	0.157	0.15	0.146	0.142	0.144	0.148	0.144	0.143	0.146	0.138	0.138	0.141	0.143
Mn	0.105	0.105	0.122	0.116	0.133	0.125	0.118	0.13	0.133	0.13	0.137	0.138	0.137	0.138
Fe	2.309	2.343	2.326	2.333	2.328	2.254	2.282	2.296	2.311	2.309	2.306	2.3	2.271	2.295
Na	0.002	0.003	0	0.003	0.005	0.006	0.007	0.005	0	0	0.003	0.006	0	0.008
Total	8.038	8.04	8.036	8.038	8.041	8.006	8.02	8.027	8.04	8.047	8.039	8.043	8.025	8.045

Appendix IF (cont.):
Microprobe Analysis of 862 Garnet (cont.)

Oxide Wt.%	862Gt1line1	862Gt1line1	862Gt1line1	862Gt1line1	862Gt1line1	862Gt1line1	862Gt1line1	862Gt1line1	862Gt1line1	862Gt1lin2	862Gt1lin2	862Gt1lin2	862Gt1lin2	862Gt1lin2
SiO_2	35.898	36.661	36.106	36.581	36.996	37.022	37.282	37.166	36.841	37.363	37.021	36.556	36.694	36.825
TiO_2	0.004	0	0	0	0	0.014	0.004	0	0	0.001	0.045	0.002	0	0.014
Al_2O_3	20.622	21.515	20.824	21.339	21.368	21.536	21.198	21.379	21.481	21.544	21.403	21.504	21.459	21.301
MgO	4.397	4.303	4.21	4.28	4.322	4.295	4.367	4.275	4.291	4.341	4.464	4.52	4.43	4.586
CaO	1.616	1.569	1.587	1.599	1.596	1.608	1.564	1.538	1.591	1.596	1.649	1.663	1.765	1.832
MnO	1.995	2.038	2.062	1.999	2.071	2.094	2.001	2.025	2.054	2.063	2.071	1.881	2.037	1.928
FeO	34.467	34.634	34.094	34.389	34.429	34.151	34.133	34.242	34.412	34.326	33.879	33.99	33.92	33.777
Na_2O	0.023	0.026	0.008	0.023	0.032	0.026	0.001	0.027	0	0.018	0.037	0.037	0.007	0.015
Total	99.022	100.746	98.891	100.21	100.814	100.746	100.55	100.652	100.67	101.252	100.569	100.153	100.312	100.278
Cation based on 12 oxygens														
Si	2.929	2.93	2.942	2.937	2.95	2.949	2.973	2.963	2.942	2.96	2.952	2.93	2.937	2.946
Ti	0	0	0	0	0	0.001	0	0	0	0	0.003	0	0	0.001
Al	1.983	2.026	2	2.019	2.008	2.022	1.992	2.009	2.022	2.012	2.011	2.031	2.024	2.008
Mg	0.535	0.513	0.511	0.512	0.514	0.51	0.519	0.508	0.511	0.513	0.531	0.54	0.529	0.547
Ca	0.141	0.134	0.139	0.138	0.136	0.137	0.134	0.131	0.136	0.135	0.141	0.143	0.151	0.157
Mn	0.138	0.138	0.142	0.136	0.14	0.141	0.135	0.137	0.139	0.138	0.14	0.128	0.138	0.131
Fe	2.352	2.315	2.323	2.309	2.296	2.275	2.276	2.283	2.298	2.274	2.259	2.279	2.271	2.259
Na	0.004	0.004	0.001	0.004	0.005	0.004	0	0.004	0	0.003	0.006	0.006	0.001	0.002
Total	8.082	8.06	8.058	8.055	8.049	8.039	8.029	8.035	8.048	8.035	8.043	8.057	8.051	8.051

Oxide Wt.%	862Gt1lin2	862Gt1lin2	862Gt1lin2	862Gt1lin2	862Gt1lin2	862Gt1lin2	862Gt1lin2	862Gt1lin2	862Gt1lin2	862Gt1lin2	862Gt1lin2	862Gt1lin2	862Gt1lin2	862Gt1lin2
SiO_2	36.655	37.073	45.485	37.914	37.371	37.337	36.604	37.213	36.924	38.891	37.4	38.521	36.294	36.841
TiO_2	0.023	0.021	0.023	0	0.004	0.104	0.036	0.018	0.006	0	0.028	0.416	0	0
Al_2O_3	21.452	21.503	19.738	21.042	21.503	21.268	21.596	20.861	21.239	20.525	21.387	21.392	20.82	21.477
MgO	4.494	4.451	3.381	3.753	4.295	4.429	4.427	4.373	4.549	4.318	4.435	3.464	4.239	4.332
CaO	1.922	1.911	1.915	2.151	2.131	2.276	2.755	2.86	2.733	2.721	2.912	2.702	2.795	2.922
MnO	1.968	1.962	1.678	1.846	1.864	1.749	1.81	1.834	1.961	1.895	2.019	2.226	2.237	2.376
FeO	33.029	33.535	29.217	32.456	33.623	33.212	33.011	32.498	32.358	31.242	32.824	32.026	31.986	32.202
Na_2O	0.042	0.028	0.121	0.044	0.006	0	0.017	0.008	0.017	0.041	0.033	0.046	0.111	0.007
Total	99.585	100.484	101.558	99.206	100.797	100.375	100.256	99.665	99.787	99.633	101.038	100.793	98.482	100.157
Cation based on 12 oxygens														
Si	2.945	2.954	3.434	3.04	2.967	2.973	2.925	2.984	2.957	3.087	2.961	3.036	2.953	2.944
Ti	0.001	0.001	0.001	0	0	0.006	0.002	0.001	0	0	0.002	0.025	0	0
Al	2.031	2.019	1.756	1.988	2.012	1.996	2.034	1.971	2.005	1.92	1.996	1.987	1.997	2.022
Mg	0.538	0.529	0.38	0.449	0.508	0.526	0.527	0.523	0.543	0.511	0.523	0.407	0.514	0.516
Ca	0.165	0.163	0.155	0.185	0.181	0.194	0.236	0.246	0.234	0.231	0.247	0.228	0.244	0.25
Mn	0.134	0.132	0.107	0.125	0.125	0.118	0.123	0.125	0.133	0.127	0.135	0.149	0.154	0.161
Fe	2.219	2.235	1.844	2.176	2.232	2.211	2.206	2.179	2.167	2.074	2.173	2.111	2.177	2.152
Na	0.006	0.004	0.018	0.007	0.001	0	0.003	0.001	0.003	0.006	0.005	0.007	0.018	0.001
Total	8.039	8.037	7.695	7.97	8.026	8.024	8.056	8.03	8.042	7.956	8.042	7.95	8.057	8.046

Oxide Wt.%	862Gt1lin2	862Gt1lin2	862Gt1lin2	862Gt1lin2	862Gt1lin2	862Gt1lin2	862Gt1lin2	862Gt1lin2	862Gt1lin2	862Gt1lin2	862Gt1lin2	862Gt1lin2	862Gt1lin2	862Gt1lin2
SiO_2	37.035	36.934	36.749	36.815	36.533	36.996	36.856	37.987	37.228	37.168	37.14	36.707	38.006	38.293
TiO_2	0.02	0.037	0.054	0.05	0.042	0	0.032	0.025	0.039	0.027	0	0.021	0.028	0.009
Al_2O_3	21.411	21.213	20.676	21.314	21.479	21.255	21.307	21.564	21.474	21.345	21.295	21.541	21.587	20.546
MgO	4.381	4.307	4.202	4.409	4.378	4.517	4.562	4.432	4.599	4.56	4.408	4.555	4.319	3.967
CaO	2.982	3.089	2.976	2.908	2.818	2.813	2.612	2.529	2.296	2.157	1.913	1.847	1.813	1.764
MnO	2.428	2.38	2.465	2.512	2.447	2.426	2.227	2.27	2.243	2.171	2.168	2.194	2.169	2.097
FeO	32.245	31.85	31.395	32.565	32.074	32.774	32.628	32.254	32.798	33.078	32.799	33.286	33.381	32.614
Na_2O	0.003	0.015	0.082	0.007	0.014	0.028	0.004	0.023	0.025	0.014	0.041	0.008	0.029	0.091
Total	100.505	99.825	98.599	100.58	99.785	100.809	100.228	101.084	100.702	100.52	99.764	100.159	101.332	99.381
Cation based on 12 oxygens														
Si	2.949	2.958	2.98	2.937	2.931	2.944	2.944	2.992	2.956	2.959	2.974	2.937	2.993	3.066
Ti	0.001	0.002	0.003	0.003	0.003	0	0.002	0.001	0.002	0.002	0	0.001	0.002	0.001
Al	2.009	2.002	1.976	2.004	2.031	1.993	2.006	2.002	2.009	2.003	2.01	2.031	2.004	1.939
Mg	0.52	0.514	0.508	0.524	0.524	0.536	0.543	0.52	0.544	0.541	0.526	0.543	0.507	0.474
Ca	0.254	0.265	0.258	0.249	0.242	0.24	0.224	0.213	0.195	0.184	0.164	0.158	0.153	0.151
Mn	0.164	0.161	0.169	0.17	0.166	0.164	0.151	0.151	0.151	0.146	0.147	0.149	0.145	0.142
Fe	2.147	2.133	2.129	2.172	2.152	2.181	2.18	2.124	2.178	2.202	2.197	2.227	2.198	2.184
Na	0	0.002	0.013	0.001	0.002	0.004	0.001	0.004	0.004	0.002	0.006	0.001	0.004	0.014
Total	8.044	8.037	8.036	8.06	8.051	8.062	8.051	8.007	8.039	8.039	8.024	8.047	8.006	7.971

Appendix IF (cont.):
Microprobe Analysis of 862 Garnet (cont.)

Oxide Wt.%	862Gt1lin2	862Gt1lin2	862Gt1lin3	862Gt1lin3	862Gt1lin3	862Gt1lin3	862Gt1lin3	862Gt1lin3	862Gt1lin3	862Gt1lin3	862Gt1lin3	862Gt1lin3	862Gt1lin3	862Gt1lin3
SiO_2	36.867	36.494	36.499	36.426	36.792	36.535	36.981	36.79	37.061	37.054	36.674	36.808	37.81	36.635
TiO_2	0	0.012	0.015	0	0.023	0	0.041	0.012	0	0	0	0	0.008	0.019
Al_2O_3	21.228	21.452	21.407	21.304	21.448	20.455	21.41	21.525	21.497	21.327	21.298	21.392	21.733	21.381
MgO	4.298	4.229	4.234	4.28	4.24	4.567	4.161	4.132	4.072	4.055	4.271	4.12	4.026	3.944
CaO	1.741	1.718	1.664	1.755	1.691	1.697	1.654	1.769	1.758	1.626	1.757	1.731	1.701	1.637
MnO	2.337	2.304	2.294	2.449	2.316	2.204	2.378	2.498	2.466	2.255	2.362	2.206	2.224	2.217
FeO	33.517	33.296	33.48	33.669	34.013	33.161	33.89	33.966	34.077	33.764	33.565	33.7	33.93	34.507
Na_2O	0.01	0.017	0.014	0.03	0.038	0.04	0.02	0.001	0.013	0.033	0.082	0	0.043	0.05
Total	99.998	99.522	99.607	99.913	100.561	98.659	100.535	100.693	100.944	100.114	100.009	99.957	101.475	100.39
Cation based on 12 oxygens														
Si	2.958	2.941	2.941	2.933	2.941	2.972	2.954	2.939	2.952	2.969	2.946	2.955	2.982	2.94
Ti	0	0.001	0.001	0	0.001	0	0.002	0.001	0	0	0	0	0	0.001
Al	2.007	2.038	2.033	2.022	2.021	1.961	2.016	2.026	2.018	2.014	2.016	2.024	2.02	2.022
Mg	0.514	0.508	0.509	0.514	0.505	0.554	0.496	0.492	0.483	0.484	0.511	0.493	0.473	0.472
Ca	0.15	0.148	0.144	0.151	0.145	0.148	0.142	0.151	0.15	0.14	0.151	0.149	0.144	0.141
Mn	0.159	0.157	0.157	0.167	0.157	0.152	0.161	0.169	0.166	0.153	0.161	0.15	0.149	0.151
Fe	2.249	2.244	2.256	2.267	2.274	2.256	2.264	2.269	2.27	2.262	2.255	2.262	2.238	2.316
Na	0.002	0.003	0.002	0.005	0.006	0.006	0.003	0	0.002	0.005	0.013	0	0.007	0.008
Total	8.039	8.04	8.043	8.059	8.05	8.049	8.038	8.047	8.041	8.027	8.053	8.033	8.013	8.051

Oxide Wt.%	862Gt1lin3	862Gt1lin3	862Gt1lin3	862Gt1lin3	862Gt1lin3	862Gt1rim1	862Gt1rim2	862Gt1rim3	862Gt1core1	862Gt1core2	862Gt1core3	862Gt6core1	862Gt6core2	862Gt6core3
SiO_2	36.666	36.392	36.06	36.289	35.652	37.13	36.831	36.419	37.183	37.075	37.057	37.349	36.9	37.15
TiO_2	0.012	0.021	0	0	0.043	0.004	0	0	0.016	0.027	0.029	0.054	0.034	0.011
Al_2O_3	21.332	21.157	21.278	21.164	20.734	21.321	20.842	21.116	21.017	21.336	21.245	21.262	21.117	21.086
MgO	4.059	3.957	3.996	3.863	3.853	3.674	3.511	3.657	4.331	4.378	4.447	4.056	3.958	4.142
CaO	1.71	1.617	1.709	2.15	2.128	2.36	2.382	2.451	2.917	2.845	2.82	3.463	2.057	3.042
MnO	2	1.93	1.846	1.785	1.698	1.456	1.29	1.372	2.704	2.229	2.135	2.142	2.383	2.159
FeO	34.259	34.233	34.337	34.085	34.281	34.791	34.85	34.788	31.789	32.654	32.468	32.094	33.105	32.252
Na_2O	0	0.01	0.025	0.033	0.027	0.029	0.028	0.035	0.02	0.014	0.035	0.037	0.016	0.024
Total	100.038	99.317	99.251	99.369	98.416	100.765	99.734	99.838	99.977	100.558	100.236	100.457	99.57	99.866
Cation based on 12 oxygens														
Si	2.947	2.948	2.927	2.94	2.927	2.964	2.975	2.942	2.974	2.952	2.957	2.972	2.972	2.975
Ti	0.001	0.001	0	0	0.003	0	0	0	0.001	0.002	0.002	0.003	0.002	0.001
Al	2.021	2.02	2.036	2.021	2.006	2.006	1.984	2.011	1.981	2.002	1.998	1.994	2.004	1.99
Mg	0.486	0.478	0.484	0.467	0.472	0.437	0.423	0.44	0.516	0.52	0.529	0.481	0.475	0.494
Ca	0.147	0.14	0.149	0.187	0.187	0.202	0.206	0.212	0.25	0.243	0.241	0.295	0.177	0.261
Mn	0.136	0.132	0.127	0.122	0.118	0.098	0.088	0.094	0.183	0.15	0.144	0.144	0.163	0.146
Fe	2.303	2.319	2.331	2.31	2.353	2.323	2.354	2.35	2.127	2.175	2.167	2.136	2.23	2.16
Na	0	0.002	0.004	0.005	0.004	0.004	0.004	0.006	0.003	0.002	0.005	0.006	0.003	0.004
Total	8.041	8.04	8.058	8.052	8.07	8.034	8.034	8.055	8.035	8.046	8.043	8.031	8.026	8.031

Oxide Wt.%	862Gt6rim1	862Gt6rim2
SiO_2	36.935	36.844
TiO_2	0.005	0.004
Al_2O_3	20.498	20.97
MgO	3.811	3.478
CaO	2.473	2.323
MnO	1.439	1.41
FeO	34.732	34.796
Na_2O	0.154	0.004
Total	100.047	99.829
Cation based on 12 oxygens		
Si	2.977	2.973
Ti	0	0
Al	1.947	1.994
Mg	0.458	0.418
Ca	0.214	0.201
Mn	0.098	0.096
Fe	2.342	2.348
Na	0.024	0.001
Total	8.06	8.031

Appendix IF (cont.):
Microprobe Analysis of 862 Biotite

Oxide Wt.%	862Gt1Biin1	862Gt1Biin2	862Gt1Biin3	862Gt1Biin3a	862Gt1Biin4	862Gt1Bith1	862Gt1Bith1a	862Gt1Biout1	862Gt1Biout1	862Gt1Biout1A	862Gt1Bith2	862Gt1Biout2	862Gt4Biin1	862Gt4Biin1A
SiO_2	38.241	37.222	37.406	36.12	36.87	37.218	36.157	36.013	36.013	35.889	37.546	36.105	38.568	37.465
TiO_2	1.715	1.553	1.58	1.907	1.32	1.546	1.54	1.412	1.412	1.573	1.548	1.753	1.637	1.527
Al_2O_3	19.298	19.533	19.003	19.152	18.885	18.847	18.78	18.93	18.93	18.699	18.217	18.696	18.367	18.225
MgO	12.629	13.343	12.668	12.352	14.141	11.541	11.551	11.596	11.596	11.625	10.76	11.432	11.398	11.829
CaO	0.111	0.114	0.039	0.021	0.052	0.097	0.08	0.057	0.057	0.026	0.073	0.017	0.089	0.105
MnO	0.01	0.083	0.024	0.022	0.047	0.039	0.033	0.041	0.041	0.014	0.055	0.025	0.035	0
FeO	14.563	15.187	15.658	16.237	13.882	17.326	17.371	17.864	17.864	18.185	17.631	18.404	16.399	16.447
Na_2O	0.465	0.503	0.404	0.382	0.366	0.341	0.389	0.355	0.355	0.318	0.345	0.33	0.403	0.48
K_2O	8.538	8.519	9.004	9.07	8.862	8.629	8.357	8.364	8.364	8.864	8.549	8.968	8.666	8.804
H_2O	4.094	4.089	4.06	4.011	4.032	4.027	3.963	3.969	3.969	3.973	3.988	3.991	4.056	4.008
Total	99.664	100.146	99.846	99.274	98.457	99.611	98.221	98.601	98.601	99.166	98.712	99.721	99.618	98.89
Cation based on 22 oxygens														
Si	5.601	5.459	5.524	5.4	5.484	5.542	5.471	5.441	5.441	5.418	5.645	5.425	5.702	5.606
Ti	0.189	0.171	0.176	0.214	0.148	0.173	0.175	0.16	0.16	0.179	0.175	0.198	0.182	0.172
Al	3.331	3.376	3.308	3.375	3.311	3.307	3.349	3.371	3.371	3.327	3.228	3.311	3.2	3.214
Mg	2.757	2.917	2.789	2.753	3.136	2.562	2.605	2.612	2.612	2.616	2.412	2.561	2.512	2.639
Ca	0.017	0.018	0.006	0.003	0.008	0.016	0.013	0.009	0.009	0.004	0.012	0.003	0.014	0.017
Mn	0.001	0.01	0.003	0.003	0.006	0.005	0.004	0.005	0.005	0.002	0.007	0.003	0.004	0
Fe	1.784	1.863	1.934	2.03	1.727	2.158	2.198	2.257	2.257	2.296	2.217	2.313	2.027	2.058
Na	0.132	0.143	0.116	0.111	0.106	0.098	0.114	0.104	0.104	0.093	0.1	0.096	0.115	0.139
K	1.595	1.594	1.697	1.73	1.682	1.639	1.613	1.612	1.612	1.707	1.64	1.719	1.634	1.681
H	0	0	0	0	0	0	0	0	0	0	0	0	0	0
Total	15.407	15.551	15.553	15.619	15.608	15.5	15.542	15.571	15.571	15.642	15.436	15.629	15.39	15.526

Oxide Wt.%	862Gt4Biin2	862Gt4Biin2A	862Gt4Bith1	862Gt4Biout1
SiO_2	36.143	36.439	36.608	36.079
TiO_2	1.709	1.615	1.539	1.528
Al_2O_3	18.587	18.804	19.218	18.69
MgO	12.274	12.046	11.787	11.716
CaO	0.096	0.011	0.022	0.075
MnO	0.031	0.027	0	0
FeO	17.2	17.311	17.082	17.485
Na_2O	0.447	0.451	0.337	0.359
K_2O	8.756	9.069	8.889	8.625
H_2O	3.995	4.013	4.017	3.966
Total	99.238	99.786	99.499	98.523
Cation based on 22 oxygens				
Si	5.426	5.445	5.465	5.455
Ti	0.193	0.181	0.173	0.174
Al	3.289	3.311	3.381	3.33
Mg	2.747	2.683	2.623	2.641
Ca	0.015	0.002	0.004	0.012
Mn	0.004	0.003	0	0
Fe	2.159	2.163	2.132	2.211
Na	0.13	0.131	0.098	0.105
K	1.677	1.729	1.693	1.664
H	0	0	0	0
Total	15.64	15.648	15.569	15.592

Appendix IF (cont.):
Microprobe Analysis of 862 Muscovite

Oxide Wt.%	Gt4mus1in	Gt4mus2in	Gt4mu3in	862Gt1musctch1	862Gt1musctch1A	862Gt1muscout1	862Gt1musctch1A	862Gt1muscout1	862Gt1Muscout2	862Gt4Musctch1	862Gt4Muscout1
SiO_2	45.596	45.118	44.643	46.356	45.632	45.348	45.632	45.348	45.863	45.737	45.001
TiO_2	0.518	0.487	0.513	0.718	0.512	0.659	0.512	0.659	0.669	0.514	0.617
Al_2O_3	35.761	36.289	36.207	35.404	35.868	35.673	35.868	35.673	35.983	35.546	35.322
MgO	0.691	0.615	0.591	0.833	0.787	0.824	0.787	0.824	0.806	0.806	0.826
CaO	0.061	0.038	0	0.022	0.007	0.044	0.007	0.044	0.032	0.023	0.011
MnO	0.031	0.018	0	0	0	0	0	0	0.018	0	0
FeO	2.287	1.803	1.578	1.905	1.8	1.679	1.8	1.679	1.677	1.885	1.711
Na_2O	1.443	1.564	1.564	1.156	1.262	1.257	1.262	1.257	1.304	1.296	1.278
K_2O	8.862	8.743	9.002	8.421	8.178	8.323	8.178	8.323	8.692	8.353	8.875
H_2O	4.505	4.489	4.457	4.517	4.486	4.469	4.486	4.469	4.52	4.483	4.442
Total	99.755	99.164	98.555	99.332	98.532	98.276	98.532	98.276	99.564	98.643	98.083
Cations based on 22 oxygens											
Si	6.069	6.027	6.006	6.154	6.1	6.085	6.1	6.085	6.085	6.118	6.076
Ti	0.052	0.049	0.052	0.072	0.051	0.066	0.051	0.066	0.067	0.052	0.063
Al	5.61	5.713	5.741	5.539	5.651	5.641	5.651	5.641	5.627	5.604	5.62
Mg	0.137	0.122	0.119	0.165	0.157	0.165	0.157	0.165	0.159	0.161	0.166
Ca	0.009	0.005	0	0.003	0.001	0.006	0.001	0.006	0.004	0.003	0.002
Mn	0.004	0.002	0	0	0	0	0	0	0.002	0	0
Fe	0.255	0.201	0.178	0.211	0.201	0.188	0.201	0.188	0.186	0.211	0.193
Na	0.372	0.405	0.408	0.297	0.327	0.327	0.327	0.327	0.335	0.336	0.334
K	1.505	1.49	1.545	1.426	1.395	1.425	1.395	1.425	1.471	1.425	1.529
H	0	0	0	0	0	0	0	0	0	0	0
Total	14.013	14.014	14.049	13.867	13.883	13.903	13.883	13.903	13.936	13.91	13.983

Appendix IF (cont.):
Microprobe Analysis of 862 Ilmenite

Oxide Wt.%	862Gt1Ilin1A	862Gt1Ilin2	862Gt1Ilrim1	862Gt1Ilin3	862Gt1Ilrim2	862Gt1Ilrim3	862Gt1Ilout1	862Gt1Ilout3	862Gt1Ilout4
SiO2	5.985	0.021	0.081	1.632	0.113	0.052	0.094	0.073	0.063
TiO2	48.853	51.726	51.454	51.033	51.15	51.069	51.068	51.454	51.681
Al2O3	0.179	0.016	0.023	0.322	0.007	0.003	0.036	0.013	0.05
MgO	0.774	0.822	0.251	0.541	0.258	0.242	0.19	0.351	0.167
CaO	0.037	0.026	0.005	0.053	0.013	0.018	0.019	0.006	0
MnO	0.285	0.37	0.228	0.438	0.286	0.257	0.302	0.23	0.237
FeO	43.356	46.242	47.133	44.081	47.291	47.359	47.058	46.298	46.458
Na2O	0.046	0.028	0	0.037	0	0	0.032	0	0.033
Total	99.515	99.251	99.175	98.137	99.118	99	98.799	98.425	98.689
Cation based on 12 oxygens									
Si	0.582	0.002	0.008	0.165	0.012	0.005	0.01	0.008	0.006
Ti	3.57	3.951	3.949	3.879	3.933	3.935	3.939	3.969	3.977
Al	0.02	0.002	0.003	0.038	0.001	0	0.004	0.002	0.006
Mg	0.112	0.125	0.038	0.081	0.039	0.037	0.029	0.054	0.025
Ca	0.004	0.003	0.001	0.006	0.001	0.002	0.002	0.001	0
Mn	0.023	0.032	0.02	0.037	0.025	0.022	0.026	0.02	0.021
Fe	3.523	3.928	4.023	3.726	4.044	4.058	4.036	3.971	3.975
Na	0.009	0.006	0	0.007	0	0	0.006	0	0.007
Total	7.843	8.049	8.042	7.939	8.055	8.059	8.052	8.025	8.017

Appendix II: Structural Data

Abbreviations

Quadrangle
SS: Sylva South
T: Tuckaseegee

Lithology
Am: Amphibolite
MetaGW: Metagraywacke
MetaSS: Metasandstone
Peg: Pegmatite

Mineral
al: aluminum (aluminum silicate)
am: amphibole
bi: biotite
chl: chlorite
cs: calcsilicate
fsp: feldspar
ky: kyanite
ms: muscovite
sill: sillimanite

Structural
Ant: antiform
Syn: synform
Ptyg: ptygmatic

Other
Intly: interlayered

Appendix II. Structural data for the Sylva South and Tuckaseegee quadrangles

		Foliation				Axial Surface		Fold Axis	
Quad	Station	Strike	Dip	Lithology	Structure	Strike	Dip	Trend	Plunge
SS	1	N54E	53NW	MetaSS					
SS	2	N47E	85NW	MetaSS					
SS	3			MetaSS	tight antiform	N30E,	55NW	30NE	12
SS	4	N50E	47NW	bi schist					
SS	5	N50E	86SE	MetaGW					
SS	6			MetaSS	tight, anti-syn	N55E	40SE	56NE	10
SS	7			MetaSS	open-closed anti-syn	N37E	65NW	50NE	46
SS	8	N355	59NWM	MetaGW, W/intlay bi-gt schist					
SS	9	N59E	V	gt MetaGW w/ pegmatite					
SS	10			MetaGW	tight plunging antiform	N30E	85NW	20NE	25
SS	11			bi gneiss					
SS	12	N43E	V	bi gneiss					
SS	13	N15E	45NW	bi gneiss					
SS	14	N20E	70NW	bi gneiss					
SS	15	N65E	70NW	bi gt schist					
SS	16	N70E	62NW	MetaSS					
SS	17	N50E	60NW	bi ms gt schist					
SS	18	N20W	40NE	bi gneiss					
SS	19	N60W	50NE	MetaGW					
SS	20	N85W	74NE	bi gneiss					
SS	21	N85W	45NE	bi gneiss					
SS	22	N50E	30SE	bi gt schist					
SS	23	N60W	75SW	ms sill schist					
SS	24	N70E	65NW	bi gt schist					
SS	25	N65E	67NW	bi ms gt schist					
SS	26	N75W	45NE	MetaSS					
SS	27	N70E	55SE	MetaSS					
SS	28	N67E	74NW	MetaGW					
SS	29	N15E	85NW	MetaGW					
SS	30	N35E	80NW	MetaGW					
SS	31	N25E	85NW	MetaGW					
SS	32	N55E	85NW	MetaGW					
SS	33	N35E	79NW	bi gneiss					
SS	34	N35E	34NW	bi gneiss					
SS	35	N56E	75NW	bi ms gt schist					
SS	36	N30E	30NW	MetaSS					
SS	37	N40E	25NW	MetaGW					
SS	38	N47E	56NW	bi gneiss					
SS	39	N75W	50NE	bi gneiss					
SS	40	N80W	80NE	bi schist					
SS	41	N81W	40NE	bi gneiss					
SS	42	N70E	60NW	bi gneiss					
SS	43	N41E	84NW	bi gneiss					
SS	44			bi gneiss	S folds	N40E	60NW	40 SW	?
SS	45	N25E	56NW	ms gt schist					
SS	46	N54E	65NW	ms gt schist					
SS	47	N40E	55NW	Am					
SS	48	N53E	76NW	bi gneiss					
SS	49	N70E	40NW	bi gneiss					
SS	50	N20E	68NW	ms bi schist					
SS	51	N44E	41NW	bi gneiss					
SS	52	N45E	30NW	bi gneiss					
SS	53	N70E	53NW	bi gneiss					
SS	54	N10E	67NW	MetaSS					
SS	55	N70E	70NW	Schist					
SS	56	N85W	66NE	bi gt schist					
SS	57	N40E	85SE	bi gneiss	gentle-open ant-syn pair	N60E	63NW	N60E	40
SS	58	N35E	80SE	bi gneiss					
SS	59	N49E	74NW	bi gneiss					
SS	60	N54E	56NW	bi gneiss					
SS	61	N54E	56NW	Am					
SS	62	N50E	35SE	bi gneiss					
SS	63								
SS	64	N22E	79SE	ms gt schist					
SS	65	N59E	88SE	MetaGW					
SS	66	N35E	78SE	gt al schist					
SS	67	N60E	52NW	gt al schist					
SS	68	N20E	67SE	gt al schist					
SS	69	N65E	62NW	bi gneiss					
SS	70	N35E	70NW	bi gneiss					
SS	71	N46E	57NW	Am gneiss					
SS	72	N20E	50NW	bi gneiss					
T	73	N65E	55NW	bi gneiss					
T	74	N60E	64NW	bi gneiss					
T	75	N31E	74SE	bi gneiss	tight inclined	N45E	80SE	N35E	28
T	76	N35E	40SE	bi gneiss	open to closed synform	N55E	54SE	N55E	29
T	77	N50E	85SE	bi gneiss					
T	78	N43E	80NW	bi gneiss					
T	79	N58E	32NW	bi gneiss					
SS	80	N45E	42NW	bi gneiss					
SS	81	N15E	58SE	MetaSS					
SS	82	N85E	58NW	bi gneiss					
SS	83	N29E	61SE	MetaSS					
SS	84	N20E	40NW	bi gneiss					
SS	85	N60E	53NW	bi gneiss					
SS	86	N20E	36SE	MetaSS					
SS	87	N50E	40SE	bi gneiss					
SS	88	N50E	55NW	bi gneiss					
SS	89	N25E	40NW	peg					
SS	90	N30E	25NW	peg					
SS	91	N25E	61SE	peg					
SS	92	N33E	75SE	bi gneiss					
SS	93	N60E	25NW	bi gneiss					
SS	94	N63E	65SE	peg					
SS	95	N55E	65NW	MetaSS					
SS	96	N25E	40SE	MetaSS					
SS	97	N44E	45SE	MetaSS					
SS	98	N40E	85SE	peg					
SS	99	N85E	73SE	bi gneiss					
SS	100	N70E	60NW	bi gneiss					
SS	101	N65E	25SE	bi gneiss					
SS	102	N35E	57NW	ms bi schist					
SS	103	N55E	50NW	MetaSS					
SS	104	N35E	62SE	MetaSS					
SS	105	N65E	55NW	MetaSS					
SS	106	N23E	50SE	MetaSS					
SS	107	N20E	58SE	MetaSS					
SS	108	N20E	80NW	ms bi schist					
SS	109	N80E	56NW	MetaSS					
SS	110	N50E	64NW	al schist					
SS	111	N40E	85NW	al gt schist					
SS	112	N20E	85NW	al gt schist					
SS	113	N26E	70NW	bi schist					
SS	114	N40E	75NW	MetaSS					
SS	115	N45E	80NW	bi gt schist					
SS	116	N70E	80NW	bi gt schist					
SS	117	N70E	75NW	bi gt schist					

Appendix II. Structural data for the Sylva South and Tuckaseegee quadrangles

		Foliation				Axial Surface		Fold Axis	
Quad	Station	Strike	Dip	Lithology	Structure	Strike	Dip	Trend	Plunge
SS	118	N25E	85NW	MetaSS					
SS	119	N55E	70NW	MetaSS					
SS	120	N67E	62NW	al schist					
SS	121	N30E	45SE	MetaSS					
SS	122	N40E	V	bi gneiss					
SS	123	N20E	70NW	al schist					
SS	124	N65E	70NW	al schist					
SS	125	N44E	85NW	MetaSS					
SS	126	N40E	80NW	bi schist					
SS	127	N64E	50NW	MetaSS					
SS	128	N55E	65NW	bi gneiss					
SS	129	N40E	68NW	bi gneiss					
SS	130	N35E	50NW	bi gneiss					
SS	131	N30E	80NW	bi gneiss					
SS	132	N60E	55NW	bi gneiss					
SS	133	N75E	82NW	MetaSS					
SS	134	N75E	55NW	MetaSS					
SS	135	N35E	56NW	MetaSS					
SS	136	N64E	81NW	MetaSS					
SS	137	N50E	40NW	al schist					
SS	138	N50E	65NW	al schist					
SS	139	N60E	73NW	al schist					
SS	140	N65E	77NW	al schist					
SS	141	N69E	88NW	Am gneiss					
SS	142	N68E	76SE	bi gneiss					
SS	143	N50E	65SE	ms schist					
SS	144	N30E	67NW	al schist					
SS	145	N50E	71NW	bi gneiss					
SS	146	N55E	64NW	al schist					
SS	147	N59E	83NW	al schist					
SS	148	N45E	62NW	al schist					
SS	149	N60E	64NW	bi gneiss					
SS	150	N73E	80NW	Am gneiss					
SS	151	N56E	61NW	MetaGW					
SS	152	N63E	64SE	MetaGW					
SS	153	N55E	48NW	MetaSS					
SS	154	N57E	55NW	al schist					
SS	155	N35E	45NW	bi gneiss					
SS	156	N50E	67NW	bi gneiss					
SS	157	N67E	50NW	al schist					
SS	158	N45E	80NW	al schist					
SS	159	N45E	75NW	al gt schist					
SS	160	N15E	87NW	Am gneiss					
SS	161	N25E	50NW	bi gneiss					
SS	162	N70W	55NE	bi gneiss					
SS	163	N40W	15NE	bi gneiss					
SS	164	N30E	50NW	MetaGW					
SS	165	N35E	70NW	bi gneiss					
SS	166	N53E	60NW	bi gneiss					
SS	167	N40E	50NW	bi gneiss					
SS	168	N20E	75SE	bi gneiss					
SS	169	N50E	35NW	bi gneiss					
SS	170	N60E	45NW	bi gneiss					
SS	171	N60E	59NW	bi gneiss					
SS	172	N65E	64NW	bi gneiss					
SS	173	N45E	30NW	bi gneiss					
SS	174	N70E	67NW	al schist					
SS	175	N54E	85NW	bi gneiss					
SS	176	N67E	77NW	bi gneiss					
SS	177	N75E	67NW	al schist					
SS	178	N75E	71NW	bi gneiss					
SS	179	N75E	75SE	al schist					
SS	180	N65E	75SE	al schist					
SS	181	N45E	75NW	bi gneiss					
SS	182	N70E	65NW	al schist					
SS	183	N35E	29NW	bi gneiss					
SS	184	N40E	67NW	bi gneiss					
SS	185			al schist	crenulated, open folds	N105	15NW	20SE	40
SS	186	N32E	62SE	al schist					
SS	187	N52E	45NW	Am gneiss					
SS	188	N35E	85NW	bi gneiss					
SS	189	N65W	25NE	Am gneiss					
SS	190	N70E	65NW	al schist	tight to recumbant	N70E	54NW	65NE	15
SS	191	N55E	60NW	bi gneiss					
SS	192	N68E	57NW	bi gneiss					
SS	193	N25E	65NW	bi gneiss					
SS	194	N23E	70NW	bi gneiss					
SS	195	N15E	55NW	bi gneiss					
SS	196	N57E	70NW	bi gneiss	open folds	N50E	25NW	40NW	55
SS	197	N60E	57NW	bi gneiss					
SS	198	N25E	65SE	peg					
SS	199	N50E	45NW	bi gneiss					
SS	200	N43E	60NW	bi gneiss					
SS	201	N44E	60NW	bi gneiss					
SS	202	N40E	70NW	bi gneiss					
SS	203	N35E	45NW	bi gneiss					
SS	204	N70E	46NW	bi gneiss					
SS	205	N40E	55NW	bi gneiss					
SS	206	N35E	33NW	bi gneiss					
SS	207	N45E	65NW	bi gneiss					
SS	208	N40E	45NW	bi gneiss					
SS	209	N60E	40SE	Granodiorite					
SS	210	N60E	67NW	bi gneiss					
SS	211	N35E	40SE	Granodiorite					
SS	212	N60E	15SE	Granodiorite					
SS	213	N45E	40NW	bi gneiss					
SS	214	N70E	50NW	bi gneiss					
SS	215	N40E	70NW	bi gneiss					
SS	216	N50E	55SE	Granodiorite					
SS	217	N50E	55NW	bi gneiss					
SS	218	N50E	65NW	bi am gneiss					
SS	219	N35E	75NW	Granodiorite					
SS	220	N62E	46NE	bi-amph gneiss	tight recumbent fold	N70W	50NE	20NE	Horizontal
SS	221	N30E	35NW	granitoid					
SS	222	N65E	41NW	MetaGW					
SS	223	N74E	40NW	MetaGW					
SS	224	N65E	20SE	MetaGW					
SS	225	N20E	45SE	MetaGW					
SS	226	N40E	76SE	MetaGW					
SS	227	N15W	82NE	MetaGW					
SS	228	N5W	45NE	MetaGW					
SS	229	N5E	55SE	MetaGW					
SS	230	N5W	62NE	MetaGW					
SS	231	N15W	50NE	Bi-gneiss					
SS	232	N5W	88NE	bi gneiss					
SS	233	N15W	39NE	MetaSS					
SS	234	N80W	75NE	bi gt schist					

Appendix II. Structural data for the Sylva South and Tuckaseegee quadrangles

Quad	Station	Foliation		Lithology	Structure	Axial Surface		Fold Axis	
		Strike	Dip			Strike	Dip	Trend	Plunge
SS	235	N40W	40NE	MetaGW inly bi schist					
SS	236	N2W	V	MetaGW					
SS	237	N12E	75SE	al schist					
SS	238	N5E	55NW	bi gneiss					
SS	239	N40E	63NW	MetaSS					
SS	240	N10E	52SE	MetaGW					
SS	241	N10W	71NE	bi gneiss					
SS	242	N10E	47SE	bi gneiss					
SS	243	N15W	70NE	bi gneiss					
SS	244	N11W	60NE	bi gneiss	inclined tight, anti-syn pair	N10E	70SE	20SE	64
SS	245	N15E	60SE	bi schist					
SS	246	N25W	55NE	MetaSS					
SS	247	N85E	30NW	MetaGW					
SS	248	N35E	70NW	bi gneiss					
SS	249			MetaGW	tight-closed recumbent folds	N55E	35NW	?	?
SS	250	N35E	70NW	al schist					
SS	251	N45E	20NW	bi gneiss					
SS	252	N64E	50NW	bi gneiss					
SS	253	N85E	67NW	MetaSS					
SS	254	N70E	69NW	MetaSS					
SS	255	N65E	73NW	MetaSS intly Al schist					
SS	256	N80W	85NE	MetaSS					
SS	257	N65E	85SE	Meta SS					
SS	258	N67E	85SE	Meta SS					
SS	259	N50E	55NW	MetaSS					
SS	260	N70E	55NW	MetaSS					
SS	261	N80E	55SE	MetaSS					
SS	262	N75E	70NW	MetaSS					
SS	263			bi gni	tight folds	N75E	62NW	75NE	?
SS	264	N22W	64NE	bi gneiss	ptyg ant-syn pair	N70W	47NE	10NE	35
SS	265	N78E	45NW	bi gneiss					
SS	266	N70E	70NW	bi gneiss					
SS	267	N75E	30NW	al schist					
SS	268	N60E	44NW	bi gneiss					
SS	269	N77E	30NW	bi gneiss					
SS	270	N68E	73NW	bi gneiss					
SS	271	N65E	75SE	Am gneiss					
SS	272	N70W	36NE	bi gneiss					
SS	273	N50E	50NW	bi gneiss					
SS	274	N75E	55NW	Am gneiss					
SS	275	N80E	75NW	al schist					
SS	276	N80E	40SE	Am gneiss					
SS	277	N60E	48NW	bi gneiss					
SS	278	N57E	67NW	Am gneiss					
SS	279	N45E	52NW	bi gneiss					
SS	280	N57E	60NW	al schist					
SS	281	N74E	65NW	bi gneiss					
SS	282	N30W	35NE	al schist					
SS	283	N30E	65SE	bi gneiss		N62E	80NW	73NE	40
SS	284	N61E	70SE	al schist					
SS	285	N65E	45NW	bi gneiss					
SS	286	N80E	65NW	Am gneiss					
SS	287	N60E	80SE	bi gneiss					
SS	288	N45E	72NW	bi gneiss					
SS	289	N40E	65SE	bi gneiss					
SS	290	N45E	75NW	Am gneiss					
SS	291	N30E	71SE	al schist					
SS	292	N40E	64SE	Am gneiss					
SS	293	N40E	50NW	Am gneiss					
SS	294	N50E	40NW	bi gneiss					
SS	295	N56E	60NW	bi gneiss					
T	296	N40E	61NW	bi gneiss					
T	297	N57E	76NW	granitoid					
T	298	N70E	71NW	bi gneiss					
T	299	N5W	40SW	bi gneiss					
T	300	N70E	70NW	MetaGW					
SS	301	N74E	81NW	MetaSS					
SS	302	N80E	79SE	MetaSS					
SS	303	N75E	87SE	MetaSS					
SS	304	N68E	87SE	MetaSS					
SS	305	N70E	71NW	MetaSS					
SS	306	N10E	75NW	Meta SS					
SS	307	N75E	75SE	MetaSS					
SS	308	N75E	73NW	MetaSS					
SS	309	N80E	76NW	MetaSS					
SS	310	N50E	35NW	MetaSS					
SS	311	N45E	65SE	Bi-gneiss					
SS	312	N73E	65NW	Meta SS					
SS	313	N80E	65NW	al schist					
SS	314	N75E	80NW	al schist					
SS	315	N80W	67NE	MetaSS					
SS	316	N68E	30NW	MetaGW					
SS	317	N80E	85NW	bi gneiss					
SS	318	N65E	64NW	bi gneiss					
SS	319	N75E	85NW	bi gneiss					
SS	320	N75E	60NW	ms bi schist					
SS	321	N50E	85NW	MetaSS					
SS	322	N75E	85NW	bi ms schist					
SS	323	N75E	53SE	bi ms schist					
SS	324	N55E	60NW	MetaSS					
SS	325	N75E	70NW	MetaSS					
SS	326	N70E	50NW	MetaSS					
SS	327	N45E	85NW	MetaSS					
SS	328	N75E	51NW	MetaGW					
SS	329	N72E	75NW	MetaSS					
SS	330	N50E	70NW	Meta SS					
SS	331	N70E	71NW	MetaSS					
SS	332	N57E	85NW	MetaSS					
SS	333	N60E	55NW	MetaSS					
SS	334	N80E	82NW	MetaSS					
SS	335	N80E	50NW	MetaSS					
SS	336	N80E	70NW	MetaSS					
SS	337	N50E	55NW	MetaSS					
	338	N70E	80SE	MetaSS					
SS	339	N80E	80SE	MetaSS					
SS	340	N80E	85NW	Meta SS					
SS	341	N75E	60SE	Meta SS					
SS	342	N60E	78NW	Meta SS					
SS	343	N85E	60SE	MetaSS					
T	344	N23W	45NE	Bi-schist					
T	345	N70W	45NE	MetaGW					
T	346	N85E	35SE	MetaGW					
T	347	N60E	36SE	Meta SS					
T	348	N50E	60NW	Bi-rich MetaSS					
T	349	N65E	30NW	Bi-rich MetaSS					
T	350	N20E	10SE	MetaSS					
T	351	N15E	25SE	Bi-schist					

Appendix II. Structural data for the Sylva South and Tuckaseegee quadrangles

Quad	Station	Foliation		Lithology	Structure	Axial Surface		Fold Axis	
		Strike	Dip			Strike	Dip	Trend	Plunge
T	352	N50E	35SE	bi schist					
T	353	N10E	15SE	bi rich MetaSS					
SS	354	N68E	70NW	MetaGW					
SS	355	N75E	65NW	MetaGW					
SS	356	N70E	65NW	MetaSS					
SS	357	N50E	75NW	MetaSS					
SS	358	N45E	70SE	MetaSS					
SS	359	N55E	78NW	bi schist					
SS	360	N55E	75NW	ms bi schist					
SS	361	N40E	50NW	ms bi schist					
SS	362	N55E	50NW	MetaGW					
SS	363	N60E	80NW	MetaGW					
SS	364	N50E	75NW	MetaGW					
SS	365	N65E	85NW	MetaGW					
SS	365A	N80E	70NW	MetaGW					
SS	366	N80E	85SE	MetaGW					
SS	367	N65E	60NW	MetaGW					
SS	368	N80E	60NW	MetaSS					
SS	369	N75E	60NW	MetaSS					
SS	370	N50E	35NW	MetaSS					
SS	371	N65E	60NW	MetaSS					
SS	372	N70E	80NW	MetaSS					
SS	373	N25E	85NW	Bi gneiss					
SS	374	N30E	45NW	Bi gneiss					
SS	375	N50E	65NW	Bi-Gneiss					
SS	376	N75E	55NW	Amphi gneiss					
SS	377	N55E	85NW	Bi-ms schist					
SS	378	N35E	55NW	Bi-Gneiss w/ amph pods					
SS	379	N40E	35NW	Coarse gr. Granite weak foli					
SS	380	N40E	45SE	Coarse gr. Granite weak foli					
SS	381	N60E	60NW	Coarse gr. Granite weak foli					
T	382	N40W	30SW	Bi-gneiss intrud by granitoid					
T	383	N10E	25SE	med gr. Bi-ms schist					
T	384	N30E	75SE	Bi gneiss					
T	385	N65E	65NW	Bi gneiss					
T	386	N30E	50NW	MetaGW					
T	387	N40E	85NW	MetaGW					
SS	388	N30E	57NW	MetaSS					
SS	389	N70E	68SE	MetaSS					
SS	390	N75E	85SE	MetaSS					
SS	391	N70E	60NW	MetaSS					
SS	392	N70E	78SE	Meta MetaSS folitated					
SS	393	N75E	50SE	Bi schist w/ fsp (plag) and gt					
T	394	N50E	65NW	bi gneiss		N30E	62NW	20NW	35
T	395	N53E	65NW	Bi gneiss					
T	396	N35E	45NW	Bi gneiss					
T	397	N60E	80NW	Bi gneiss					
T	398	N60E	80NW	Bi gneiss					
T	399	N55E	45NW	bi ms schist					
T	400	N50E	45NW	granitoid					
T	401	N60E	35NW	granitoid					
T	402	N50E	40NW	granitoid					
T	403	N70W	50NE	granitoid					
T	404	N70W	38NE	granitoid					
T	405	N45E	50NW	Bi gneiss					
T	406	N45E	85SE	Bi gneiss					
T	407	N60E	65SE	granitoid					
T	408	N65E	75SE	granitoid					
T	409	N55E	85SE	MetaSS					
T	410	N55E	75NW	granitoid					
T	411	N60E	45NW	granitoid					
T	412	N65E	25NW	bi ms schist					
T	413	N55E	65NW	granitoid					
T	414	N55E	80SE	Bi gneiss					
T	415	N45E	42SW	granitoid					
T	416	N40E	45NW	ms bi schist					
T	417	N45E	75NW	bi schist					
T	418	N50E	57NW	bi ms schist					
T	419	N40E	35NW	granitoid					
T	420	N45E	60NW	granitoid					
T	421	N40E	30SE	granitoid					
T	422	N45E	75NW	Bi gneiss					
T	423	N60E	80NW	Bi gneiss					
T	424	N30E	70NW	Bi gneiss					
T	425	N50E	70NW	al schist					
T	426	N55E	55NW	Bi gneiss					
T	427	N45E	85NW	MetaGW					
T	428	N58E	85NW	bi-ms-gt schist					
T	429	N50E	60NW	bi ms schist					
T	430	N43E	85NW	bi schist	crenulations	N30E	50SE	N30E	?
T	431	N25E	65NW	bi schist					
T	432	N50E	53NW	bi ms schist					
T	433	N50E	67NW	bi ms gt schist					
T	434	N55E	85NW	bi ms gt schist					
T	435	N55E	85SE	Bi gneiss					
T	436	N40E	80SE	bi ms schist					
T	437	N53E	85NW	bi gneiss					
T	438	N50E	65SE	bi gneiss					
T	439	N32E	75NW	bi ms schist					
T	440	N45E	62NW	bi ms schist					
T	441	N45E	70SE	bi ms schist					
T	442	N50E	60NW	bi ms schist					
T	443	N65E	85SE	bi ms schist					
T	444	N30E	85NW	bi gneiss					
T	445	N40E	85NW	Bi gneiss					
T	446	N40E	70NW	Bi gneiss					
T	447	N40E	67NW	Bi gneiss					
T	448	N45E	85NW	bi gn					
T	449	N40E	80NW	Bi gneiss					
T	450	N30E	58NW	bi gneiss					
T	451	N85E	60NW	Bi gneiss					
T	452	N50E	85NW	Bi gneiss					
T	453	N15E	35SE	Bi gneiss					
T	454	N50E	65NW	Bi gneiss					
T	455	N80E	60NW	pegmatite					
T	456	N37E	60NW	pegmatite					
T	457	N60E	55NW	granitoid					
T	458	N50E	63NW	pegmatite					
T	459	N50E	55NW	pegmatite					
T	460	N50E	40NW	Bi gneiss					
T	461	N55E	45NW	Bi gneiss					
T	462	N50E	55NW	bi ms schist					
T	463	N47E	52NW	Bi gneiss					
T	464	N45E	75SE	bi ms schist					
T	465	N50E	85NW	bi ms schist					
T	466	N55E	75NW	Bi gneiss	S-FOLD	N30E	80NW	35NE	70
T	467	N60E	75NW	Bi gneiss					

Appendix II. Structural data for the Sylva South and Tuckaseegee quadrangles

Quad	Station	Foliation		Lithology	Structure	Axial Surface		Fold Axis	
		Strike	Dip			Strike	Dip	Trend	Plunge
T	468	N70E	40SE	Bi gneiss					
T	469	N80E	45SE	Bi gneiss					
T	470	N70E	55NW	Bi gneiss					
T	471	N50E	85NW	Bi gneiss					
T	472	N45E	45SE	Bi gneiss					
T	473	N30E	75SE	bi ms gt schist					
T	474	N45E	50NW	Bi gneiss					
T	475	N45E	75NW	Bi gneiss					
T	476	N40E	60NW	bi ms gt schist					
T	477	N60E	65NW	Bi gneiss					
T	478	N55E	67NW	Bi gneiss					
T	479	N40E	55NW	Bi gneiss					
T	480	N55E	85NW	Bi gneiss					
T	481	N60E	65SE	Bi gneiss					
T	482	N50E	70SE	Bi gneiss					
T	483	N55E	85SE	MetaSS					
T	484	N55E	85NW	ms bi schist					
T	485	N60E	88NW	Bi gneiss					
T	486	N60E	70NW	ms bi gt schist					
T	487	N60E	80NW	bi gneiss					
T	488	N50E	80NW	bi schist					
T	489	N20E	50SE	bi gneiss					
T	490	N45E	70NW	ms bi gt schist					
T	491	N45E	50NW	bi gneiss	recumbent, tight, fold	N45E	55NW	40NE	50
T	492	N50E	40NW	bi ms schist	crenulations	N75W	50NE	recumbent	
T	493	N45E	57NW	bi gneiss					
T	494	N25E	75NW	bi gneiss					
T	495	N30E	65NW	Bi gneiss					
T	496	N50E	70NW	gt bi schist					
T	497	N50E	65NW	bi ms schist					
T	498	N55E	75SE	bi ms schist					
T	499	N60E	60NW	bi ms schist					
T	500	N60E	60NW	bi ms schist					
T	501	N50E	85NW	Bi gneiss					
T	502	N50E	70NW	Bi gneiss					
T	503	N60E	75NW	Bi gneiss					
T	504	N60E	70NW	Bi gneiss					
T	505	N20W	40SW	granitoid					
T	506	N25W	10SW	granitoid					
T	507	N55E	65SE	bi ms schist	crenulation	N35W	85SW	45SE	63
T	508	N35W	45SW	granitoid					
T	509	N50E	75NW	ms bi schist					
T	510	N45E	70NW	ms bi gt schist					
T	511	N45E	80NW	ms bi gt schist					
T	512	N55E	70NW	ms bi gt schist					
T	513	N55E	70NW	sill gt schist					
T	514	N55E	70NW	ms gt schist					
T	515	N50E	75SE	ms gt schist					
T	516	N45E	50NW	granitoid					
T	517	N45E	80NW	Bi gneiss					
T	518	N50W	45NE	granitoid					
T	519	N30E	80SE	Bi gneiss					
T	520	N20E	60SE	Bi gneiss					
T	521	N55E	70SE	bi ms schist					
T	522	N55E	75SE	bi ms schist					
T	523	N70E	55NW	Bi gneiss					
T	524	N60E	65NW	Bi gneiss	Tight-closed ant-syn pair	N40E	65NW	20NE	60
T	525	N60E	65NW	bi gneiss					
T	526	N70E	80NW	Bi gneiss					
T	527	N50E	80NW	Bi gneiss					
T	528	N50E	80NW	bi gneiss					
T	529	N55E	40SE	granitoid					
T	530	N50E	70NW	bi gneiss					
T	531	N30E	75SE	granitoid					
T	532	N55E	50NW	granitoid					
T	533	N40E	55NW	bi gneiss					
T	534	N45E	70NW	Am					
T	535	N20W	80NE	bi gneiss					
T	536	N60E	15SE	granitoid					
T	537	N43E	80NW	bi gneiss					
T	538	N40E	75NW	bi gneiss					
T	539	N45E	55NW	bi gneiss					
T	540	N50E	70NW	bi gneiss					
T	541	N40E	80NW	bi gneiss					
T	542	N50E	80NW	sill ms bi schist					
T	543	N40E	60NW	bi gneiss					
T	544	N35E	85NW	bi gneiss					
T	545	N45E	60NW	Bi gneiss					
T	546	N45E	50NW	al schist					
T	547	N45E	80NW	bi gneiss					
T	548	N40E	60NW	Bi gneiss					
T	549	N50E	65NW	bi gneiss					
T	550	N45E	45NW	bi gneiss					
T	551	N55E	80NW	bi gneiss					
T	552	N50E	75NW	Bi gneiss					
T	553	N45E	55NW	bi gneiss					
T	554	N20W	35SW	granitoid					
T	555	N50E	85SE	ms bi schist					
T	556	N40E	70SE	ms bi gt schist					
T	557	N55E	70SE	ms bi gt schist					
T	558	N50E	85NW	ms bi gt schist					
T	559	N55E	85NW	Bi gneiss					
T	560	N50E	80NW	bi gneiss					
T	561	N60E	40SE	bi gneiss					
T	562	N40E	80NW	bi ms gt schist					
T	563	N45E	85NW	Bi gneiss					
T	564	N55E	70SE	bi gneiss					
T	565	N40E	80SE	bi gneiss					
T	566	N50E	70SE	bi gneiss					
T	567	N55E	55SE	ms bi schist					
T	568	N60E	50NW	ms bi schist					
T	569	N45E	70NW	ms bi gneiss					
T	570	N65E	85NW	ms bi gneiss					
T	571	N50E	40NW	ms bi gt schist					
T	572	N40E	75NW	ms bi gt schist					
T	573	N50E	65NW	bi ms gneiss	crenulated	N15W	60NE	15NW	65
T	574	N50E	75NW	bi ms gneiss					
T	575	N55E	50NW	bi ms gneiss					
T	576	N25E	55NW	bi ms gneiss					
T	577	N30E	62NW	ms bi gneiss					
T	578	N55E	50NW	ms bi gneiss					
T	579	N55E	65NW	ms bi gneiss					
T	580	N50E	75NW	ms bi gneiss					
T	581	N60E	45NW	bi ms schist					
T	582	N60E	55NW	bi gneiss					
T	583	N60E	35NW	bi gneiss					
T	584	N60E	35NW	bi gneiss					

Appendix II. Structural data for the Sylva South and Tuckaseegee quadrangles

Quad	Station	Foliation		Lithology	Structure	Axial Surface		Fold Axis	
		Strike	Dip			Strike	Dip	Trend	Plunge
T	585	N50E	70NW	bi gneiss					
T	586	N80E	55NW	bi gneiss					
T	587	N70E	70NW	bi gneiss					
T	588	N65E	55NW	bi gneiss					
T	589	N50E	60NW	bi gneiss					
T	590	N55E	70NW	bi gneiss					
T	591	N50E	70NW	bi gneiss					
T	592	N50E	60NW	bi schist					
T	593	N55E	50NW	bi schist					
T	594	N50E	70NW	bi gneiss					
T	595	N55E	65NW	Bi gneiss					
T	596	N65E	80NW	bi gneiss					
T	597	N55E	80NW	bi schist					
T	598	N65E	65NW	Bi gneiss					
T	599	N45E	30NW	granitoid					
T	600	N60E	65NW	bi gneiss					
T	601	N50E	75NW	bi gneiss					
T	602	N50E	75NW	ms bi schist					
T	603	N50E	65NW	ms bi schist					
T	604	N55E	50NW	Bi gneiss					
T	605	N50E	85NW	bi gneiss					
T	606	N50E	60NW	bi gneiss					
T	607	N50E	55NW	bi ms gneiss					
T	608	N45E	85NW	bi ms gneiss					
T	609	N45E	65NW	bi ms gneiss					
T	610	N45E	70NW	bi ms gneiss					
T	611	N45E	55SE	bi ms gneiss					
T	612	N50E	85NW	bi ms gneiss					
T	613	N50E	65NW	bi ms gneiss					
T	614	N50E	85NW	bi ms gneiss					
T	615	N55E	60NW	bi ms gneiss					
T	616	N50E	60NW	bi ms gneiss					
T	617	N60E	62NW	bi ms gneiss					
T	618	N50E	75NW	bi ms gneiss					
T	619	N40E	80NW	bi ms gneiss					
T	620	N50E	70NW	bi ms gneiss					
T	621	N70E	40NW	bi gneiss					
T	622	N60E	55NW	bi ms gneiss					
T	623	N55E	80NW	ms bi schist					
T	624	N40E	65NW	ms bi schist					
T	625	N40E	45NW	ms bi schist					
T	626	N50E	65NW	ms bi schist					
T	627	N55E	80NW	bi gneiss					
T	628	N50E	55NW	bi gneiss					
T	629	N45E	80NW	bi ms schist					
T	630	N65E	57NW	Am					
T	631	N45E	40SE	bi gneiss					
T	632	N30E	70SE	bi schist					
T	633	N35E	60SE	bi ms gneiss	, tight, inclined folded leucosomal layer	N15W	55NE	axial planar	
T	634	N50E	75SE	bi gneiss					
T	635	N55E	50NW	bi schist					
T	636	N30E	40SE	bi ms gneiss					
T	637	N55E	75SE	bi ms gneiss					
T	638	N45E	60NW	bi gneiss					
T	639	N60E	70NW	bi gneiss					
T	640	N55E	40SE	bi gneiss					
T	641	N55E	55NW	bi gneiss					
T	642	N20E	55SE	bi gneiss					
T	643	N40E	80SE	bi gneiss					
T	644	N35E	80SE	bi ms gneiss					
T	645	N40E	75SE	bi ms gneiss					
T	646	N40E	70SE	bi gneiss					
T	647	N45E	35SE	bi gneiss					
T	648	N10E	45SE	bi ms gneiss					
T	649	N15E	65SE	ms bi gneiss					
T	650	N10E	60SE	bi gne					
T	651	N15E	70SE	bi-ms gneiss					
T	652	N15E	45SE	bi-ms gneiss					
T	653	N15E	40SE	bi gneiss					
T	654	N15E	80SE	bi ms gneiss					
T	655	N10E	65SE	bi ms gneiss					
T	656	N10E	45SE	bi ms gneiss					
T	657	N65E	55NW	bi gneiss					
T	658	N55E	65NW	bi ms schist					
T	659	N50E	75NW	bi ms gneiss					
T	660	N60E	45NW	bi ms gneiss					
T	661	N50E	55NW	bi ms gneiss					
T	662	N20E	80SE	bi ms schist					
T	663	N50E	60SE	bi ms gneiss					
T	664	N40E	65SE	bi ms gneiss					
T	665	N20W	60SW	metasandstone, bi rich					
T	666	N25E	40SE	MetaGW, bi rich					
T	667	N25E	55SE	MetaGW, bi rich					
T	668	N20E	70SE	MetaGW					
T	669	N20E	75NW	bi, gt, sill schist					
T	670	N40E	35NW	MetaGW					
T	671	N20E	80NW	bi, gt, sill schist					
T	672	N10E	55SE	bi schist					
T	673	N55E	38SE	MetaGW, bi rich					
T	674	N40E	35SE	bi schist					
T	675	N40E	80SE	MetaGW, bi and ms					
T	676	N35E	55SE	MetaGW, bi rich					
T	677	N40E	80NW	MetaGW, intly bi and ms schist	crenulations	N40E	30SE	35NE	25
T	678	N50E	80NW	bi, ms, gt and sill schist					
T	679	N25E	75SE	MetaGW, bi					
T	680	N60E	80SE	bioite, ms and gt schist					
T	681	N45E	85SE	bioite, ms and gt schist					
T	682	N60E	80SE	bi schist, lesser ms					
T	683	N15W	25NE	MetaGW					
T	684	N20E	70NW	MetaGW					
T	685	N45E	85NW	MetaGW, ms and bi					
T	686	N85E	25SE	MetaGW					
T	687	N75E	25NW	MetaGW					
T	688	N70E	40NW	bi schist w/intly qtz & plag					
T	689	N45W	45NE	bi schist w/intly qtz & plag					
T	690	N20W	40NE	MetaGW, gt					
T	691	N20E	80SE	bi rich ms schist					
T	692	N45E	70SE	bi gneiss					
T	693	N40E	80SE	bi rich ms schist					
T	694	N55E	80SE	bi schist					
T	695	N50E	70SE	bi gneiss					
T	696	N40E	70SE	bi ms gneiss					
T	697	N25E	60SE	bi ms gneiss					
T	698	N5E	85SE	bi gneiss					
T	699	N10E	75SE	bi schist					
T	700	N15E	50SE	tronjemite					
T	701	N10E	70SE	bi schist					

Appendix II. Structural data for the Sylva South and Tuckaseegee quadrangles

Quad	Station	Foliation		Lithology	Structure	Axial Surface		Fold Axis	
		Strike	Dip			Strike	Dip	Trend	Plunge
T	702	N30E	60SE	bi gneiss					
T	703	N30E	67NW	bi gneiss					
T	704	N52E	55NW	bi gneiss					
T	705	N50E	55NW	bi gneiss					
T	706	N55E	75NW	bi ms gneiss					
T	707	N40E	55NW	bi rich ms schist					
T	708	N35E	70NW	bi schist					
T	709	N30E	85NW	bi ms gneiss					
T	710	N60E	77NW	bi gneiss	similar, axial planar folds	N50E	55NW	N10E	55
T	711	N65E	75NW	bi ms gneiss					
T	712	N50E	85NW	bi ms gneiss					
T	713	N40E	65NW	bi ms schist					
T	714	N40E	75NW	bi ms schist					
T	715	N45E	85NW	bi ms gneiss	pytgmatic folds, leuco layer, ~0.7cm	N55E	50NW	30NW	75
T	716	N40E	70SE	bi ms gneiss					
T	717	N40E	65NW	bi ms gneiss					
T	718	N55E	60NW	bi rich ms schist					
T	719	N40E	75SE	bi ms schist					
T	720	N60E	65NW	bi gneiss					
T	721	N30E	75NW	bi ms schist					
T	722	N45E	85NW	bi ms schist					
T	723	N50E	80NW	bi ms schist					
T	724	N50E	45NW	bi gneiss					
T	725	N50E	85NW	bi ms gneiss					
T	726	N35E	40NW	ms bi schist					
T	727	N70E	35NW	ms bi schist					
T	728	N55E	45SE	bi gneiss					
T	729	N50E	45NW	pegmatite					
T	730	N10W	35SW	bi ms schist					
T	731	N70E	35SE	bi ms schist					
T	732	N15W	60NE	bi ms gneiss					
T	733	N60E	30NW	bi ms schist	crenulations	N50E	70SE	40NE	50
T	734	N70E	75NW	bi ms schist					
T	735	N50E	50NW	bi ms schist					
T	736	N50E	70NW	bi ms gneiss					
T	737	N45E	50NW	bi-ms gneiss					
SS	738	N65W	15NE	bi ms gneiss					
SS	739	N50E	67NW	bi ms gneiss	lineation of leucosomal layer			80NE	55
SS	740	N80E	75NW	bi gneiss					
SS	741	N40E	80NW	bi ms gneiss					
SS	742	N80E	67NW	bi gneiss					
SS	743	N75E	80NW	bi ms gneiss					
SS	744	N80E	85NW	bi ms gneiss					
SS	745	N10E	88NW	bi ms gneiss					
SS	746	N15W	85NE	bi ms gneiss					
SS	747	N75E	31NW	sill schist					
SS	748	N78E	45NW	ms bi schist					
SS	749	N65E	70NW	Am					
SS	750	N40W	50NE	bi ms schist					
T	751	N65E	85NW	chl schist					
T	752	N10W	25NE	MetaGW					
T	753	N55W	43NE	bi ms schist					
T	754	N55W	60NE	MetaSS					
T	755	N40W	55NE	bi ms schist					
T	756	N55W	40NE	MetaSS					
T	757	N35W	55NE	MetaSS w/ intly schist					
T	758	N50E	35SE	MetaGW					
T	759	N45E	27SE	bi gneiss					
T	760	N20E	50SE	bi gneiss					
T	761	N20E	70SE	ms gt schist					
T	762	N40E	27SE	bi gneiss					
T	763	N25E	70SE	bi gneiss					
T	764	N20E	45SE	bi ms schist					
T	765	N20E	54SE	bi gneiss					
T	766	N50E	60NW	bi ms gneiss					
T	767	N60E	48NW	bi ms gneiss					
T	768	N55E	50NW	bi ms gniess					
T	769	N60E	59NW	bi ms gneiss					
T	770	N55E	55NW	bi ms schist					
T	771	N40E	70NW	bi ms schist					
T	772	N50E	63NW	bi ms gneiss					
T	773	N55E	55NW	bi ms gneiss					
T	774	N60E	30NW	bi ms gneiss					
T	775	N65E	65NW	MetaGW					
T	776	N50E	57NW	MetaGW					
T	777	N60E	60NW	bi ms schist					
T	778	N65E	35NW	granitoid					
T	779	N55E	73NW	bi schist					
T	780	N55E	45NW	bi schist					
T	781	N50E	45NW	MetaGW					
T	782	N40E	30NW	MetaGW					
T	783	N80E	60NW	MetaGW					
T	784	N65E	58NE	MetaGW					
T	785	N50E	80NW	MetaGW					
T	786	N50E	55NW	MetaGW					
T	787	N35E	85NW	bi gt schist					
T	788	N30W	65NW	MetaGW					
T	789	N35E	65NW	Bi-schist					
T	790	N35E	45NW	bi ms gt schist					
T	791	N42E	85NW	MetaGW					
T	792	N35E	85NW	bi schist					
T	793	N35E	60NW	MetaGW					
T	794	N45E	70NW	MetaGW					
T	795	N35E	75NW	MetaGW					
T	796	N40E	75NW	MetaGW					
T	797	N30E	67NW	MetaGW					
T	798	N45E	60NW	MetaGW					
T	799	N30E	70NW	MetaGW					
T	800	N50E	75NW	MetaGW					
T	801	N40E	85NW	bi ms gt schist					
T	802	N35E	70SE	bi ms gt schist					
T	803	N45E	65NW	MetaGW					
T	804	N45E	65NW	bi ms gneiss					
T	805	N35E	75SE	MetaGW					
T	806	N35E	60NW	bi ms gt schist	crenulated	N40E	60SE	55SW	35
T	807	N70W	40SW	bi ms gt schist					
T	808	N45W	85NE	ms bi gneiss					
T	809	N30E	77NW	bi ms gt schist					
T	810	N40E	75SE	MetaGW					
T	811	N55E	75SE	MetaGW					
T	812	N40E	60SE	MetaGW					
T	813	N30E	65SE	Bi-schist					
T	814	N10E	50SE	bi-ms MetaGW					
T	815	N50E	35NW	MetaGW					
T	816	N40E	75NW	ultramafic with talc					
T	817	N40E	45SE	Meta sandstone					
T	818	N15W	40NE	MetaGW					

Appendix II. Structural data for the Sylva South and Tuckaseegee quadrangles

Quad	Station	Foliation		Lithology	Structure	Axial Surface		Fold Axis	
		Strike	Dip			Strike	Dip	Trend	Plunge
T	819	N20E	35NW	MetaGW					
T	820	N20E	60NW	MetaGW					
T	821	N25E	88NE	bi gneiss					
T	822	N23E	85NW	MetaGW					
T	823	N35E	60SE	MetaGW					
T	824	N35E	50NW	MetaGW					
T	825	N40E	60NW	MetaGW					
T	826	N20W	72NE	MetaGW					
T	827	N75E	20NW	MetaGW					
T	828	N55E	60NW	MetaGW					
T	829	N55E	65NW	MetaGW					
T	830	N55E	45NW	MetaGW					
T	831	N55E	55NW	MetaGW					
T	832	N30E	65NW	MetaGW					
T	833	N30E	75SE	MetaGW					
T	834	N40E	67NW	schist	crenulated				
T	835	N28E	69NW	bi and ms granular schist					
T	836	N33E	65NW	bi and ms granular schist					
T	837	N25E	60NW	bi, ms, gt schist					
T	838	N35E	80NW	MetaGW w/ intly schist					
T	839	N40E	80NW	MetaGW					
T	840	N43E	80NW	ms schist					
T	841	N32E	80NW	ms and bi schist w/ porphyroclasts of plagioclase					
T	842	N25E	78NW	bi schist w/ qtz and plag					
T	843	N30E	65NW	MetaGW w/ intly schist					
T	844	N40E	47NW	MetaGW					
T	845	N35E	80NW	MetaGW					
T	846	N35E	75NW	schist	S-C fabric				
T	847	N45E	70NW	bi gneiss, lesser ms					
T	848	N40E	60NW	MetaGW					
T	849	N50E	85NW	schist					
T	850	N40E	77SE	bi gneiss					
T	851	N30E	70NW	bi and ms schist					
T	852	N65E	79NW	ms schist					
T	853	N65E	25NW	bi gneiss	tight closed fold, refolded into open-closed fold	E	55N	NE?	85
					refold:	N75W	85SW	75NW	55
T	854	N75W	25NE	bi gneiss					
T	855	N55E	25SE	Bi rich MetaGW					
T	856	N55W	48NE	Bi rich MetaGW, lesser ms					
T	857	N70W	30NE	MetaGW					
T	858	N65W	60NE	MetaGW					
T	859	N70W	35NE	MetaGW					
T	860	N85W	50NE	bi ms gt schist					
T	861	N70W	50NE	bi ms gt schist					
T	862	N20E	65SE	bi ms gt schist					
T	863	N30E	75SE	bi ms gt schist					
T	864	N20E	70SE	MetaGW					
T	865	N30E	80SE	bi ms gt schist					
T	866	N30E	73NW	pegmatite					
T	867	N40E	40SE	bi ms schist					
T	868	N25E	35NW	MetaGW	closed asymmetrical folds	N55E	50NW	35SW	50
T	869	N20E	65SE	ultramafic					
T	870	N20E	70SE	MetaGW					
T	871	N30W	72SW	MetaGW					
T	872	N65E	15NW	Am cs					
T	873	N65W	30NE	Am gneiss					
T	874	N30E	15NW	Am gneiss					
T	875	N30W	36SW	Am gneiss					
T	876	N80W	20NE	bi gneiss					
T	877	N70E	35NW	bi gt schist					
T	878	N65E	30NW	Meta GW intly schist					
T	879	N20E	75SE	Meta GW intly schist					
T	880	N15W	30NE	MetaGW intly schist					
T	881	N70W	25NE	Am gneiss					
T	882	N70W	35NE	Am gneiss					
T	883	N73W	36NE	bi gneiss					
T	884	N60W	10NE	bi gneiss					
T	885	N85E	55NW	MetaGW					
T	886	N30W	52NE	MetaGW intly schist					
T	887	N40W	44NE	Am gneiss					
T	888	N65W	32NE	Am					
T	889	N40W	30NE	Am gneiss	open fold	N50E	55NW	40NE	75
T					tight folds anti-syn pair	N40W	42NE	35NW	55
T	890	N55E	30NW	bi ms gt schist					
T	891	N10E	40SE	ms bi gt schist					
T	892	N25E	65SE	bi gneiss					
T	893	N35E	55SE	bi ms gt schist					
T	894	N60W	39NE	Am gneiss					
T	895	N60W	41SW	ultramafic					
T	896	N40W	60SW	ultramafic					
SS	897	N20E	68SE	Am gneiss					
SS	898	N35W	35SW	Am gneiss					
SS	899	N15W	30NE	MetaSS					
SS	900	N10W	55NE	MetaSS					
SS	901	N10W	40NE	MetaSS					
SS	902	N35W	50NE	sill ms bi gt schist					
SS	903	N20W	40NE	MetaGW					
SS	904	N40E	33SE	Am gneiss					
SS	905	N40E	72SE	Am gneiss					
SS	906	N25E	65NW	MetaGW					
SS	907	N45E	60NW	MetaGW					
SS	908	N30E	63NW	MetaGW	pegmatite N20E@72NW				
SS	909	N40E	60NW	bi gt schist					
SS	910	N35E	50NW	MetaGW					
SS	911	N10E	75SE	MetaGW					
SS	912	N60E	50NW	ms bi gt sill schist					
SS	913	N50E	55NW	MetaGW					
SS	914	N35E	55NW	MetaGW					
SS	915	N45E	40NW	MetaGW					
SS	916	N45E	85NW	bi ms gt schist					
T	917	N45E	60NW	bi ms gt schist					
T	918	N45E	55NW	bi ms gt schist					
T	919	N30E	65NW	granitoid	pegmatite N20E@65NW				
T	920	N25E	35NW	granitoid					
T	921	N40E	60NW	MetaGW	open and closed anti-syn pair, inclined	N40E	60NW	25NE	30
T	922	N42E	35NW	granitoid					
T									
T	923	N40E	45NW	granitoid					
T	924	N45E	45NW	granitoid					
T	925	N50E	65SE	pegmatite					
T	926	N55E	70NW	MetaGW					
T	927	N32E	64NW	MetaGW					
T	928	N25E	45NW	MetaGW					
T	929	N10E	45SE	granitoid					
T	930	N52E	74NW	bi gneiss					
T	931	N45E	55NW	granitoid					
SS	932	N60E	52NW	MetaGW					

Appendix II. Structural data for the Sylva South and Tuckaseegee quadrangles

Quad	Station	Foliation		Lithology	Structure	Axial Surface		Fold Axis	
		Strike	Dip			Strike	Dip	Trend	Plunge
SS	933	N60E	55NW	MetaGW					
SS	934	N50E	70SE	MetaGW					
SS	935	N58E	87SE	MetaGW					
SS	936	N60E	48NW	MetaGW					
SS	937	N60E	32NW	MetaGW					
SS	938	N40E	72NW	MetaGW					
T	939	N80W	20NE	bi gneiss					
T	940	N60E	50NW	ultramafic					
T	941	N10E	78SE	MetaGW					
T	942	N60E	52NW	bi ms gt schist	crenulated open-closed, ant-syn	N75W	30SW	78SW	15-20
T	943	N45E	39NW	MetaGW					
T	944	N50E	78NW	ultramafic					
T	945	N30E	60NW	ultramafic					
T	946	N35E	67NW	MetaGW					
T	947	N70E	55NW	Am					
T	948	N40E	70NW	bi ms gt schist					
T	949	N55W	50NE	MetaGW					
T	950	N60E	36NW	MetaGW					
T	951	N5E	40SE	MetaGW					
T	952	N25E	50SE	bi gneiss					
T	953	N20W	70NE	bi gneiss					
T	954	N10E	50SE	bi gneiss					
T	955	N20E	70SE	bi ms gniess					
T	956	N10E	15SE	bi ms gneiss					
SS	957	N15E	85NW	MetaGW	qtz-rich layer	N50W	60SE		
SS									
SS	958	N20E	85NW	saprolite					
T	959	N45E	72SE	bi gneiss					
T	960	N35E	62SE	saprolite					
T	961	N40E	70SE	ms bi gt schist	, open, crenulations	N55W	65SE	65SE	40
T	962	N25E	75SE	MetaGW					
T	963	N35E	70SE	bi ms gt schist	crenulations	N40E	46SE	45NE	20
T	964	N54E	35NW	MetaGW	, tight, recument	N55E	53NW	67SW	53
T					refolded, , open fold	N35W	60SW	45NW	36
T	965	N65W	77NE	ms gt schist					
T	966	N55W	63NE	MetaGW					
T	967	N43E	62SE	bi ms gt schist					
T	968	N45E	70SE	bi ms schist					
T	969	N47E	77SE	MetaGW					
T	970	N58E	45SE	bi ms schist	, closed kink folds ant-syn pair	N80W	30NE	85SE	23
T	971	N80E	75NW	granitoid					
T	972	N35E	85NW	ultramafic					
T	973	N35E	85NW	ultramafic					
T	974	N37E	70NW	ultramafic					
T	975	N25E	83NW	ultramafic					
T	976	N30E	70SE	ultramafic					
T	977	N32E	57SE	bi ms gt schist					
T	978	N5E	39NW	Am					
T	979	N10E	35SE	Am					
T	980	N20E	55SE	ultramafic					
T	981	N20E	35NW	UM semi-schist					
T	982	N30E	40NW	ultramafic					
T									
T	983	N60E	51NW	ms bi schist					
T	984	N57E	49NW	Am					
T	985	N50E	82NW	bi ms schist					
T	986	N15E	64NW	ms bi schist					
T	987	N57E	82NW	ms bi schist					
T	988	N54E	60NW	MetaSS					
T	989	N35E	54NW	MetaGW					37558
T	990	N45E	47NW	MetaGW					
T	991	N30E	50NW	MEtaGW					
T	992	N45E	62NW	ms bi schist					
T	993	N43E	58NW	saprolite					
T	994	N40E	54NW	bi ms schist					
T	995	N47E	61NW	MetaGW					
T	996	N58E	45NW	ms schist					
T	997	N40E	60NW	ms bi gt schist					
T	998	N45E	57NW	bi rich MetaGW	x-cut tronj dike N20E,50NW				
SS	999	N66E	40NW	Granodiorite					
SS	1000	N52E	57NW	Granodiorite					
SS	1001	N65E	75SE	Granodiorite					
SS	1002	N84E	74NW	bi rich MetaGW					
SS	1003	N75E	59NW	bi MetaGW, gt	tight recumbent fold	N85E	59NW	N15W	60
SS	1004	N87E	65NW	bi rich gt schist					
SS	1005	N85W	68NE	amph and bi gneiss w/intly cs					
SS	1006	N80W	46NE	amph and bi gneiss w/intly cs					
SS	1007	N85E	70NW	bi,gt schist	open to gentle fold	N5W	55NE	N5W	61
SS	1008	N85W	57NE	bi rich MetaGW					
SS	1009	N70E	37NW	bi MetaGW					
SS	1010	N65E	61NW	bi MetaGW					
SS	1011	N80E	55NW	bi MetaGW					
SS	1012	N65W	70SW	large qtz lenses bi rich, amph					
SS	1013	N50W	45NE	bi MetaGW, felsic layers ~2-5cm apart					
SS	1014	N80E	75SE	amph-bi gneiss w/ cs					
SS	1015	N55E	80NW	amph MetaGW w/ cs					
SS	1016	N75E	77NW	bi MetaGW w/ms, minor gts					
SS	1017	N50E	65NW	al schist, v. weathered ms,bi,gt schist. Med-coarse gr.					
SS	1018	N55E	55NW	bi,ms,gt,sill Schist	open to closed crenulations	N50E	34NW	50SW	10
SS	1019	N74E	75NW	bi MetaGW, dark grey, intlylay fine gr. Schist	crenulated				
SS	1020	N65E	60NW	bi rich MetaGW intly schist	open to gentle crenulations	N74W	20SW	50SW	7
SS	1021	N67E	85SE	bi,ms,gt schist	open to gentle crenulations	N20E	7SE	55SW	11
SS	1022	N75E	75NW	bi,amph MetaGW					
T	1023	N5W	45NE	amph,bi gneiss					
T	1024	N14W	70NE	amph					
T	1025	N20E	85NW	gt-amph poorly foliated, small mylonite zone (~2-3cm)					
T	1026	N7E	57SE	qtz-rich gneiss (cs) w/ bi and amph					
T	1027	N25E	64SE	qtz-rich gneiss (cs) w/ bi and amph (bi rich)					
T	1028	N20E	75SE	qtz-rich gneiss (cs) w/ bi and amph (bi and amph rich)					
T	1029	N5E	50NW	mafic/um, rounded and poor foliation					
T	1030	N25E	75SE	bi rich, bi,ms,gt schist, med gr. (gt ~1-2mm across)					
T	1031	N25E	60SE	bi rich gneiss, poorly formed boudins					
T	1032	N40E	45SE	bi rich, bi, ms gneiss w/ intlylay bi,ms,gt schist					
T	1033	N41E	67SE	bi,ms,chl schist (mafic/UM?)					
T	1034	N20E	65SE	bi rich, bi, ms gneiss w/ intlylay bi, ms, gt schist					
T	1035	N5E	65NW	UM semi-schist					
SS	1036	N85W	71NE	meta SS, med-fine gr. Poorly foliated, light grey					
SS	1037	N78E	76NW	bi,ms,gt,chl schist, med-fine gr., red and yellow staining					
SS	1038	N84E	50NW	bi,ms,gt,chl schist, med-fine gr., red and yellow staining					
SS	1039	N40E	65NW	MetaGW, w/ intlylay ms,gt,bi schist(med-fine gr)	gently-open fold	N24E	40NW	75NW	35
T	1040	N55E	45SE	qtz rich metagreywacke, ms and bi, med to med-fine gr.					
T	1041	N20W	52NE	qtz rich bi ms gneiss w/ intly schist, grey/tan	open fold	N85E	60NW	70NE	85
T	1042	N25W	60NE	qtz rich bi ms gneiss w/ intly schist, grey/tan , migmatitic	tight to closed fold	N5W	65SE	55NW	5
T	1043	N25W	60NE	qtz rich bi ms gneiss w/ intly schist, grey/tan					
T	1044	N45W	70NE	qtz rich bi ms gneiss w/ intly schist, grey/tan					
T	1045	N45W	40NE	qtz rich bi ms gneiss w/ intly schist, grey/tan					
T	1046	N85W	55NE	qtz rich bi ms gneiss w/ intly bi and gt rich sill? schist,					

Appendix II. Structural data for the Sylva South and Tuckaseegee quadrangles

		Foliation				Axial Surface		Fold Axis	
Quad	Station	Strike	Dip	Lithology	Structure	Strike	Dip	Trend	Plunge
T	1047	N10W	75NE	qtz rich bi,ms gneiss w/ intly ms,bi,gt,sill schist					
T	1048	N45W	85NE	qtz rich ms,bi gneiss	tight to isoclinal fold	N50W	80NE	17SE	40
T	1049	N17E	80NW	qtz rich ms,bi gneiss					
T	1050	N5E	50SE	quartz rich bi ms gneiss					
T	1051	N75W	67NE	bi ms					
T	1052	N80W	40NE	bi ms					
T	1053	N10E	75NW	Ultramafic					
T	1054	N25E	40NW	ultramafic					
T	1055	N45E	40NW	al schist					
T	1056	N85W	22NE	chl schist					
T	1057	N70E	44NW	bi ms gneiss	tight to isoclinal folds	N88W	50NE	88W	45
T									
T	1058	N75E	55NW	bi ms gneiss					
T	1059	N80E	0	bi ms gneiss					
T	1060	N77E	85NW	ultramafic					
T	1061	N40E	72NW	bi ms gneiss w/ intly al schist	crenulations	N30E	10SE	55NE	7
T	1062	N55E	60SE	intly bi schist	open to gentle synform	N70E	55NW	70NE	10
T	1063	N10W	48NE	bi ms					
T									
T	1064	N12W	54NW	bi ms gneiss w/ intly al schist	tight to isoclinal fold	N55W	27NE	W-NW	
T	1065	N35W	45NE	bi ms gneiss w/ intly schist	tight upright fold	N84E	54SE	84NE	31
SS	1066	N79E	30NW	bi ms					
T	1067	N50E	67NW	ultramafic					
T	1068	N61E	60SE	ultramafic					
T	1069	N45E	40SE	ultramafic					
T	1070	N45W	65NE	al schist					
T	1071	N55W	81NE	MetaGW					
T	1072	N70W	71SW	Ultramafic					
T	1073	N45E	55NW	granitoid					
T	1074	N60E	67NW	bi rich ms					
T	1075	N15E	42NW	Granodiorite					
T	1076	N60E	75NW	bi gneiss					
T	1077	N48E	70NW	bi rich, contact b/t bi gneiss and granite					
T	1078	N55E	54NW	bi gneiss intly schist					
T	1079	N55E	57NW	bi gneiss intly schist					
T	1080	N40E	22NW	bi gneiss intly bi ms schist					
T	1081	N35E	70SE	al, bi ms gt sill schist					
T	1082	N64E	64NW	bi ms gneiss					
T	1083	N10W	60NE	bi ms					
T	1084	N85E	43NW	al, bi ms gt sill schist					
T	1085	N22W	42NE	bi gneiss					
T	1086	N20W	43NE	bi gneiss					
T	1087	N45E	40SE	amph Bi, finely layered					
T	1088	N40W	28NE	qtz rich w/ bi and amph					
T	1089	N16W	62NE	qtz rich w/ bi and amph					
T	1090	N38W	20NE	qtz rich w/ bi and amph					
T	1091	N38W	48NE	qtz rich w/ bi and amph					
T	1092	N10W	54NE	qtz rich metaSS w/ bi and amph					
T	1093	N21E	70SE	qtz rich w/ bi and amph					
T	1094	N45W	25NE	qtz rich bi gneiss					
T	1095	N20E	70SE	qtz rich bi gneiss					
SS	1096	N44E	55NW	qtz rich metaSS					
SS	1097	N60E	55NW	bi rich ms gt schist					
SS	1098	N50E	55NW	ms schist					
SS	1099	N45E	62NW	gt rich schist					
SS	1100	N40E	62SE	ms rich gt bi sill schist					
SS	1101	N11W	75NE	Al schist					
SS	1102	N40E	80SE	bi ms amph metaSS w/ intly schist					
SS	1103	N40E	85SE	bi ms amph metaSS w/ intly schist					
SS	1104	N70E	82SE	bi ms amph metaSS w/ intly schist					
SS	1105	N17W	45NE	gt rich al schist w/ amph?					
SS	1106	N13W	54NE	gt rich bi sill schist					
SS	1107	N20E	80NW	gt sill schist					
SS	1108	N20E	60SE	amph gniess					
T	1109	N30E	60SE	qtz rich metaSS bi ms gt					
T	1110	N60E	60NW	bi ms gt sill schist					
T	1111	N45E	52SE	ms gt schist					
T	1112	N50E	80SE	granodiorite					
T	1113	N45E	40NW	bi ms gt schist					
T	1114	N35E	55SE	Bi rich gneiss					
SS	1115	N35E	60NW	ms gt schist					
SS	1116	N35E	60NW	ms bi gt schist					
SS	1117	N50E	82NW	ms bi gt schist					
SS	1118	N35E	52SE	metaSS					
SS	1119	N60W	65NE	metaSS w/intly schist					
SS	1120	N60E	67NW	metaSS w/intly schist					
SS	1121	N45E	55NW	gt bi ms schist					
SS	1122	N40E	63NW	gt bi ms schist					
SS	1123	N55E	52NW	gt bi ms schist					
SS	1124	N40E	54NW	ms gt schist					
SS	1125	N55E	65NW	bi ms					
T	1126	N10E	60NW	ultramafic					
T	1127	N62E	54NW	bi gneiss					
T	1128	N65E	60NW	al schist					
T	1129	N40E	67NW	bi gneiss					
T	1130	N75E	53NW	bi rich MetaSS					
T	1131	N65E	57NW	bi rich lesser ms					
T	1132	N45E	55NW	al schist					
T	1133	N50E	67NW	intly bi schist					
SS	1134	N50E	39NW	bi gneiss w/intly amph					
SS	1135	N75W	35NW	bi schist					
SS	1136	N85W	54NE	bi rich gneiss w/intly amph					
SS	1137	N80W	55NE	bi amph gneiss w/ minor Csilicate					
SS	1138	N50W	70SW	bi schist, amph					
SS	1139	N25E	25NW	bi ms schist					
SS	1140	N50W	55NE	bi ms al schist	open to closed synform	N80W	60NE	45NE	45
T	1141	N62E	80NW	bi ms gneiss w/intly bi ms schist					
T	1142	N65E	64NW	pegmatite					
T	1143	N65E	50NW	bi rich gniess w/intly bi ms schist					
T	1144	N55E	57NW	bi rich gniess					
T	1145	N50E	61NW	bi rich gniess w/intly bi ms gt schist	crenulated schist	N40E	62SE	45NE	30
T	1146	N50E	55NW	bi rich gneiss					
T	1147	N58E	80SE	bi rich gneiss					
T	1148	N60E	73NW	ms rich bi gt schist					
T	1149	N65E	75SE	bi ms gt schist					
T	1150	N70E	77NW	bi ms gneiss					
T	1151	N63E	52NW	bi rich ms schist					
T	1152	N65E	58NW	bi rich gneiss and granodiorite contact	tight to isoclinal folds in gneiss	N60E	50NW	20NE	50
SS	1153	N62E	67NW	qtz rich metaSS					
SS	1154	N65E	75NW	qtz rich metaSS					
SS	1155	N75E	31NW	metaSS w/Csilicate					
SS	1156	N60E	65NW	mafic/UM					
SS	1157	N70E	77NW	metaSS					
T	1158	N75E	71NW	bi gneiss	tight anitform	N60E	82NW	55SW	20
T	1159	N51E	87NW	bi gneiss					
T	1160	N45E	75SE	bi gneiss w/intly Csilicate					
T	1161	N41E	87SE	bi gneiss					

Appendix II. Structural data for the Sylva South and Tuckaseegee quadrangles

Quad	Station	Foliation		Lithology	Structure	Axial Surface		Fold Axis	
		Strike	Dip			Strike	Dip	Trend	Plunge
T	1162	N55E	65NW	bi ms gt schist					
T	1163	N60E	81NW	Al schist					
T	1164	N40E	67SE	Al bi ms gt schist					
T	1165	N50E	65SE	Al bi ms gt schist					
T	1166	N45E	65NW	bi ms gt schist					
T	1167	N63E	70NW	Bi gneiss w/intly bi ms gt schist					
T	1168	N45E	65NW	bi gneiss w/ intly bi ms gt schist					
T	1169	N35E	54SE	MetaGW					
T	1170	N60E	80NW	bi ms qtz rich metaSS					
T	1171	N20E	39NW	bi gneiss w/intly schist					
T	1172	N40E	71SE	bi ms schist					
T	1173	N35E	65SE	bi rich ms gneiss w/ intly ms bi gt schist					
T	1174	N50E	40SE	bi rich ms gneiss					
T	1175	N5W	53NE	bi ms gneiss					
T	1176	N5W	57NE	bi ms gneiss					
T	1177	N4W	45NE	bi ms gneiss					
T	1178	N10W	55NE	ms gt schist					
T	1179	N10W	25SW	amph					
T	1180	N40E	50NW	metaSS gt					
T	1181	N40E	75NW	bi gneiss					
T	1182	N55E	75NW	bi gneiss					
T	1183	N55E	80NW	bi ms gneiss					
SS	1184	N35E	45NW	bi ms schist					
SS	1185	N35W	80SW	granodiorite					
SS	1186	N50E	40NW	granodiorite					
SS	1187	N60E	80SE	ms bi gt schist					
T	1188	N85W	60SW	mafic/UM					
T	1189	N20E	30SE	granodiorite					
T	1190	N30E	10NW	granodiorite					
T	1191	N15W	35NE	qtz rich metaSS					
T	1192	N50W	60NE	qtz rich metaSS					
T	1193	N65W	49NE	qtz rich metaSS					
T	1194	N75W	57NE	metaSS					
T	1195	N30W	60NE	metaSS					
T	1196	N20W	50NE	metaSS w/intly bi ms schist					
T	1197	N50E	75NW	MetaSS w/ intly schist					
T	1198	N35E	55NW	MetaSS intly Al schist					
T	1199	N40E	75NW	MetaSS					
T	1200	N55E	65SE	MetaSS					
T	1201	N60E	57NW	MetaSS					
T	1202	N10E	85NW	bi rich					
T	1203	N5E	58NW	MetaSS					
T	1204	N35E	57NW	MetaSS					
T	1205	N35E	82NW	bi rich					
T	1206	N45E	70NW	intly bi ms gt schist					
T	1207	N30E	70NW	MetaSS					
T	1208	N30E	75NW	MetaSS					
T	1209	N60E	62NW	MetaSS					
T	1210	N87W	50NE	MetaSS					
T	1211	N10E	57NW	MetaSS					
T	1212	N45E	70NW	MetaSS					
T	1213	N60E	30NW	intly bi ms gt schist					
T	1214	N45E	77SE	bi ms					
T	1215	N50W	55NE	metaSS					
T	1216	N45W	44NE	metaSS					
T	1217	N60E	75SE	metaSS					
T	1218	N20E	65SE	metaSS w/minor amph					
T	1219	N50W	55NE	bi ms metaSS					
T	1220	N50W	20NE	bi ms metaSS					
T	1221	N39W	30NE	bi ms gt sill schist					
T	1222	N20W	85SW	bi ms metaSS					
T	1223	N10W	65NE	metaSS w/intly amph					
T	1224	N65E	79NW	bi ms gt					
T	1225	N60E	52NW	bi ms					
T	1226	N30E	72NW	bi ms					
T	1227	N40E	80NW	chl bi ms gt					
T	1228	N62E	85SE	chl bi ms gt					
T	1229	N85E	80NW	MetaSS					
T	1230	N45E	71SE	ms					
T	1231	N40E	45NW	bi ms					
T	1232	N45E	40SE	chl gt					
T	1233	N50E	60SE	schist					
T	1234	N80E	60NW	bi ms gt					
T	1235	N20E	45SE	bi ms gt chl					
T	1236	N10W	15NE	ms					
T	1237	N20E	40SE	MetaSS					
T	1238	N60E	58NW	bi ms metasandstone					
T	1239	N50E	67NW	bi ms gt					
T	1240	N60E	45NW	cs					
T	1241	N5W	57NE	MetaSS					
T	1242	N55E	67SE	ms chl gt					
T	1243	N55E	49NW	ms chl gt					
TSS	1244	N60E	25NW	MetaSS					
T	1245	N30E	77NW	bi ms MetaSS					
T	1246	N20W	65NE	al schist					
T	1247	N45W	41NE	al schist					
T	1248	N20W	54NE	MetaSS					
T	1249	N35W	51NE	MetaSS					
T	1250	N45W	54NE	al schist					
T	1251	N45W	65NE	MetaSS					
T	1252	N35W	65NE	bi ms MetaSS					
T	1253	N25W	45NE	bi ms MetaSS					
T	1254	N22W	30NE	bi ms MetaSS					
T	1255	N55W	57NE	MetaSS intly Al schist					
T	1256	N25W	35NE	MetaSS					
T	1257	N30W	40NE	MetaSS intly Al schist					
T	1258	N25E	27NW	al schist					
T	1259	N35E	40NW	bi ms MetaSS					
T	1260	N50E	70SE	cs					
T	1261	N60W	40NE	MetaSS intly Al schist	tight fold	N50W	45NE	50NW	75
T	1262	N30W	35NE	MetaSS intly Al schist					
T	1263	N45W	35NE	MetaSS intly Al schist					
T	1264	N40W	80NE	MetaSS intly Al schist					
T	1265	N55E	50NW	bi ms MetaSS					
T	1266	N55E	85NW	MetaSS intly Al schist					
T	1267	N32W	65NE	MetaSS intly Al schist					
T	1268	N35W	40NE	MetaSS					
T	1269	N35W	50SE	MetaSS					
T	1270	N12W	55NE	al schist					
T	1271	N45W	55NE	MetaSS					
T	1272	N37E	80NW	bi ms MetaSS					
T	1273	N45E	83SE	bi ms MetaSS					
T	1274	N46E	55NW	bi ms MetaSS					
T	1275	N25W	37NE	MetaSS					
T	1276	N75W	65NE	MetaSS					
T	1277	N45E	80NW	MetaSS					
T	1278	N25E	45NW	cs					

Appendix II. Structural data for the Sylva South and Tuckaseegee quadrangles

Quad	Station	Foliation		Lithology	Structure	Axial Surface		Fold Axis	
		Strike	Dip			Strike	Dip	Trend	Plunge
T	1279	N35E	85NW	bi ms gt MetaSS					
T	1280	N43E	67NW	bi ms gt MetaSS					
T	1281	N43E	85NW	Al schist					
T	1282	N30E	60SE	MetaSS					
T	1283	N40E	75SE	bi ms gt schist	open to closed crenulations	N40E	35SE	30NE	10
T	1284	N15E	85NW	al schist					
T	1285	N10W	50NE	cs					
T									
T	1286	N45E	65NW	bi ms MetaSS					
T	1287	N40W	46NE	bi ms MetaSS					
T									
T	1288	N40E	80SE	ms chl gt schist					
T	1289	N10E	55SE	MetaSS					
T	1290	N72E	53NW	bi ms gneiss					
T	1291	N70E	55NW	al schist					
T	1292	N65E	67NW	bi gneiss					
T	1293	N85E	55NW	Ultramafic					
T	1294	N65E	72NW	Ultramafic					
T	1295	N65E	67NW	bi ms bi MetaSS					
T	1296	N61E	60NW	bi ms chl schist					
T	1297	N20E	34NW	Ultramafic					
T	1298	N43E	46NW	MetaSS					
T	1299	N58E	65NW	bi ms MetaSS					
T	1300	N70W	65NE	pegmatite					
T	1301	N75E	63NW	bi ms metaSS					
T	1302	N67W	38NE	Ultramafic					
T	1303	N70W	37NE	bi ms MetaSS					
T	1304	N75E	50NW	bi ms MetaSS					
T	1305	N55E	45NW	bi ms MetaSS					
T	1306	N80E	45NW	bi ms MetaSS					
T	1307	N75E	45NW	bi ms MetaSS					
T	1308	N60E	70NW	bi ms MetaSS					
T	1309	N78W	50NE	bi ms MetaSS					
T	1310	N75E	73SE	MetaSS					
T	1311	N65E	37NW	MetaSS					
T	1312	N15W	55NE	bi gneiss					
T	1313	N70E	45NW	bi ms gt schist	crenulations	N33E	85NW	40NE	27
T	1314	N45E	60NW	ms rich bi gt sill schist					
T	1315	N35E	49SE	qtz metaSS					
T	1316	N30E	65SE	bi rich gneiss	tight synform	N20E	50SE	25SW	45
T	1317	N35E	80SE	bi rich gneiss					
T	1318	N30E	45SE	bi rich gneiss					
T	1319	N20E	55NW	bi rich metaSS					
T	1320	N64E	80SE	bi rich gneiss w/intly bi ms gt schist					
T	1321	N40E	72SE	bi gneiss w/intly bi schist					
T	1322	N55E	45SE	bi rich gneiss					
T	1323	N70E	45NW	bi rich gneiss w/intly bi ms schist					
T	1324	N65E	50SE	bi ms metaSS					
T	1325	N45E	85NW	bi rich gneiss					
T	1326	N70E	60NW	bi gneiss w/intly bi schist	open crenulation	N75E	16SE	47SW	28
T	1327	N65E	50NW	bi rich gneiss					
T	1328	N25E	37SE	metagrawacke					
T	1329	N70E	57NW	bi rich gneiss					
T	1330	N50E	80SE	bi rich gneiss					
T	1331	N50E	85SE	bi rich gneiss					
T	1332	N25E	57SE	gt ms schist					
T	1333	N25E	75NW	bi rich gneiss					
T	1334	N15W	31NE	MetaSS					
T	1335	N30W	50NE	MetaSS					
T	1336	N45E	82SE	MetaSS					
T	1337	N25E	82SE	MetaSS					
T	1338	N85W	45NE	bi ms gneiss	open to closed fold	N35E	63NW	37NE	30
T					open fold	N50E	55NW	35NE	35
T	1339	N30W	75NE	MetaGW					
T	1340	N40E	70SE	MetaSS					
T	1341	N70E	43NW	MetaGW					
T	1342	N50E	68NW	MetaGW					
T	1343	N45E	80NW	MetaSS					
T	1344	N40E	40SE	MetaGW					
T	1345	N43E	55SE	bi ms gneiss	tight ant/syn pair	N45E	76NW	50SW	25
T	1346	N20E	70NW	bi ms gneiss	isoclinal fold	N10W	77SW	10NW	65
T	1347	N40E	54SE	bi ms gneiss	tight fold, thickens in hinge	N33E	75SE	35NE	52
T	1348	N65E	50SE	bi ms gneiss					
T	1349	N60E	80NW	bi ms gt schist					
T	1350	N50E	63SE	bi ms metaSS					
T	1351	N20W	60NE	amph					
T	1352	N50W	65SW	bi ms gt schist					
T	1353	N20E	85NW	bi ms gt schist					
T	1354	N70E	45NW	MetaSS w/intly schist					
T	1355	N80E	40NW	MetaSS					
T	1356	N10W	67NE	w/intly bi ms schist					
T	1357	N30W	45NE	w/intly bi ms schist					
T	1358	N50W	15SW	w/intly bi ms schist					
T	1359	N20W	50NE	w/intly bi ms schist					
T	1360	N43E	78NW	w/intly bi ms schist					
T	1361	N40W	43NE	intlylyered cs	open fold	N30E	55NW	25NE	35
T	1362	N85W	57NE	bi and lesser ms schist					
T	1363	N60E	74NW	bi ms gt schist					
T	1364	N55E	75NW	bi and ms MetaSS					
T	1365	N45E	77NW	bi ms gt chl schist					
T	1366	N65E	55NW	bi rich gneiss					
T	1367	N60W	35NE	Ky bi gt schist					
T	1368	N30W	40NE	MetaSS w/intly schist					
T	1369	N60W	45NE	v. qtz rich bi ms MetaSS					
T	1370	N22E	75SE	chl bi schist					
T	1371	N20E	62NW	gt chl talc ultramafic					
T	1372	N10E	80NW	ms schist					
T	1373	N34E	77SE	talc gt chl ultramafic					
T	1374	N61W	70NE	talc gt chl ultramafic					
T	1375	N15W	60NE	MetaSS w/ intly ms ky schist					
T	1376	N20E	55SE	MetaSS intly ms gt schist					
T	1377	N45W	60NE	bi rich gt gneiss					
T	1378	N80E	77NW	qtz rich MetaSS w/ cs					
T	1379	N30W	60NE	MetaSS w/ intly ms ky schist					
T	1380	N75E	70NW	bi rich ms gt schist					
T	1381	N75W	57NE	MetaSS					
T	1382	N50E	60NW	MetaSS intly bi ms gt schist					
T	1383	N60E	70SE	bi ms gt schist					
T	1384	N35E	65SE	MetaSS					
T	1385	N70E	30NW	MetaGW					
T	1386	N45E	65NW	Am					
T	1387	N35E	55SE	bi ms schist					
T	1388	N45E	85SE	bi ms gt schist					
T	1389	N20E	60NW	bi ms gneiss					
T	1390	N55E	77SE	bi ms schist					
T	1391	N65E	56NW	pegmatite					
T	1392	N80E	75NW	pegmatite					

Appendix II. Structural data for the Sylva South and Tuckaseegee quadrangles

Quad	Station	Foliation		Lithology	Structure	Axial Surface		Fold Axis	
		Strike	Dip			Strike	Dip	Trend	Plunge
T	1393	N37E	60NW	pegmatite					
T	1394	N60E	35NW	pegmatite					
T	1395	N50E	75NW	pegmatite					
T	1396	N50E	60SE	granodiorite					
T	1397	N50E	55NW	pegmatite					
T	1398	N25W	35SW	granodiorite					
T	1399	N65W	60NE	pegmatite					
T	1400	N60E	80NW	pegmatite					
T	1401	N55E	35SE	bi ms gneiss					
T	1402	N75E	40NW	bi gneiss					
T	1403	N80E	63NW	bi gneiss					
T	1404	N60E	55NW	bi gneiss					
T	1405	N35E	70SE	saprolite					
T	1406	N60E	70NW	bi gneiss					
T	1407	N65E	85SE	saprolite					
T	1408	N45E	65SE	bi gneiss	tight to isoclinal anti-syn pair	N50E	65SE	47NE	70
T	1409	N50E	60SE	bi gneiss	isoclinal synform	N70E	45SE	60NW	70
T	1410	N69E	70NW	bi schist					
T	1411	N50E	80NW	bi ms schist					
T	1412	N65E	78NW	bi schist					
T	1413	N50E	70SE	bi schist					
T	1414	N32E	80NW	saprolite cs					
T	1415	N15W	50NE	bi ms gneiss					
T	1416	N50E	75SE	saprolite					
T	1417	N50E	80SE	saprolite	crenulation open	N10W	20NE	70NE	10
T	1418	N40E	80NW	ms schist					
T	1419	N45E	80NW	ms schist					
T	1420	N45E	80NW	saprolite					
T	1421	N35E	80SE	saprolite					
T	1422	N45E	82NW	bi ms gt sill schist					
T	1423	N41E	77SE	bi ms gneiss					
T	1424	N65E	35NW	gt bi chl schist					
T	1425	N64E	N38W	bi ms gt schist					
T	1426	N45E	50NW	bi ms gt schist					
T	1427	N75E	65NW	ms rich gt bi schist					
T	1428	N65E	45NW	qtz rich bi ms gneiss					
T	1429	N37E	40SE	qtz rich bi ms gneiss					
T	1430	N30E	75SE	qtz rich bi ms gneiss					
T	1431	N50E	40NW	pegmatite					
T	1432	N40E	35NW	bi gt chl ms schist					
T	1433	N23E	60SE	bi ms gt schist					
T	1434	N45E	50SE	bi ms gneiss					
T	1435	N59E	60NW	bi ms gt schist					
T	1436	N25E	35SE	bi rich lesser ms schist					
T	1437	N20E	45SE	bi ms qtz rich gneiss gneiss					
T	1438	N50E	65SE	bi rich, gt, lesser ms schist					
T	1439	N50E	53SE	bi rich, gt, lesser ms schist					
T	1440	N30E	57SE	bi rich, gt, lesser ms schist					
T	1441	N30E	85SE	plag and qtz rich w/ ms and bi gneiss					
T	1442	N30E	47SE	bi rich, lesser ms schist					
T	1443	N50E	40NW	bi rich, gt, lesser ms schist					
T	1444	N40W	80NE	schist					
T	1445	N20E	50SE	bi ms MetaSS					
T	1446	N20E	30SE	MetaSS					
T	1447	N60E	80SE	bi ms gt schist					
T	1448	N62E	75SE	bi ms gt schist					
T	1449	N45E	75NW	bi ms gt schist	open crenulations	N42E	20SE	40NE	15
T	1450	N50E	70NW	ms schist					
T	1451	N64E	75NW	bi ms gt gneiss					
T	1452	N46E	70NW	ms bi gt schist					
T	1453	N55E	76NW	saprolite	open folds	N50E	67NW	50SW	60
T	1454	N35E	83SE	MetaSS	tight fold	N15W	50NW	15SW	45
T					gentle to open folds	N45E	65NW	45NE	43
T	1455	N75E	80NW	MetaSS					
T	1456	N40E	81NW	MetaSS					
T	1457	N67E	70NW	MetaSS intly Am					
T	1458	N15E	65SE	granodiorite					
T	1459	N63E	84NW	cs					
T	1460	N20E	85NW	saprolite					
T	1461	N12W	70NE	granodiorite					
T	1462	N40E	75SE	cs					
T	1463	N47E	87NW	cs					
T	1464	N50E	70SE	Am					
T	1465	N30E	80NW	Am					
T	1466	N20E	55NW	bi gneiss					
T	1467	N70E	40SE	saprolite					
T	1468	N40E	40NW	bi schist					
T	1469	N20E	57NW	Am					
T	1470	N20E	80NW	bi ms gt schist					
T	1471	N43E	60NW	bi ms gneiss					
T	1472	N40E	45NW	bi gneiss					
T	1473	N35E	71NW	bi gneiss					
T	1474	N27E	40NW	bi gneiss					
T	1475	N35E	51SE	granitoid					
T	1476	N55E	70NW	bi ms gt schist					
T	1477	N50E	60NW	bi ms gt schist					
T	1478	N10E	59SE	granitoid					
T	1479	N63E	85NW	granitoid					
T	1480	N68E	59NW	granitoid					
T	1481	N65E	72NW	granitoid					
T	1482	N45E	55NW	bi ms gt schist					
T	1483	N44E	60NW	bi gneiss					
T	1484	N64E	67NW	saprolite					
T	1485	N41E	78NW	bi gneiss	gentle inclined fold	N55W	60NE	55SE	85
T	1486	N46E	80NW	bi ms schist	tight crenulations	N49E	30SE	70NE	5
T	1487	N41E	80NW	bi ms gt schist	open to closed crenulations	N35E	34SE	35NE	2
T	1488	N35E	85Nw	bi ms gt schist					
T	1489	N45E	85SE	bi ms gneiss					
T	1490	N41E	70SE	bi ms schist					
T	1491	N7E	40SE	bi ms gneiss					
T	1492	N50E	65SE	saprolite					
T	1493	N60E	87NW	saprolite					
T	1494	N20E	37SE	bi gneiss					
T	1495	N40E	80NW	bi ms gt schist					
T	1496	N65E	70NW	ms schist	crenulations	N22W	30NE	65NE	30
T	1497	N56E	68NW	bi gneiss					
T	1498	N50E	64NW	bi ms gt schist					
T	1499	N50E	65NW	bi gneiss					
T	1500	N55E	60NW	bi gneiss					
T	1501	N65E	60NW	bi ms gneiss					
T	1502	N65E	57NW	bi ms gneiss					
T	1503	N60E	70NW	bi ms gneiss					
T	1504	N60E	75SE	MetaSS					
T	1505	N50E	55NW	qtz rich bi ms MetaSS w/ intly bi rich ms gt schist					
T	1506	N50E	67NW	qtz rich bi ms MetaSS w/ intly bi rich ms gt schist					
T	1507	N40E	35NW	qtz rich bi ms MetaSS w/ intly bi rich ms gt schist					
T	1508	N35E	30SE	ms rich gt schist					

Appendix II. Structural data for the Sylva South and Tuckaseegee quadrangles

Quad	Station	Foliation		Lithology	Structure	Axial Surface		Fold Axis	
		Strike	Dip			Strike	Dip	Trend	Plunge
T	1509	N73E	75SE	bi ms gneiss					
T	1510	N51E	50NW	ms ky gt al schist					
T	1511	N60E	50NW	bi ms gt schist					
T	1512	N65E	50NW	qtz rich MetaSS w/ intly ms ky gt schist					
T	1513	N10E	61SE	bi ms gt schist					
T	1514	N7E	80NW	bi ms gt schist					
T	1515	N6W	57NE	bi ms gt schist					
T	1516	N17E	67SE	bi ms gt schist					
T	1517	N45E	65NW	bi gneiss					
T	1518	N65E	45NW	bi gneiss					
T	1519	N50W	25NE	bi gneiss	recumbent anti-syn pair	N20W	32NE	20NW	20
T	1520	N70E	45NW	bi gneiss					
T	1521	N55E	67NW	bi gneiss					
T	1522	N65E	45NW	bi gneiss					
T	1523	N57E	40NW	bi gneiss					
T	1524	N60E	45NW	bi gneiss					
T	1525	N50E	63NW	bi gneiss					
T	1526	N45E	55NW	bi gneiss					
T	1527	N46E	75NW	bi ms gneiss	closed to tight crenulation	N30E	35SE	35NE	40
T	1528	N45E	70SE	bi ms gneiss					
T	1529	N40E	70NW	bi ms gneiss					
T	1530	N37E	65NW	bi ms gneiss					
T	1531	N54E	75NW	bi gneiss					
T	1532	N60E	67NW	bi gneiss					
T	1533	N29W	51SW	bi gneiss					
T	1534	N62E	74SE	granitoid					
T	1535	N45E	57NW	granodiorite					
T	1536	N65E	75NW	bi gneiss					
T	1537	N45E	80NW	qtz rich, ms bi MetaSS					
T	1538	N45E	65SE	ms bi gt schist					
T	1539	N40E	67NW	ms bi gt schist					
T	1540	N55E	70SE	ms bi gt schist					
T	1541	N56E	61NW	ms bi gt schist					
T	1542	N50E	75NW	ms bi gt schist					
T	1543	N55E	67NW	ms bi gt schist					
T	1544	N40E	68NW	ms bi gneiss					
T	1545	N57E	64NW	ms rich, bi, gt schist					
T	1546	N52E	80SE	ms rich, bi, gt schist					
T	1547	N65E	85NW	ms rich, bi, gt schist					
T	1548	N50E	75SE	ms rich, bi, gt schist					
T	1549	N51E	75NW	bi rich, ms, gt schist					
T	1550	N60E	80NW	ms rich schist					
T	1551	N65E	83NW	ms bi gt					
SS	1552	N40E	67SE	MetaSS					
SS	1553	N10W	74NE	MetaSS					
SS	1554	N10E	84SE	MetaSS					
SS	1555	N20W	75NE	bi ms gneiss					
SS	1556	N70E	47NW	Am gneiss					
SS	1557	N10E	58SE	saprolite					
SS	1558	N10E	58SE	bi gneiss					
SS	1559	N25E	79NW	saprolite					
	1560	N65E	55NW	bi ms schist					
T	1561	N35E	74NW	bi gneiss					
T	1562	N50E	72NW	saprolite					
T	1563	N70E	65NW	bi gneiss					
T	1564	N55E	67NW	pegamtite					
T	1565	N47E	46NW	bi gneiss					
T	1566	N51E	63NW	bi gneiss					
T	1567	N68E	72NW	granodiorite					
T	1568	N67E	47NW	ms bi gt schist					
T	1569	N39E	46NW	bi schist					
T	1570	N55W	75SW	qtz rich ms bi MetaSS					
T	1571	N80E	54SE	qtz rich ms bi MetaSS					
T	1572	N21E	52SE	MetaSS w/intly ms rich schist					
T	1573	N30E	54SE	gt MetaSS					
T	1574	N20E	41SE	ms bi gneiss					
T	1575	N37E	56SE	qtz rich ms bi MetaSS					
T	1576	N20E	62SE	qtz rich ms bi MetaSS					
T	1577	N35E	43SE	qtz rich ms bi MetaSS					
T	1578	N25E	57SE	bi ms gt schist					
T	1579	N35E	60SE	bi ms schist					
T	1580	N26E	60SE	qtz rich MetaSS					
T	1581	N35E	80SE	qtz rich MetaSS					
T	1582	N25E	70NW	bi ms schist					
T	1583								
T	1584	N30E	62NW	gt ms bi MetaSS					
T	1585	N30E	80SE	bi ms MetaSS					
T	1586	N25E	55SE	bi rich ms gneiss					
T	1587	N30E	73SE	qtz rich ms bi gt MetaSS					
T	1588	N35E	75SE	ms bi schist					
T	1589	N33E	57SE	bi rich ms schist					
T	1590	N28E	60SE	ms rich bi gt schist					
T	1591	N19E	65SE	bi ms metagreywacke					
T	1592	N15E	46SE	bi rich ms gneiss					
T	1593	N30E	70SE	bi rich ms MetaGW					
T	1594	N24E	84SE	bi ms MetaGW					
T	1595	N37E	76SE	ms bi schist					
T	1596	N35E	72SE	bi ms MetaGW					
T	1597	N35E	75SE	ms bi gt schist					
T	1598	N35E	77SE	bi rich ms MetaGW					
T	1599	N15W	38NE	ms bi gt ky schist					
T	1600	N74E	40NW	MetaSS					
T	1601	N40W	45NE	MetaSS					
T	1602	N85E	46NW	ms MetaSS					
T	1603	E	51NW	bi ms MetaSS					
T	1604	N70E	34NW	bi ms MetaSS					
T	1605	N79E	30NW	bi ms MetaSS					
T	1606	N73E	40NW	bi ms MetaSS					
T	1607	N50E	37NW	MetaSS					
T	1608	N80E	50NW	MetaSS					
T	1609	N80E	65NW	bi ms gt MetaSS					
T	1610	N60E	62NW	bi ms gt schist					
T	1611	N65E	45NW	qtz rich ms bi MetaSS					
T	1612	N43E	60NW	bi ms MetaSS					
T	1613	N5W	70NE	qtz rich ms bi MetaSS					
T	1614	N12E	27NW	MetaSS	gentle fold	N48E	90	40NE	10
T	1615	N88W	45NE	MetaSS					
T	1616	N71W	36NE	qtz rich ms bi					
T	1617	N80W	51NE	MetaSS					
T	1618	N85W	35NE	qtz rich					
T	1619	N45E	65NW	bi ms gt					
T	1620	N80E	45NW	MetaGW					
T	1621	N80E	37NW	bi ms gt schist					
T	1622	N75E	70NW	MetaGW					
T	1623	N75E	70NW	al schist					
T	1624	N10E	80SE	MetaGW					
T	1625	N60E	55SE	bi gneiss					

Appendix II. Structural data for the Sylva South and Tuckaseegee quadrangles

Quad	Station	Foliation		Lithology	Structure	Axial Surface		Fold Axis	
		Strike	Dip			Strike	Dip	Trend	Plunge
T	1626	N50E	75NW	bi ms gt schist					
T	1627	N20E	60SE	bi ms gt sill schist					
T	1628	N35E	61SE	MetaGW					
T	1629	N70W	42NE	MetaGW					
T	1630	N10E	50NW	ms bi gt schist					
T	1631	N40E	37SE	MetaGW					
SS	1632	N60E	75NW	al schist					
SS	1633	N38E	70NW	ms schist					
SS	1634	N40E	77SE	bi ms gt schist	open inclined crenulations	N50W	60SW	40SE	55
T	1635	N55E	68NW	MetaSS	isoclinal synform	N50E	65NW	50SW	76
SS	1636	N30E	85NW	MetaGW					
T	1637	N35E	75NW	MetaGW					
T	1638	N65E	78NW	granitoid					
T	1639	N45E	60NWE	granodiorite					
T	1640	N67E	69NW	MetaGW					
T	1641	N44E	47NW	granitoid	anti syn pair	N50E	60NW	50SE	46
T	1642	N60E	70NW	granitoid					
T	1643	N50E	70NW	MetaGW					
T	1644	N45E	56NW	MetaGW					
T	1645	N50E	70NW	ms gt schist					
SS	1646	N70E	84SE	bi gneiss					
T	1647	N40W	54NE	bi ms schist					
T	1648	N35W	49NE	Am gneiss					
T	1649	N80E	70NW	ms bi schist					
T	1650	N48E	75NW	MetaGW					
	1651	N40W	44NE	MetaGW					
	1652	N41E	79NW	MetaGW					
	1653	N35E	69SE	MetaGW	closed folds	N80E	55NW	57NE	36
	1654	N15E	75NW	bi ms schist					
	1655	N51E	75SE	MetaGW					
	1656	N80E	80SE	MetaGW					
	1657	N55E	40NW	bi gneiss					
	1658	N50E	80NW	MetaGW					
	1659	N75E	64NW	MetaGW					
	1660	N49E	54NW	ms bi gt schist					
	1661	N44E	50NW	MetaGW					
	1662	N49E	70NW	MetaGW					
	1663	N45E	44NW	bi gneiss					
	1664	N55E	63NW	MetaGW					
	1665			MetaGW					
	1666			bi gneiss					
	1667	N50E	70SE	MetaGW					
	1668	N30E	77SE	MetaGW					
	1669	N80E	84NW	MetaGW					

Vita

Shawna Renee Cyphers was born February 12, 1981 in Amarillo, TX, to Robert and Sue Ellen Cyphers, and younger sister to Aaron. In 1985 the family moved to Chattanooga, TN where Shawna attended the Chattanooga School for the Arts and Sciences from which she graduated in 1999.

Upon finishing high school Shawna moved to Knoxville, TN and spent her freshman and sophmore year at UTK changing majors every other semester, from undecided to music education to a Bachelor of Arts in music. The summer before her junior year she recalled the 101 and 102 geology courses that she enjoyed as a freshman and decided to change majors one last time. She received her B.S degree in Geology May, 2004 and entered graduate school at the University of Tennessee at Knoxville, Fall of 2004.